Characterization of distal vessel remodelling in chronic thromboembolic pulmonary hypertension

Inaugural Dissertation submitted to the
Faculty of Medicine in partial fulfilment of the requirements
for the Degree of Doctor in Human Biology (Doctor biologiae hominis -
Dr. biol. hom.) of the Justus Liebig University Giessen

by Dijana Iloska-Leyer
from Ohrid, Macedonia

Gießen 2020

Characterization of distal vessel remodelling in chronic thromboembolic pulmonary hypertension

Inauguraldissertation

zur Erlangung des Grades eines Doktors der Humanbiologie

des Fachbereichs Medizin

der Justus-Liebig-Universität Gießen

vorgelegt von Dijana Iloska-Leyer

aus Ohrid, Mazedonien

Gießen 2020

From the Max-Planck-Institute for Heart and Lung Research. Department IV Lung Development and Remodelling (Prof. Dr. Med. Werner Seeger) of the Faculty for Medicine of the Justus-Liebig-Universität Gießen

Supervisor: Prof. Dr. Seeger
Supervisor: Prof. Dr. Dorresteijn

Day of disputation: 17.07.2020

Dedicated to:

My parents, Ratka and Nikola!

На моите родители, Ратка и Никола!

Т’га за југ

Орелски крилја как да си метнех,
И в наши ст’рни да си прелетнех!
На наши места ја да си идам,
Да видам Стамбол, Кукуш да видам,
Да видам дали с’нце и тамо
Мрачно угревјат како и вамо.

Ако как овде с’нце ме стретит,
Ако пак мрачно с’нцето светит
На п’т далечни ја ќе се стегнам
И в други ст’рни ќе си побегнам,
К’де с’нцето светло угревјат,
К’де небото звезди посевјат.

Овде је мрачно и мрак м’ обвива
И темна м’гла земја покрива:
Мразој и снегој и пепелници,
Силни ветришча и вијулици;
Околу м’гли и мразој земни,
А в гр’ди студој и мисли темни.

Не, ја не можам овде да седам,
Не, ја не можам мразој да гледам!
Дајте ми крилја ја да си метнам,
И в наши ст’рни да си прелетнам:
На наши места ја да си идам,
Да видам Охрид, Струга да видам.

Тамо зората греит душата
И с’нце светло зајдвит в гората:
Тамо дарбите природна сила
Со с’та роскош ги растурила:
Бистро езеро гледаш белеит
Или од ветар сино – темнеит;
Поле погледниш или планина,
Сегде божева је хубавина.

Тамо по срце в кавал да свирам,
С’нце да зајдвит, ја да умирам.

Константин Миладинов

Longing for the South

If I had an eagle's wings
I would rise and fly on them
To our shores, to our own parts,
To See Stambol, to see Kukus,
And to watch the sunrise: is it
dim there too, as it is here?

If the sun still rises dimly,
If it meets me there as here,
I'll prepare for further travels,
I shall flee to other shores
Where the sunrise greets me brightly
And the sky is sewn with the stars.

It is dark here, dark surrounds me,
Dark covers all the earth,
Here are frost and snow and ashes,
Blizzards and harsh winds abound,
Fogs all around, the earth is ice,
And in the breast are cold, dark thoughts.

No, I cannot stay here, no;
I cannot sit upon this frost.
Give me wings and I will don them;
I will fly to our own shores,
Go once more to our own places,
Go to Ohrid and to Struga.

There the sunrise warms the soul,
The sun gets bright in mountain woods:
Yonder gifts in great profusion
Richly spread by nature's power.
See the clear lake stretching white-
Or bluely darkened by the wind,
Look at the plains or mountains:
Beauty everywhere divine.

To pipe there to my heart's content.
Ah! Let the sun set, let me die.

Konstantin Miladinov

Table of contents

List of Tables

List of Figures

List of Abbreviations

ACTB	β-actin
AF	Adventitial fibroblast
ANGPT1	Angiopoetin 2
ANGPT2	Angiopoetin 2
APA	Antiphospholipid antibody
ATX	Autotaxin
BPA	Balloon angioplasty
BSA	Bovine serum albumin
BrdU	Bromodeoxyuridine
B2M	Beta-2-Microglobulin
CCL2	C-C Motif Chemokine Ligand 2
cGMP	cyclic Guanosine monophosphate
CHI3L1	Chitinase-3-like-1
CTEPH	Chronic thromboembolic pulmonary hypertension
CTE	Chronic thromboembolism
CRP	C-reactive protein
CKS1B	Cyclin-Dependent Kinases Regulatory Subunit 1
DAPI	4′,6-Diamidin-2-phenylindol
DMSO	Dimethyl sulfoxide
DVT	Deep vein thrombosis
EC	Endothelial cell
EEL	External lamina elastica
ELISA	Enzyme-linked immunosorbent assay
ENA-78	Neutrophil-activating protein
ENPP2	Ectonucleotide Pyrophosphatase/Phosphodiesterase 2
eNOS	Endothelial Nitric Oxide Synthase
ET-1	Endothelin-1
FCS	Fetal calf serum
FGF	Fibroblast growth factor
FOXO	Forkhead box O
GAPDH	Glyceraldehyde 3-phosphate dehydrogenase
GF	Growth factor
HIF1-α	Hypoxia Inducible Factor 1α

HOXC6	Homeobox C6
IBS	Inflammatory bowel disease
IEL	Internal elastic lamina
IL	Interleukin
IPAH	Idiopathic pulmonary arterial hypertension
IP-10	Interferon-γ-inducible 10 kDa
KDR	Kinase insert domain protein receptor
KEGG	Kyoto Encyclopedia of Genes and Genomes
KLF2	Kruppel-like factor 2
LCM	Laser capture microdissection
LPA	Lysophosphatidic acid
MCEMP1	Mast Cell-Expressed Membrane Protein
mRNA	messenger Ribonucleic Acid
NFATC2	Nuclear factor of activated T-cells, cytoplasmic 2
NO	Nitric oxide
NOS 3	Nitric Oxide Synthase 3
PA	Pulmonary artery
PAI-1	Plasma plasminogen activator inhibitor
PAAF	Pulmonary adventitial fibroblast
PACP	Pulmonary artery capillary pressure
PAEC	Pulmonary artery endothelial cell
PAH	Pulmonary arterial hypertension
PASMC	Pulmonary arterial smooth muscle cell
PAP	Pulmonary artery pressure
PAWP	Pulmonary artery wedge pressure
PCLS	Precision cur-lung slide
PDGF	Platelet Derived Growth Factor
PDPN	Podoplanin
PECAM 1	Platelet endothelial cell adhesion molecule
PF4	Platelet factor 4
PE	Pulmonary embolism
PEA	Pulmonary endarterectomy
PH	Pulmonary hypertension
RHC	Right heart catheterization

PMEC	Pulmonary microvascular endothelial cells
PRPG6	Pre-MRNA Processing Factor 6
PVR	Pulmonary vascular resistance
PVOD	Pulmonary veno-occlusive disease
RV	Right ventricle
sGC	Soluble guanylate cyclase
t-PA	Tissue plasminogen activator
TNF-α	Tumour Necrosis Factor-α
Tyr	Tyrosine
VEGF	Vascular endothelial growth factor
VE-catherin	Vascular endothelial cadherin
VTE	Venous thromboembolism
vWf	von Willebrand factor
WT	Wildtype
α-SMA	alpha- smooth muscle actin

1. Theoretical background

1.1. Pulmonary vasculature: composition and function

The pulmonary vasculature is exclusive in its structure, volume and function. The lung is the only organ displaying two different types of circulation: the **pulmonary circulation**, with main function of gas exchange, and the **bronchial circulation**, a systemic vascular supply that provides oxygenated blood to the walls of the conducting airways, pulmonary arteries and veins. (Suresh & Shimoda, 2016). During embryonic stage of development, pulmonary circulation is a low compliance and high resistance system (Suresh & Shimoda, 2016), while postnatally, it is directed towards high compliance and low resistance in order to effectively accomplish the gas exchange (Townsley, 2013). In fact, the pulmonary vascular resistance (PVR) is approximately one-tenth of the one of systemic circulation. In comparison to their systemic counterparts, the pulmonary arteries have thinner walls, smaller smooth muscle layer, balancing between high production of endogenous vasodilators and low production of vasoconstrictors (Suresh & Shimoda, 2016) in order to accommodate a large volume of blood with little increase in mean pulmonary arterial pressure (mPAP) (Lammers et al., 2012). The pulmonary circulation arises from the right ventricle (RV), while the bronchial vessels usually originate from the aorta or the intercostal arteries, draining into the right heart. Bronchial vessels also supply the intrapulmonary airways, at a level of terminal bronchioles, where they anastomose with the pulmonary vasculature (Baile, 1996).

The pulmonary vasculature is composed of three anatomic compartments associated in a sequence: the arterial tree, an extensive capillary bed and the venular tree (Townsley, 2013). Further on, the arterial wall comprises of three layers, tunica intima, tunica media and tunica adventitia, each contributing in a different extent to the total vessel thickness (Figure 1).

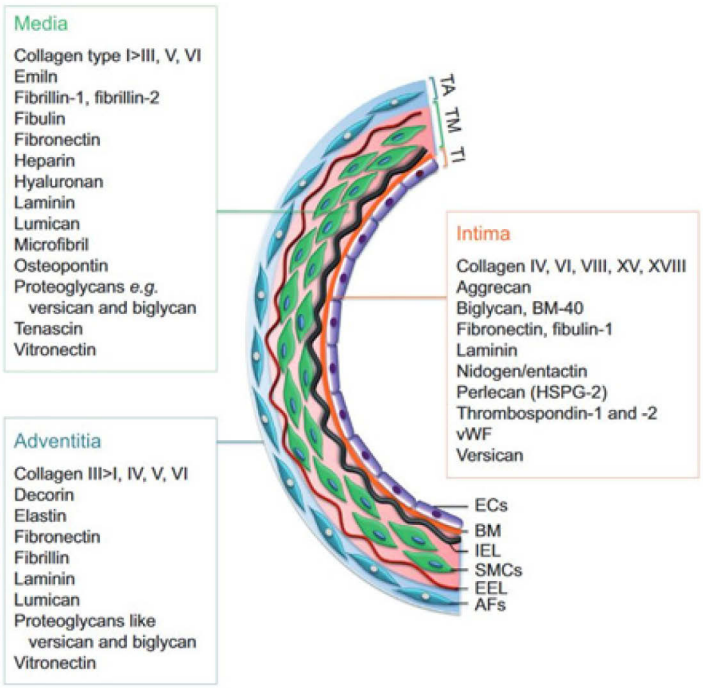

Figure 1: Architecture of the arterial wall and its extracellular matrix (ECM) components. The major components of the vessel wall are: tunica intima (TI), tunica media (TM) and tunica adventitia (TA). TI is represented by endothelial cells (ECs), further supported by basal membrane (BM) and internal elastic lamina (IEL); TM corresponds to the smooth muscles cells (SMCs) layer connected to the TA, defined by adventitial fibroblasts (AF) via external elastic lamina (EEL) (Chelladurai, Seeger, & Pullamsetti, 2012). Reproduced with permission of the © ERS 2019: *European Respiratory Journal 40 (3) 766-782; DOI: 10.1183/09031936.00209911 Published 31 August 2012*

Tunica intima is the innermost layer of the vascular wall, under direct influence of the blood flow. It is comprised of continuous monolayer of endothelial cells (ECs), supported by a sub-endothelial layer of connective tissue and supportive cells, ultimately forming a tightly regulated semipermeable barrier. The gas exchange takes place in the capillary segment (normally around 3-4µm in size), dispersed from the small arteries and comprised only of ECs, surrounded by the alveolar epithelial cells. In addition to tunica intima towards the tunica media, in muscular arteries, the internal elastic lamina can be identified as a concentric layer of elastic tissue.

Tunica media is comprised of a single layer (arterioles) or multiple layers (pulmonary arteries) of smooth muscle cells (SMCs) and elastic and connective fibres arranged circumferentially around the vessel. It is a substantial part of the vessel, playing a role in contraction and relaxation of the blood vessel, in order to decrease and increase the diameter of the vessel lumen, respectively. The media is demarcated from the adventitia with a thick layer of external elastic lamina.

Tunica adventitia is the outermost layer composed of adventitial fibroblasts (AFs) as a predominant cell type, interstitial cells, connective fibres, a vasa vasorum and neuronal network, providing a structural integrity and a damage protection of the vessel. Tunica adventitia as well hosts resident progenitor stem cells and infiltrating immune cells (Chelladurai et al., 2012).

Any kind of mechanical or structural alterations in the vascular wall can affect the pressure in the pulmonary circulation, contributing to initiation and maintenance of pulmonary hypertensive state.

1.2. Pulmonary hypertension

Pulmonary hypertension (PH) is a progressive, multi-etiological disease of the pulmonary vasculature characterized by pathological remodelling of the resistance pulmonary arteries, resulting in RV failure and ultimately death (Farber & Loscalzo, 2004). Clinically, PH confers mPAP greater or equal to 25 mmHg and PVR greater or equal to 3 Wood units at rest, measured by right heart catheterization (RHC), which is a reference standard for assessing PH patients. During the RHC, an additional measurement of pulmonary artery wedge pressure (PAWP) or pulmonary artery capillary pressure (PACP) is performed to differentiate between pre-capillary and post-capillary PH (M. M. Hoeper et al., 2013). Recently, a new definition has been proposed by the 6th WSPH Task Force on PH diagnosis and classification, suggesting that pre-capillary PH is best defined by the concomitant presence of mPAP >20 mmHg, PAWP ≤15 mmHg and PVR ≥3 WU (Gérald Simonneau et al., 2019). All forms of PH are estimated to affect over 100 million people worldwide. Once diagnosed and left untreated, the median survival rate of patients is only 2.8 years (D'Alonzo et al., 1991).

1.3. Classification of pulmonary hypertension

Based on their clinical presentation, pathological findings, haemodynamic characteristics and treatment strategy (Galiè et al., 2016), updated clinical classification from the 6th World PH symposium, PH has been classified into five main groups, Group 1 to 5 (Galiè et al., 2016; Gérald Simonneau et al., 2019). As presented in Table 1, the **Group 1** is Pulmonary Arterial Hypertension (PAH), represented by wide range of clinical manifestations, including the pulmonary veno-occlusive disease. The other clinical groups are as following: **Group 2**: PH due to left heart disease; **Group 3**: PH due to lung diseases and/or hypoxia; **Group 4**: Chronic thromboembolic pulmonary hypertension and **Group 5**: PH with unclear multifactorial mechanisms.

Table 1: Comprehensive clinical classification of pulmonary hypertension (PH) (Gérald Simonneau et al., 2019)

1. **Pulmonary arterial hypertension (PAH)**
1.1. Idiopathic PAH 1.2. Heritable PAH 1.2.1 BMPR2 mutation 1.2.2 ALK-1, ENG, SMAD9, CAV1, KCNK3 1.2.3 Unknown 1.3. Drugs and toxins induced 1.4. PH associated with: 1.4.1 Connective tissue disease 1.4.2 Human immunodeficiency virus (HIV) infection 1.4.3 Portal hypertension 1.4.4 Congenital heart disease 1.4.5 Schistosomiasis 1.5. PAH long-term responders to calcium channel blockers 1.6. PAH with overt features of venous/capillaries (PVOD/PCH) involvement 1.7. Persistent PH of the newborn syndrome
2. Pulmonary hypertension due to left heart disease
2.1. PH due to heart failure with preserved left ventricular ejection fraction 2.2. PH due to heart failure with reduced left ventricular ejection fraction 2.3. Valvular heart disease 2.4. Congenital/acquired left cardiovascular conditions leading to post-capillary PH
3. Pulmonary hypertension due to lung diseases and/or hypoxia
3.1. Obstructive lung disease 3.2. Restrictive lung disease 3.3. Other lung disease with mixed restrictive/obstructive pattern 3.4. Hypoxia without lung disease 3.5. Developmental lung diseases
4. Pulmonary hypertension due to pulmonary artery obstructions
4.1. Chronic thromboembolic pulmonary hypertension 4.2. Other pulmonary artery obstructions 4.2.1. Sarcoma (high or intermediate grade) or angiosarcoma

4.2.2. Other intravascular tumours (renal, uterine carcinoma, germ cell tumours of the testis, other tumours) 4.2.3. Non-malignant tumours (Uterine leiomyoma) 4.2.4. Arteritis without connective tissue disease 4.2.5. Congenital pulmonary arteries stenoses 4.2.6. Parasites (hydatidosis)
5. Pulmonary hypertension with unclear and/or multifactorial mechanisms
5.1. Hematologic disorders: chronic hemolytic anemia, myeloproliferative disorders, splenectomy 5.2. Systemic and metabolic disorders: pulmonary Langerhans cell histiocytosis, Gaucher disease, glycogen storage disease, neurofibromatosis, Sarcoidosis 5.3. Others: fibrosing mediastinitis, chronic renal failure with or without haemodialysis 5.4. Complex congenital heart disease

1.4. Group 1 PH: Pulmonary arterial hypertension (PAH)

In spite of the classification, featured by the clinical parameters, every PH group (or subgroup), regardless of the clinical manifestations and histopathological characteristics, exhibits pulmonary vasoconstriction and excessive pulmonary vascular remodelling, leading to increased PVR, RV overload and failure. PAH as the first group in the classification system of PH, appears to involve multiple aetiologies, including the idiopathic PAH (IPAH), heritable PAH (BMPR2 mutation, ALK-1, ENG, SMAD9 etc.), drugs and toxins induced PAH, as well PAH associated with several other diseases such as collagen vascular disease, PA shunts, portal hypertension, HIV infection and other conditions that include congenital heart disease, hemoglobinopathy, and hereditary haemorrhagic telangiectasia.

1.4.1. Pathogenesis of PAH

Sustained pulmonary vasoconstriction, lumen obliteration of small- and medium-sized arteries and arterioles, formation of plexiform lesions and in situ thrombosis, and concentric thickening of pulmonary arteries are the main cause for elevated mPAP and PVR in patients with PAH regardless of the initial pathogenic trigger (J. X. Yuan & Rubin, 2005).

It is well appreciated that patients with PAH exhibit imbalanced levels of vasodilators and vasoconstrictors. Endothelin-1 (ET-1) levels are elevated in PH patients (Giaid et al., 1993), as a major player in the vasodilator/vasoconstrictor imbalance. It is primarily produced by pulmonary artery ECs (PAECs). Through the action on its receptor expressed on pulmonary

artery SMCs (PASMCs), it induces vasoconstriction, proliferation and the production of cytokines and growth factors (Luscher & Barton, 2000; Pollock, Keith, & Highsmith, 1995).
Similarly, PH patients have reduced circulating levels of the vasodilators such as prostacyclin and nitric oxide (NO) relative to levels of the vasoconstrictor such as thromboxane (Christman et al., 1992). It was shown that prostacyclin induces vasodilation, inhibits platelet activity and exhibits anti-proliferative effects on PASMCs, therefore it is considered as a therapeutic target for the treatment of PH (Olschewski et al., 2004). On the other hand, NO levels are as well decreased in PAH patients due to high arginase levels (substrate of nitric oxide synthase) or increased asymmetric dimethyl arginine (competitive inhibitor of nitric oxide synthase) (S. Pullamsetti et al., 2005). NO stimulates soluble guanylate cyclase (sGC) to produce cyclic guanosine monophosphate (cGMP), which in turn activates cGMP-dependent protein kinase G in PASMCs, causing vasodilatory and anti-proliferative effects as well as PASMC relaxation. Phosphosdiesterase-5 (PDE-5) is the enzyme responsible for breakdown of cGMP in response to increase of NO. Consequently, PDE-5 inhibitors are used effectively in treatment of PAH, as they can increase intracellular cGMP and enhancing PASMCs relaxation and vasodilation (Wilkins, Wharton, Grimminger, & Ghofrani, 2008).
Circulating levels of serotonin (5-Hydroxy tryptamine) are elevated in PH patients. Serotonin is mainly produced in PAECs and via the serotonin transporter, expressed in PASMCs and pulmonary artery adventitial Fibroblasts (PAAFs), leading to vasoconstriction and proliferation (Naeije & Eddahibi, 2004).
Voltage gated potassium channels (Kv channels), Kv1.2 and Kv1.5 are known to be downregulated in PASMCs from PH patients (X.-J. Yuan, Wang, Juhaszova, Gaine, & Rubin, 1998). Downregulation of these channels, along with subsequent membrane depolarization and opening of the voltage-gated Ca^{2+} channels results in vasoconstriction (Archer et al., 2008). Mitochondrial abnormalities such as pathological activation of pyruvate dehydrogenase kinase (PDK) are known to inhibit Kv channels and activate vasoconstrictive, pro-proliferative and anti-apoptotic signalling cascades (Moudgil, Michelakis, & Archer, 2006).

Although the causal PAH pathomechanisms are still largely unclear, recently, a cancer-like concept for PAH has emerged, rationalized by *in situ* and *in vitro* observations (Rai et al., 2008; Sakao et al., 2011). According to this concept, a monoclonal expansion of ECs has been found in IPAH when compared with ECs found in lungs of patients with congenital heart malformations (S. D. Lee et al., 1998). Next, instability of short DNA microsatellite sequences within plexiform lesions in IPAH has been evident (Yeager, Halley, Golpon, Voelkel, & Tuder,

2001) and the presence of somatic chromosome abnormalities in the lungs of patients with PAH and cultured cells has been reported (Aldred et al., 2010). PAECs and PASMCs derived from patients with PAH maintain their abnormal hyperproliferative, apoptosis-resistant phenotype (Tu et al., 2012; Tu et al., 2011) and human pulmonary vascular cells derived from PAH patients exhibit an altered energy metabolism *in situ* and *in vitro* (Michelakis et al., 2002; Sutendra et al., 2010; Tuder, Davis, & Graham, 2012; Xu et al., 2007). Yet, one should consider that there are crucial differences between PAH pathogenesis and carcinogenesis.

1.4.2. Pulmonary vascular remodelling

PAH pathophysiology is represented by endothelial dysfunction and a persistent vasoconstriction, resulting in obliterative remodelling of small pulmonary arteries (< 500 μm diameter) and pre-capillary (< 70μm diameter) due to proliferation of PAECs and PASMCs (K. R. Stenmark, Meyrick, Galie, Mooi, & McMurtry, 2009; Tuder et al., 2009). Indeed, the remodelling is primarily a result of excessive proliferation of vascular cells and affects all the layers (intima, media and adventitia), leading to intimal thickening, media hypertrophy, adventitial thickening, plexiform lesions and vascular pruning (S. S. Pullamsetti et al., 2014). Recruitment of inflammatory and progenitor cells within the vessel wall is also contributing to the vascular remodelling (A. L. Firth, Mandel, & Yuan, 2010).

Endothelial cells regulate the vascular tone and their injury or dysfunction can cause a switch from quiescent phenotype towards a pro-proliferative and apoptotic-resistant phenotype, leading to neointima formation (Meyrick, Clarke, Symons, Woodgate, & Reid, 1974; Sakao et al., 2005; Tuder, Groves, Badesch, & Voelkel, 1994). Dysfunctional endothelium then releases growth factors (fibroblast growth factor (FGF)-2 and angipoetin-1 and 2 (ANGPT-1; ANGPT-2)), vasoconstrictors (ET-1), pro-thrombotic mediators (thromboxane-A2) and pro-inflammatory cytokines (bone morphogenetic proteins (BMPs)) that stimulate proliferation of PASMCs (Morrell et al., 2009; Thompson & Rabinovitch, 1996). A network of vascular channels, called plexiform lesions, is formed at later stage of the disease evolving from monoclonal expansion of apoptosis-resistant PAECs, migration and proliferation of PASMCs and accumulation of circulating cells such as macrophages and endothelial progenitor cells (S. D. Lee et al., 1998; Rabinovitch, 2012).

Medial hypertrophy and hyperplasia is featured by expansion of apoptosis-resistant smooth muscle cells, as well as differentiating cells present in the vessels or migration and de-differentiation of PAAFs (Davie et al., 2006). In larger pulmonary arteries, hypertrophy of PASMCs and extracellular matrix deposition are most effective in enlarging the vessel wall,

while hyperplasia is prevalent in smaller resistance vessels (Jeffery & Morrell, 2002). As mentioned before, several growth factors are released after endothelial injury affecting the SMCs as one of the remodelling effectors. Platelet derived growth factor (PDGF), is shown to induce proliferative and migratory phenotype of PASMCs. Pulmonary arteries of IPAH patients are shown to highly express PDGF ligands and the receptors (PDGFR-α, PDGFR-β) (Perros et al., 2008). Administration of imatinib, a PDGFR antagonist, reversed the vascular remodelling in hypoxia model of PH (Schermuly et al., 2005). Furthermore, a transcription factor FoxO1, is downregulated in IPAH, negatively regulating pro-proliferative and anti-apoptotic PASMC phenotype by affecting some proliferative genes as Cyclin D1, p27, and apoptotic genes like BCL6 and GADD45a (Savai et al., 2014).

Tunica adventitia is collagen-enriched vessel platform containing mainly fibroblast and adrenergic nerves. Additionally, it accommodates many immunomodulatory cells, such as macrophages, mast cells, T-cells, dendritic cells, CD34+/Sca1+ progenitor cells, ECs of vasa vasorum, pericytes and adipocytes (Majesky, Dong, Hoglund, Mahoney, & Daum, 2011). The vascular remodelling also includes thickening of the adventitia, as PAAFs proliferate and secrete chemokines thus facilitating the recruitment of inflammatory cells in response to environmental stress (Kurt R. Stenmark et al., 2012). In fact, increased levels of tumour necrosis factor (TNF)-α, Interleukin (IL)-1β, IL-6, and IL-8 have been reported in severe hypoxic pulmonary hypertension (Soon et al., 2010). Several of these cytokines are multifunctional, directly regulating proliferation, migration and differentiation of vascular cells. IL-6, for instance, induces PASMCs proliferation via elevation of FGF-2. When overexpressed in mice it caused exaggerated pulmonary hypertensive response to hypoxia (Golembeski, West, Tada, & Fagan, 2005). Elevated TFG-β in PH can induce PAAFs to differentiate into myofibroblasts, leading to increased production of extracellular matrix proteins like collagen or can further migrate to the medial or intimal layer supporting the extensive pathological remodelling (Davie et al., 2006).

1.4.3. Vascular inflammation

One of the features observed from histopathologic specimens and serum/ plasma samples from patients with PAH is the presence of inflammation. Inflammation represents a complex series of interactions among soluble factors and cells that can arise in response to traumatic, infectious, post-ischemic, toxic, or autoimmune injury (Chatelain & Dardik, 1988).

Patients with IPAH have elevated serum levels of cytokines, including IL-1- β, IL-6, and IL-8 (Humbert et al., 1995; Soon et al., 2010) and chemokines such as chemokine (C-C motif) ligand (CCL)2/monocyte chemotactic protein (MCP)-1 (Sanchez et al., 2007), CCL5/regulated upon activation, normal T cell expressed and secreted (RANTES) (Peter Dorfmüller et al., 2002) and CXC3CL1/fractalkine (Balabanian et al., 2002). TNF-α, IL-6, MCP-1, and C-reactive protein (CRP) are also increased in congenital heart disease associated PAH (Diller et al., 2008). However, increased levels of such mediators are common to the pathology of PAH *per se* and are not restricted to one particular subtype.

1.4.4. Transcription factors in PAH

Growing evidence indicates that transcription factors (TFs) have been implicated in the pathogenesis of PH and RV dysfunction (S. S. Pullamsetti et al., 2017). The activity of the TFs can be targeted by different stimuli converging the PH vascular phenotype (S. S. Pullamsetti et al., 2017). TFs are sequence-specific DNA-binding proteins controlling the process of transcription. TFs regulate the gene expression by direct binding to the core promoter elements in proximity to transcriptional start sites to recruit transcriptional machinery and regulate gene expression (Goodrich & Tjian, 2010) or by utilizing regulatory DNA elements called enhancers, the general transcriptional machinery, and Pol II (RNA polymerase II) complexes (Goodrich & Tjian, 2010; Lelli, Slattery, & Mann, 2012).

As known, several TFs are key regulators of cellular proliferation and may directly be involved in the pathogenesis of PH and most likely CTEPH. Evidence that Forkhead box O1 (FoxO1) transcription factor, among all FoxO isoforms, is centrally involved in the hyperproliferative and apoptosis-resistant phenotype of PASMCs, the hallmark of PAH, has been recently presented by Savai et al. (2014). FoxO TFs belong to a family of transcriptional regulators characterized by a conserved DNA-binding domain termed the Forkhead box (Eijkelenboom & Burgering, 2013) and can act as transcriptional activators and repressors. In mammals, four FoxO isoforms have been identified: FoxO1, FoxO3, FoxO4 and FoxO6. FoxOs control various cellular responses (Eijkelenboom & Burgering, 2013) and have been implicated in vascular structural maintenance (Mahajan et al., 2012; Oellerich & Potente, 2012). FoxO1 and FoxO3 are described in the literature to regulate essential set of genes involved in angiogenesis as well as vascular remodelling (Potente et al., 2005).

GATA-6 is a member of GATA family of zink-finger TFs, expressed in a wide spectrum of tissues, heart, lung, liver, kidney, pancreas, spleen etc. maintaining the differential cell

composition (Suzuki et al., 1996). It is highly expressed in quiescent vasculature, particularly in vascular SMCs, maintaining their contractile phenotype and lost upon vascular injury (Mano, Luo, Malendowicz, Evans, & Walsh, 2015; Nishida et al., 2002). GATA-6 may play a role in the pathogenesis of PH by regulating ET-1, plasminogen activator inhibitor-1 (PAI-1), matrix metallopeptidase 1 (MMP1), matrix metallopeptidase 10 (MMP10) etc (Ghatnekar et al., 2013).

KLF-2 belongs to the Kruppel-like factors (KLFs), a subclass of the zinc finger family of TFs which regulates cellular differentiation and tissue development (Bieker, 2001). Within the vessel wall it is exclusive to EC and induced when cultured ECs were exposed to sustained shear stress (Dekker et al., 2002). Share stress induced KLF-2 is directly affecting the eNOS levels, as an essential regulator of vascular reactivity and tone (Huang et al., 1995).

1.5. Chronic thromboembolic pulmonary hypertension (CTEPH)

Chronic thromboembolic pulmonary hypertension (CTEPH) is a rear, complex, multifactorial and severe vascular disease that is life threatening if untreated (I. M. Lang, Dorfmuller, & Vonk Noordegraaf, 2016; J. Pepke-Zaba, 2010). It represents the group 4 of the current clinical classification of PH. CTEPH has a distinguishable nature when compared to other types of PH, with regard to the pathophysiological features, as well as the treatment options (I. Lang, 2015). Extensive clinical evidence indicates that it might be initiated by a spectrum of thrombotic or inflammatory lesions of the pulmonary vasculature, although the acute pulmonary embolism (PE) emerge as a most common reason (J. Pepke-Zaba, 2010). A large international registry confirmed that approximately around 75% of the patients had a history of acute PE, despite the fact that there were some reservations in regard to the thromboembolic nature of the disease (J. Pepke-Zaba et al., 2011).

Several ongoing studies suggest that CTEPH is a disease of dual vascular compartments, presented by major vessel remodelling and small vessel arteriopathy, characterized by medial hypertrophy, obstructive intimal thickening, microthrombi formation and plexiform lesions (Figure 2) (Galiè & Kim, 2006; I. Lang, 2010; Piazza & Goldhaber, 2011). CTEPH usually starts with a persistent thrombi obstruction in the proximal (main, lobar and segmental) arteries which fails to resolve (G. Simonneau, Torbicki, Dorfmuller, & Kim, 2017). Small vessel disease occurs distally to the obstructed areas and most likely due to excessive collateral blood supply from high pressure pulmonary and systemic circulation (G. Simonneau et al., 2017).

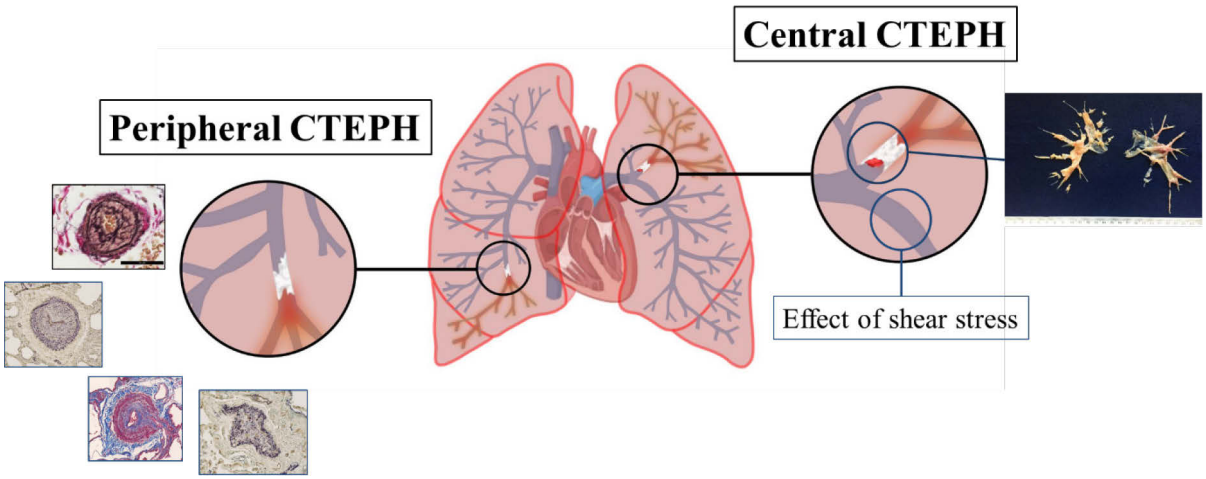

Figure 2: CTEPH as a dual compartment disease. Major vessel remodelling and microvascular arteriopathy characterized by medial hypertrophy, intimal thickening, intimal fibrosis and plexiform lesions

CTEPH diagnosis is confirmed if after 3 months of effective anticoagulation, the patient has mPAP greater or equal to 20 mmHg, pulmonary capillary wedge pressure (PCWP) smaller or equal to 15 mmHg and at least one mismatched segmental perfusion defect (I. M. Lang et al., 2016; I. M. Lang, Pesavento, Bonderman, & Yuan, 2013; Gérald Simonneau et al., 2019). The cut-off inclusion criteria is based on different scanning tests, such as multidetector computed tomography angiography or pulmonary angiography and most importantly ventilation/perfusion (V′/Q′) scanning (Galiè et al., 2009). V′/Q′ scanning is used to distinguish between CTEPH and PAH, as PAH patients will have normal or small peripheral perfusion defects (N. H. Kim et al., 2013).

The clinical signs of CTEPH are not specific (I. M. Lang & Madani, 2014), therefore setting on the early diagnosis is challenging (P. F. Fedullo, Augur, Kerr, & Rubin, 2001). Clinically significant pulmonary hypertension can manifest months or years later, after the “honeymoon period” for the majority of the patients (McNeil & Dunning, 2007). After the disease has been established, as in other PH forms, patients experience progressive dyspnoea on exertion as a prevailing symptom. Additionally, patients might present fatigue, syncope, haemoptysis, and signs of right-heart failure (Marius M. Hoeper et al., 2014).

Despite the fact that estimating the overall incidence and prevalence of CTEPH correctly has been a challenging process, prospective studies are reporting the incidence of CTEPH after acute PE between 0.4 and 9.1% (I. M. Lang & Madani, 2014). The prevalence of CTEPH in overall population is estimated at 17-20 per million (I. M. Lang et al., 2016).

1.5.1. CTEPH classification

The treatment of patients with CTEPH is largely contingent on eligibility of the patient for surgical excision and/or balloon angioplasty. Recently, a refined classification of surgical CTEPH has been introduced and proposed by University of California, San Diego - (UCSD) (unpublished data), presented at the International CTEPH conference 2017 (Jenkins, Madani, Fadel, D'Armini, & Mayer, 2017). According to this classification, based on location of the disease and degree of difficulty in dissection/excision/resection, there are "levels" of thromboembolic disease (Table 2).

Table 2: A proposed new surgical classification of CTEPH, University of California, San Diego, preliminary results (M. Madani, Ogo, & Simonneau, 2017)

Surgical level	Location of the thromboembolic disease
0	No evidence of CTE (chronic thromboembolic disease)
I	CTE at the level of main pulmonary arteries
II	CTE at the level of lobar or intermediate arteries
III	CTE at the segmental level
IV	CTE at the subsegmental level

1.5.2. Current treatment for CTEPH

The management of the therapeutic strategies for each individual patient is proceeded in expert centres, supported by a multidisciplinary team of surgeons, cardiologists, pulmonologists and radiologists (Dartevelle et al., 2004; M. M. Hoeper, Mayer, Simonneau, & Rubin, 2006).

Depending on the clinical manifestation, as CTEPH represents dual compartment disease, patients with major vessel obliterations are endorsed for surgical therapy; while patients experiencing distal vascular arteriopathy, not accessible to surgery are referred to medical therapy or non-invasive interventions (Figure 3).

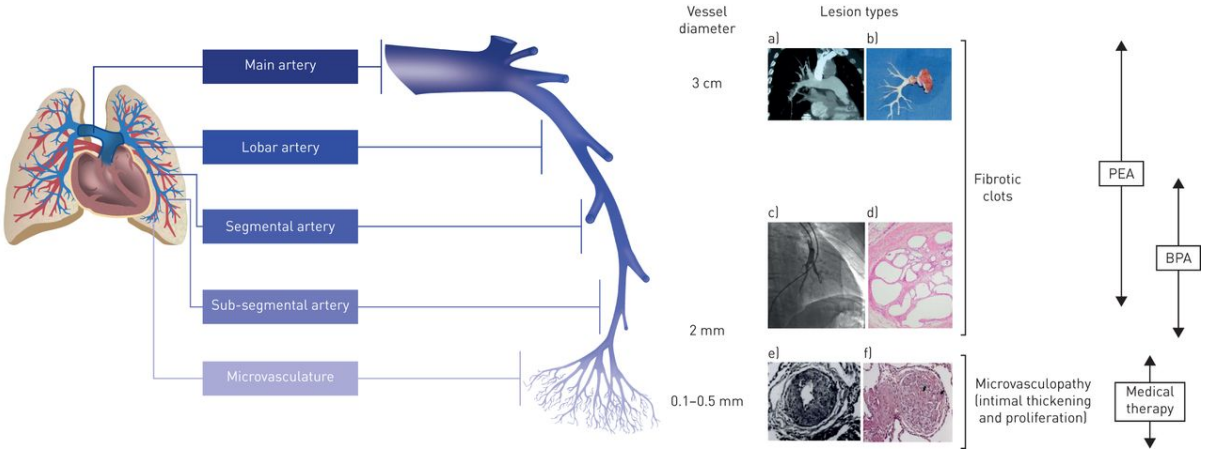

Figure 3: The treatment options for chronic thromboembolic pulmonary hypertension (CTEPH) (M. Madani et al., 2017, p. 4) Reproduced with permission of the © ERS 2019: *European Respiratory Review 26 (146) 170105; DOI: 10.1183/16000617.0105-2017 Published 20 December 2017*

1.5.2.1. Pulmonary endarterectomy

The surgical resection known as pulmonary endarterectomy (PEA) comprises of full bilateral endarterectomy in order to remove the scaring obstruction at the level of intima-media, proximally in the main, lobar and segmental arteries; while mid-segmental and sub-segmental affected areas require experienced surgeon or are technically inoperable (Galiè et al., 2016; Jenkins, 2015; M. Madani et al., 2017).

The procedure is performed under deep hypothermic circulatory arrest to provide clear operating field and protect the deterioration of the brain function (Galiè et al., 2016; M. Madani et al., 2017). Many parameters influence whether patients are available for surgery, at first their age and general health (Jenkins et al., 2017). Furthermore, considering the hemodynamic measures, assessed by right heart catheterization, patients with high PVR, have greater mortality risks, yet, show better improvement after PEA (Jenkins et al., 2017). Once the right place for resection is identified, the surgeon “cleaves/scrap” the obstruction till smooth vessel wall, accessible for continual blood flow (M. M. Madani & Jamieson, 2006). Data regarding the clinical outcomes after PEA, indicate not only hemodynamic enhancement, but higher 10-year post-surgical survival rates as well as improvement of the WHO (World Health Organization) functional class (Cannon et al., 2016; I. M. Lang et al., 2013; Mayer et al., 2011; Skoro-Sajer et al., 2007).

1.5.2.2. Balloon angioplasty

Emerging therapeutic strategy, termed as percutaneous balloon pulmonary angioplasty (BPA) has been proven recently as a considerable measure for patients with inoperable CTEPH,

patients with limited benefit from PEA or with persistent or recurrent PH after PEA (I. Lang et al., 2017). BPA is usually accompanied by a medicated therapy.

BPA as non-invasive, catheter based intervention in comparison to PEA and is performed to open distal obstructed vessels or widen stenotic lesions, in order to improve haemodynamics and pulmonary perfusion, ultimately preventing right ventricular failure (I. Lang et al., 2017). A balloon is inserted via the femoral or jugular vein at the site of the obstruction using a guide wire with a help of imaging techniques and inflated to break the webs and bands (Ogawa & Matsubara, 2015; Ogo et al., 2017).

Improvements in clinical parameters and haemodynamics, as well as the functional class and the exercise capacity are notable after successful single or multiple session/s of BPA (Ogo et al., 2017).

BPA is not a risk-free procedure as pulmonary artery injury and haemorrhage can occur very easily (Inami et al., 2015). Despite that, further development of BPA and/or bridging it with PEA allows expanded application for delicate patients experiencing both proximal and distal vascular lesions (I. Lang et al., 2017).

1.5.2.3. Medical therapy

Presence of microvascular disease in inoperable CTEPH patients has been a challenging issue when designing the therapeutic strategy of each individual patient. As histopathological changes described in CTEPH are similar to those of PAH, medical treatment with PAH approved drugs targeting nitric oxide, endothelin and prostacyclin pathway have been evaluated in CTEPH patients (Moser & Bioor, 1993; J. Pepke-Zaba, Ghofrani, & Hoeper, 2017).

Similar to PAH, NO levels have been reduced in CTEPH patients. Importantly, sGC stimulator, known as riociguat is used to compensate the loss of NO by further activating the production of cyclic guanosine monophosphate (cGMP), a secondary signalling molecule. The final consequence of increased cGMP is decreased intracellular calcium and smooth muscle relaxation (Klinger, Abman, & Gladwin, 2013; Tonelli, Haserodt, Aytekin, & Dweik, 2013). The results of the CHEST-1 study suggest improvement in PVR, N-terminal pro-brain natriuretic peptides and WHO functional class in patients with CTEPH. Furthermore, and most striking, an improvement in the 6-min walking distance in contrast to placebo treated CTEPH patients has been noted (H. A. Ghofrani et al., 2013).

Reesink et al. (2006) reported deteriorated endothelin pathway in patients with CTEPH. Plasma levels of ET-1 are augmented and this correlates with the haemodynamic parameters and severity of the disease. ET-1, *per se* is a potent vasoconstrictor, contributing to proliferation of smooth muscle cells in both, proximal and distal CTEPH, as ET-1 receptors have been identified in PEA surgical dissection (Southwood et al., 2016). Endothelin receptor antagonists are well established for treatment of patients with PAH, while they aren't licenced yet for CTEPH patients, but rather used "off-label" (Southwood et al., 2016). Bosentan significantly improved the PVR and cardiac index, although it failed because it didn`t meet the criteria for the 6-min walking test. However, another endothelin receptor antagonist, macitentan undoubtedly improved cardiopulmonary haemodynamics and clinical variables in patients with inoperable CTEPH, regardless of the use of PAH therapies at baseline (MERIT-1 study) (H.-A. Ghofrani et al., 2017).

Prostacyclin levels in PAH patients are reduced (Irene M. Lang & Gaine, 2015), therefore drugs targeting the prostacyclin pathway have been used. A little less is known on the efficacy of prostacyclin therapies in CTEPH patients, particularly because the lack of defining the subgroup in the clinical trials. However, within a PH study, effect of inhaled iloprost was evaluated in inoperable CTEPH patients and the general outcome confirmed the positive effect in 6 min walking distance and the functional class (Olschweski et al., 2002).

1.5.2.4. Supportive medical therapy

Lifelong anticoagulation therapy, use of antidiuretics and oxygen in case of hypoxemia, are indispensable for patients with CTEPH, even after PEA (J. Pepke-Zaba et al., 2017). Despite the fact that, there are no randomized controlled clinical trials, the reasoning behind is to prevent *in situ* thrombosis or recurrent venous thromboembolism (VTE) (Joanna Pepke-Zaba, Jansa, Kim, Naeije, & Simonneau, 2013; Wilkens et al., 2018). According to the Updated Recommendations from the Cologne Consensus Conference 2018, both coumarin-derived and non-vitamin-K-dependent anticoagulants are used as an additional therapy in the post-acute phase of a PE (Wilkens et al., 2018).

So far, as stated in the current guidelines by Wilkens et al. (2018), vitamin K antagonists (especially warfarin) are still considered the standard supportive treatment for CTEPH. The need of bypassing the limitations of vitamin K antagonists, accustomed the usage of new oral anticoagulants such as dabigatran (a direct thrombin inhibitor) and rivaroxaban, apixaban, and edoxaban (direct activated factor X inhibitors). The advantages of the new oral anticoagulants

are that they do not require laboratory monitoring, have limited food and drug interactions, and doses are convenient for most of the patients (Roca & Roca, 2015). Furthermore, a study conducted by Gavilanes-Oleas et al. (2018) reported the use of new direct oral anticoagulants on twenty patients with CTEPH monitored for 21 months. In this time period, beyond a major bleeding caused by a traumatic fall there was no recurrence of VTE (Gavilanes-Oleas et al., 2018). In the long run, extensive clinical studies can provide detailed knowledge on the safety and the conventional use of these particular anticoagulants.

As mentioned before, CTEPH diagnosis is based on measures of the mPAP > 20 mmHg by the latest suggestion from the 6th WSPH Task Force on PH diagnosis and classification) and PCWP ≤ 15mmHg, after ≥ 3 months effective anticoagulation and one perfusion defect, at most (Galiè et al., 2016; I. M. Lang et al., 2013; Gérald Simonneau et al., 2019). It is well known that patients with surgically assessable obstructions have greater chance in functional and improvement of the hemodynamic parameters (J. Pepke-Zaba et al., 2017). However, according to the international registries data, 10-50% of the CTEPH patients with distal vascular arteriopathy aren`t qualified for a surgical dissection of the organized vascular obstruction. (Mayer et al., 2011; Peacock, Simonneau, & Rubin, 2006; J. Pepke-Zaba et al., 2011). Significant portion of patients, with consideration of approximately 50%, endure a persistent or recurrent pulmonary hypertension, even after successful surgery and may require further treatment (Cannon et al., 2016; J. Pepke-Zaba et al., 2017). In the past few years, the treatment of operable and non-operable CTEPH patients evolved, as surgical techniques advance and the medical and percutaneous interventions expand.

Nonetheless, even after supposedly successful PEA or BPA, CTEPH patients can suffer further from persistent or recurrent PH. Persistent PH may evolve from incomplete removal of more distal vascular obstruction or presence of microvascular disease in patients with proximal disease (Jenkins, 2015). Recurrent PH may be a consequence of poor anticoagulation and distal arteriopathy (Cannon et al., 2016).

1.5.3. Pathophysiology of CTEPH

Current evidence on the pathogenesis of CTEPH, suggests the unlikelihood that a single factor, but rather a combination of factors causing chronic vascular scaring, that subsequently leads to PH and RV dysfunction (Matthews & Hemnes, 2016). The initial event indeed, is an acute PE, following venous thromboembolism (VTE) (P. Fedullo, Kerr, Kim, & Auger, 2011). The incomplete resolution of the acute PE is advancing into occlusive vascular remodelling of

proximal and segmental vessels, displayed by the presence of intraluminal webs and bands, stenotic lesions etc. (Marius M. Hoeper et al., 2014). The "completely occluded" arterial tree, distal to the organized thrombus is not affected by the high pressure, while the non-completely (stenotic, patent, open) occluded arterial tree is exposed to shear stress, leading to an increased PVR and secondary pulmonary arteriopathy and ultimately to CTEPH (Figure 4) (Southwood et al., 2016).

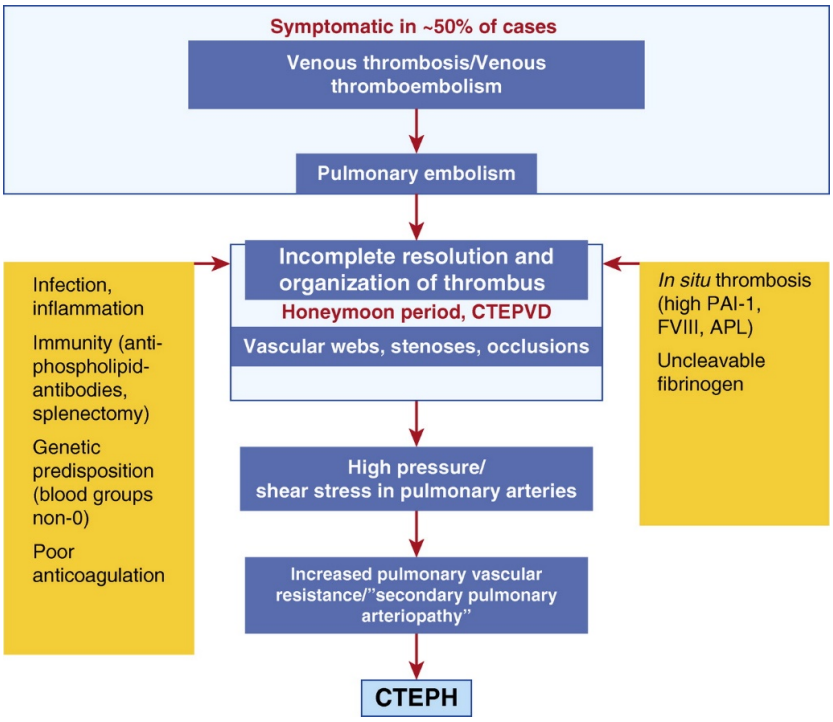

Figure 4: Schematic representation of the current pathophysiological concept of CTEPH. Reprinted with permission of the American Thoracic Society. Copyright © 2019 American Thoracic Society (I. M. Lang et al., 2016) Reproduced with permission of the © ERS 2019: *European Respiratory Review 26 (143) 160112; DOI: 10.1183/16000617.0112-2016 Published 29 March 2017*

The factors affecting the incomplete resolution and the formation of the chronic vascular scaring are as follows:

Inherited thrombophias. Mutations of factor V Leiden, the prothrombin, anti-thrombin, protein C and S are inherent in the development of VTE (Cohn, Roshani, & Middeldorp, 2007), although their contribution to the progression to CTEPH is not very well understood. Wong, Szydlo, Gibbs, and Laffan (2010), demonstrated that there are no differences in the prevalence of the indicated mutations, except for a higher incidence of the factor V in a subset of Caucasian CTEPH patients, in comparison to patients within other PH groups. Other studies evaluated statistically non-significant association in CTEPH with the general population for factor V (I. Lang, 2010), suggesting the absence of the cause and effect between inherited thrombophilias and CTEPH.

Acquired thrombophilias. Antiphospholipid antibodies (APA) and anticardiolipin antibodies are associated with various medical conditions, being specific for anionic phospholipids, phospholipid-binding proteins, or phospholipid-protein complexes (Parthvi et al., 2017). APA are the most prevalent aberration contemplating approximately 20% of the CTEPH cases, in contrast to 10% found in IPAH patients (Wolf et al., 2000). Given that the CTEPH patients had higher titers of APA than IPAH patients, their prothrombic character is quite significant in the initiation and the development of the disease. A study conducted between four European centres, revealed a prevalence of 10% among the CTEPH patient population, in comparison to 4% of the group of non-thromboembolic PH (Bonderman, Wilkens, Wakounig, Schafers, et al., 2009). Further research on the presence of lupus anticoagulant has confirmed that 10.6% of the CTEPH patients are positive for its presence.

Elevated factor VIII levels. Factor VIII (antihemophilic factor) is a protein from the coagulation cascade, which has an ability to facilitate the factor IXa-mediated activation of factor X. The mechanism of action is not very well understood, while the major effects is to increase the rate of the reaction. Factor VIII possess no enzymatic activity, has capacity to be activated by thrombin and factor Xa and inactivated by activated protein C and by human antibodies to factor VIII (Chavin & Weidner, 1984). In plasma, factor VIII forms a complex with von Willebrand factor (vWf) as his carrier protein (Vlot et al., 1996). As a response to an injury, factor VIII dissociates from its carrier, being released in the plasma, contributing to clot formation (Sharma & Lang, 2018). Elevated levels of factor VIII has been described to contribute to a single and/or recurrent venous thromboembolic events (Kyrle et al., 2000). Aligned with that, study has presented that in comparison to healthy controls and non-thromboembolic PH patients, the levels of factor VIII were elevated in CTEPH patients (Bonderman et al., 2003). Whether the elevated factor VIII levels are the cause or the consequence of CTEPH, requires further investigation (Matthews & Hemnes, 2016).

Inefficient/defective fibrinolysis and fibrinogen. Several thrombotic disorders, such as coronary artery disease (Hamsten, Wiman, de Faire, & Blombäck, 1985; Paramo, Colucci, & Collen, 1985) and VTE (Nillson, Ljungnér, & Tengborn, 1985) are represented by reduction in the plasma fibrinolysis. This modification is most likely due to an increased plasma plasminogen activator inhibitor (PAI-1) activity or deficient tissue plasminogen activator (t-PA) (Olman et al., 1992). Fibrinolysis as an antagonistic process of fibrin formation, comprises of synergistic cleavage of cross-linked fibrinogen, via plasminogen, t-PA, PAI-1 and other interaction proteins. Tranexamic acid, as an antifibrinolytic agent was used in a canine model

of acute PE, where a persistent elevation of PAP and thrombus non-resolution was noted (Moser et al., 1991).

On one hand, plasma levels of PAI-1 and t-PA were elevated in patients with CTEPH in contrast to the corresponding controls, although there was no difference in the enzymatic activity between them (Olman et al., 1992). Induction of venous occlusion in CTEPH patients, has been shown to result in increased t-PA antigen and PAI-1 activity, suggesting that the defective or deficient fibrinolysis might not be one of the major contributors to the development of CTEPH (Olman et al., 1992). Another consequence is, once formed, the thromboemboli is resistant to fibrinolysis (Nijkeuter, Hovens, Davidson, & Huismann, 2006).

On the other hand, patients with CTEPH often bear a point mutation of fibrinogen Aα-Thr312Ala (Le Gal et al., 2007; Li et al., 2013; Suntharalingam et al., 2008), which leads to formation of fibrin clots and increased cross-linking of α-chains (Toshner & Pepke-Zaba, 2014). Further, other β-chain mutations, P235L/γR357W,P235L/γY114H and P235L, along with α-chain mutations L69H and R554L were found in CTEPH patients (Morris et al., 2009). Taken together, all fibrin defects in CTEPH patients lead to ineffective thrombolysis, thus directly influencing the thrombus non-resolution (I. M. Lang et al., 2016; Marsh, Chiles, Liang, & Morris, 2013).

Endothelial dysfunction. Endothelial cells (ECs) isolated from PEA biorepositories, possess cobblestone morphology and are positive for endothelial markers. The same study confirmed their hyperproliferative and apoptosis resistant phenotype, reduced tube formation capacity, lower rates of mitochondrial membrane potential and reduction of mitochondrial content in comparison to control PAECs (Tura-Ceide et al., 2016).

In another study, ECs isolated from CTEPH were compared to donor ECs for the production of PAI-1 and t-PA, and there were no significant differences in the basal t-PA levels as well as the PAI-1 activity. Similar response was obtained when the ECs were exposed to thrombin (I. M. Lang, Marsh, Olman, Moser, & Schleef, 1994).

As a response to increased pressure, inflammation or acute lung injury, endothelial permeability upsurge (Bogatcheva, Garcia, & Verin, 2002; J. Garcia & Schaphorst, 1995). Share stress is yet another factor affecting the ECs function, influencing their production of vasoactive factors (Sacks et al., 2006). Apart of its function in a thrombus formation, it has been reported that, α-thrombin increased albumin clearance via the endothelial monolayer (J. G. Garcia et al., 1986). In these circumstances, ECs became shorter, which leads to formation

of intracellular gaps and ECs permeability, through activation of T-type voltage gated Ca^{2+} channels and increase of cytosolic calcium (Moser & Bioor, 1993; Wu et al., 2003). ECs isolated from PEA material, indeed confirm the different calcium homeostasis in comparison to control hPAECs. The positive identification of the angiostatic factors, such collagen type I, platelet factor 4 (PF4) and interferon-γ-inducible 10 kDa (IP-10) certainly confers towards endothelial dysfunction (Zabini et al., 2012).

Platelets aggregation. Thyroid hormone replacement therapy and splenectomy are platelet-activating conditions, suggesting the platelet involvement in the pathogenesis of CTEPH (Bonderman, Wilkens, Wakounig, Schafers, et al., 2009; J. Pepke-Zaba et al., 2011). Platelet activation after splenectomy, *per se*, has been identified by an increase of thrombus volume in a mouse model of defective thrombus resolution (Frey et al., 2014). Platelet microparticles has been shown to be generated in splenectomised patients in the same study, in contrast to non-splenectomised CTEPH patients. Further research on the potential role of platelets in the development of CTEPH is presenting that the platelets from CTEPH or PAH were activated compared to non-PH controls by their increased surface expression of p-selectin, PAC-1 binding and the GTP-bound GTPase RhoA, involved in their aggregation (Yaoita et al., 2014). On the other hand, patients with CTEPH have a decreased platelet count, higher mean platelet volume and decreased aggregation in response to agonists (Remková, Šimková, & Valkovičová, 2015). These findings suggest the possible contribution of the dysfunctional platelets in the pathogenesis of CTEPH, given that platelets are also activated in PAH patients.

Medical conditions associated with CTEPH.

Splenectomy. An increased prevalence of splenectomy as a risk factor for CTEPH has been reported in a retrospective study by Jaïs and colleagues (Jais et al., 2005). History of splenectomy has been detected in 8.6% (95% CI 5.2 to 12.0) of patients with CTEPH, in contrast to 2.5% (96% CI 0.7 to 4.4) and 0.56% (95% CI 0 to 1.6) in IPAH and other pulmonary conditions, respectively. The most common reason for splenectomy is a ruptured spleen, which is often caused by an abdominal injury, some blood disorders, certain cancers, infection, and noncancerous cysts or tumours. The mechanisms associating splenectomy with CTEPH are still not well understood. One of the possible reasons is the loss of splenic filtering which leads to abnormal circulating erythrocytes, thrombin generation (Kuypers, 1998) and pro-inflammatory cytokine expression (Moshtaghi-Kashanian, Gholamhoseinian, Hoseinimoghadam, & Rajabalian, 2006). After splenectomy, platelet count returns to normal, and the risk of thromboembolism and ultimately CTEPH is noticeable from 7 to 25 years later

(Jais et al., 2005), suggesting that increased risk of CTEPH cannot be addressed only by elevated platelet count. Research evidence is furthermore, suggesting the phospholipid accumulation in PEA thrombi after splenectomy, as well as in a mouse model of venous thromboembolism undergoing splenectomy (Frey et al., 2014). Taken together, the role of the phospholipid factor, post splenectomy in supplemental development of pathophysiological conditions and CTEPH cannot be undermined.

Ventriculoatrial (VA) shunts and infected pacemakers. Staphylococcal infection may play a significant role, as patients with CTEPH have been described to have VA shunts and infected pacemakers with higher frequency than other PH etiologies. Despite the fact that, a precise mechanism connecting VA shunts and CTEPH is lacking, Bonderman et al. (2008) suggested that staphylococcal infection can delay thrombus resolution in addition to upregulation of profibrotic molecules, in a murine model of venous thrombosis.

Non-O blood group. Individuals with non-O blood group have been demonstrated to bear increased levels of von Willebrand factor (vWf), factor VIII, p-selectin and TNF-α, all highly susceptible for VTE and CTEPH (Gándara et al., 2013). Although, the underlying mechanisms addressing the association between ABO blood group and factor VIII-vWf are unclear, studies have shown that healthy, O-blood group individuals have 25-30% lower levels of plasma vWf, than non-O carriers (Gill, Endres-Brooks, Bauer, Marks, & Montgomery, 1987; McCallum, Peake, Newcombe, & Bloom, 1983; Mohanty et al., 1984; Orstavik et al., 1985). Another study has suggested that the modulated glycosylation, can affect the vWf clearance and further on the plasma levels of factor VIII-vWf complex (Gallinaro et al., 2008).

Chronic inflammatory diseases. Finally, several inflammatory diseases such as inflammatory bowel disease (IBS), osteomyelitis, venous ulcers, thyroid hormone replacement and malignancy have been listed in the literature to have direct effect towards an increased risk of development of CTEPH (Bonderman et al., 2005; Bonderman, Wilkens, Wakounig, Schäfers, et al., 2009; P. Fedullo et al., 2011; N.H. Kim & Lang, 2012).

1.5.4. Histopathology of CTEPH

1.5.4.1. Proximal major vessel obliterations in CTEPH

CTEPH is dual vascular disorder, comprising of major and microvascular vessel remodelling. The proximal (major) vessel remodelling represented as persistent organized thrombi at a level of main, lobar and segmental arteries is the initial step in orchestrating the further development of CTEPH (G. Simonneau et al., 2017). The organized thrombi, also called neointima is tightly

adhered to the medial layer of the pulmonary arteries, which may completely obstruct the lumen of the artery (I. Lang, 2015). As a consequence, the intimal surface roughens and in order to restore the blood circulation and potentially decrease the PVR, recanalization (bands and webs) takes place (P. F. Fedullo et al., 2001). The intimal layer mainly displays collagen and elastic fibres deposition and presence of α-smooth-muscle actin (α-SMA) positive cells, possibly from SMCs migrated from the media or from circulating progenitor cells (A. L. Firth, Yao, et al., 2010; Owens, Kumar, & Wamhoff, 2004). A clinicopathologic study of 200 consecutive PEA samples revealed the presence of organized thrombi, inflammation, cholesterol clefts, calcification and increased cellularity (Bernard & Yi, 2007). Rozenn Quarck, Wxnants, Verbeken, Meyns, and Delcroix (2015) analysed the major-vessel lesions of CTEPH patients using immunohistochemistry and identified the presence of four types of lesions: neointima, thrombotic, atherosclerotic and recanalized lesions. Regarding the composition of infiltrated cells in the organized thrombi, several studies confirmed presence and similar distribution of macrophages, T- and B- lymphocytes and neutrophils (Arbustini et al., 2002; Bernard & Yi, 2007; Rozenn Quarck et al., 2015).

Recanalization, or the neo-angiogenesis is regulated by both pro- and anti-angiogenic factors (Ribatti, 2009). A study reported that several angiostatic factors, such as collagen type I, PF4 and IP-10 are present in PEA material (Zabini et al., 2012). In addition, it is shown that these factors contribute to endothelial dysfunction. In contrast to this study, Naito et al. (2018) has been able to demonstrate that ECs isolated from PEA not only demonstrate high proliferative potential, but also extensive angiogenic capacity.

Certain discrepancies appear in regard to the presence of fresh thrombus in PEA material of operable CTEPH patients. Some studies are reporting a high percentage of appearance of fresh clot (Arbustini et al., 2002), while in some, these changes is rarely observed (Blauwet, Edwards, Tazelaar, & McGregor, 2003; Rozenn Quarck et al., 2015), which is most likely a result of different interpretation of the pathologist or the effectiveness of the anticoagulation therapy.

1.5.4.2. Microvascular disease in CTEPH

Small vessel arteriopathy (also referred as microvascular disease) in CTEPH was at first described by Moser and Bloor in a lung tissues obtained from biopsy or at autopsy of CTEPH patients (Moser & Bioor, 1993). The histological features of distal pulmonary microvasculopathy include intimal thickening, eccentric intimal fibrosis, intimal fibromuscular

proliferation, medial hypertrophy and presence of plexiform lesions (Moser & Bioor, 1993; G. G. Pietra et al., 2004). Distal pulmonary vessels with diameter of 100-500 µm are highly affected by the remodelling, including the vessels with less than 100 µm (I. M. Lang et al., 2016). Hypertrophy and hyperplasia of all three cell types of pulmonary vascular wall (PAECs, PASMCs and PAAFs) and accumulation of endothelial progenitor cells underline the histopathological features of CTEPH (Ogawa et al., 2009; Sakao et al., 2011); (I. Lang, 2015).

The vascular remodelling distal to the organized thromboembolic obstruction may be similarly distributed in the lung areas of complete and non-complete occlusion. The areas distal of non-completely occluded arteries are affected by high pressure and share stress, triggering the increase of PVR and at the end leading to CTEPH (G. Simonneau et al., 2017).

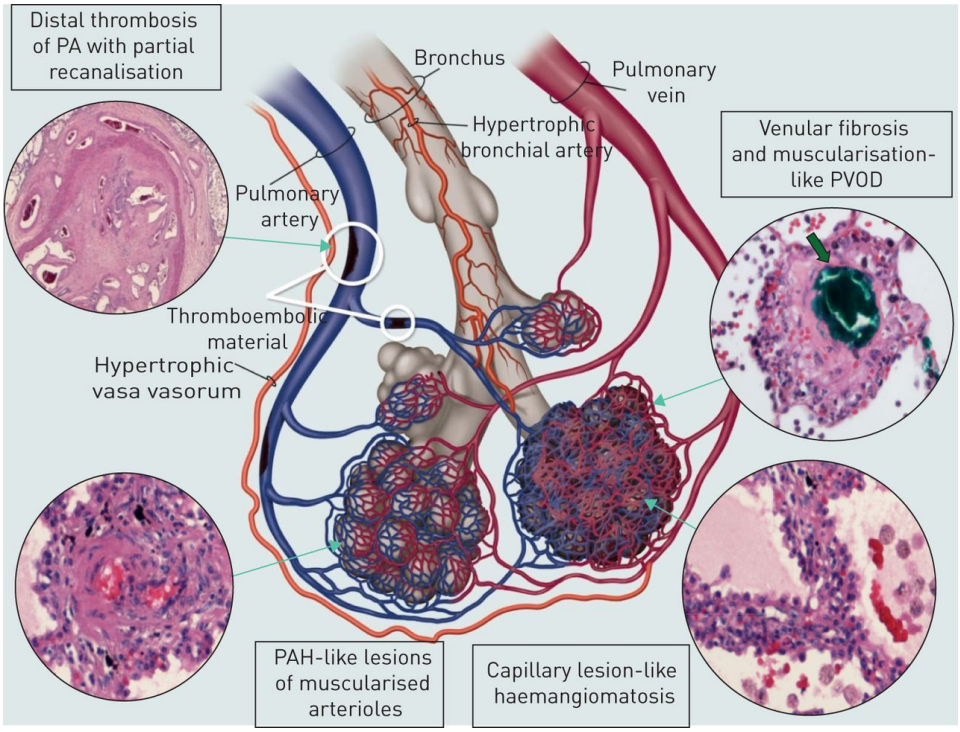

Figure 5: Microvascular disease in CTEPH affecting the pulmonary arterioles, venules and capillaries. Presence of hypertrophied vasa vasorum and bronchial arteries showing the anastomoses between pulmonary and systemic circulation (G. Simonneau et al., 2017).

Furthermore, the importance of the bronchial circulation in pulmonary vascular and airways disease has been appreciated. In patients with CTEPH anastomoses between bronchial and pulmonary arterial circulation appears via hypertrophied bronchial arteries and vasa vasorum (Figure 5) (P. Dorfmüller et al., 2014). These anastomoses are similar lesions as in capillary haemangiomatosis and pulmonary veno-occlusive disease (PVOD). Although their function is not yet fully understood, it is estimated that they help the perfusion and support ischaemic tissue downstream of the proximal obstruction (P. Dorfmüller et al., 2014; G. Simonneau et al.,

2017). In addition, P. Dorfmüller et al. (2014) confirmed that the disease not only affects the pre-capillary arterioles, but also the post-capillary venules and small veins.

The presence of plexiform lesions in CTEPH patients has been a topic of controversial discussion up to date. Plexiform lesions in CTEPH patients, and especially in autopsies, rather than lung biopsies have been reported in a systematic study by Moser and Bloor (1993). Plexiform lesions are complex, glomeruloid-like vascular structures, morphologic hallmark of obstructive intimal remodelling, which correlate with the severity of PH (Giuseppe G. Pietra et al., 1994; Yi et al., 2000). Plexiform lesions are described as a dynamic proliferating networks of endothelial-lined vascular channels, surrounded by apoptosis-resistant myofibroblasts, smooth muscle cells, or even undifferentiated mesenchymal cells (Cool et al., 1999; Jonigk et al., 2011). The three-dimensional characterization of plexiform lesions in CTEPH using microvascular corrosion casting has been reported by Ackermann et al. (2017). Case study report of a 64-years old woman with severe CTEPH have identified vascular channels expressing endothelial markers of differentiation, supported by concentric accumulation of a tightly layered mesenchymal cells. The study provides the first evidence that the formation of plexiform lesions is driven by sprouting and intussusceptive angiogenesis. Sprouting angiogenesis is growth of new blood vessels from pre-existing vasculature, while intussusceptive angiogenesis represents creation of two vessels from one using transcapillary tissue pillars (Ranchoux et al., 2018).

1.5.5. Molecular mechanisms in CTEPH

The pathogenesis of CTEPH in terms of cellular and molecular mechanisms is not fully exemplified. As CTEPH arises as a sequela of acute PE, the pathophysiological mechanisms preventing thrombus resolution are associated to defective angiogenesis and delayed fibrinolysis along with endothelial dysfunction (I. M. Lang et al., 2013). Presence of pro-inflammatory mediators and platelet aggregation has been highly associated with proximal CTEPH (Figure 6). Furthermore, little is known on the molecular mechanisms underlying the development and the progression of microvascular disease in CTEPH. So far, as the histopathological changes in CTEPH are similar to those in PAH and the PAH approved therapies are also implicated in the treatment of CTEPH, it is presumed that the similar cellular mechanisms and key pathways may play an important role in the initiation and progression of distal CTEPH.

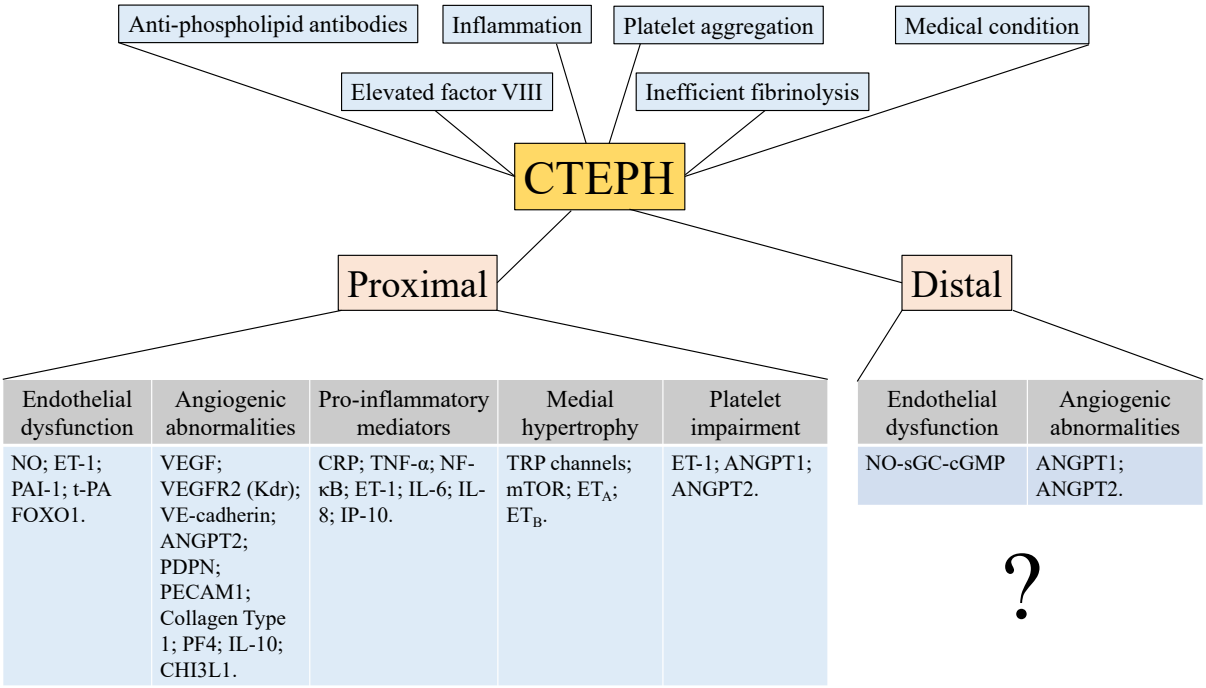

Figure 6: Pre- and post- elements of pathobiology of CTEPH. Factors involved in the development of CTEPH and consequent molecular markers discovered so far, featuring proximal and distal CTEPH.

1.5.5.1. Angiogenic abnormalities

The occlusive thrombus while healing or organization is affected by positive regulators of angiogenesis (Distler, Hirth, Kurowska-Stolaroska, Gay, & Distler, 2003). The venous thrombus recanalization has been noticed in rats after single injection of vascular endothelial growth factor (VEGF) recombinant protein in the freshly formed thrombi (Waltham et al., 2003). Another study, conducted in a rat model of deep vein thrombosis (DVT) is appreciating the induction of angiogenesis by basic fibroblast growth factor (bFGF) and epithelial neutrophil-activating protein (ENA-78), while having no effect on the thrombus resolution (Varma et al., 2004). Furthermore, in the mouse model of venous thrombi in inferior vena cava (IVF) has been found that the formation of occlusive thrombus causes a relative hypoxia in the surrounding vein wall, leading to increased levels of hypoxia- inducible factor 1 alpha (HIF1α). HIF1α upregulates the expression of angiogenic factors that promote vein recanalization and thrombus resolution (Evans et al., 2011). Utilizing another IVF model, generated with endothelial cell-specific deletion of kinase insert domain protein receptor (*Kdr*), a predominant cell receptor for VEGF in endothelial cells, a delayed thrombus resolution has been perceived (Alias et al., 2014). Consistently to the findings, the gene expression profiles of the organized white human PEA thrombi, manifest lower levels of several vascular specific genes such as KDR, vascular endothelial cadherin (VE-catherin) and podoplanin (PDPN), as well as

angiopoetin 2 (ANGPT2), platelet endothelial cell adhesion molecule (PECAM 1), vascular endothelial growth factor A (VEGFA) etc. (Alias et al., 2014).

Furthermore, increasing evidence suggest that expression changes of chitinase-3-like-1 (CHI3L1) is associated with the pathogenesis of various human diseases (Francescone et al., 2011). It has been shown that CHI3L1 plays a role in cancer through enhanced production of pro-inflammatory/pro-tumourigenic and angiogenic factors (Libreros, Garcia-Areas, & Iragavarapu-Charyulu, 2013). Furthermore, studies have shown an important link between CHI3L1 and inflammation or metabolic diseases, including asthma (Chupp et al., 2007), hypertension (Ma et al., 2012), diabetes mellitus (Rathcke & Vestergaard, 2009; Rondbjerg, Omerovic, & Vestergaard, 2011), insulin resistance (Kyrgios et al., 2012) and atherosclerosis (Gong, Xing, Zheng, & Xing, 2014; Michelsen et al., 2010). Family 18 of glycosyl hydrolases encompasses chitinases, which can enzymatically cleave chitin and chitinase-like proteins that bind, but do not cleave this polysaccharide (Bussink, Speijer, Aerts, & Boot, 2007). Despite the fact that, mammals lack endogenous chitin, both types of proteins are expressed in the lung and other organs (Bussink et al., 2007; Funkhouser & Aronson, 2007).

Chitinase-3-like-1 (CHI3L1) also known as YKL-40 (cartilage-glycoprotein 39) is a 40-kDa secreted heparin-, chitin- and collagen-binding lectin without chitinase activity, due to a mutation of an essential glutamic acid to leucine in the catalytic domain (Fusetti, Pijning, Kalk, Bos, & Dijkstra, 2003; Renkema et al., 1998). CHI3L1 is secreted by broad spectrum of cells, such as neutrophils, macrophages, synovial cells, fibroblasts, connective tissue cells, endothelial cells, vascular smooth muscle cells, epithelial cells and tumour cells (Di Rosa, Malaguarnera, De Gregorio, Drago, & Malaguarnera, 2013).

However, the role of CHI3L1 in pulmonary vascular homeostasis and disease is poorly understood (Kawada, Hachiya, Arihiro, & Muizoguchi, 2007), although could be presumed from the cellular functions mediated by CHI3L1. CHI3L1 is suggested to affect the proliferation and differentiation of connective tissue cells (De Ceuninck et al., 2001; Recklies, White, & Ling, 2002), inflammation and matrix remodelling (Di Rosa et al., 2013), recruitment of macrophages (Ref), activation of vascular endothelial cells (Malinda, Ponce, Kleinmann, Shackelton, & Millis, 1999) and angiogenesis (Francescone et al., 2011). In addition, studies from other lung diseases confirmed the potential role of CHI3L1. Zhou et al. demonstrated increased expression of CHI3L1 in patients with idiopathic pulmonary fibrosis (IPF) and the plasma levels correlate with the disease progression (Zhou et al., 2014). The same study has demonstrated that, during injury, CHI3L1 plays a protective role enhancing inflammation and

cell death, while in repair it plays a profibrotic role by contributing to fibroblast proliferation and matrix deposition. Increased CHI3L1 is associated with asthma and chronic obstructive pulmonary disease, suggesting its potential as a biomarker, as it is related to chronic inflammatory disease processes (Chupp et al., 2007; James et al., 2016). Based on the studies listed above, we hypothesised the potential role of CHI3L1 in the pathogenesis of CTEPH.

1.5.5.2. Presence of pro-inflammatory markers

Inflammatory markers, such as CRP (R. Quarck, Nawrot, Meyns, & Delcroix, 2009), TNF-α (Langer et al., 2004) and MCP-1 (Kimura et al., 2001) are elevated in plasma and proximal thrombi of CTEPH patients, in correlation with the patient hemodynamic parameters. A study has reported that CRP induced NF-κB activation may be involved in the pathogenesis of CTEPH (Wynants et al., 2013). CRP stimulated ECs isolated from PEA, resulted in differential expression of genes related to NF-κB pathway. On the other hand, the effects of pyrrolidine-dithio-carbamate ammonium (PDTC), NF-κB inhibitor has been demonstrated on CRP-induced adhesion of monocytes to PAECs, adhesion molecule expression, ET-1, IL-6, and vWF secretion (Wynants et al., 2013). As shown, CRP-NF-κB link might contribute to the persistence of the proximal thrombi and subsequently to CTEPH.

1.5.5.3. Vascular remodelling

The endarterectomised material from occluded regions of the proximal PAs consist of SMCs, ECs and myofibroblasts (Amy L. Firth, Yuill, & Smirnov, 2008). Patients with PH, including CTEPH confer extensive vascular wall thickening and remodelling, as a result of proliferation of PASMCs. Store-operated Ca^{2+} entry (SOCE), cytosolic free Ca^{2+} and transient receptor potential (TRP) channels are known to be important in cell proliferation and vascular remodelling in PH (A. L. Firth, Remillard, & Yuan, 2007; Lin et al., 2004). Mammalian target of rapamycin (mTOR) acts via AKT pathway and is involved in cancer cell proliferation (Gao et al., 2004). The proliferation of wide varieties of cells (cancer cells, coronary arterial smooth muscle cells, embryonic stem cells and vascular progenitor cells) can be inhibited by blockage of the mTOR signalling using rapamycin (Ogawa et al., 2009). When SMCs isolated from PEA material are acutely treated with rapamycin, the levels of SOCE are significantly reduced; while chronic treatment of rapamycin will inhibit SOCE, towards decrease cell proliferation (Ogawa et al., 2009). These findings suggest the potential role of mTOR signalling pathway in the proximal pulmonary vascular remodelling in CTEPH and potential therapeutic benefit of rapamycin for operable CTEPH patients.

1.5.5.4. Endothelial dysfunction

As ET-1 levels are elevated in patients with CTEPH and in animal models resembling CTEPH (Hojoong Kim, 2009; Reesink et al., 2006) increasing evidence is suggesting the role of ET-1 in proliferation of SMCs within the obstructed artery and in microvascular disease (Southwood et al., 2016).

Furthermore, increased levels of angiopoetin 1 (ANGPT-1) are perceived in CTEPH lung samples (M. M. Hoeper et al., 2006), while increased levels of ANGPT-2 negatively correlate with the outcome of PEA (Lankeit et al., 2013). ANG-1, is involved in angiogenesis and SMC proliferation (M. M. Hoeper et al., 2006). It is known that, ANGPT-1 blocks BMPR2 signalling even in the absence of germline BMPR2 mutations. This mechanism seems to play a role in several forms of PH including CTEPH (Du et al., 2003).

Nitric oxide (NO) pathway may play a significant role in the pathogenesis of CTEPH (G. Simonneau et al., 2017). NO levels in CTEPH patients are decreased, while the levels of asymmetric dimethylarginine (NO synthase inhibitor) are increased in contrast to the respective controls (Skoro-Sajer et al., 2007). Patients not being candidates for PEA or with recurrent/persistent PH after surgery are medically treated with sGC stimulator – riociguat, emphasising the role of NO-sGC-cGMP pathway in pathogenesis of CTEPH (H. A. Ghofrani et al., 2013).

1.5.5.5. Platelet aggregation

Patients with CTEPH, and in general, PH patients present thrombotic pulmonary vascular lesions, suggesting the role of abnormal blood coagulation factors and dysfunctional platelets in the pathogenesis of the disease (Shlyonsky, Naeije, & Mies, 2014). Platelets activation can be driven by thyroid hormone replacement therapy and splenectomy (Bonderman, Wilkens, Wakounig, Schafers, et al., 2009; Karimi & Cohan, 2010; J. Pepke-Zaba et al., 2011). Hypoxia can also influence the platelet activation, which results in release of distinct mediators, including IL-1, bioactive lipids and chemokines in inflammation (Jurk & Kehrel, 2005; von Hundelshausen & Weber, 2007). One of the known bioactive lipid mediators generated by activated platelets is lysophosphatidic acid (LPA). LPA is a product of hydrolysis of the lysophospholipids, precisely lysophosphatidylcholine (Kondo et al., 2014), by mediation of Ectonucleotide Pyrophosphatase/Phosphodiesterase 2 (ENPP2), also known as Autotaxin (ATX). ENPP2 is a secreted lysophospholipase D, a member of the nucleotide pyrophosphatase

(NPP) family of ectoenzymes and exoenzymes (van Meeteren et al., 2006). The physiological function of ENPP2 involves wide variety of processes such as cell migration, neurogenesis, angiogenesis, smooth-muscle contractions, platelet aggregation, and wound healing (Moolenaar, van Meeteren, & Giepmans, 2004). LPA binds to G-protein coupled receptors to affect the proliferation, differentiation and the cell migration (Shlyonsky et al., 2014). Literature evidence suggest that LPA affects the airway inflammation and remodelling (Zhao & Natarajan, 2013) (Park et al., 2013) and protects the pulmonary vasculature from hypoxia induced remodelling (Cheng et al., 2012). However, the role of LPA in the pathogenesis of CTEPH is not yet known, but highly suggestive due the following reasons: (i) ENPP2 is stored in the α-granules of resting human platelets and released upon platelet aggregation, leading to the production of LPA (Leblanc et al., 2014). LPA is also known to promote human platelet activation by inducing platelet shape change and calcium mobilization, thereby potentially playing a role in thrombosis and thrombus formation (Teo, Yung, Herr, & Chun, 2009). (ii) LPA released in the plasma with a concentration of ≥100 nM, operates via eight selective G-protein coupled receptors (GPCRs), LPA_{1-8} (Cheng et al., 2012), from which LPA_1 and LPA_2 are predominantly expressed in vascular ECs and SMCs (J. Kim, Keys, & Eckhart, 2006; H. Lee, Goetzl, & An, 2000). LPA may modulate endothelial cell function and endothelial permeability (Ishii, Fukushima, Ye, & Chun, 2004; Moolenaar et al., 2004; Sarker, Hu, & Fraser, 2010). It may alter the endothelial nitric oxide synthase (eNOS) activity and as a consequence affecting the pulmonary vascular tone, which is maintained by both NO and ET-1 levels (Brinkmann, 2007). (iii) LPA promotes fibroblast and monocyte differentiation into myofibroblast and fibrocyte, respectively (Shao, Suresh, Vakil, Gomer, & Pilling, 2008; Tang et al., 2014) and dedifferentiation, proliferation and migration of cultured vascular SMCs (Boguslawski et al., 2002; Gennero et al., 1999). (iv) LPA signalling was shown to protect the mouse pulmonary vasculature from hypoxia induced remodelling, highlighting that LPA deficiency affects the endothelin signalling, indulging endothelin-A receptor, in contrast to endothelin-B signalling (Cheng et al., 2012). Hence, LPA can undoubtedly influence the vascular homeostasis, creating a PH sequelae. Further studies are needed in order to delineate the effect of ENPP2-LPA axis in the pathogenesis of PH, and specifically CTEPH, both conditions overwhelmed by platelet aggregation.

1.5.6. Animal models for CTEPH

Acute PE may be easily reproduced and induced by glass beads or autologous blood clot in different animal species. Additionally, animal models of deep vein thrombosis (DVT), murine

vena cava ligation has been utilized to investigate the mechanisms involved in thrombus formation and resolution (Alias et al., 2014; Evans et al., 2011). A promising large-animal model of chronic PH replicating the vascular abnormalities seen in both obstructed and unobstructed territories in human CTEPH, as well as RV remodelling has been established by O. Mercier et al. (2013). The model employs ligation of the left pulmonary artery (PA), combined with repeated embolization of hystoacryl into the right lower lobe. Within this model, the mean PAP of the animals exceeded 20 mmHg for 5 weeks, increased PVR, increased medial wall thickness (MWT) of distal to obstruction pulmonary arteries, RV hypertrophy, increased tricuspid annular plane systolic excursion (TAPSE) were observed, even up to one month after embolization (O. Mercier et al., 2013). However, a small animal model for chronic CTEPH, resembling all the human pathophysiological features has been a challenging issue to date in the field, probably due to the efficient endogenous fibrinolytic system that subsequently result in thrombus resolution in small animals (Olaf Mercier & Fadel, 2013).

2. Aims and objectives

Chronic thromboembolic pulmonary hypertension (CTEPH) stands for a complex, multifactorial and severe vascular disease, initiated by a spectrum of thrombotic or inflammatory events in the pulmonary vasculature. The dual disease nature is represented by major vessel remodelling and/or small vessel arteriopathy, characterized by medial hypertrophy, obstructive intimal thickening, microthrombi formation and plexiform lesions. However, the histological and molecular hallmarks of proximal and distal CTEPH are still largely unclear, rising the scientific interest as the presence of microvascular disease in inoperable CTEPH patients has been a challenging issue for many years. For these patients, in recent years a single medical treatment has been approved, thus deciphering the molecular mechanisms, driving the microvascular disease is indispensable and can possibly contribute to identifying novel therapeutic targets.

We undertook a non-hypothesis driven approach, to head-to-head compare the histopathological and molecular features within end-stage CTEPH and IPAH, as well as proximal and distal CTEPH. Consequently, the aims of this study were:

- To compare the histopathological and molecular signature of small vessel arteriopathy of human CTEPH to donors and IPAH
- To compare the histopathological and molecular signature of distal vessel remodelling in central CTEPH to peripheral CTEPH
- To assess whether the distal vascular remodelling is homogeneously distributed, independently of the affected by the disease site (or in the hypo- and hyperperfused areas, distal to the obstruction)
- To histopathologically and molecularly characterize CTEPH patients undergoing pulmonary endarterectomy
- To assess the functional role of the microarray identified target CHI3L1 on pulmonary vascular cells and on living human precision cut lung slices
- To assess the functional role of the microarray identified target ENPP2 on pulmonary vascular cells and on living human precision cut lung slices.

3. Materials and Methods

3.1. Materials

3.1.1. Reagents and chemicals

Table 3: List of reagents and chemicals

Reagent	Company
4′,6-Diamidin-2-phenylindol (DAPI)	Invitrogen, USA
Acetic acid, glacial	Sigma, USA
Acetone	Carl Roth, Germany
Acrylamide solution (30%)	Sigma Aldrich, USA
Agarose, low gelling temperature, Type VII	Sigma Aldrich, USA
Ammonium Persulfate (APS)	Sigma Aldrich, USA
Blue ink	TBS Lab Products, USA
Bovine serum albumin (BSA)	Carl Roth, Germany
Bromophenol blue	Roche, Germany
BSA solution (2mg/ml)	BioRad, USA
Citrate buffer	Life technologies, USA
Chloroform	Carl Roth, Germany
Crystal violet	Sigma Aldrich, USA
Dako Fluorescence Mounting Media	Dako, Denmark
Dimethyl sulfoxide	Sigma Aldrich, USA
Diphenylacetohydroxamic acid	Sigma Aldrich, USA
DirectPCR® lysis reagent	Peqlab, Germany
Di-sodium hydrogen phosphate	Carl Roth, Germany
DNA ladder	Fermentas, USA
Sigma Aldrich	Sigma Aldrich, USA
Ethanol absolute	Carl Roth, Germany
Ethidium Bromide	Carl Roth, Germany
Ethylenediamine-Tetraceticacid (EDTA)	Carl Roth, Germany
Fluorescence mounting medium	Dako, USA
Ferric-hematoxylin A	Waldeck, Germany
Ferric-hematoxylin B	Waldeck, Germany
Halt™ protease and phosphotase inhibitor cocktail	Thermo Fisher Scientific, USA
Hanks' Balanced Salt solution	Thermo Fisher Scientific, USA
Hematoxylin Solution	Life technologies, USA
Hydrochloric acid	Carl Roth, Germany
Hydrogen peroxide	Merck, Germany
Ficoll-Paque PLUS	GE Healthcare
Isopropanol	Carl Roth, Germany
iTaq™ Universal SYBR® Green Supermix	BioRad, USA
Mayer's Hematoxylin Solution	Sigma Aldrich, USA
Methanol	Carl Roth, Germany
Methyl-green	Vector, USA
Milk powder	Carl Roth, Germany
N,N,N′,N′-Tetramethyl-1,2-diaminomethane (TEMED)	Sigma Aldrich, USA
Page Ruler Prestained Protein Ladder	Thermo Scientific, USA
Paraformaldehyde	Carl Roth, Germany
Picric acid	AppliChem, Germany
Pertex Mounting Medium	Medite, Germany
Ponceau S Solution	Sigma Aldrich, USA
Potassium chloride	Carl Roth, Germany

Potassium dihydrogen phosphate	Carl Roth, Germany
Proteinase K	Peqlab, Germany
Proteinase K Diluent	Dako, Denmark
Proteinase K 40x	Dako, Denmark
Rainbow protein molecular weight marker	AmershamBiosciences, USA
Resorcin-Fuchcin	Waldeck, Germany
RNase Away	Invitrogen, USA
Scott′s Tap Water Substitute Concentrate 10X	Sigma Aldrich, USA
Sodium bicarbonate	Carl Roth, Germany
Sodium chloride	Carl Roth, Germany
Sodium dodecylsulfate (20% w/v)	Carl Roth, Germany
Sodium hydroxide	Carl Roth, Germany
Stripping Buffer	Thermo Scientific, USA
Tetramethylrhodamine methyl ester (TMRM)	Invitrogen, USA
Tris 0.5 M (pH 6.8)	Amresco, Germany
Tris 1.5M (pH 8.9)	Amresco, Germany
Tris base	Sigma Aldrich, USA
Triton X-100	Carl Roth, Germany
TRIzol™	Thermo Fisher Scientific, USA
Trypsin Concentrate and Diluent	Life technologies, USA
Tween 20	Sigma, USA
Xylol	Carl Roth, Germany
β mercaptoethanol	Sigma Aldrich, USA

3.1.2. Kits

Table 4: List of the used kits

Names	**Company**
BrdU Incoportation assay kit	Roche, Germany
DAB Substrate kit	Vector, USA
DC Protein assay kit	BioRad, USA
High Capacity cDNA synthesis kit	Applied Biosystems, USA
ImmPRESS kit	Vector, USA
In situ cell death detection kit	Roche, Germany
NovaRED substrate kit	Vector, USA
Ovation PicoSL WTA System V2 kit	NuGEN Technologies, USA
Picro-Sirius red Stain kit	Abcam, UK
RNeasy Micro kit	Qiagen, USA
RNeasy Plus Micro kit	Qiagen, USA
Sircol insoluble collagen kit	Biocolor, UK
Sircol soluble collagen kit	Biocolor, UK
Supersignal west femto maximum sensitivity substrate kit	Thermo Scientific, USA
Trichrome Stain (Masson) kit	Sigma, USA
Vectastain kit	Vector, USA
Vector VIP Substrate kit	Vector, USA

3.1.3. Cell culture medium and reagents

Table 5: List of cell culture medium and reagents

Names	Company
A549	ATCC, USA
Albumin, Fraction V, fatty acid free	Roth, Germany
Collagen I, Rat Tail	Thermo Fisher Scientific, USA
DMEM GlutaMAX™	Gibco, Germany
DMEM/F-12	Gibco, Germany
Dulbecco's Phosphate Buffer saline (DPBS)	Sigma, USA
Endothelial Cell GM MV2	PromoCell GmbH, Germany
Fetal calf serum (FCS)	PAA, USA
Fibroblast medium	ScienCell Research Labs, USA
Human Pulmonary Arterial Adventitial Fibroblasts	ScienCell Research Labs, USA
Human Pulmonary Arterial smooth muscle cells (PASMCs)	Lonza, USA
Human Pulmonary Microvascular Endothelial Cells (HPMEC)	PromoCell GmbH, Germany
LPS	Sigma, USA
Oleoyl-L-α-lysophosphatidic acid	Sigma, USA
PF 8380	Tocris, UK
Pencillin/Streptomycin	Lonza, USA
Pericyte medium	ScienCell Research Labs, USA
Poly-L-Lysine	ScienCell Research Labs, USA
Recombinant human CHI3L1	R&D systems, USA
Recombinant human IL4	Peprotech, USA
Recombinant human IL6	Sigma, USA
Recombinant human IL8	Peprotech, USA
Recombinant human IL13	Peprotech, USA
Recombinant human IL18	R&D systems, USA
Recombinant human IFN-γ	Peprotech, USA
Recombinant human CCL2	R&D systems, USA
Recombinant human PDGF-BB	Peprotech, USA
Recombinant human TGF-β	R&D systems, USA
Recombinant human TNF-α	Peprotech, USA
Recombinant human VEGF	Peprotech, USA
RPMI media	Thermo Fisher Scientific
Smooth muscle cell medium (SmGM)	Lonza, USA
Trypsin/EDTA	Lonza, USA

3.1.4. Other materials

Table 6: List of additionally used materials

Names	Company
Cell culture dishes (10cm, 6cm, 6well, 48well, 96well)	Greiner bio-one, Germany
Cell scrapers	BD Falcon, USA
Centrifugal protein concentrators	Millipore, USA
Culture inserts	Ibidi, Germany
Filter tips (10, 100, 1000 µl)	Greiner bio-one, Germany

Gel blotting paper	Whatman, USA
Microcentrifuge tubes	Eppendorf, USA
Milk powder	Carl Roth, Germany
PEN membrane slides	Leica, Germany
Polyvinylidene fluoride (PVDF) membrane	Carl Roth, Germany
Polypropylene tubes (15ml, 50ml)	Greiner bio-one, Germany
Precellys Tubes with beads	PeQLab, Germany
PVDF membrane	Carl Roth. Germany
Real time PCR plates	BioRad, USA
Transwell (8µm pore size)	BD Biosciences, USA
QIAshredder	Qiagen

3.1.5. Equipment

Table 7: List of used equipment

Names	Company
Agarose electrophoresis chambers	Biometra, USA
Cell culture incubator, Hera cell	Heraus, Germany
Centrifuge	Life Technologies, Germany
CFX96 tm Real-Time PCR detection system	BioRad, USA
Fluorescence microscope Leica DM 2500	Leica, Germany
Fujifim LAS 4000	Fujifilm, Japan
Leica DM 6000B	Leica, Germany
LMD6000	Leica, Germany
Microplate reader Infinite 200	TECAN, Germany
NanoDrop2000 Sprectrophotometer	Thermo Scientific, USA
PCR thermocycler	Eppendorf, USA
Power supply	BioRad, USA
PowerLab	AD Instruments, Australia
Precellys Homogenizer	PeQLab, Germany
Nanozoomer 2.0 HT	Hamamatsu, Japan
Leica VT1200 S	Leica, Germany
Water bath (cell culture)	Heraus, Germany
Western blot chambers	BioRad, USA

3.2. Methods

3.2.1. Human tissues

The work was performed employing human explanted lung tissues and biorepository from PEA. Human lung tissues were collected from 12 healthy donor controls, 12 IPAH disease controls and 12 CTEPH patients undergoing lung transplantation. Additionally, the explanted central and peripheral CTEPH lung samples were kindly provided by Dr. Maria Rosa Ghigna from the Service Anatomie Pathologique, Hôpital Marie Lannelongue, Paris, France and Peter Dorfmüller from the Institute of Pathology, University Clinic Giessen and Marburg. CTEPH explanted lung samples as well as ink-injected experiment was kindly supplied and performed

by Dr. Lavinia Neubert from Hannover Medical School. Samples were snap frozen for mRNA isolation, or paraformaldehyde (4%) fixed and paraffin embedded. The PEA biorepository were warmly supplied by Dr. med. Eckhard Mayer and Dr. Stefan Guth, from Kerckhoff Clinic, Bad Nauheim, Germany. Intact, unaffected by disease proximal and distal pulmonary arteries from cancer patients were used as controls for endarterectomised material, proximal fibrous tissue, distal patent (stenotic) and distal completely occluded material, respectively. These samples were kindly provided by Prof. Dr. med. Ludger Fink from the Institute of Pathology and Cytology, UEGP, Wetzlar, Germany. The study protocol and the tissues usage for the Giessen cohort were approved by the Ethics committee (Ethik Kommission am Fachbereich Humanmedicin der Justus Liebig Universität Giessen). Written informed consent was obtained from all patients before any procedure.

3.2.2. Staining

3.2.2.1. Weigart – Van Gieson staining

Formalin fixed, paraffin embedded human lung tissues were cut into 4 µm thick sections and deparaffinised starting with incubation at 59°C for 60 min. Sections were then rehydrated with a continuous flow of xylol-ethanol 99,6%- ethanol 96%- ethanol 70% and incubated for 10-24 h in Resorcin-Fuchsin prepared in advance. Next, slides were washed in running tap water for 15 min, shortly in distilled H_2O (dH_2O) and incubated with *Weigert's* iron haematoxylin for 5 min, followed by running tap water washing for 15 min. Van Gieson solution was applied for 10 min, slides were then shortly washed in dH_2O, dehydrated with ascending ethanol concentrations (70%, 96%, 99.6%) and finally mounted with Pertex mounting medium. Slides were scanned with Nanozoomer 2.0 HT equipped with NDP operating software. Morphometric analysis was carried out employing Leica DM6000B microscope supplied with Leica Qwin V3 software. Medial wall thickness (MWT) was calculated as the distance between lamina elastica interna and lamina elastic externa, using the following formula: %MWT = (2 x medial wall thickness/external diameter) x 100.

3.2.2.2. Double immunohistological staining

Paraffin embedded human lung tissues were cut into 4 µm thick sections and slides were incubated for 60 min at 60°C, followed by deparaffinization in xylol and rehydration in series of grade-decreasing ethanol solutions. For the next 15 min, peroxidase quenching was performed with 3% H_2O_2-methanol solution, followed by extensive washing with dH_2O and PBS. Antigen retrieval was performed with trypsin solution, for 10-15 min at 37°C heating

block. After three washing steps with PBS, blocking solution containing 10% BSA was added for 20 min. Serumblock1 horse serum (Vectastain kit) was applied after the washing steps for 10 minutes followed by incubation with a primary antibody (α-SMA) (A-4), after which ready-to-use biotinylated secondary antibody was used. Before application of the Streptavidin/Peroxidase, followed by three washing steps, Vector Vip Substrate Kit was used for antibody-colour development under optical control of Leica DM6000B microscope. Further on, the slides were washed with tap water and prepared for the next primary antibody staining, by blocking with 10% BSA for 20 min ImmPRESS Serumblock 1 was applied for the next 20 min, followed by incubation of the second primary antibody (vWf) (A-4), for 30 min. Secondary antibody from the ImmPRESS kit was applied after three PBS wash steps and developed with DAB Substrate kit. Counter staining was performed with Methyl green for 3 min at 60°C. As last, dehydration was performed in series of grade-increasing ethanol solutions and xylol and slides were mounted with Pertex Mounting medium. Preserved slides were scanned with Nanozoomer 2.0 HT equipped with NDP operating software. The degree of muscularization was evaluated employing Leica DM6000B microscope using Leica Qwin V3 software.

3.2.2.3. Masson`s Trichrome staining

Formalin fixed paraffin embedded human lung tissues were cut into 4 µm thick sections and at first deparaffinized in xylol and rehydrated with series of gradual decrease of ethanol concentration. Sections were then washed in distilled H_2O and incubated in preheated Bouin`s solution at 56°C for 15 min in a water bath. Slides were then washed in running tap water until complete elimination of the yellow color and shortly rinsed in $ddH_2O$. Further, slides were incubated with Mayer`s hematoxylin for 5 min, washed subsequently with running tap water and double dH_2O (ddH_2O) and proceeded to Biebrich Scarlet-Acid Fuchsin staining for 5 min. Sections were then rinsed in ddH_2O, incubated in phosphotungstic/phosphomolybdic acid/ddH_2O (1:1:2) for 6 min, followed by 15 min incubation with Aniline Blue solution. Afterwards, slides were settled into 1% acetic acid solution for 2 min, washed with double dH_2O, gradually dehydrated with ethanol and xylol and mounted with Pertex Mounting medium. Preserved slides were scanned with Nanozoomer 2.0 HT equipped with NDP operating software.

3.2.2.4. Sirius Red staining

The 4 µm thick sections were cut from formalin fixed paraffin embedded human lung tissues and incubated at 58°C for 60 min. Further deparaffinization was carried out in xylol, followed by gradual rehydration with ethanol solutions. Sections were washed in dH_2O shortly prior incubation with 0.1% Picro Sirius Red, light protected for 60 min. Three consecutive washes with 1% acetic acid were carried out and sections were dehydrated with ethanol and xylol and mounted with Pertex Mounting medium. In a modified protocol, used later in this work, we benefited of a ready to use kit, supplied by Picro-Sirius Red solution and 0.5% acetic acid solution. The preparation protocol remained the same. Preserved slides were analysed for total collagen deposition using Leica DM6000B microscope supplied with Leica Qwin V3 software.

3.2.2.5. Double immunofluorescent staining

Paraffin embedded lung tissues were sectioned at 4 µm thickness and slides were incubated for 20 minutes at 65°C, followed by deparaffinization in xylene and rehydration in series of grade-decreasing ethanol solutions. Antigen retrieval was performed in boiling 10mM citrate (pH 6.0) for 10 minutes at 630 watt in microwave. Next, three washing steps were applied before trypsin retrieval for the second primary antibody, by 10 min incubation at room temperature. After extensive washing, blocking solution (3%BSA, 0.2% Triton X in PBS) was applied for one hour, followed by three PBS washing steps and an overnight incubation at 4°C with the primary antibodies diluted in blocking buffer (A-4). On next day, slides were washed three times with PBS and incubated with secondary antibodies (A-5), for 1h at room temperature in dark. After three PBS washing steps, tissues were stained with 4′,6-Diamidin-2-phenylindol (DAPI) in an 1:1000 dilution in PBS for 10 min and washed trice with PBS. At last, slides were covered by mounting medium and stored in 4°C or examined under Leica DM 6000B microscope using Leica LCM2000 imaging software.

3.2.2.6. Single immunohistological staining

Sections with 4 µm-thickness from paraffin embedded lung tissues were incubated for 1h at 60°C, followed by deparaffinization in xylol and dehydration in series of grade-decreasing ethanol solutions and two consecutive washes with distilled water. Antigen retrieval was performed in boiling 10mM citrate (pH 6.0) for 20 min and until cooling for about 30 min. Peroxidase quenching was achieved with 15% H_2O_2. After washing with PBS three times, proteinase K solution was applied for 15 min at room temperature, followed by blocking step with 10% BSA for 1h and two additional washing steps. Primary antibody was added, and

slides were incubated overnight at 4°C (A-4). Next day, slides were washed with PBS, three times and biotinylated secondary antibody was added and incubated for 10 min. Application of the Streptavidin/Peroxidase, followed by three washing steps, was performed prior NovaRed kit was used for antibody-colour development under optical control of Leica DM6000B microscope. Hematoxylin was used as a counterstain, followed by dehydration step (with 70%, 96% & 99.6%) and xylol at the end. Slides were then mounted with Pertex Mounting medium and scanned with Nanozoomer 2.0 HT equipped with NDP operating software.

3.2.2.7. Haematoxylin & Eosin (H&E) staining

H&E staining was applied to lung sections with 4 µm thickness, after their dehydration in xylol and dehydration in series of grade-decreasing ethanol solutions. Slides were for 10 min incubated with haematoxylin and bluing nuclear colour developed after their reaction to tap water for the next 3 min. Eosin staining followed for 6 min and slides were rehydrated shortly in ethanol and finished by xylol for the 5 last minutes. Pertex Mounting medium was used to cover the slides and then, Nanozoomer 2.0 HT scan was performed.

3.2.3. Laser capture microdissection of pulmonary vessels

Laser capture microdissection (LCM) of eight donors, IPAH and CTEPH lung tissues (pool of two) including three central and four peripheral CTEPH, was performed as previously described (Savai et al., 2014) with some modifications. 10 µm cryosections from human lung tissue were mounted on membrane coated glass slides, rapidly dehydrated, briefly stained with Mayer's haematoxylin. Bluing reagent (Scott's tap water) was applied to the slides for 15sec, then slides were washed in increasing gradient of 70 to 100% ethanol, air-dried and transferred to LCM. Approximately 200 intrapulmonary vessels with a diameter less than 100 µm were selected and microdissected under optical control using the Laser microdissection device LMD6000 (Leica, Wetzlar, Germany). The microdissected material was collected in Eppendorf tubes filled with 50 µl RNA lysis buffer (RLT+β-mercaptoethanol). After collection, the dissected material was directly frozen in liquid nitrogen until isolation of the RNA was carried.

3.2.4. Cell culture

Experiments were carried out on human donor PMECs, PASMCs and hPAAFs. Additionally for the basal screening, lung adenocarcinoma cell line (A549), lung pericytes and polarized macrophages were used. Donor PMECs were purchased from PromoCell GmbH and maintained in Endothelial Cell GM MV2, supplemented with 0.05 mL/mL FBS, 5 ng/mL EGF,

bFGF 10 ng/mL, IGF-1 20 ng/mL, VEGF165 0.5 ng/mL, ascorbic acid 1 µg/mL and Hydrocortisone 0.2 µg/mL. Donor-PASMCs were purchased from Lonza and maintained in SmGM growth medium supplemented with 0.5 ml/ml FBS and growth factors (GFs), provided by the company. hPAAFs were provided by ScienCell Research Labs and maintained in Fibroblast medium, supplemented with GFs provided with the kit. Importantly, when hPAAFs were cultured, plates were coated with poly-L-lysine prior experiment, in order to promote better cell adhesion. For the basal screening experiments, A549 cells were acquired from ATCC and maintained in DMEM GlutaMAX supplemented with 10% FCS, 100U/ml penicillin and 0.1mg/ml streptomycin. Human lung pericytes were maintained in pericyte medium supplemented with FCS, GFs and P/S.

Prior stimulation or functional assays, when serum starvation was required, cells were kept in the corresponding basal medium, supplied with 0.1% FCS, 100U/ml penicillin and 0.1mg/ml streptomycin for 24 hr, then stimulated accordingly. All cells types were cultured at 37˚C and 5% CO_2 in a humidified chamber until a confluency of 90-95% and then sub-cultured in a ratio of 1:3. For sub-culturing, the cells were washed once with DPBS and incubated with Trypsin/EDTA for 4-5min, followed by trypsin neutralization with equal volume of FCS. The cells were centrifuged at 1200 rpm for 8 min (except for hPMECs 1050 rpm, 5 min), supernatant was removed and pellet was gently resuspended in the appropriate growth medium and seeded into new culture dishes.

Freezing of the cells, was performed after the trypsinization step, using 5% DMSO in FCS. When needed, cryovials were kept at 37˚C and once thawed, cell were seeded immediately into a new culture dish. To avoid any residual DMSO, the medium was changed the next day.

3.2.5. RNA isolation

3.2.5.1. RNA isolation from LCM vessels

RNA isolation was carried out using Qiagen RNeasy Plus Micro Kit (Cat. No.74034), according to manufacturer`s protocol, including the step with carrier RNA. Incubation of the caps at 42°C, 30 min, followed by vortexing, before storage of the samples was not performed at this point. The final volume of RNase free water to dilute the RNA was 18 µL. cDNA synthesis was carried out right after the RNA isolation.

3.2.5.2. RNA isolation from PEA material

Total RNA was isolated from PEA material using Qiagen Rneasy Micro kit according to manufacturer`s instructions, with some modifications. Approximately 5 mg of tissue was

disrupted using ceramic mortar and pestle by adding liquid nitrogen until converted into powder. Mortar was equilibrated to room temperature, 300 µL RLT with β-ME were added to the tissue powder, gently mixed and agitated until liquid and transferred into QIAshredder columns for homogenization. Columns were span for 2 min at maximum speed. Tissue lysate (supernatant from previous step) was transferred into sterile eppendorf, 590 µL RNase-free water and 10 µL Proteinase K (Qiagen Cat No. 19131) were added and mixed thoroughly by pipetting. Samples were then incubated at 55°C for 10 min, followed by centrifugation for 3 min at 10,000 rpm (small pellet was formed, sometimes accompanied by a thin layer of film on the top of the supernatant). Approximately 900 µL of the supernatant was transferred into a new microcentrifuge tube and 0.5 volumes (≈450 µL) of ethanol (96-100%) were added and mix well by pipetting. 700 µL of the sample was transferred to RNeasy MinElute spin column and centrifuged for 15 s at 10,000 rpm. Flow through was discarded and the previous step was repeated until all lysate is used. RW1 buffer (350 µL) was used for stringent washing to efficiently remove biomolecules such as carbohydrates, proteins, fatty acids etc. followed by 15s centrifugation at 10,000 rpm. Traces of salts were removed by performing washing step with RPE buffer twice. To eliminate the possibility of carryover of ethanol, column was placed into new 2 mL collection tube and centrifuged 1-2 min at full speed. RNeasy MinElute spin column was placed in new sterile 1.5 ml tube, 10-15 µL RNase-free water was added (decide by the amount of used tissue), incubated for 2-3 min at RT, and centrifuged for 1 min at full speed. Elution step was repeated using the eluate from the previous step.

3.2.5.3. RNA isolation from cells

RNA isolation from primary hPMECs, hPASMCs and hPAAFs was carried out using TRIzol™ reagent. Media was aspirated and cells were washed with PBS. 250 µL of TRIzol™ was directly added to each of 6 well plates and after 2 min incubation lysates were scratched with cell scrappers and transferred into microcentrifuge tubes. Chloroform (1/5 of TRIzol™ volume) was added to each sample, followed by vortexing and 10 min incubation at RT, prior centrifugation for 30 min at 4°C at 12,000 g. The upper aqueous phase was carefully transferred into a new tube, without disturbing the precipitate, mixed with 125µL ice-cold isopropanol to precipitate the RNA. The samples were incubated at RT for 10 min and further centrifuged for 20 min at 4°C at 12,000 g. After discarding the supernatant, RNA samples were twice washed with ice-cold 75% ethanol for 15 min and spined at 4°C at 7,500g. RNA pellets were dried for 15 min and resuspended in 12-15 µL of RNase free water while incubated for 10 min at 60°C.

RNA concentration and purity was assessed by using NanoDrop, where 1 µL was applied and absorbance analysis was set as a ratio of 260/280.

3.2.6. Microarray analysis

Genome-Wide Expression Profiling of donor, CTEPH and IPAH lung samples was done using purified total RNA (n = 8 per group), amplified after pooling two by two samples, using the Ovation PicoSL WTA System V2 kit (NuGEN Technologies). Additionally, three central and four peripheral CTEPH were amplified, in order to be compared to donor samples. The amplified cDNA was Cy5-labeled using the SureTag DNA labeling kit (Agilent) and hybridization to oligonucleotide spotted microarray slides (Human Whole Genome, SurePrint G3 Human GE v2 8 3 60K Microarray; Agilent Technologies). Image analysis was performed with GenePix Pro 5.1 software, and calculated values for all spots were saved as GenePix results files. Log fold changes in CTEPH and IPAH lung samples are changes relative to donors. Data analysis was performed using R version 3.5.1.

The microarray analysis was performed at the Microarray facility of Dr. Jochen Wilhelm at Justus-Liebig University, Giessen, Germany.

3.2.7. Reverse transcription of RNA

A total 1000 ng of RNA or full amount for LCM vessels was used for cDNA synthesis using ImProm-II™ Reverse transcription system according to the manufacturer's instructions. RNA concentration and purity was checked after isolation using NanoDrop2000TM Spectrophotometer by determining the ratio of 260/280nm wavelengths. The RNA samples with 260/280 ratio around 1.8 were used for further experiments. cDNA synthesis was performed with High Capacity cDNA Synthesis Kit according to the manufacturer's instructions using the following Mastermix composition (Table 8):

Table 8: Compounds of mastermix for reverse transcription and their concentration

Components	Final concentration	Volume (µl)
10x RT buffer	1X	2
25x dNTP mix, 100mM	4mM	0.8
10x random primers	1X	2
Ribonuclease inhibitor	10U	0.5
MultiScribe reverse transcriptase	50U	1
Nuclease free water		3.7

3.2.8. Quantitative real time PCR (qRT-PCR)

Quantitative real time PCR was performed from the cDNA samples of 40 µL reactions using iQ™SYBR® Green Supermix and CFX96 tm Real-Time PCR detection system. The primer pairs (A-3), were at first designed using an online Primer-Blast program (http://www.ncbi.nlm.nih.gov/tools/primer-blast/) and then purchased from Sigma-Aldrich. The product size was kept in between 100-300 bp. β-2 microglobulin (B2M) was used as a reference gene for all the performed reactions. Reaction mix was prepared according to the following scheme:

Table 9: qRT PCR reaction mix composition

Components	Volume (µl)
iTaq™ Universal SYBR® Green Supermix	7
Forward primer, 10 µM	0.5
Reverse primer, 10 µM	0.5
cDNA template	2
Nuclease free water	10

The PCR reaction was accomplished by the following protocol:

Table 10: qRT PCR reaction steps

qRT PCR steps	Temperature	Time	Number of repeats
Initial denaturation	95°C	3 min	1
Denaturation	95°C	10 sec	
Annealing	58°C/60°C*	30 sec	40
Elongation	72°C	30 sec	
Denaturation	95°C	10 sec	1
Melting curve	65°C to 95°C	Increment 0.5°C for 5 sec	1

3.2.9. Sircol collagen assay

Both, soluble and insoluble collagen from PEA material and their respective controls were assessed using commercially available kits and experiments were carried according to manufacturer`s instructions.

3.2.9.1. Sircol soluble collagen assay

For measuring the soluble collagen from the PEA samples 30 mg of the extracted tissue were homogenized in RIPA buffer containing protease and phosphatase inhibitor. Tissues were homogenized, centrifuged and 15 µl of each lysate was taken into 1.5 mL tube and the final volume was adjusted to 100 µL with water. Standard solutions containing 15 µl of RIPA buffer and 1, 5, 10, 25, and 50 and 100 µg of collagen were as well prepared. Blank solution was prepared with 15 µL RIPA buffer and 85 µL H_2O. Furthermore, 1 mL of Sircol dye reagent was added to the blank, standards and samples and tubes were mixed by inverting and incubated at RT for 30 min with a gentle shaking. After the incubation step, tubes were centrifuged at 12,000 rpm for 10 min and supernatants were removed. Next, 750 µL of ice-cold Acid-Salt Wash reagent was applied and the samples were span. The pellets were resuspended in 450 µL of Alkali Reagent and 200 µL from each tube was transferred to a 96-well plate. Experiment was performed in duplicates. Absorbance was measured at λ = 555 nm in a TECAN plate reader.

3.2.9.2. Sircol insoluble collagen assay

Measurement of the insoluble collagen from the PEA samples and their controls, required 50 µL of Fragmentation reagent for each mg of tissue and incubation at 65°C for 2-3 h. Every 30 min, vigorous vortexing was performed in order to help the tissue disintegration. With this method, insoluble collagen fibres are converted into water-soluble denatured collagen, without generation a release of the hydroxyproline residues. After the incubation, tubes were removed from the heating block and centrifuged at 12,000 rpm for 10 min. Standards were prepared containing 0, 20, 40, and 60 µg of denatured collagen. Deionized water was used as a blank control. Next, 1 mL of Sircol Dye reagent was applied to each tube and they were gently mixed for 30 min. During this time period a collagen-dye complex will form and precipitate out from the soluble unbound dye. After centrifugation at 12,000 rpm for 10 min, tubes were gently inverted and 750 µL ice-cold Acid-Salt Wash Reagent to the pellet was added to remove unbound dye and again forwarded to centrifugation. Supernatant was gently removed and 1 mL of Alkali reagent was added to the pellets of the blanks, standards and samples. 200 µL from each tube was transferred to a 96-well plate in duplicates and the absorbance was measured at 555 nm in a TECAN plate reader.

3.2.10. Protein isolation

3.2.10.1. Protein isolation from cells

Protein isolation from cultured hPMECs, hPASMCs and/or hPAAFs was performed using RIPA buffer containing protease and phosphatase inhibitor cocktail (PPi). At first, media was aspirated and cells were washed with PBS. Corresponding amount of lysis buffer was added and plates were incubated on ice for 10 min. Cell lysates were collected after vigorous scratching and centrifuged at 13,000 g for 30 min at 4°C was carried. Supernatant was collected into 1.5 mL tube and directly quantified or stored at -80°C.

3.2.10.2. Protein quantification

Bio-Rad DC Protein Assay kit was employed for protein quantification according to manufacturer`s instructions. Briefly, the assay is based on Lowry`s method, the principle behind it lies in the reactivity of the peptide nitrogen with Cu^{2+} under alkaline conditions and the subsequent reduction of the Folin-Ciocalteay phosphomolybdic phosphotungstic acid to heteropolymolybdenum blue by the copper-catalyzed oxidation of aromatic acids. BSA standard at different concentration, ranging from 0.125-2.0 mg/mL was used to generate the standard curve. Protein samples were pre-diluted according to the standard. Duplicates of standards and samples were pipetted and the absorbance was measured at 750 nm using TECAN Infinite M200 plate reader.

3.2.10.3. Western blotting

After protein estimation, equalization of the proteins was performed and samples were mixed with 5X loading buffer and denatured at 95°C for 10 min. Protein samples and molecular weight markers were loaded for separation on polyacrylamide gels (7.5% or 10%) (Table 12). Gels were run in vertical electrophoretic assembly using at 80-100V until the protein of interest were nicely separated.

Table 11: Composition of the 5X loading buffer

Components	Final concentration
Tris-HCl (2M, pH-6.8)	375mM
SDS	10% (w/v)
Glycerol	50%(v/v)
β-Mercaptoethanol	12.5%(v/v)
Bromophenol Blue	0.02%(w/v)
Water	Up to the final volume

Table 12: Resolving and stacking gel constituents

Components	Final concentration
Stacking gel (6%)	
Tris-HCl (2M, pH-6.8)	125mM
Acrylamide/Bis-acrylamide	6%
SDS 10% (w/v)	0.10%
APS 10% (w/v)	0.05%
TEMED	0.10%
Water	Up to the final volume
Resolving gel (7.5-10%)	
Tris-HCl (2M, pH-6.8)	375mM
Acrylamide/Bis-acrylamide	7.5-10%
SDS 10% (w/v)	0.10%
APS 10% (w/v)	0.05%
TEMED	0.10%
Water	Up to the final volume

The content of the running buffer is given in the following table:

Table 13: Running buffer composition

Components	Final concentration
Tris	25mM
Glycine	250mM
SDS 10% (w/v)	0.10%
Water	Up to the final volume

Next, proteins were transferred on Polyvinylidene difluoride (PVDF) membrane by electrophoretic transfer. The transfer was carried out for 1h and 15 min at 100 V in blotting buffer (Table 14). Protein transfer was checked by Ponceau S solution, and once confirmed a proper transfer, membranes were incubated in blocking buffer containing 5% non-fat dry milk or BSA in 1X TBST (Table 15) for 1 h with gentle shaking at room temperature. Incubation of the membranes with primary antibodies was performed overnight (A-4) at 4°C. Secondary

HRP-coupled antibody incubation followed after three washing steps of 10 min with TBST for 1 h at room temperature. Membranes were incubated with Supersignal West Femto maximum sensitivity substrate and signal detection was evaluated by Fujifim LAS 4000.
Membranes were stripped with stripping buffer for 20 minutes, washed with TBST three times for 15 min, blocked and probed again with another primary antibody.

Table 14: Blotting buffer composition

Components	Final concentration
Tris	50mM
Glycine	40mM
Methanol (v/v)	20%
Water	Up to the final volume

Table 15: TBST constituents

Components	Final concentration
Tris	20mM
Sodium chloride	137mM
Tween 20 (v/v)	0.1%
HCl	to set the pH to 7.4
Water	Up to the final volume

3.2.10.4. Densitometric analysis of the Western blots

ImageJ was employed for quantification of the Western blots, by evaluating band intensity values (in arbitrary units), which were normalized to the loading controls glyceraldehyde 3-phosphate dehydrogenase (GAPDH) or β-actin (ACTB). Ratios were plotted as percentage in regard to the control.

3.2.11. Cell proliferation

Cellular proliferation of hPMECs, hPASMCs and hPAAFs was assessed using colorimetric BrdU Cell Proliferation ELISA Kit in accordance with the manufacturer's instructions. The kit is based on the principle of measurement of 5-Bromo-2′-deoxycitidine (BrdU) incorporation into DNA as a direct indicator of cell proliferation using anti-BrdU HRP-linked antibody.

Prior stimulation, cells were seeded in 96-well plates and serum starved for 24 h. Stimulated cells were incubated with BrdU labelling solution for 2 h. Further the 2 h incubation, cell were washed with PBS and then fixed with FixDenat solution for 30 min. Fixed cells were subsequently incubated with anti-BrdU-POD antibody for 90 min, washed three times with PBS and further incubated with TMB (tetramethyl-benzidine) solution until colour development. Absorbance was measured at λ = 370 nm with reference at λ = 492 nm in a TECAN Infinite M200 plate reader. Cell proliferation was plotted as a percentage of absorbance compared to control cells absorbance measured at 370 nm.

3.2.12. Cell apoptosis

Detection of cell apoptosis employed ELISA based *In situ* cell death assay according to the manufacturer's instructions. The assay is based on *in vitro* determination of the cytoplasmic enrichment of histone-associated DNA fragments (mono- and oligonucleosomes), applying two antibodies directed against DNA and histones.

Briefly, stimulated cells were centrifuged for 10 min at 200 g. Media was aspirated, cells were lysed at RT for 30 min and further centrifugation was carried at 200 g for 10 min. 40 µl of lysate was pipetted into a streptavidin-coated microplate together with 80 µl of an immunoreagent-containing anti-histone (biotin-labeled) and anti-DNA (HRP-labeled) antibodies followed by incubation for 2 h at 300 rpm at RT. After incubation, plates were washed thrice with incubation buffer and further determination of the amount of peroxidase retained in the immunocomplex with ABTS (2,2'-azino-di-[3-ethylbenzthiazoline sulfonate (6)]), until colour development. Absorbance was measured at 405 nm with reference at 490 nm in the TECAN Infinite M200 plate reader. Apoptosis of cells was plotted as percentage of absorbance compared to control cells absorbance measured at 405 nm.

3.2.13. Macrophages polarization

Human macrophages were generated prom peripheral blood mononuclear cells as previously described (S. S. Pullamsetti et al., 2017). Human macrophages were generated from blood monocytes. Briefly, peripheral blood leukocytes were prepared from buffy coats obtained from the UGMLC blood bank. Cells were then separated by density gradient using Ficoll-Paque PLUS (GE Healthcare). Platelets present in the enriched monocyte fraction were removed by three washing steps in PBS with 2% FCS. Finally, monocytes were seeded in RPMI containing 10% FCS, 4 mML-glutamine, and penicillin/streptomycin at a concentration of 5×10^5 cells/ml in six-well tissue culture plates. M1 and M2 macrophages were achieved from naïve

macrophages by addition of 100 ng/mL LPS + 100 U/mL IFN-γ and 20ng/mL IL-4, respectively.

3.2.14. Cell migration

Migration of the cells was determined using Boyden chamber transwell migration assay, using 8 μm pore size, uncoated membranes. Briefly, cells were serum starved for 24 h and basal medium containing 2% FCS along with recombinant CHI3L1 or LPA in 0.2% fatty acid free BSA was provided at the in the lower part of the transwell chamber, while resuspended cells in serum-free medium were introduced on the upper part of the Boyden chamber. Cells were left to migrate for 18 h, washed, fixed with methanol and at the end stained with crystal violet. Membranes were extracted from the chambers, fixed on a glass slide and mounted with Pertex Mounting medium. Nanozoom files were acquired and migrated cells were counted using Image G software. Cell migration was presented as percentage of control.

3.2.15. Animal experiments and genotyping

A breeding couple of two white female mice (*Enpp2*+/+ genotype, also known as *Atx*+/+) and a male mouse (*Enpp2*+/- genotype) on FVB genetic background, were kindly provided by Prof. Susan S. Smyth, MD, PhD from the University of Kentucky, College of Medicine, Lexington KY, USA.

To study the effect of *Enpp2* reduction on thrombus maintenance and/or resolution, a murine stagnant flow inferior vena cava (IVC) thrombosis model was employed in collaboration with Prof. Dr. Irene Lang and Smriti Sharma from Medical University of Vienna. All animals used were under the care and supervision of the Department and Core Unit of Biomedical Research, Medical University of Vienna (MUW). Procedures were approved by the MUW Institutional Animal Care Committee and the Austrian Ministry of Science. Induction of thrombosis was performed by partial ligation of IVC in *Enpp2*+/- mice and wild type controls. Ultrasound measurements and thrombi harvest were assessed at day 3, 7 and 14 after surgery, where thrombus area, length and weight were evaluated. Platelets, neutrophils, and lymphocytes number was determined at day 7 and 14 after the ligation.

Mice tail tissues were incubated overnight with DirectPCR® lysis reagent containing 0.3mg/mL Proteinase K at 55°C with a moderate shaking. Further on, lysis was carried at 85°C for 1h to inactivate Proteinase K. Next, 2 μl of lysate was used to perform genotyping PCR. Genotyping of homozygous *Enpp2*+/+ and heterozygous *Enpp2*+/- mice was performed using primers in

Table 16. Primers Enpp2_P640 and Enpp2_P643 detect the allele 500bp and 700bp. PCR reaction mixture and reactions steps are summarized in Table 17 and Table 18.

Table 16: Primer sequences for genotyping protocol

Primer name	Primer sequence 5'-3'
Enpp2_P640	GCA CAT ACC TTT AAT TCC AGC AC
Enpp2_P643	ACA GAC TTC TCT GAA GCT GAC

Table 17: Mastermix composition

Components	Volume (µl)
5x Green Go Tag Flexi Buffer	3
$MgCl_2$ [25mM]	1.2
dNTPs [5mM]	0.6
ENPP2_P640 [10pmol/µl]	3
ENPP2_P643 [10pmol/µl]	3
GoTag Polymerase [5U/µl]	0.25
DNase/RNase free water	16.95
DNA	2
Total volume	30

Table 18: PCR protocol

PCR steps	Time (min)	Temperature (°C)	Number of cycles
Initial denaturation	5	94	1
Denaturation	0.5	94	
Annealing	0.5	60	35
Elongation	0.5	72	
Final elongation	5	72	1
Cool down	∞	4	

3.2.16. Contractility assay

hPASMCs were cultured to 80-90% confluency, serum starved for 24 h, trypsinized and cell population was adjusted to $1.5x10^5$ cells/mL in 0.1% FCS basal media. From this cell suspension, 0.4 mL were transferred to Eppendorf tube and mixed with 0.2 mL rat tail collagen type 1 solution (3 mg/mL) (Life technologies, Carlsbad, CA, USA). 1M NaOH (7 µL) were added to the mixture and mixed well. 500 µL of this mixture was transferred into a 24-well plate. Gels were solidified for 30 min at room temperature. Add 600 µL of basal media plus stimulation factors to the wells and release the gels from the well using sterile needle. Plates were swirled gently and observed under the microscope to make sure that the gels are released. Plates were incubated for 72 h and scanned the plates to obtain the images.

3.2.17. Ink injected CTEPH case study

Fresh pulmonary explants diagnosed with CTEPH were picked-up from the operation theatre immediately after surgery. The pulmonary arteries were cannulated by a preparation of the pulmonary hilus. Blue ink (TBS Lab Products, Hilsborough, NC), diluted in a liquid adhesive, was injected via catheter and distributed into the pulmonary vasculature. Representative samples from proximal to distal arteries were formalin-fixed and paraffin-embedded. Serial cut slices were prepared at a routine microtome for further staining and histopathologic examination.

3.2.18. Precision cut lung slides (PCLS)

Human, intact lung biopsies from non-cancerous part, subsequent to lung resection for peripheral cancer were used. The biopsies were initially inflated by injecting 3% warm (37°C) low-melting agarose–PCLS growth media. After complete solidification of agarose in the inflated samples on ice, tissue blocks of approximately 0.5-1 cm in each dimension were prepared. Lung slices (300 µm thick) were cut perpendicularly to the visible airway with a vibratome Leica VS1200 S on ice-cold HBSS. After overnight incubation at 37°C in 5% CO_2 and DMEM/F-12 supplemented with antibiotics and growth factors, the collected lung slices were placed for the following experiments. At first, organ culture tissues were washed twice with medium, and cultured for 24 h in serum deprived medium before experiments. Then, they were incubated for total 8 days in the experimental condition, with full replenishment of the media, after the fourth day. A total of four lung biopsies were used in our study and samples were proceeded for histology or genome screening/PCR.

3.2.19. Statistical analysis

In order to test the data several tests were used. First, data was tested for each comparison whether it was normally distributed or not using the commmonly applied adjusted Kolmogorov-Smirnov-test which is recommended for small sample sizes (Yazici & Yolacan, 2007). In case of normally distributed data, parametric tests were applied. A T-test was performed for statistical analysis of two groups or one-way ANOVA for more than two groups followed by post-hoc tests. In the latter case, the Levene test was applied and in case of homogeneous variance (Levene test, $p > 0.5$) a Tukey-test was used, while for heterogeneous variance a Dunnet/Games-Howell test was used. For non-parametric data either the Kruskal-Wallis or Mann-Whitney U-Test were used. For multiple comparisons over time or different conditions of the same cells, repeated measurement ANOVA was applied.

4. Results

4.1. Chapter I: Histopathological and molecular characterization of distal vessel remodelling in explanted CTEPH, and in comparison, to IPAH and donor lung tissues

4.1.1. Characterization and comparison of vascular remodelling in explanted CTEPH and in comparison, to IPAH and donor lung tissues

As an initial step, the histopathological changes and the vascular remodelling were comprehensively evaluated in explanted CTEPH lung samples and compared with the already known and studied PH form, IPAH. In these human lung sections, we assessed the medial hypertrophy, the neointima-media ratio, the degree of muscularization and the collagen deposition by Weigert–Van Gieson, double immunohistochemical staining of von Willebrand factor (vWF) and α-smooth muscle actin (α-SMA) and Sirius Red/Trichrome staining, respectively.

4.1.1.1. Assessment of the medial hypertrophy in explanted CTEPH and in comparison, to IPAH and donor lung tissues

The combined Weigert–van Gieson staining is used for differential staining and visualization of elastic fibres and connective tissue in donor, CTEPH and IPAH explanted lung tissue sections. Thus, this staining not only allows visualization of the vascular thickening and remodelling, but also facilitates the morphometric analysis. After the staining, using Leica DM6000B microscope supplied with Leica Qwin V3 software donor, CTEPH and IPAH vessels were divided into three groups depending on their size (Group 1: diameter `d` = 20-70 µm, Group 2: d = 70-150 µm and Group 3: d > 150 µm), followed by measurement of medial

wall thickness (MWT). As presented in Figure 7, in CTEPH as well as in IPAH lung samples, increased thickness of the vessel wall is detectable in all sizes of vessels, mainly in the media and intima compartments, in comparison to the thin vessel wall of the donors.

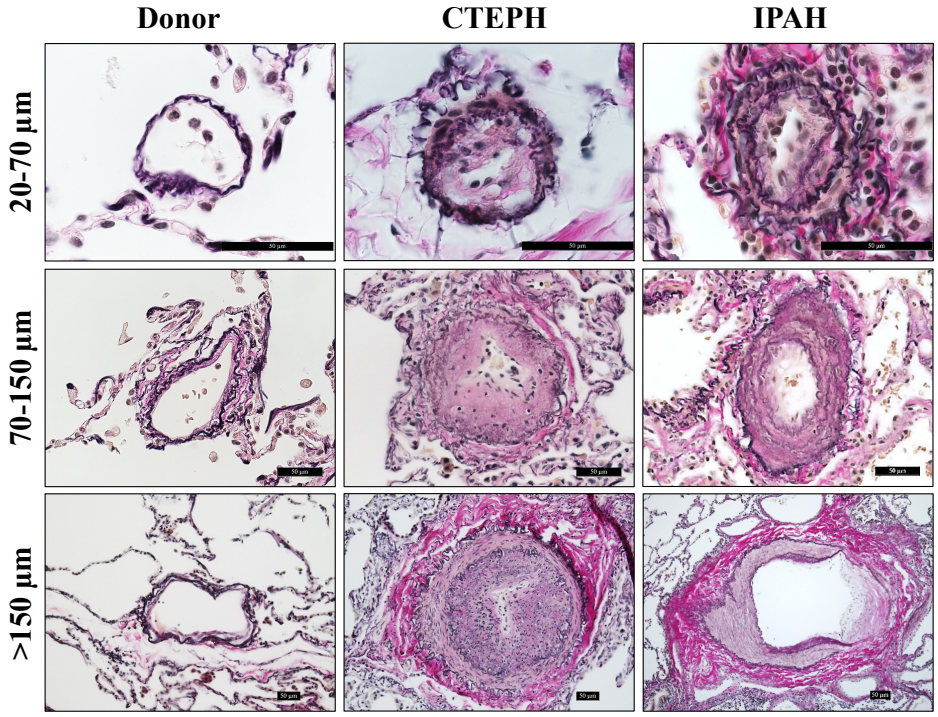

Figure 7: Visualization of severe vascular wall thickening in human lung samples from CTEPH and IPAH patients compared to donors. Representative microphotographs of vessels within three groups (dark blue-dark brown: nuclei; dark violet: elastic fibres; red-pink: collagen fibres and yellow: stained muscles and cytoplasm.): Group 1: d = 20-70 µm; Group 2: d = 70-150 µm and Group 3: d >150 µm. Scale bar 50 µm, n=12. Details of the staining protocol are listed in materials and methods section.

Further, MWT of CTEPH or IPAH in comparison to donors using ANOVA showed a significant difference between the groups $F(2, 33) = 54.351$, $p < .001$) in all three groups of vessels. The post-hoc tests showed that for the vessels with diameter 20-70 µm, donors are having significantly lower values with 17.71% MWT, compared to CTEPH (38.30%; Tukey-HSD, $p < .001$) and IPAH (37.42%; Tukey-HSD, $p < .001$) which are not different from each other (Tukey-HSD, ns) (Figure 8A). The results of the comparison of the MWT for the vessels with diameter 70-150 µm exhibited a significant difference between the groups $F(2, 33) = 34.102$, $p < .001$). The post-hoc tests showed that donors are having significantly lower values with 16.99% compared to CTEPH (38.34%; Dunnett, $p < .001$) and IPAH (42.71%; Dunnett, $p < .001$) which are not different from each other (Dunnett, ns) (Figure 8B). The results of the morphometric analysis of the vessels with $d > 150$ µm displayed a significant difference between the groups $F(2, 33) = 10.295$, $p < .001$). The post-hoc tests showed that donors are having significantly lower values with 18.36% compared to CTEPH (39.07%; Dunnett, $p <$

.001) and IPAH (33.67%; Dunnett, p < .01) which are not different from each other (Dunnett, ns) (Figure 8C).

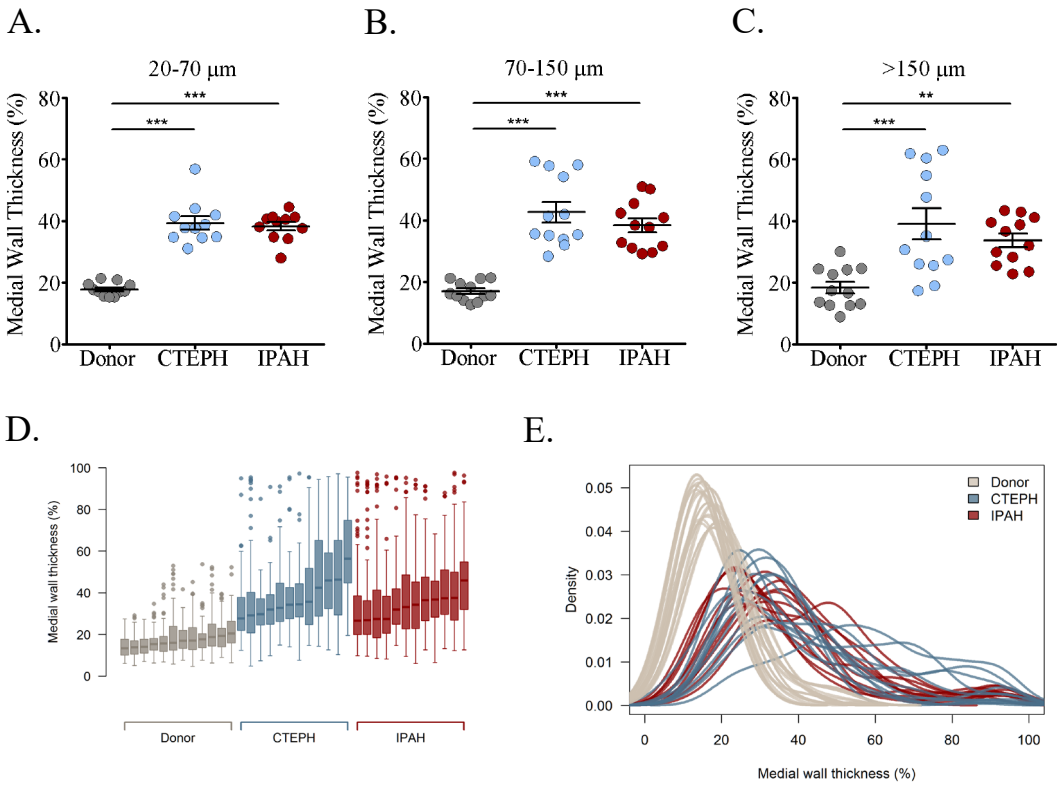

Figure 8: Medial hypertrophy quantification of donor, CTEPH and IPAH patients following the Weigert–van Gieson staining. Measurement of medial wall thickness (MWT) of pulmonary vessels is shown as a percentage. A. Group 1: d = 20-70 µm; B. Group 2: d = 70-150 µm; C. Group 3: d > 150 µm; D. Boxplot of individual patients displaying the distribution of the MWT; E. Distribution of the individual densities of MWT for each individual donor or patients' sample. Data is represented as mean±SEM (n=12; *p<0.05, **p<0.01, ***p<0.001)

Next, as appreciated from Figure 8D, the distribution of the MWT values for each individual patient of CTEPH was similar to IPAH, in contrast to the donor samples. On one hand, the IPAH samples showed more homogenous distribution of MWT values, in comparison to CTEPH, where some patients displayed higher variability to the rest of the corresponding samples. On the other hand, the distribution of the individual densities of the MWT, exhibited similar Gaussian curve distribution between CTEPH and IPAH samples (Figure 8E).

4.1.1.2. Evaluation of the neointima/media ratio in explanted CTEPH and in comparison, to IPAH and donor lung tissues

From the same van Gieson stained lung sections, we also analyzed the ratio neointima/media in all three categorized vessel sizes using the Leica Qwin V3 software, in order to evaluate the vascular remodelling in the CTEPH and IPAH samples in comparison to the donor controls.

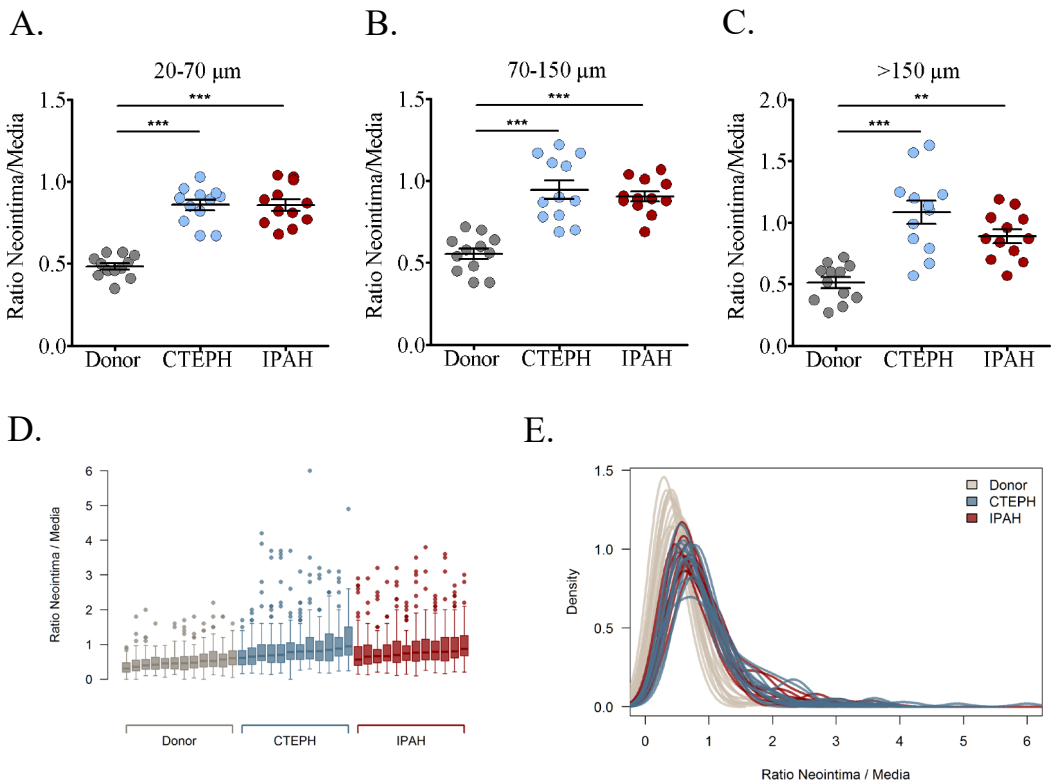

Figure 9: Computational assessment of the neointima/media ratio of pulmonary vessels from donor, CTEPH and IPAH lung samples. A. Group 1: d = 20-70 µm; B. Group 2: d = 70-150 µm; C. Group 3: d > 150 µm; D: Boxplot of individual patients displaying the distribution of the ratio neointima/media; E. Distribution of the individual densities of the ratio neointima/media for each individual donor or patients' sample. Data is represented as mean±SEM (n=12; *p<0.05, **p<0.01, ***p<0.001)

The results of the comparison of the neointima/media ratio of vessels with diameter 20-70 µm showed a significant difference between the groups $F(2, 33) = 52.357$, $p < .001$). The post-hoc tests presented that donors are having significantly lower values with 0.48 compared to CTEPH (0.86; Tukey-HSD, $p < .001$) and IPAH (0.86; Tukey-HSD, $p < .001$) which are not different from each other (Tukey-HSD, ns) (Figure 9A). The assessment of the ratio of 70-150 µm vessels size showed a significant difference between the groups $F(2, 33) = 27.062$, $p < .001$). The post-hoc tests displayed that donors are having significantly lower values with 0.56 compared to CTEPH (0.95; Dunnett, $p < .001$) and IPAH (0.91; Dunnett, $p < .001$) which are not different from each other (Dunnett, ns) (Figure 9B). At last, the ratio of the vessels with d > 150 µm showed a significant difference between the groups $F(2, 33) = 18.173$, $p < .001$). The post-hoc tests revealed that donors are having significantly lower values with 0.51 compared to CTEPH (1.08; Tukey-HSD, $p < .001$) and IPAH (0.89; Tukey-HSD, $p < .01$) which are not different from each other (Tukey-HSD, ns) (Figure 9C).

Following the evaluation of the ratio, we analysed the distribution of the values for each individual patient of CTEPH, IPAH, and donors. Similar to the MWT distribution, CTEPH and IPAH patients present indistinguishable and even more homogeneous distribution of the values of the ratio, in contrast to the donor samples (Figure 9D). The distribution of the individual densities of the ratio showed similar Gaussian curve distribution between CTEPH and IPAH samples (Figure 9E).

4.1.1.3. Evaluation of the degree of muscularization in explanted CTEPH and in comparison, to IPAH and donor lung tissues

In order to evaluate the degree of muscularization we performed double immunohistochemical staining with von Willebrand factor (vWF) for endothelial cells and α-smooth muscle actin (α-SMA) for smooth muscle cells (Figure 10A). Leica Qwin V3 software was applied to quantify the degree of muscularization in vessels from donors, CTEPH and IPAH lung samples. The vessels were again divided into three groups depending on their size (Group 1: d = 20-70 µm, Group 2: d = 70-150 µm and Group 3: d > 150 µm. Immunofluorescent visualization was used to show the localization of the endothelial (by vWf) and smooth muscle cell (α-SMA) markers within arteries of CTEPH and IPAH patients, as well as donors. As observed from Figure 10 B, CTEPH samples showed increased immunoreactivity of α-SMA a marking the vascular remodelling similar to IPAH.

For the 20-70 µm cohort of non-muscularized vessels, the results revealed a significant difference between the groups ($F(2, 32) = 28.105$, $p < .001$). The post-hoc tests showed that in donors, the percentage of non-muscularized vessels is significantly different to IPAH (Tukey, $p < .001$) and CTEPH (Tukey, $p < .001$). IPAH and CTEPH are not significantly different from each other (Tukey, ns). Regarding the partially-muscularized vessels in a range of 20-70 µm there wasn't a significant difference between the groups ($F(2, 32) = 0.580$, ns). Further, the percentage of fully-muscularized showed a significant difference between the groups ($F(2, 32) = 14.484$, $p < .001$). The post-hoc tests show that donors are significantly different to IPAH (Tukey, $p < .001$) and CTEPH (Tukey, $p < .001$). IPAH and CTEPH are not significantly different from each other (Tukey, ns) (Figure 10C). The quantification for the non-muscularized vessels with d = 70-150 µm showed a significant difference between the groups ($F(2, 32) = 3.491$, $p < .05$). The post-hoc tests presented that non-muscularized vessels in donors are statistically significantly different to IPAH (Games-Howell, $p < .05$), but not to CTEPH (Games-Howell, ns). IPAH and CTEPH are also significantly different from each other (Games-Howell, $p < .05$). There was no significant difference between the groups, for the

partially-muscularized ($F(2, 32) = 0.049$, ns) and fully-muscularized vessels ($F(2, 32) = 1.060$, ns) (Figure 10D). For the vessels with diameter greater than 150 µm condition, no significant difference between the groups was observed: the non-muscularized ($F(2, 32) = 1.101$, ns), partially-muscularized ($F(2, 32) = 0.737$, ns) and fully muscularized ($F(2, 32) = 0.210$, ns), respectively (Figure 10E).

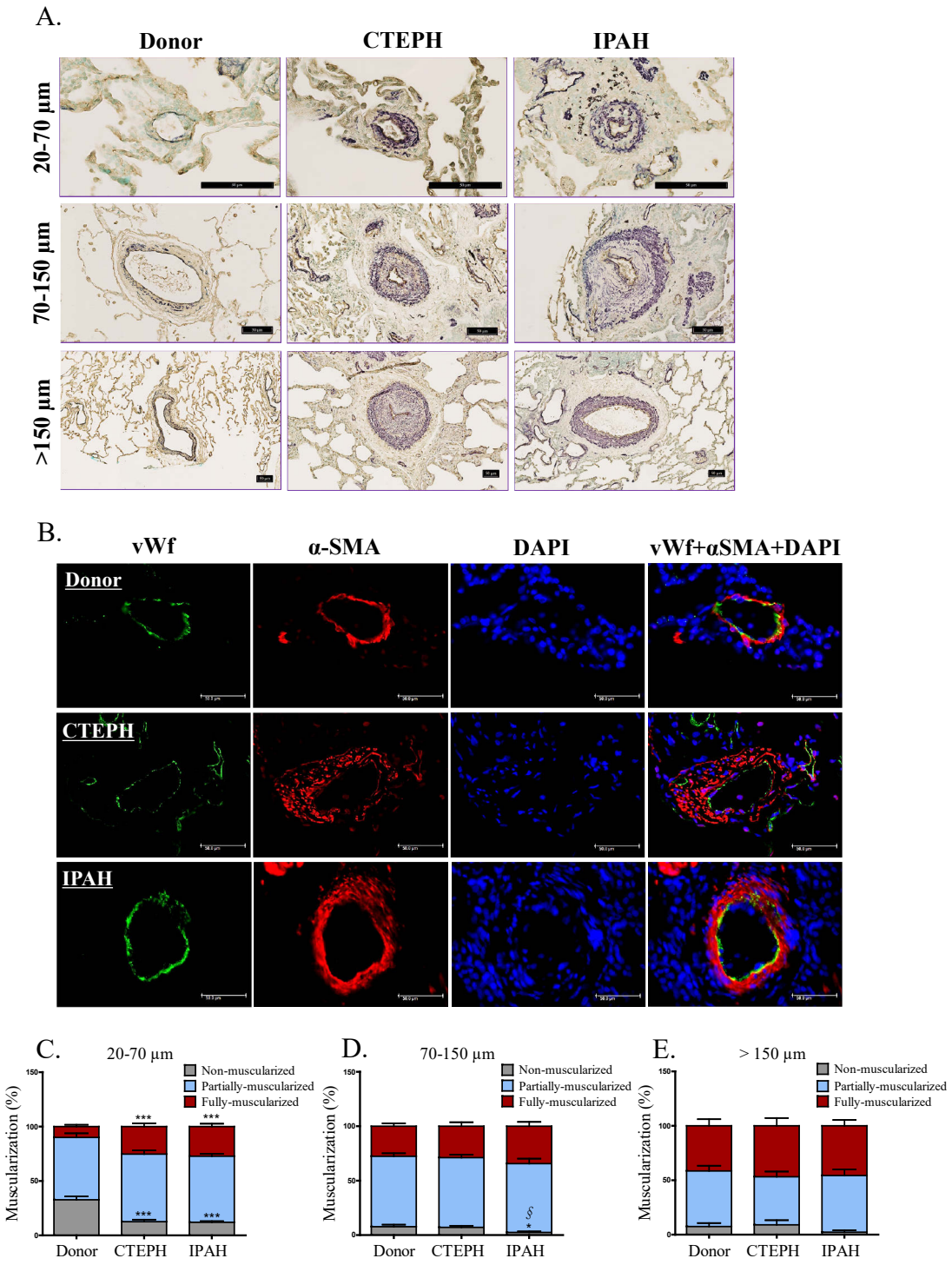

Figure 10: Visualization and quantification of the degree of muscularization for patients with CTEPH and IPAH, in comparison to control (donor samples). Immunohistochemistry with vWF and α-SMA for vessels with: A. Group 1: d = 20-70 µm; Group 2: d = 70-150 µm; Group 3: d > 150 µm; B. Representative microphotographs of immunolocalization of vWf (green), α-SMA (red) and DAPI (nuclei, blue). Quantification of the degree of muscularization for C. Group 1; D. Group 2; E. Group 3. Scale bar 50µm. Data is represented as mean±SEM (n=12 (donor and CTEPH), n=11 (IPAH); *p<0.05, **p<0.01, ***p<0.001 versus donor; §p<0.05, §§p<0.01, §§§p<0.001 versus CTEPH).

4.1.1.4. Collagen deposition in explanted CTEPH and in comparison, to IPAH and donor lung tissues

To investigate the total collagen deposition within the CTEPH and IPAH lung samples, two different staining techniques were employed: Sirius Red and Masson`s Trichrome staining. As visible in the representative images, the CTEPH and IPAH patients, display increased collagen staining by both methods within the vascular wall (Figure 11A). Furthermore, the total collagen was quantified using Leica Qwin V3 software. The results of the quantification were then compared using an ANOVA test and show a significant difference between the groups $F(2, 33) = 14.196$, $p < .001$). The samples were normalized to controls (donor samples). The post-hoc tests showed that CTEPH samples have significantly higher values of the total collagen area (212.40%; Dunnett, $p < .001$) in contrast to the donors, which are also significantly different from IPAH (159.58%; Dunnett, $p < .05$). Furthermore, the CTEPH and IPAH samples were also significantly different from each other (Dunnett, $p < .05$), suggesting a more prominent total collagen deposition in CTEPH (Figure 11B).

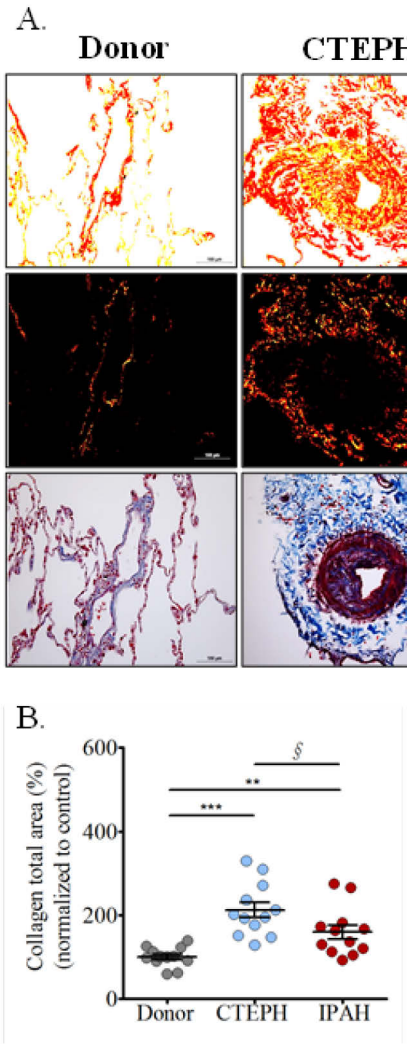

Figure 11: Visualization and quantification of total collagen area in explanted CTEPH and IPAH lungs in comparison to donor. A. Representative microphotographs of vessels with extensive collagen deposition characteristic for severe vascular remodelling, as noticed in CTEPH and IPAH samples, in contrast to donors (Sirius red colours collagen fibres in red; in polarized light, the thickest collagen fibres appear yellow/orange, while the finest are green; Trichrome distinguishes between the blue collagen, the muscle fibres in red, red cytoplasm and the blue nuclei). B. Measurement of the total collagen area in the respective samples. Scale bar 100 µm, n=12. Data is expressed as a percentage of donor controls and represented as mean±SEM (n=12; *p<0.05, **p<0.01, ***p<0.001; §p<0.05, §§p<0.01, §§§p<0.001 versus CTEPH)

4.1.1.5. Differential gene expression of laser capture microdissected vessels from explanted CTEPH and in comparison to IPAH and donor lung tissues

To investigate and compare the distal pulmonary vasculature-specific differential gene expression, laser capture microdissection (LCM) followed by microarray–based profiling was performed on lung samples from donors and explanted CTEPH and IPAH tissues. Vessels with

diameter < 100 µm were selected under optical control of LMD6000 device (Figure 12A and 12B).

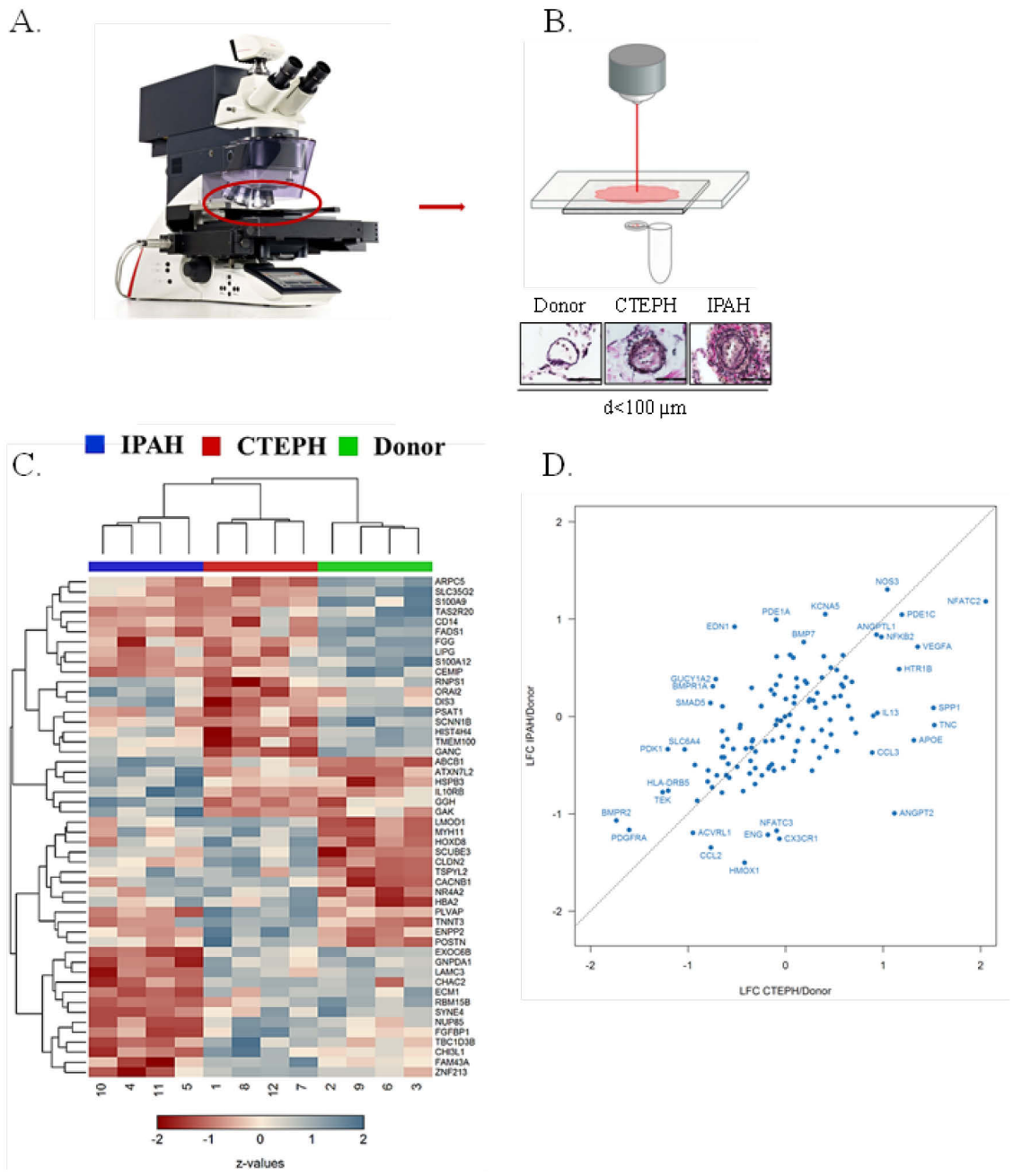

Figure 12: Gene regulation patterns of CTEPH, IPAH and donor lung samples employing laser capture microdissection and microarray screening. A. Laser microdissection device LMD6000 (Leica, Wetzlar, Germany); B. Schematic representation of the LCM performed on 10 µm tissue sections. C. Heatmap of supervised clustering of the top 50 differentially regulated genes selected by F value. n=8 (each sample represents a pool of two different biological replicates). Red indicates relatively low expression, while blue relatively high expression D. LogFC correlation of the identified genes in CTEPH *vs*. donor and IPAH *vs*. donor within the PH known genes.

To visualize the global transcriptome, we accounted a heatmap displaying hierarchical clustering of the top 50 selected by F-value, similarly and differently regulated genes in the

given experimental setup. The biological signature of the CTEPH revealed a subset of genes, similarly regulated as in the IPAH, as well as genes which were differently regulated, when all together were compared to the donor (Figure 12C). Next, we evaluated the log fold change (LogFC) >1 correlation of all the known PH associated genes with the genes identified for the LCM-microarray asset. Many of the genes (such as NFATC2 - Nuclear Factor of Activated T Cells 2, NOS3 - Nitric Oxide Synthase 3, VEGFA - Vascular Endothelial Growth Factor A, PDE1C - Phosphodiesterase 1C, PDGFRA - Platelet Derived Growth Factor Receptor Alpha etc.) regulated in CTEPH vs. donor, showed significant positive correlation with IPAH vs donor, while many of them (PDE1A - Phosphodiesterase 1A, EDN1 - Endothelin 1, CCL3 - Chemokine (C-C motif) ligand 3 , ANGPT2 - Angiopoietin 2 etc.) presented significant negative correlation (Figure 12D).

Microarray analysis identified 2074 protein-coding genes with LogFC > 1 differential expression in CTEPH-Donor, in comparison to IPAH-Donor. Interestingly, as shown in Figure 13A, only 17.65% of the total number of up- and down- regulated genes with LogFC > 1 are commonly regulated between CTEPH *vs.* donor and IPAH *vs.* donor. From the total number of upregulated genes (909), only 19.80% are commonly regulated (Figure 13B); while from the total number of downregulated genes (1169), only 15.57% (Figure 13C). The Volcano plots showed the statistical significance of differential expression against the mean log fold difference $-\log_2$ (fold change). Among the gene selection of LogFC > 1, one of the commonly regulated genes in both, CTEPH *vs.* donor and IPAH *vs.* donor was NFATC2. As presented in the Volcano plots (Figure 13D) and in Table 19, CHI3L1 came as a gene which is upregulated in CTEPH, while down regulated in IPAH. Several other genes were regulated in opposite direction in CTEPH and IPAH, both in contrast to the donor (Table 19). Furthermore, one of the differentially regulated genes, ENPP2, showed a significant upregulation in CTEPH, while no change was detected in IPAH (Figure 13D). The list of the top 25 up- and downregulated genes is given in the Appendix as A-1 and A-2.

Table 19: List of genes regulated in CTEPH with opposite direction to IPAH

Symbol	Entrez gene name	LogFC CTEPH-Donor	LogFC IPAH-Donor	LogFC CTEPH-IPAH
FGFBP1	Fibroblast growth factor binding protein 1	1.00	-1.44	NA
SCIMP	SLP adaptor and CSK interacting membrane protein	1.30	-1.03	2.33
FAM43A	Family with sequence similarity 43. member A	1.18	-1.41	2.59
ANGPT2	Angiopoietin 2	1.20	-1.05	2.25
CHI3L1	Chitinase 3-like 1 (cartilage glycoprotein-39)	1.28	-1.66	2.93
D2HGDH	D-2-hydroxyglutarate dehydrogenase	1.21	-1.03	2.24

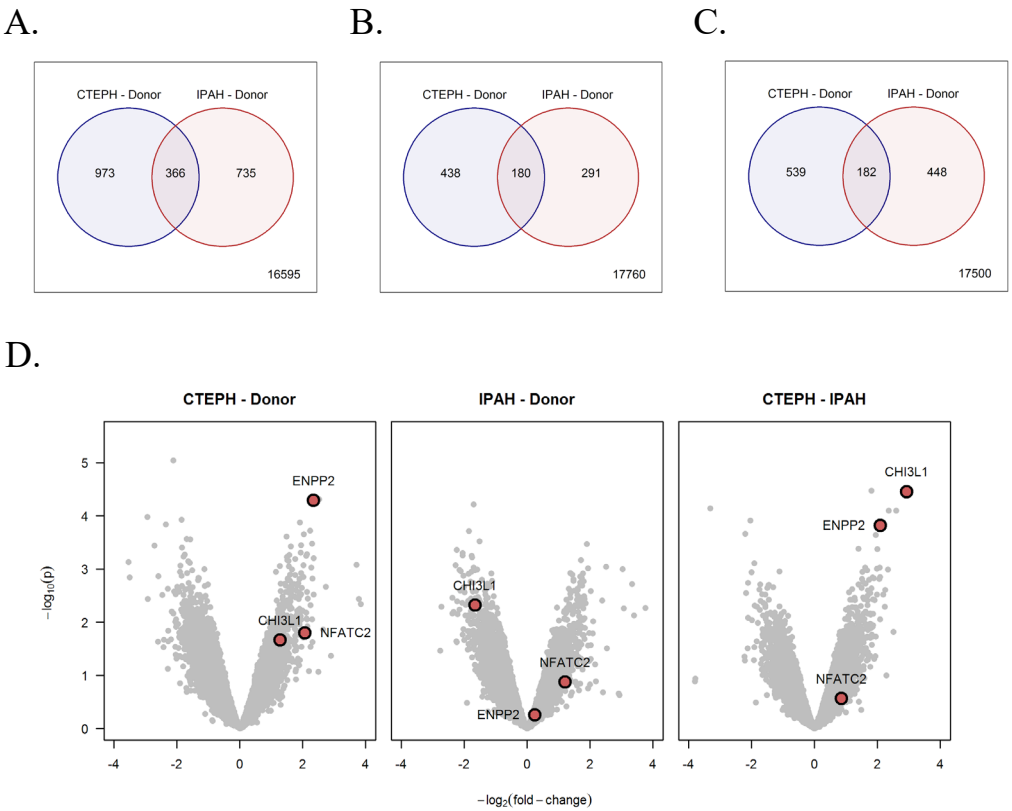

Figure 13: Transcriptional similarities and differences between CTEPH and IPAH. Venn diagram of: A. both, up- and down- regulated genes based on LogFC > 1; B. Upregulated genes by LogFC > 1; C. Downregulated genes by LogFC > 1; D. Volcano plots of the distribution of genes selected under $-\log_{10}$ of p values (y axis), plotted against the $-\log_2$ of fold change for CTEPH-Donor, IPAH-Donor and comparison of CTEPH vs IPAH with selected targets, NFATC2, CHI3L1, ENPP2 (red dots), as similarly and differently regulated in all the three contrasts, respectively.

4.1.1.6. KEGG pathway analysis of the differential gene expression of LCM vessels from explanted CTEPH and in comparison to IPAH and donor lung tissues

In order to further obtain biological insight into number of up- and down- regulated signalling pathways, Kyoto Encyclopedia of Genes and Genomes (KEGG) pathways analysis was performed.

KEGG pathway analysis revealed enrichment of several signalling pathways in both CTEPH and IPAH, among which increased number of differentially regulated genes are associated with metabolic pathways and protein processing in endoplasmic reticulum (Figure 14A and 14B). Surprisingly, the most prominently regulated pathways in CTEPH and in contrast to IPAH according to the gene enrichment were alcoholism, systemic lupus erythematosus and viral carcinogenesis (Figure 14A and 14B). With regard to the IPAH, processes in lysosome and oxidative phosphorylation were among the most prominently regulated pathways. As observed

from Figure 14C, the majority of the genes determined by LogFC >1 fall into metabolic pathways (being downregulated, while upregulated in IPAH) (Figure 14D). Significant portion of the genes related to alcoholism and viral carcinogenesis in CTEPH are downregulated, along with all downregulated genes in systemic lupus erythematosus Figure (14C). In IPAH, most of the genes predicting the lysosomal processes are upregulated, along with all upregulated genes in oxidative phosphorylation pathway (Figure 14D). As mentioned above, when CTEPH and IPAH were compared, most of the regulated and especially downregulated genes are falling into metabolic pathways, followed by pathways regulated in cancer, which are more prominently activated in IPAH, in comparison to CTEPH (Figure 14C).

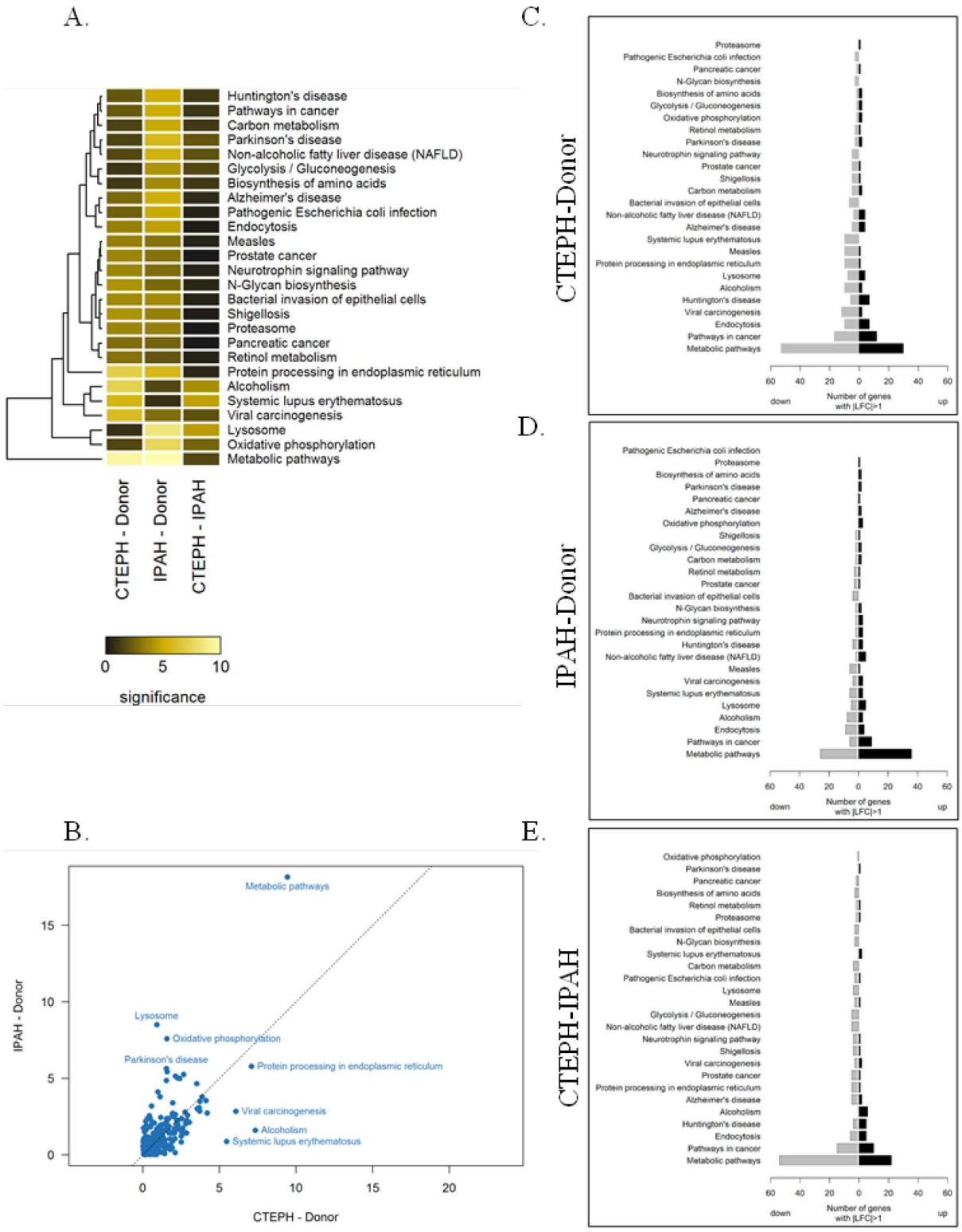

Figure 14: In silico KEGG pathway analysis of CTEPH and IPAH in contrast to donor samples and their comparison. A. Heatmap showing the significance (-$\log_{10}$ p-value) of the perturbation of KEGG pathways obtained from the gene set tests, presenting the Top 26 regulated pathways. B. LogFC correlation of the identified pathways in CTEPH *vs*. donor and IPAH *vs*. donor; (C-E) Visualization of the number and subset of up- and down- regulated genes in C. CTEPH *vs.* donor; D. IPAH *vs.* donor; E. CTEPH *vs.* IPAH depending on the corresponding pathway.

4.2. Chapter II: Histopathological and molecular characterization and comparison of distal vessel remodelling in explanted central and peripheral CTEPH in comparison to donor lung tissues

4.2.1. Characterization and comparison of vascular remodelling in explanted central and peripheral CTEPH in comparison to donor lung tissues

In order to evaluate whether the distal histopathological changes between central (proximal) and peripheral (distal) CTEPH are similar or distinct with each other, we systematically evaluated the vascular remodelling by assessing the medial hypertrophy, the ratio neointima/media and the collagen deposition employing the methods described in Chapter 4.1.

4.2.1.1. Assessment of the medial hypertrophy in explanted central and peripheral CTEPH in comparison to donor lung tissues

As described in section 4.1.1, vessels from central and peripheral CTEPH were selected and divided into three groups based on their size (Group 1: d = 20-70 µm, Group 2: d = 70-150 µm and Group 3: d > 150 µm) and compared with corresponding vessels from donors. Both, central and peripheral CTEPH samples presented increased thickness of the vessel wall and apparent neointima formation in all sizes of vessels in comparison to respective donor controls (Figure 15).

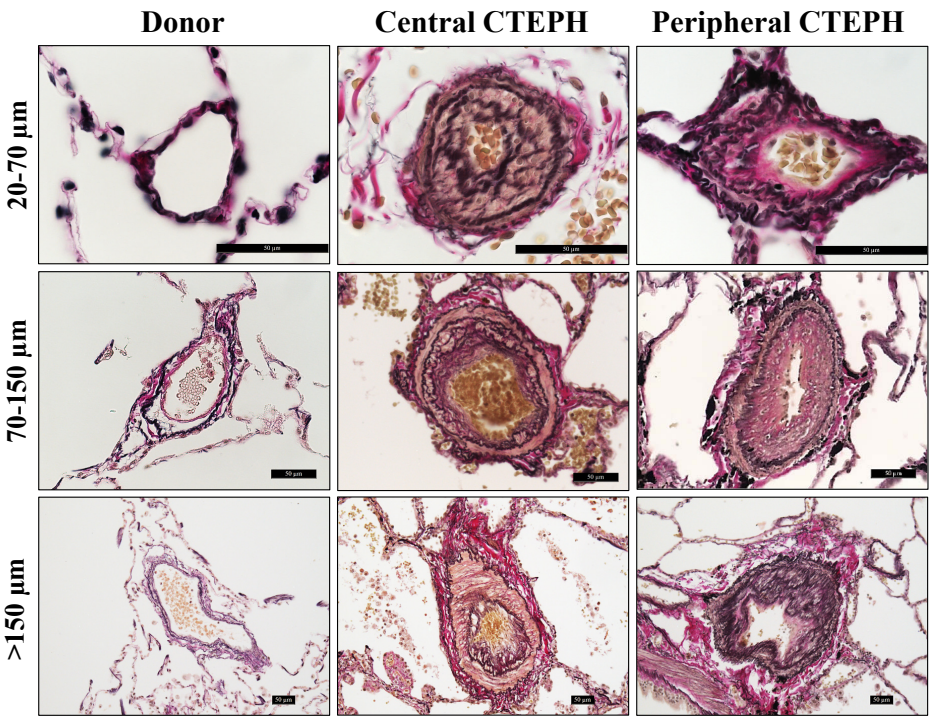

Figure 15: Visualization of severe vascular wall thickening in human lungs from central CTEPH and peripheral CTEPH and respective controls. Representative microphotographs of vessels within three groups: Group 1: d = 20-70 µm; Group 2: d = 70-150 µm and Group 3: d > 150 µm. Scale bar 50 µm, n(donor) = 9, n(Central CTEPH) = 3 patients x 2 regions, n(Peripheral CTEPH) = 4 patients x 2 regions. Details of the staining protocol are listed in the materials and methods section.

Further in order to address the regional heterogeneity in terms of vascular remodelling, two sections from different areas of the patients`s lung were taken for evaluation of the MWT, as well as for the ratio of neointima/media. Cumulatively, the results of the comparison of MWT of vessels with d = 20-70 µm manifested a significant difference between the groups $F(2, 20) = 52.441$, $p < .001$). The post-hoc tests showed that donors possess significantly lower values with 17.94% compared to central CTEPH (38.07%; Dunnett, $p < .01$) and peripheral CTEPH (36.33%; Dunnett, $p < .001$) which are not different from each other (Dunnett, ns) (Figure 16A). The MWT of vessels with d = 70-150 µm presented a significant difference between the groups $F(2, 20) = 28.300$, $p < .001$). The post-hoc tests revealed that donors are having significantly lower values with 17.72% of the MWT compared to central CTEPH (38.75%; Tukey-HSD, $p < .001$) and peripheral CTEPH (37.64%; Tukey-HSD, $p < .001$) which are not different from each other (Tukey-HSD, ns) (Figure 16B).

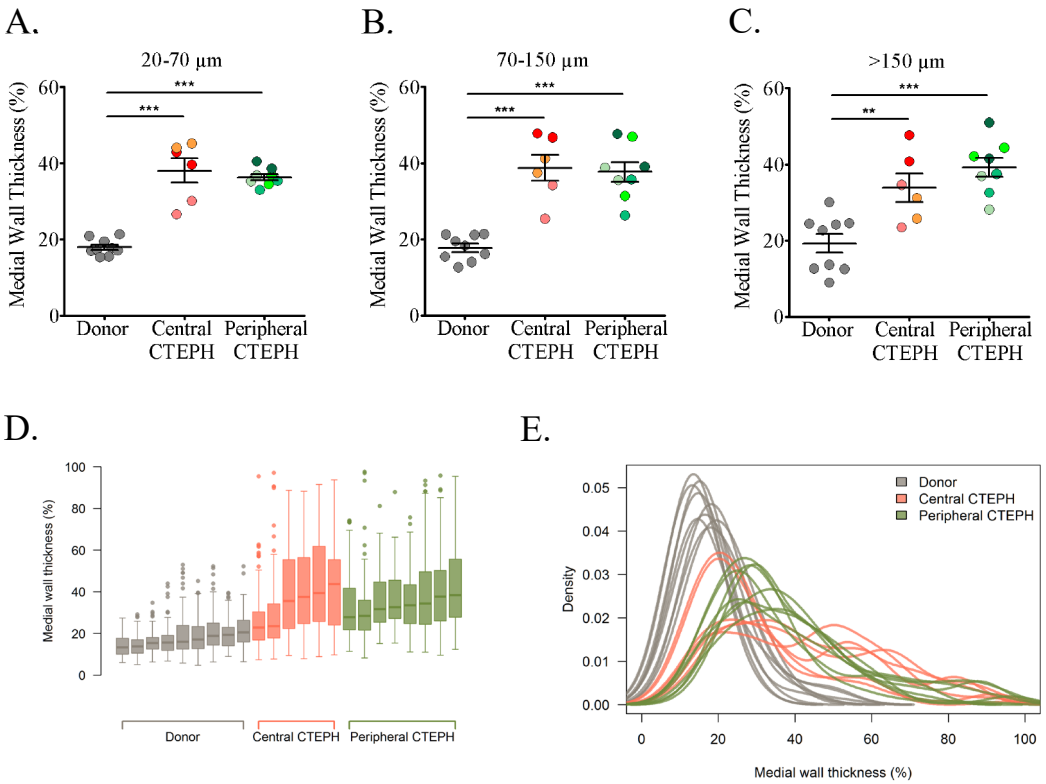

Figure 16: Medial hypertrophy quantification of donor, central CTEPH and peripheral CTEPH following the Weigert–van Gieson staining. Each patient is represented in different colour, containing two different area sections. Measurement of medial wall thickness (MWT) of pulmonary vessels is shown as a percentage. A. Group 1: d = 20-70 µm; B. Group 2: d = 70-150 µm; C. Group 3: d > 150 µm; D: Boxplot of individual patients displaying the distribution of the MWT; E. Distribution of the individual densities of MWT for each individual donor or patients sample. Data is represented as mean±SEM (n(donor) = 9, n(Central CTEPH) = 3 patients x 2 regions, n(Peripheral CTEPH) = 4 patients x 2 regions; *p<0.05, **p<0.01, ***p<0.001)

At last, the comparison of the MWT for vessels with d > 150 µm revealed a significant difference between the groups $F(2, 20) = 14.973$, $p < .001$). The post-hoc tests showed that donors are having significantly lower values with 19.26% as compared to central CTEPH (33.89%; Tukey-HSD, $p < .01$) and peripheral CTEPH (39.23%; Tukey-HSD, $p < .001$), which are not different from each other (Tukey-HSD, ns) (Figure 16C).

Further, the distribution of the MWT values within each patient of central or peripheral CTEPH is similar, independently of the site where the section was taken, which is apparently different from the donor. The thickness of the vessels accounted for MWT in peripheral CTEPH seems to be more homogenous, in contrast to central CTEPH (Figure 16D). The individual densities of the MWT, showed Gaussian distribution for peripheral CTEPH and partially bimodal distribution for central CTEPH (Figure 16E).

4.2.1.2. Evaluation of the ratio neointima/media in explanted central and peripheral CTEPH in comparison to donor lung tissues

Next, in sequence to the measurement of the medial wall thickness, we assessed the ratio neointima/media to further confirm the neointima formation, as a significant factor of vascular remodelling in central and peripheral CTEPH, in contrast to the healthy, donor controls.

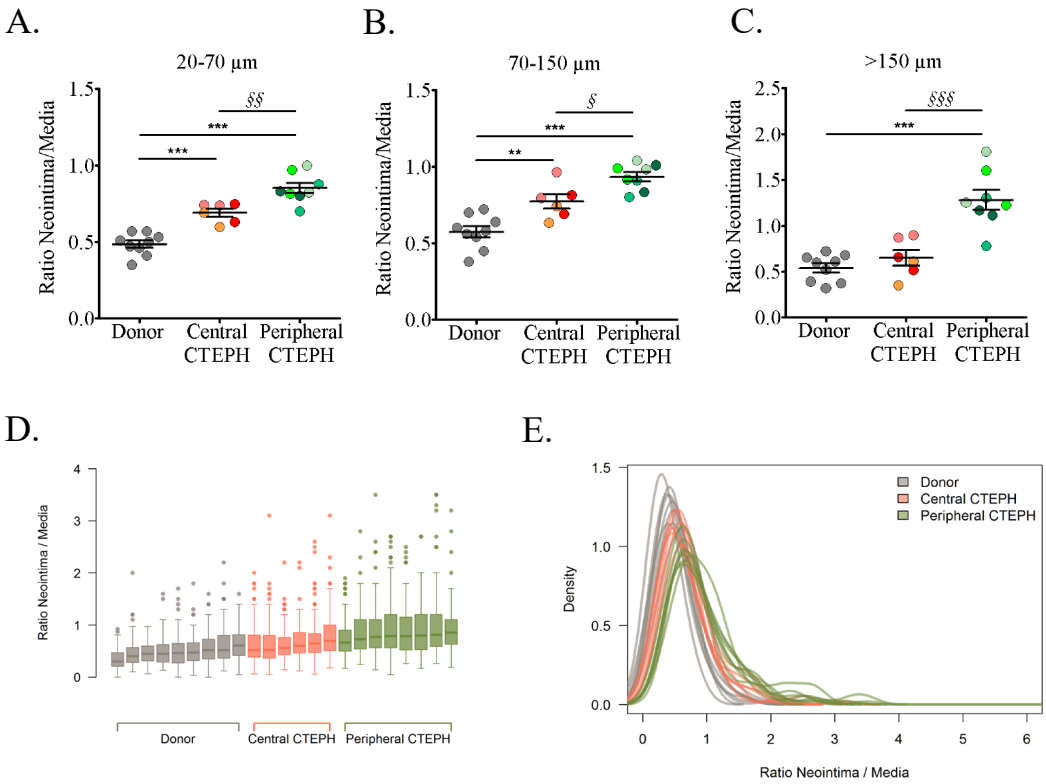

Figure 17: Computational assessment of the ratio neointima/media of pulmonary vessels from donor, central CTEPH and peripheral CTEPH lung samples. Each patient is represented in different colour, containing two different area sections. A. Group 1: d = 20-70 µm; B. Group 2: d = 70-150 µm; C. Group 3: d > 150 µm; D: Boxplot of individual patients displaying the distribution of the ratio neointima/media; E. Distribution of the individual densities of the ratio neointima/media for each individual donor or patients sample. Data is represented as mean±SEM (n(donor) = 9, n(Central CTEPH) = 3 patients x 2 regions, n(Peripheral CTEPH) = 4 patients x 2 regions.; *p<0.05, **p<0.01, ***p<0.001)n=12; *p<0.05, **p<0.01, ***p<0.001; §p<0.05, §§p<0.01, §§§p<0.001 versus Central CTEPH)

The ratio neointima/media of the vessels with d = 20-70 µm showed a significant difference between the groups F(2, 20) = 45.027, p < .001). The post-hoc tests confirmed that donors are having significantly lower values with 0.49 compared to central CTEPH (0.69; Tukey-HSD, p < .001) and peripheral CTEPH (0.85; Tukey-HSD, p < .001) which are also different from each other (Tukey-HSD, p < .01) (Figure 17A). The results of the comparison of 70-150 µm vessels showed a significant difference between the groups F(2, 20) = 26.060, p < .001). The post-hoc tests revealed that donors are having significantly lower values with 0.57 compared to central

CTEPH (0.77; Tukey-HSD, $p < .01$) and peripheral CTEPH (0.93; Tukey-HSD, $p < .001$) which are also different from each other (Tukey-HSD, $p < .05$) (Figure 17B). The comparison of $d > 150$ µm show a significant difference between the groups $F(2, 20) = 24.190$, $p < .001$). The post-hoc tests showed that donors are having significantly lower values with 0.54 compared to peripheral CTEPH (1.28; Tukey-HSD, $p < .001$) but not significant to central CTEPH (0.65; Tukey-HSD, ns) (Figure 17C). Central CTEPH and peripheral CTEPH are significantly different from each other in terms of ratio neointima/media (Tukey-HSD, $p < .001$). Following the evaluation of the ratio, we assessed the distribution of the values for each individual patient of central CTEPH and peripheral CTEPH, and in comparison, to the donor samples. Similarly, as the MWT distribution, central and peripheral presented indistinguishable and even more homogeneous distribution of the values of the ratio, in contrast to the donor samples (Figure 17D). The distribution of the individual densities of the ratio showed Gaussian curve similitude for both, central and peripheral CTEPH (Figure 17E).

4.2.1.3. Collagen distribution in explanted central and peripheral CTEPH in comparison to donor lung tissues

As presented by the representative microphotographs, both central and peripheral CTEPH, display increased collagen staining within the vascular wall (Figure 18A). The total collagen area (%) was measured and the values of total collagen area of central and peripheral CTEPH samples were normalized to controls (donor samples). The post-hoc tests showed that central CTEPH had significantly higher values of total collagen area (314.84%; Dunnett, $p < .001$), in contrast to controls, which are also different from peripheral CTEPH (217.35%; Dunnett, $p < .01$). Central and the peripheral CTEPH are also different from each other (Dunnett, $p < .05$) (Figure 18B).

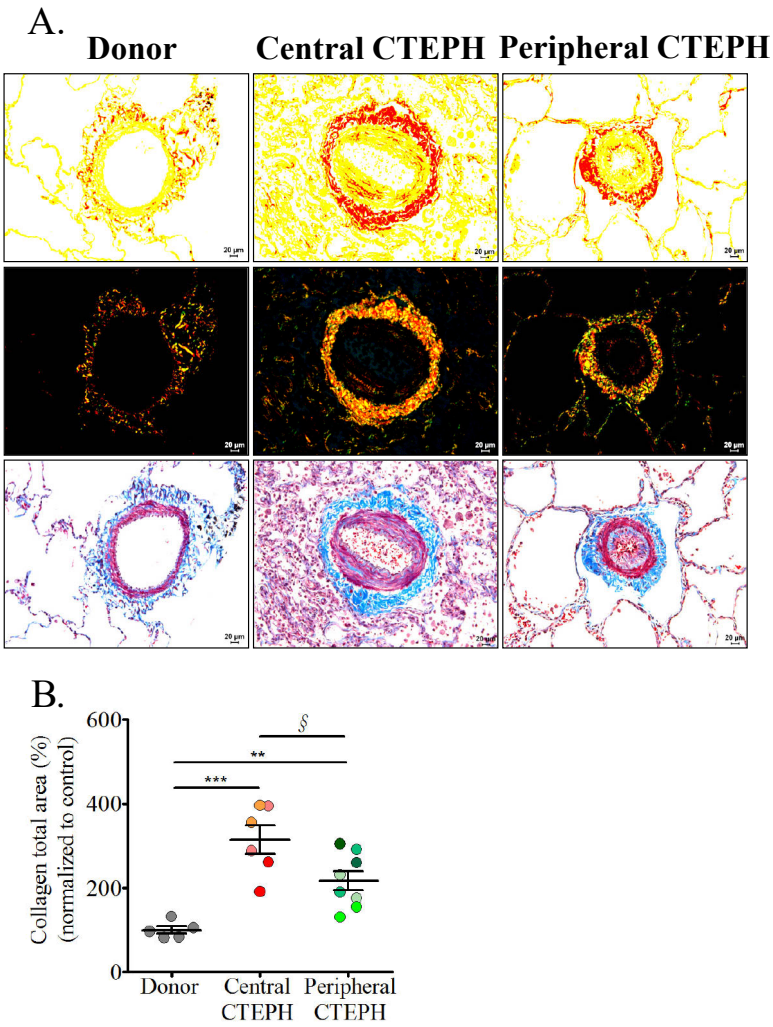

Figure 18: Visualization and quantification of total collagen area in human donor and explanted central and peripheral CTEPH. A. Representative microphotographs of vessels with extensive collagen deposition characteristic for severe vascular remodelling, as noticed in both, central and peripheral CTEPH samples, in contrast to donors B. Measurement of the total collagen area in the respective samples. Scale bar 20 µm. Data is expressed as a percentage of donor controls and represented as mean±SEM (n(donor) = 9, n(Central CTEPH) = 3 patients x 2 regions, n(Peripheral CTEPH) = 4 patients x 2 regions; *p<0.05, **p<0.01, ***p<0.001; §p<0.05, §§p<0.01, §§§p<0.001 versus Central CTEPH).

4.2.2. Genome wide expression profiling of explanted central and peripheral CTEPH in comparison to donor lung tissues

4.2.2.1. Differential gene expression of LCM vessels from explanted central and peripheral CTEPH in comparison to donor lung tissues

To evaluate whether there is specific gene signature associated with peripheral *vs.* central part of the disease, vessels with diameter < 100 µm from both, central and peripheral CTEPH (Figure 19A) were laser capture microdissected (LCM), followed by microarray–based approach of genome wide expression profiling.

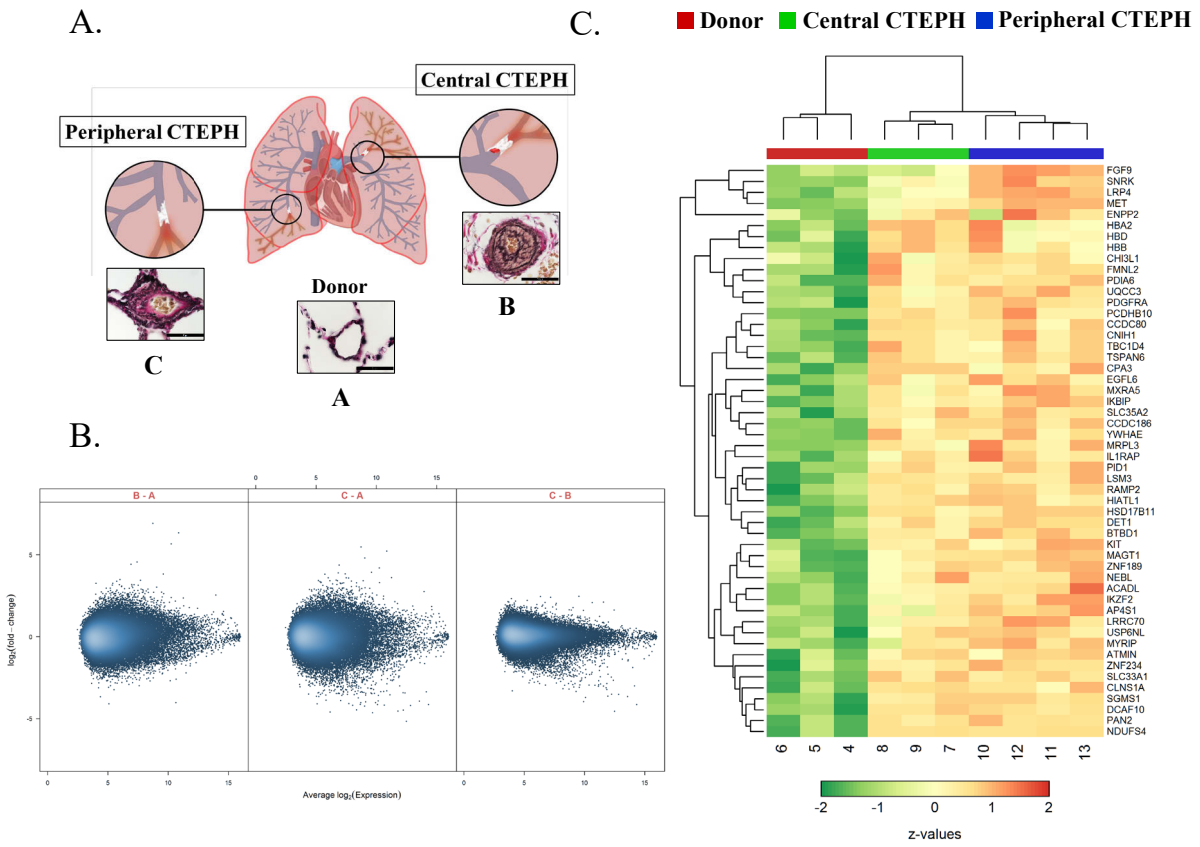

Figure 19: Gene regulation patterns of central and peripheral CTEPH in contrast to donor lung samples based on combined LCM-microarray approach. A. Schematic representation of the location of the disease (central and peripheral CTEPH), and typical appearance of the dissected material. B. MDPlots to visualise the transcriptional difference between central CTEPH (B) and donor (A), peripheral CTEPH (C) and donor and central vs. peripheral CTEPH based on $\log_2$ (fold change) of p values plotted against the average $\log_2$ of the expression. C. Heatmap of the top 50 differentially regulated genes plus CHI3L1 and ENPP2 selected by F value. n(donor)=3, n(central CTEPH)=3, n(peripheral CTEPH)=4 (each sample of central and peripheral CTEPH represents a pool of two experimental replicates, chosen from different parts of the same patient)

The global transcriptome of all (up-, down- and non-) regulated genes of central CTEPH *vs.* donor, peripheral CTEPH *vs.* donor and peripheral *vs.* central CTEPH was represented by mdplots. Peripheral CTEPH showed higher enrichment of regulated genes, whereas the comparison between peripheral and central revealed diminished enrichment (Figure 19B). Next, we accounted a heatmap displaying hierarchical clustering of the top 50 (selected by F-value), similarly and differently regulated genes in donor, central and peripheral CTEPH, including in addition CHI3L1 and ENPP2, which came to be significantly regulated and biologically endorsed in the previous experimental setup. The genome wide expression profiling, revealed that the molecular imprint of both central and peripheral CTEPH presented a general similarity, in contrast to the donor samples (Figure 19C).

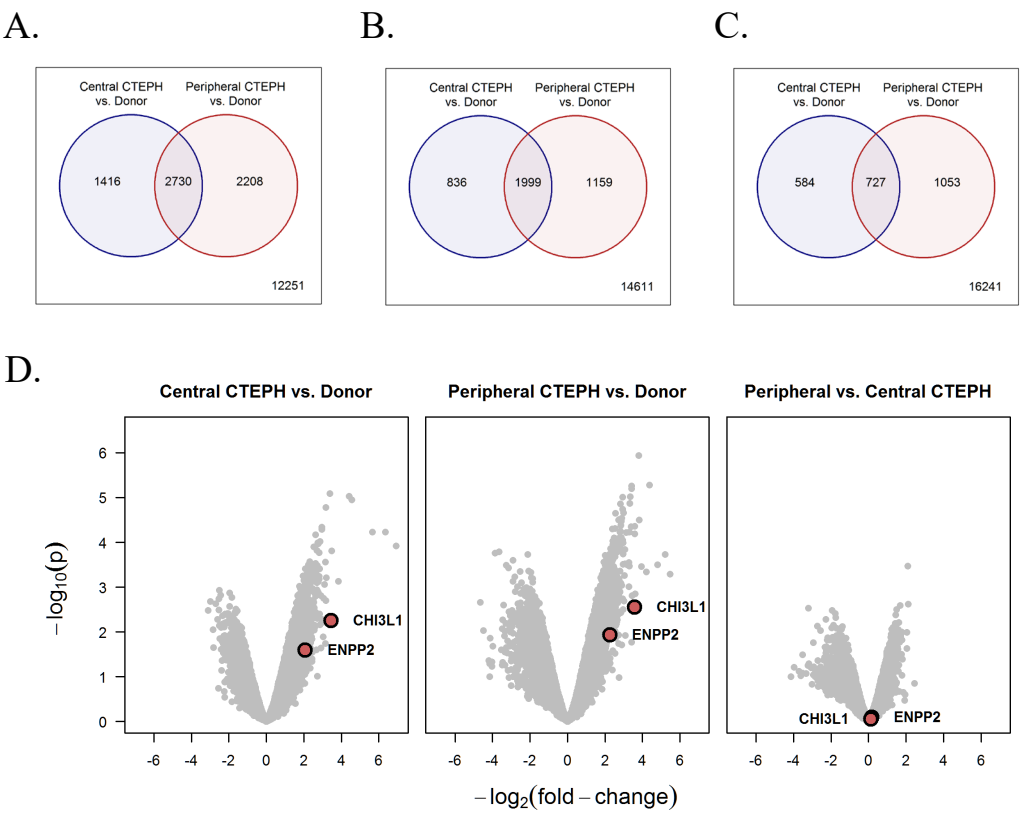

Figure 20: Transcriptional similarities and differences between central and peripheral CTEPH. Venn diagram by LogFC > 1 of: A. both, up- and down- regulated genes; B. upregulated genes; C. downregulated genes; C. Volcano plots of the distribution of genes selected under $-\log_{10}$ of p values (y axis), plotted against the $-\log_2$ of fold change for central CTEPH-Donor, peripheral CTEPH-Donor and comparison of peripheral *vs*. central CTEPH with selected targets CHI3L1 and ENPP2 (red dots), as similarly regulated in both, central and peripheral CTEPH.

Microarray analysis identified 6354 protein-coding genes with LogFC > 1 differential expression in Central CTEPH-Donor, in comparison to Peripheral CTEPH-Donor. Interestingly, as shown in Figure 20A, 43.02% of the total number of up- and down- regulated genes with LogFC > 1 are commonly regulated between central CTEPH *vs.* donor and peripheral CTEPH *vs.* donor. From the total number of upregulated genes 50.05% (1999) are commonly regulated (Figure 20B); whereas from the total number of downregulated genes, 30.75% (727) (Figure 20C). The Volcano plots acknowledged the statistical significance of differential expression against the mean log fold difference $-\log_2$ (fold change), depicting the already selected target genes, from the general non-biased screening of CTEPH. Among the gene selection of LogFC > 1, CHI3L1 and ENPP2 are the commonly regulated genes in a similar direction in both, central and peripheral CTEPH. When both conditions compared

together, there isn't a significant difference in the expression of these genes, as expected (Figure 20D).

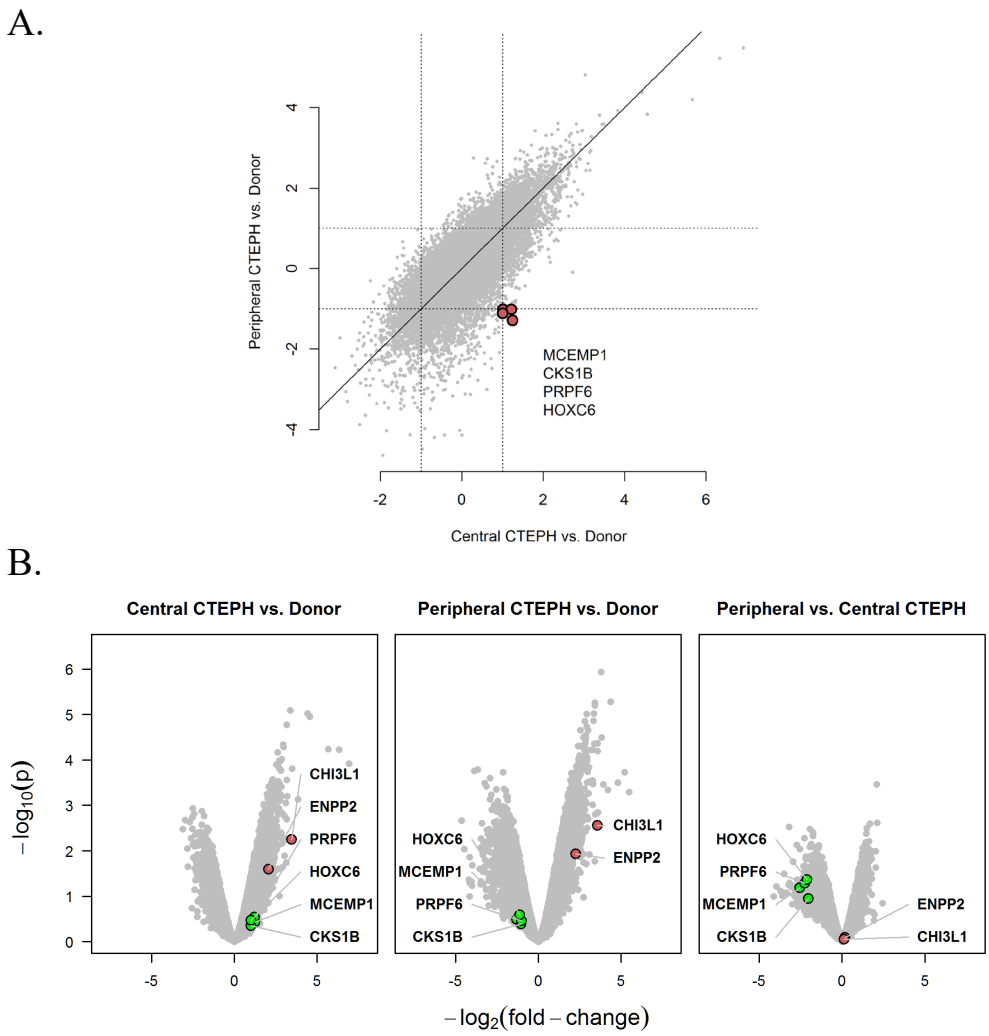

Figure 21: Genes with opposite direction of regulation in central and peripheral CTEPH, both in contrast to donor. A. Correlation of Log FC between central and peripheral CTEPH; B. Volcano plots of the depicted commonly and oppositely regulated genes (red dots - commonly regulated genes, green dots - oppositely regulated genes) selected under $-\log_{10}$ of p values (y axis), plotted against the $-\log_2$ of fold change for central CTEPH-donor, peripheral CTEPH-donor and comparison of peripheral *vs*. central CTEPH.

Several genes were regulated differentially in central and peripheral CTEPH, both in contrast to the donor. As presented in Figure 21A, MCEMP1 (Mast Cell-Expressed Membrane Protein), CKS1B (Cyclin-Dependent Kinases Regulatory Subunit 1), PRPF6 (Pre-MRNA Processing Factor 6) and HOXC6 (Homeobox C6) are upregulated in central CTEPH, while downregulated in peripheral CTEPH. Similarly, as presented in the Volcano plots, CHI3L1 and ENPP2 are among the commonly regulated genes between central and peripheral CTEPH, while MCEMP1, CKS1B, PRPF6, HOXC6 showed significantly different behaviour or are down regulated, when peripheral is compared to central CTEPH (Figure 21B).

4.2.2.2. KEGG pathway analysis of the differential gene expression of LCM vessels from explanted central and peripheral CTEPH in comparison to donor lung tissues

KEGG pathway analysis revealed enrichment of several signalling pathways, similarly in both central and peripheral CTEPH, among which increased number of differentially regulated genes are associated with metabolic pathways, pathways in cancer and PI3K-Akt signalling pathway (Figure 22A and 22B). Surprisingly, the most prominently regulated pathway, according to where the most of the regulated genes fall in, is systemic lupus erythematosus (Figure 22A). As observed from Figure 22B, the majority of the genes determined by LogFC >1 fall into metabolic pathways, being upregulated, in both, central and peripheral CTEPH. Significant portion of the genes related to cancer and PI3K-Akt are upregulated in both central and peripheral CTEPH (Figure 22B). The most affected pathways common to the one taking place in the ribosome, phagosome, followed by oxidative phosphorylation (Figure 22C and 22D). As mentioned before, the most significantly differently regulated pathway, enriched by corresponding genes is systemic lupus, followed by alcoholism and interestingly vascular smooth muscle contraction, which predominantly takes place in the peripheral part (Figure 22E).

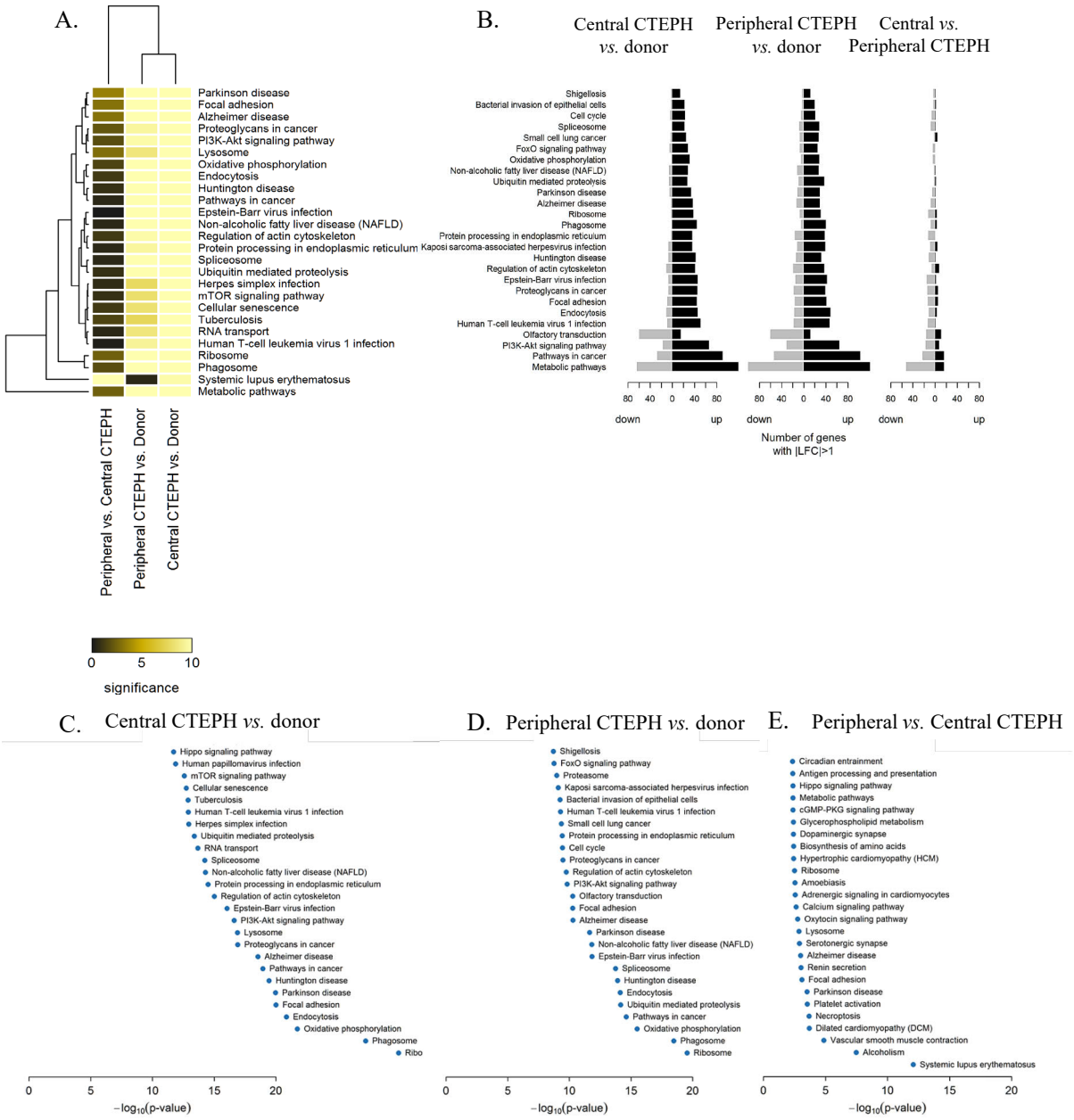

Figure 22: In silico KEGG pathway analysis of central and peripheral CTEPH in contrast to donors and their correlation A. Heatmap showing the significance (-$\log_{10}$ p-value) of the perturbation of KEGG pathways obtained from the gene set tests presenting the Top 26 regulated pathways; B. Visualization of the number and subset of up- and down- regulated genes in central CTEPH *vs.* donor, followed by peripheral CTEPH *vs.* donor and their comparison; (C-E) Individual signalling pathways regulated in C. Central CTEPH *vs.* donor; D. Peripheral CTEPH *vs.* donor; E. Peripheral *vs.* Central CTEPH.

4.3. Chapter III: Histopathological characterization of distal vessel remodelling in a case study of a patient with central (proximal) and recurrent CTEPH

4.3.1. Characterization of distal vascular lesions in central CTEPH – ink-injected case study

With the intention to assess profoundly and systematically the vascular changes taking place within centrally diagnosed CTEPH patient with the recurrent aetiology, in collaboration with Dr. Lavinia Neubert from Hannover Medical School, we performed *ex-vivo* ink injection procedure of a patient lung after transplantation (Figure 23). A 57 years old female patient, was diagnosed with lung embolism in 1998 and PEA was performed in 10/2010 and 10/2011, followed by 2 times balloon angioplasty (last session in 07/2016). She received Bosentan and Sildenafil since 01/2011, switched from sildenafil to riociguat in 04/2015. Her haemodynamic parameters were: mPAP 66 mmHg, PAP_{syst} 115 mmHg, PAP_{diast} 41 mmHg, PAWP 10 mmHg and she underwent lung transplantation in 08/2017.

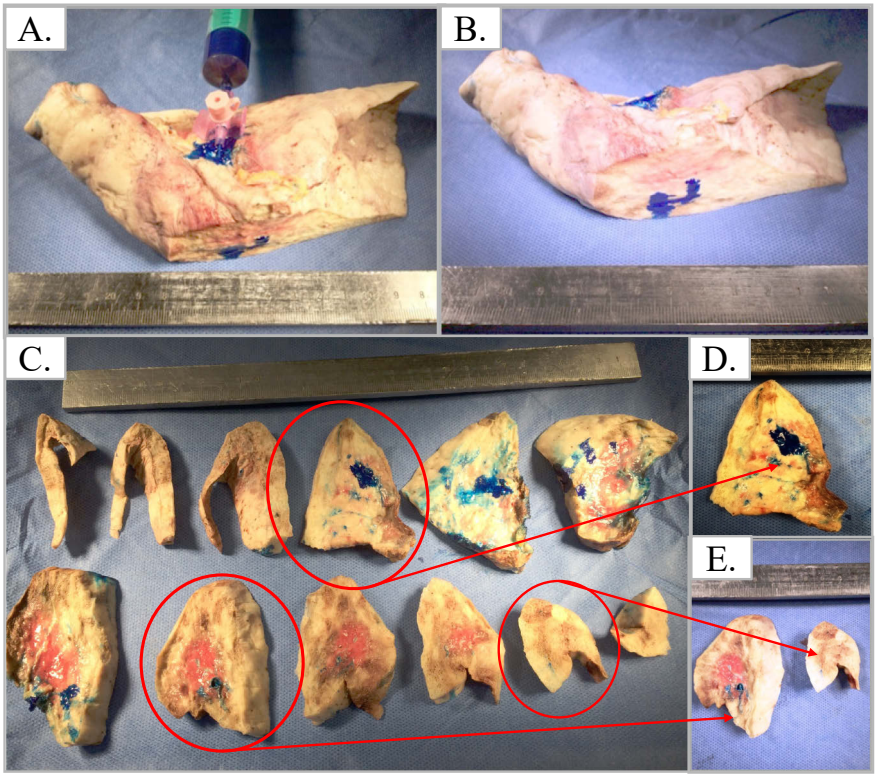

Figure 23: Labeling of pulmonary arteries through blue color in a fresh lung CTEPH explant. Fresh explant of the left lung with cannulation of the pulmonary artery at the level of the lung hilus. A. Distribution of blue color within the pulmonary arteries of the lobe; B. Distribution of blue color within the pulmonary arteries of the lobe and within serial lungs slices from basal to apical (C). Central (D) and peripheral (E) Lung slices with marked pulmonary arteries (blue).

Vascular remodelling of the macro- and micro- vasculature was assessed within areas proximal to, thromboembolism and distal to thromboembolism. The distribution of the blue ink was clearly visible at the areas proximal to thromboemboli (Figure 24A, 24B, 24D, 24E), as well presence of extensive remodelling of the pulmonary vasculature, presented by concentric intimal lesions and medial hypertrophy (Figure 24C and 24F). As observed from Figure 24G, H, and I, the area of the thromboemboli, or large, muscular arteries were affected by considerable intimal fibrosis and recanalization. Similarly, the distal to thromboemboli regions revealed existence of concentric, highly remodelled vascular lesions, characterized by intimal and medial thickening and extensive matrix deposition (Figure 24J-24O).

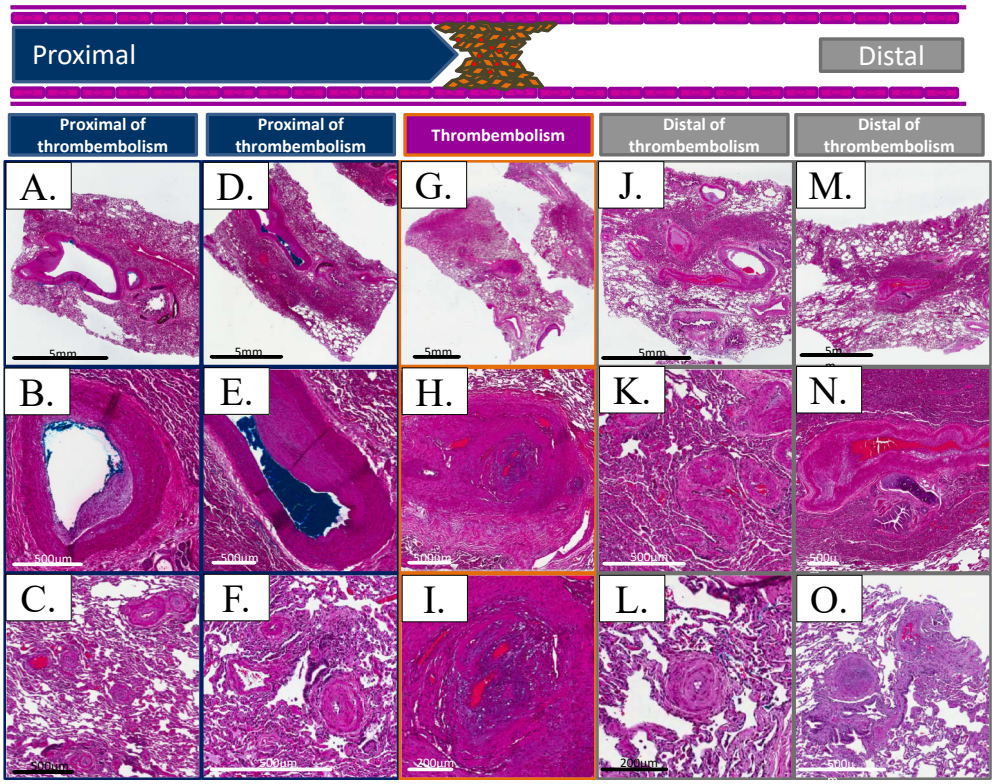

Figure 24: Thromboembolism of a pulmonary artery in a fresh lung explant of a patient suffering from chronic thromboembolic pulmonary hypertension (CTEPH). (A), (D), (G), (J), (M) show overview of lung slices taken from central to peripheral pulmonary artery with thromboembolism (G). (A) to (F) show colored lumen of artery proximal to thromboembolus and formation of concentric and plexiform lesions in the surrounded lung tissue. (G) to (I) show thromboembolus with occlusion of the vascular lumen and recanalization. (J) to (O) reveal no colored lumen of the artery distal to thrombembolus, but also formation of concentric and plexiform lesions in the surrounded lung tissue. Scale bars 5 mm (A, D, G, J, M), 500 µm (B, C, E, F, H, K, N, O) and 200 µm respectively (I, L).

4.3.1.1. Assessment of the distal medial hypertrophy in pre-thrombus, thrombus and post-thrombus area of a central and recurrent CTEPH

As presented in Figure 25, Weigert–van Gieson staining displayed severe vascular remodelling represented by intimal thickening, medial hypertrophy and adventitial stiffening in all pre-, thrombus- and post-thrombus related areas of all three groups of vessels (Group 1: d = 20-70 µm, Group 2: d = 70-150 µm and Group 3: d > 150 µm).

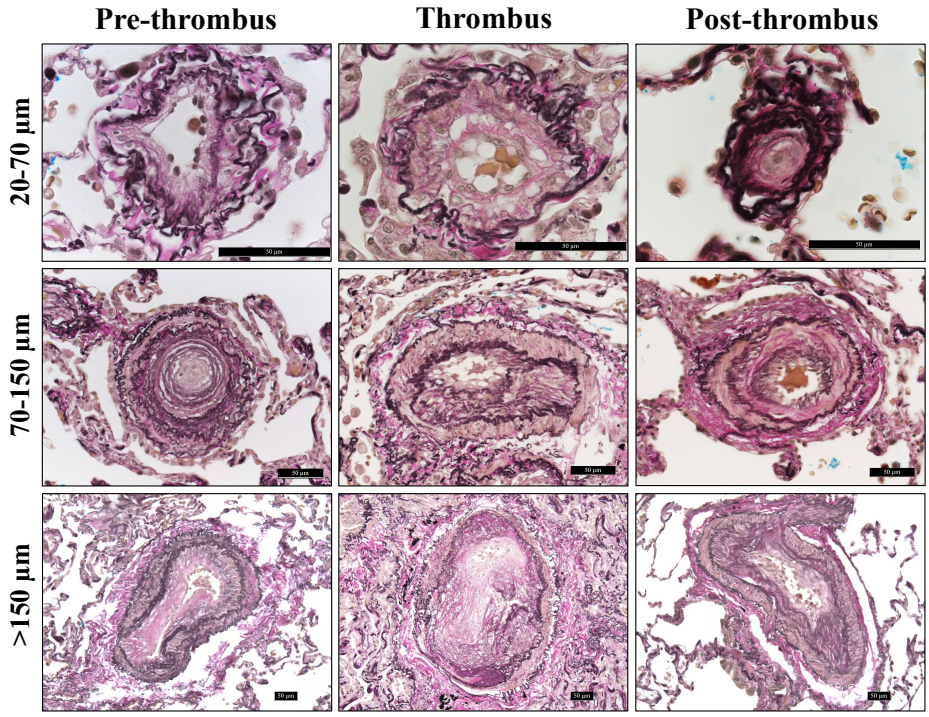

Figure 25: Visualization of severe vascular wall remodelling in pre-, thrombus and post-thrombus of case study explanted CTEPH. Weigert–van Gieson staining was applied to differentiate between the nuclei, elastic and collagen fibres and yellow-stained muscles and cytoplasm. Representative microphotographs of vessels within three groups: Group 1: d = 20-70 µm; Group 2: d = 70-150 µm and Group 3: d >150 µm. Scale bar 50 µm, n=1.

Medial wall thickness (MWT) was again assessed for the different vessel sizes of the pre-, thrombus, and post-thrombus and compared to a baseline (extracted as a mean value of MWTs from donor samples from Giessen cohort). As observed from Figure 26A, the pre-thrombus, thrombus and the post-thrombus manifest severe vascular remodelling in terms of increased MWT in comparison to the baseline. Next, the distribution of the MWT values for each individual site was similar for all the vessels, independently of the area they were taken from (Figure 26B). The distribution of the individual densities of the MWT, exhibited fairly bimodal Gaussian curve resemblance for the pre-, post- and the thrombus part itself (Figure 26C).

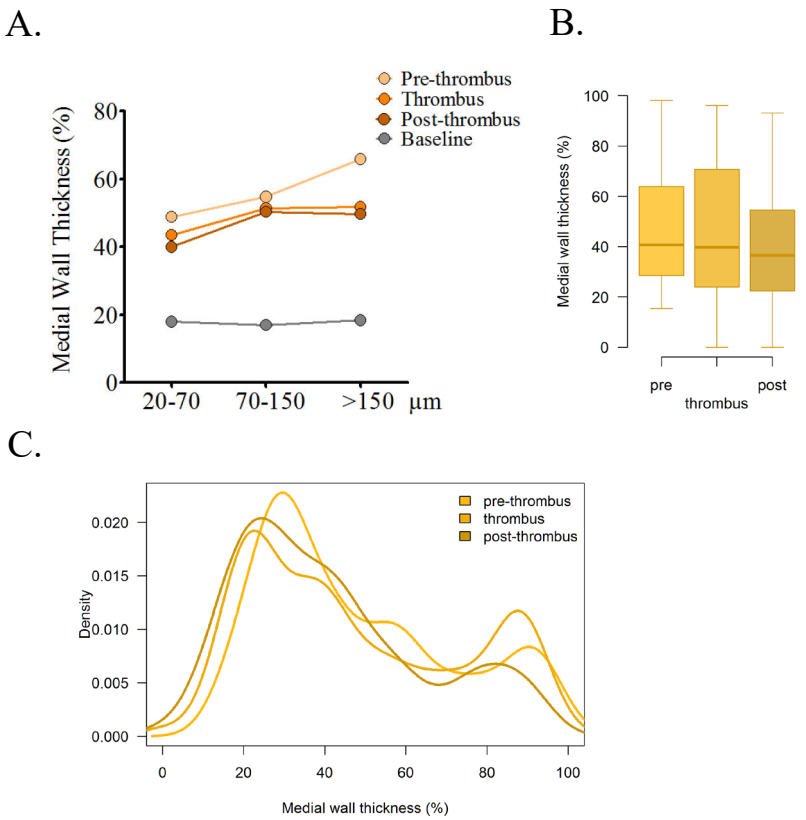

Figure 26: Quantification of the medial hypertrophy of pulmonary vessels from pre-, thrombus and post-thrombus area of explanted CTEPH lung in comparison to a mean value of 12 donor samples. A. Measurement of medial wall thickness (MWT) of pulmonary vessels is shown as a percentage for Group 1: d = 20-70 µm, Group 2: d = 70-150 µm, and Group 3: d > 150 µm; B. Boxplot of the MWT values for each part, displaying the distribution of the MWT; C. Distribution of the individual densities of MWT for vessels falling into pre-, thrombus and post-thrombus area.

4.3.1.2. Ratio neointima media evaluation in pre-thrombus, thrombus and post-thrombus area of a central and recurrent CTEPH

In addition, vascular remodelling, in terms of neointima formation suggested that vessels with diameter 20-70 µm belonging to the pre-thrombus part, revealed similar ratio as to the baseline, which was different to the ratio neointima/media of the thrombus and the post-thrombus. For the 70-150 µm and > 150 µm vessels, the ratio was similarly increased in comparison to the baseline (Figure 27A). Similarly, the pre-, thrombus-and the post-thrombus presented homogeneous distribution of the values of the ratio (Figure 27B). The distribution of the individual densities of the ratio neointima/media resembled Gaussian curve for all CTEPH sites (Figure 27C).

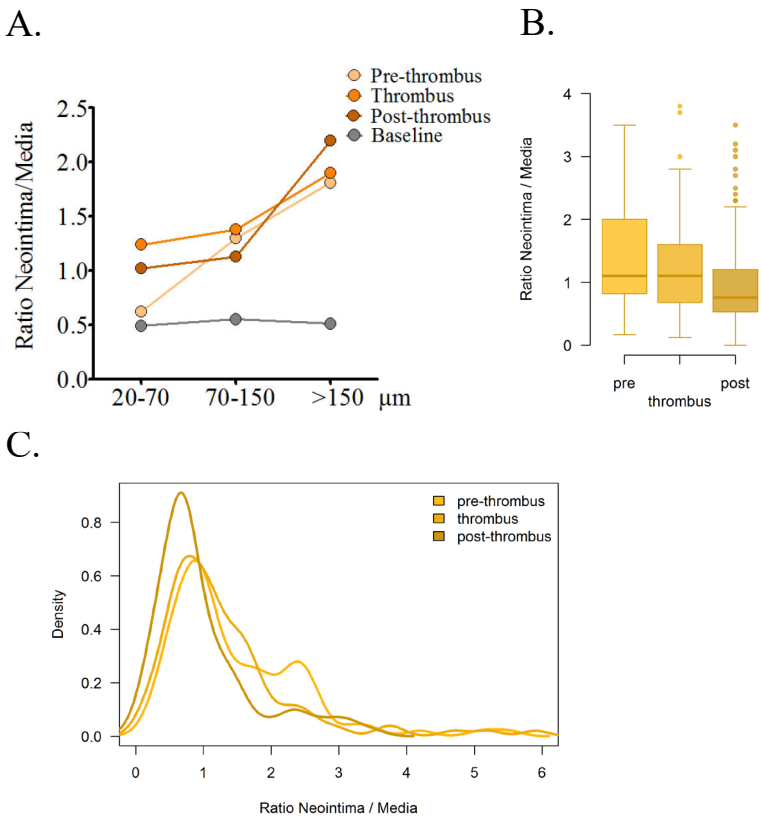

Figure 27: Computational assessment of the ratio neointima/media of pulmonary vessels from pre-, thrombus and post-thrombus area of explanted CTEPH lung in comparison to a mean value of 12 donor samples. Pulmonary vessels were classified in Group 1: d = 20-70 µm, Group 2: d = 70-150 µm, and Group 3: d > 150 µm; B. Boxplot for each part displaying the distribution of the neointima/media ratio; C. Distribution of the individual densities of the neointima/media ratio for each individual part.

4.3.1.3. Collagen deposition in pre-thrombus, thrombus and post-thrombus area of a central and recurrent CTEPH

Next, the analysis of the total collagen area of the ink-injected CTEPH lung displayed that vessels from the pre-thrombus, thrombus and the post-thrombus were characterized with extensive remodelling in terms of collagen deposition (Figure 28A). Further the evaluation of total collagen area (%) confirmed that all, the pre-thrombus, thrombus and the post-thrombus have increased collagen deposition in comparison to the baseline. The pre-thrombus had the highest value of total collagen area (%), followed by the thrombus, and the post-thrombus (Figure 28B).

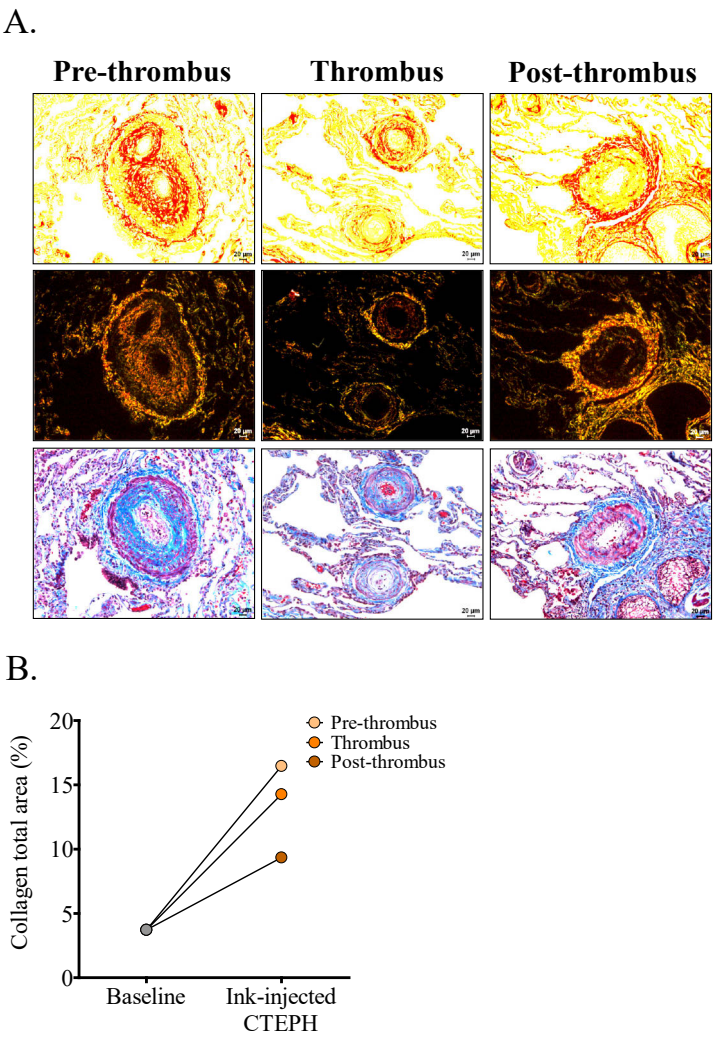

Figure 28: Visualization and quantification of total collagen area from pre-, thrombus and post-thrombus part of explanted, ink-injected CTEPH lung in comparison to a mean value of five donor samples. A. Representative microphotographs of vessels with extensive collagen deposition characteristic for severe vascular remodelling, as noticed in all, pre-, thrombus and post-thrombus; B. Measurement of the total collagen area of the respective samples in contrast to baseline. Scale bar 20 µm.

4.4. Chapter IV: Histopathological characterization of distal vessel remodelling in central and peripheral lobes from central CTEPH in comparison to donor lung tissues

4.4.1. Characterization of vascular remodelling in central and peripheral lobes from central CTEPH in comparison to donor lung tissues

Further to investigate the vascular changes within different lobes of two patients with central, yet inoperable CTEPH (one with atherosclerotic plaques in the central pulmonary arteries and the other with central thromboembolic occlusion), we again systematically evaluated the vascular remodelling intensity by assessing the medial hypertrophy, the ratio neointima/media

and the collagen deposition. The samples were kindly provided by Dr. Lavinia Neubert from Hannover Medical School.

4.4.1.1. Assessment of medial hypertrophy in central and peripheral lobes from central CTEPH in comparison to donor lung tissues

As presented in Figure 29, severe vascular remodelling was observed as represented by intimal thickening, medial hypertrophy and adventitial stiffening exhibits the vessel phenotype in both central and peripheral lobes of central CTEPH patients.

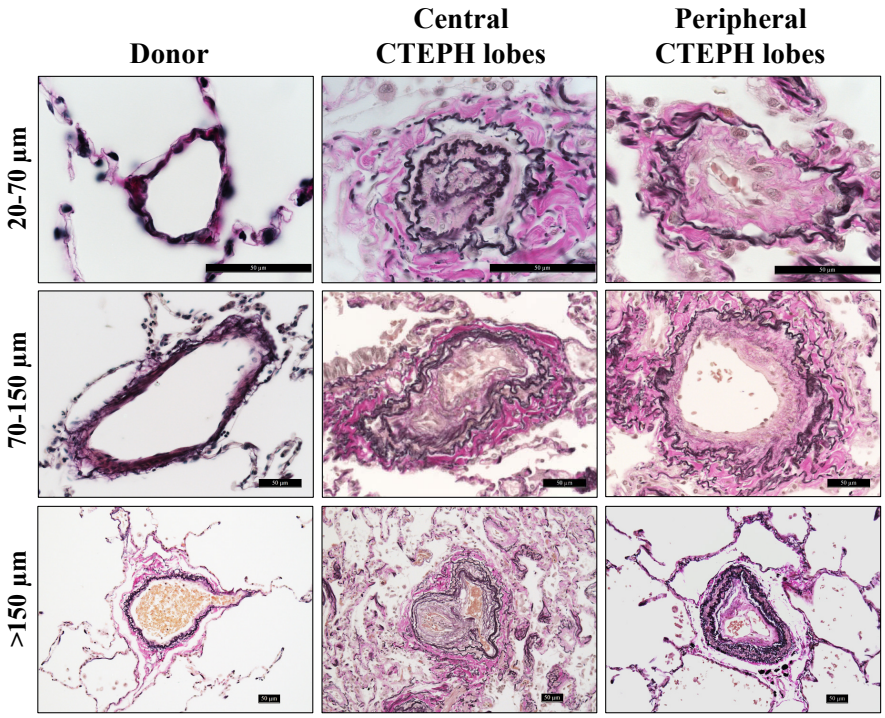

Figure 29: Visualization of severe vascular wall thickening in human lungs from central and peripheral lobes of central CTEPH and respective controls. Representative microphotographs of vessels within three groups: Group 1: d = 20-70 µm; Group 2: d = 70-150 µm and Group 3: d >150 µm. Scale bar 50 µm, n(donor) = 5, n(Central CTEPH lobes)=4, n(Peripheral CTEPH lobes)=4.

The results of the comparison of the MWT of vessels with diameter 20-70 µm showed a significant difference between the groups $F(2, 9) = 15.704$, $p < .01$). The central CTEPH lobes were having significantly higher values of MWT (43.20%; Tukey-HSD, $p < .01$). The peripheral CTEPH lobes as well, showed similar behaviour of increased MWT (43.06%; Tukey-HSD, $p < .01$), while they were not different from each other (Tukey-HSD, ns) (Figure 30A). Similarly, the results of the comparison of MWT for the group of 70-150 µm revealed a significant difference between the groups $F(2, 9) = 13.291$, $p < .01$). Central (46.96%; Dunnett, $p < .01$), as well as peripheral CTEPH lobes (44.23%; Dunnett, $p < .01$) preserved the significant increase of MWT in comparison to the donor samples and were not different from each other (Dunnett, ns) (Figure 30B). The results of the comparison of the MWT for the

vessels with d > 150 µm displayed a significant difference between the groups F(2, 9) = 12.848, p < .01). Donors were having significantly lower values with MWT of 23.06% compared to the central CTEPH lobes (40.29%; Tukey-HSD, p < .01) and peripheral CTEPH (37.17; Tukey-HSD, p < .01) which are not different from each other (Tukey-HSD, ns) (Figure 30C). The distribution of the MWT values within the central or the peripheral CTEPH lobes was similar, independently of the site where the section was taken, which were apparently different from the donor (Figure 30D). The individual densities of the MWT, showed Gaussian distribution for both central and peripheral CTEPH lobes (Figure 30E).

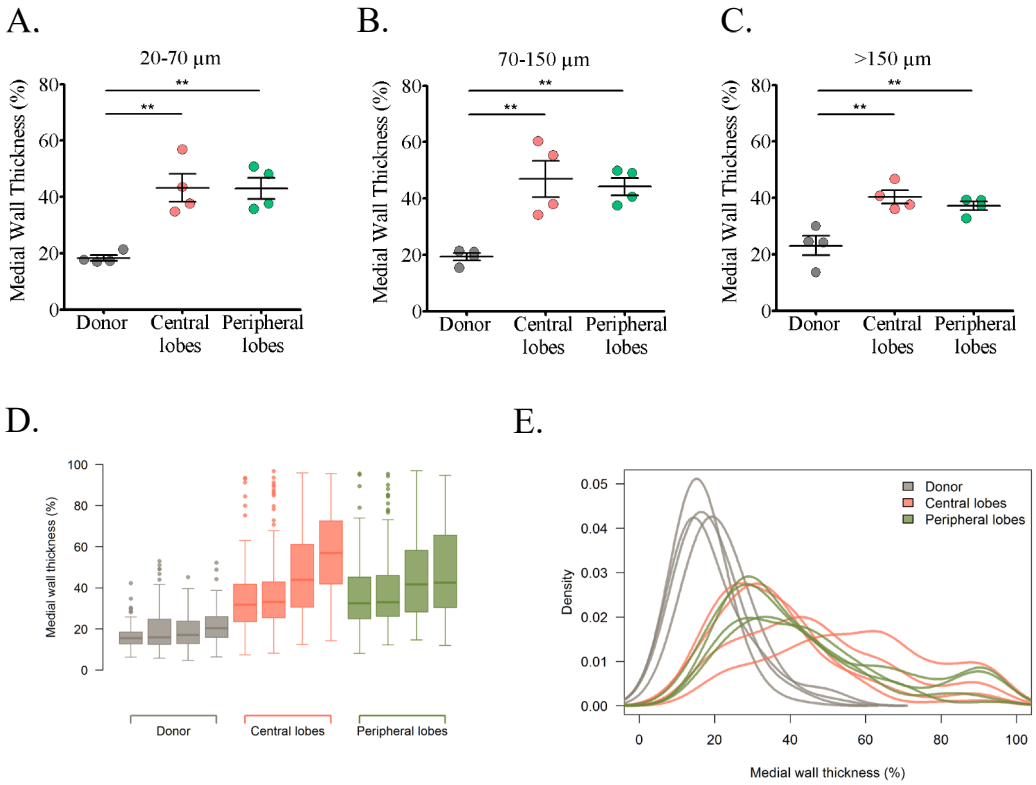

Figure 30: Medial hypertrophy quantification of donor, central and peripheral CTEPH lobes following the Weigert–van Gieson staining. Measurement of medial wall thickness (MWT) of pulmonary vessels is shown as a percentage. A. Group 1: d = 20-70 µm; B. Group 2: d = 70-150 µm; C. Group 3: d > 150 µm; D: Boxplot of individual patients displaying the distribution of the MWT; E. Distribution of the individual densities of MWT for each individual donor or patients sample. Data is represented as mean±SEM (n(donor) = 5, n(Central lobes) = 4, n(Peripheral lobes) = 4; from 2 different regions of 2 patients *p<0.05, **p<0.01, ***p<0.001)

4.4.1.2. Ratio neointima/media evaluation in central and peripheral lobes from central CTEPH in comparison to donor lung tissues

In addition, the results of the comparison of neointima/media ratio within 20-70 µm vessels showed a significant difference between the groups F(2, 9) = 44.693, p < .001). The central (0.88; Tukey-HSD, p < .001) and peripheral CTEPH lobes (0.93; Tukey-HSD, p < .001) are

exhibiting significantly higher values in comparison to the respective donors and are not different from each other (Tukey-HSD, ns) (Figure 31A). The vessels with d=70-150 µm presented a significant difference for the ratio between the groups $F(2, 9) = 28.592$, $p < .001$). The central CTEPH lobes (0.92; Tukey-HSD, $p < .001$) as well as the peripheral CTEPH (0.98; Tukey-HSD, $p < .001$) presented significantly higher values in contrast to the donors, and were not different from each other (Tukey-HSD, ns) (Figure 31B). The results of the ratio comparison of >150 µm showed a significant difference between the groups $F(2, 9) = 6.478$, $p < .05$). The post-hoc tests showed that donors exhibit significantly lower values with 0.50 compared to central CTEPH (0.88; Tukey-HSD, $p < .05$) and peripheral CTEPH (0.96; Tukey-HSD, $p < .05$) which are not different from each other (Tukey-HSD, ns) (Figure 31C).

The distribution of the ratio neointima/media values within the central or the peripheral CTEPH lobes was similar, independently of the site, which were apparently different from the donor (Figure 31D). The individual densities of the ratio, showed Gaussian distribution for both central and peripheral CTEPH lobes (Figure 31E).

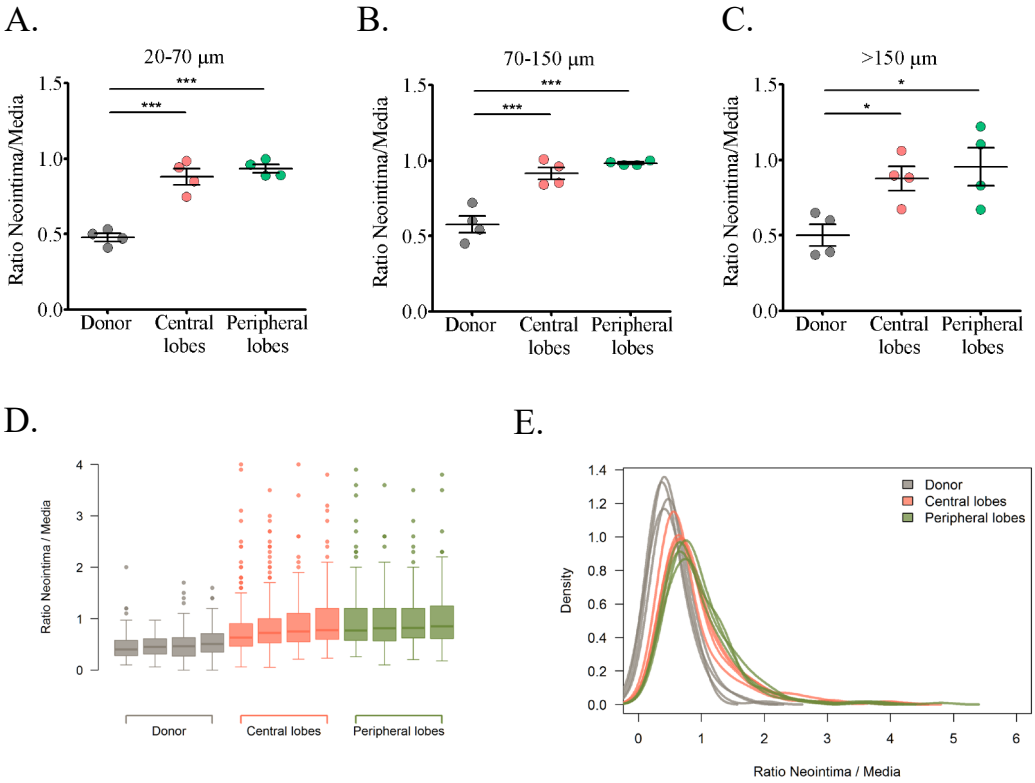

Figure 31: Computational assessment of the ratio neointima/media of pulmonary vessels from donor, central and peripheral CTEPH lung lobes. Ratio neointima/media in A. Group 1: d = 20-70 µm; B. Group 2: d = 70-150 µm; C. Group 3: d > 150 µm; D: Boxplot of individual patients displaying the distribution of the ratio neointima/media; E. Distribution of the individual densities of the ratio neointima/media for each individual donor or patients sample. Data is represented as mean±SEM (n(donor)=4, n(Central CTEPH lobes) = 4, n(Peripheral CTEPH lobes) = 4; *p<0.05, **p<0.01, ***p<0.001)n=12; *p<0.05, **p<0.01, ***p<0.001)

4.4.1.3. Collagen distribution in central and peripheral lobes from central CTEPH in comparison to donor lung tissues

As displayed in Figure 32A, increased collagen within the vascular wall was observed in both central and peripheral lobes of inoperable CTEPH. Notably, central CTEPH lobes were exhibiting significantly higher values of total collagen area (373.8%; Tukey-HSD, $p < .05$) in contrast to the respective controls. Likewise, the peripheral lobes were significantly different to donors (354.25%; Tukey-HSD, $p < .05$), while central and peripheral CTEPH were not significantly different from each other (Tukey-HSD, ns) (Figure 32B).

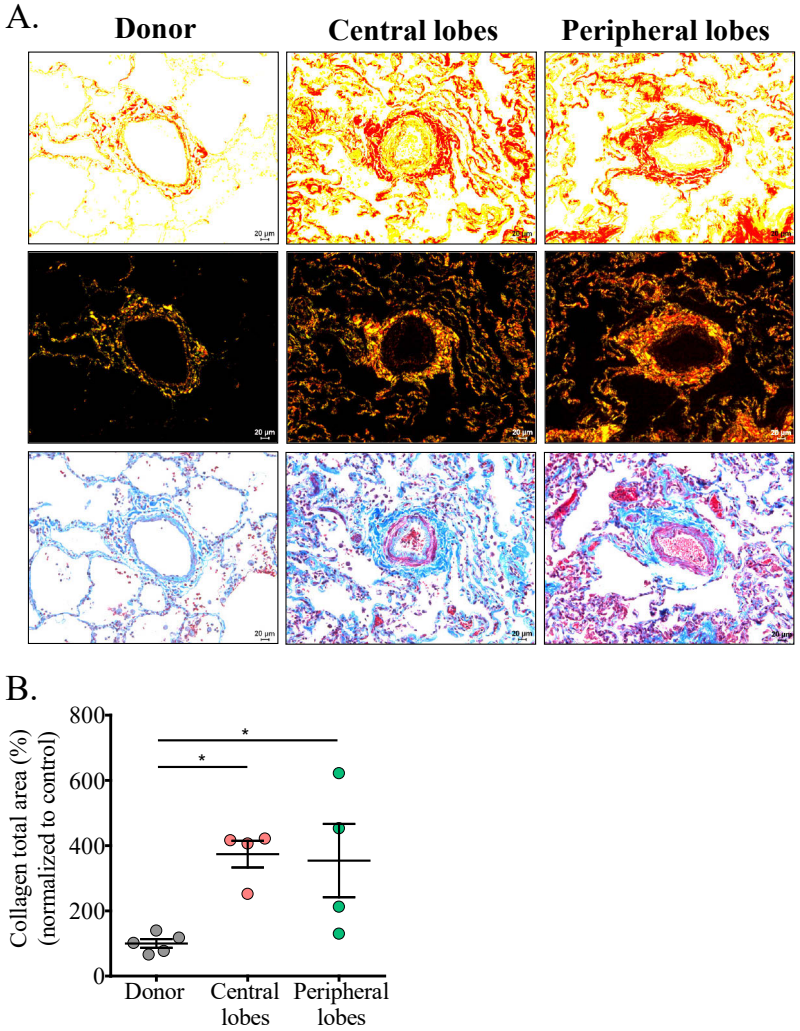

Figure 32: Visualization and quantification of total collagen area in human donor and explanted central and peripheral CTEPH lobes. A. Representative microphotographs of vessels with extensive collagen deposition characteristic for severe vascular remodelling, as noticed in both, central and peripheral CTEPH samples, in contrast to donors B. Measurement of the total collagen area in the respective samples. Scale bar 20 µm. Data is expressed as a percentage of donor controls and represented as mean±SEM (n(donor) = 5, n(Central CTEPH lobes) = 4, n(Peripheral CTEPH lobes) = 4; *p<0.05, **p<0.01, ***p<0.001)

4.5. Chapter V: Histopathological characterization of distal vessel remodelling in sarcoma-CTEPH patients in comparison to donors

4.5.1. Characterization of vascular remodelling in sarcoma-CTEPH patients in comparison to donors

To further confirm the vascular remodelling distribution, lung biopsies of patients who developed pulmonary hypertension (CTEPH) due to sarcoma and underwent PEA surgery were used, in order to evaluate the degree of vascular remodelling and whether their histopathological profile will resemble the findings describes so far. We evaluated the MWT, the ratio neointima/media and the collagen deposition from the lung biopsies of these patients.

4.5.1.1. Assessment of medial hypertrophy in sarcoma-CTEPH patients in comparison to donors

At first, sarcoma CTEPH samples were similarly visualized as before, and vessels were categorized in 3 groups. Increased vessel remodelling was noticed within all vessel sizes (Figure 33).

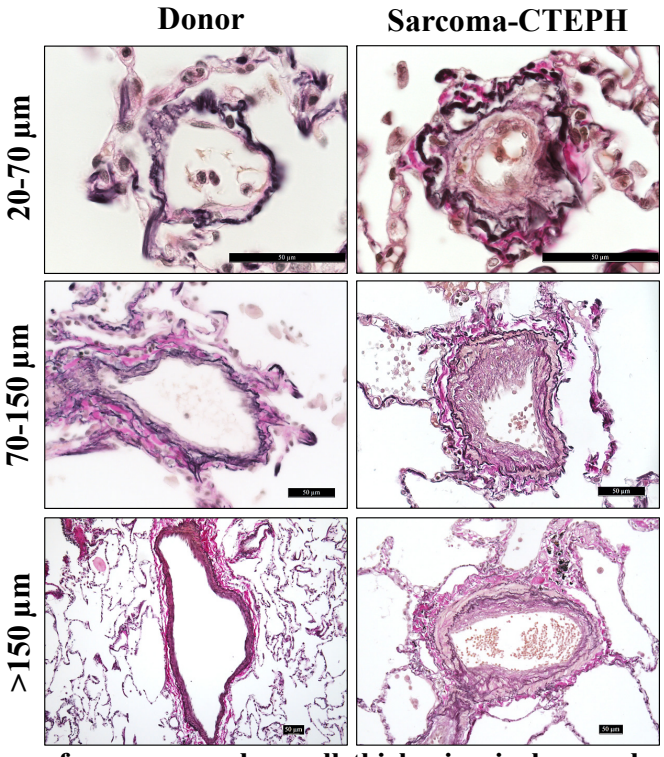

Figure 33: Visualization of severe vascular wall thickening in human lungs sarcoma-CTEPH patients and respective controls. Representative microphotographs of vessels within three groups: Group 1: d = 20-70 µm; Group 2: d = 70-150 µm and Group 3: d >150 µm. Scale bar 50 µm, n = 4.

The results are compared using one-sided t-tests for each condition (20-70 µm, 70-150 µm, >150 µm). The results of the comparison of 20-70 µm for the MWT, revealed a significant higher MWT of the Sarcoma-CTEPH with 39.10% in contrast to the donor samples with

18.32% (T(6) = -4.002, p < .01) (Figure 34A). The results of the comparison of 70-150 µm showed a significant difference (T(6) = -3.593, p < .01) between donors (19.31%) and sarcoma (40.50%) (Figure 34B). The results of the comparison of >150 µm regarding MWT displayed a significant increase of MWT in sarcoma patients (40.44%) in comparison to the respective donors (23.06%) (T(6) = -2.700, p < .05) (Figure 34C).

The distribution of the MWT values within the sarcoma patients is higher than the donors, (Figure 34D). The individual densities of the MWT, showed a shifted Gaussian distribution in comparison to the donors (Figure 34E).

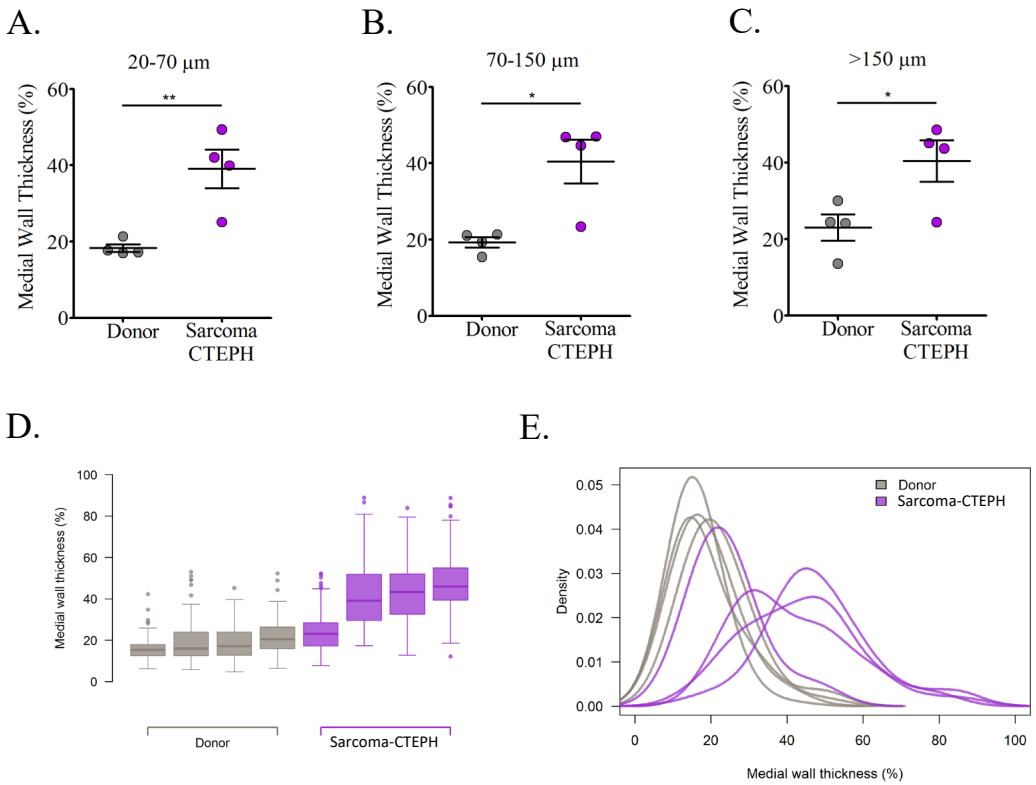

Figure 34: Medial hypertrophy quantification of donor and sarcoma- CTEPH lobes following the Weigert–van Gieson staining. Measurement of medial wall thickness (MWT) of pulmonary vessels is shown as a percentage. A. Group 1: d = 20-70 µm; B. Group 2: d = 70-150 µm; C. Group 3: d > 150 µm; D: Boxplot of individual patients displaying the distribution of the MWT; E. Distribution of the individual densities of MWT for each individual donor or patients sample. Data is represented as mean±SEM; n=4 (*p<0.05, **p<0.01, ***p<0.001).

4.5.1.2. Ratio neointima/media evaluation in sarcoma-CTEPH patients in comparison to donors

Further, the evaluation of neointima/media ratio of 20-70 µm sized vessels showed a significant difference (T(5) = -8.803, p < .001) between donors (0.48) and sarcoma (0.78) (Figure 35A). Similarly, the results of the comparison of 70-150 µm revealed a significantly higher ratio in sarcoma (0.87) in comparison to the ratio neointima/media of donors (0.58) (T(5) = -2.234, p

< .05) (Figure 35B). The results of the comparison of >150 µm showed a significant difference (T(5) = -5.688, p < .01) between donors (0.50) and sarcoma (1.16) (Figure 35C).

The distribution of the ratio neointima/media values in the sarcoma patients is higher than the donors (Figure 35D). The individual densities of the MWT, showed a Gaussian distribution in comparison to the donors (Figure 35E).

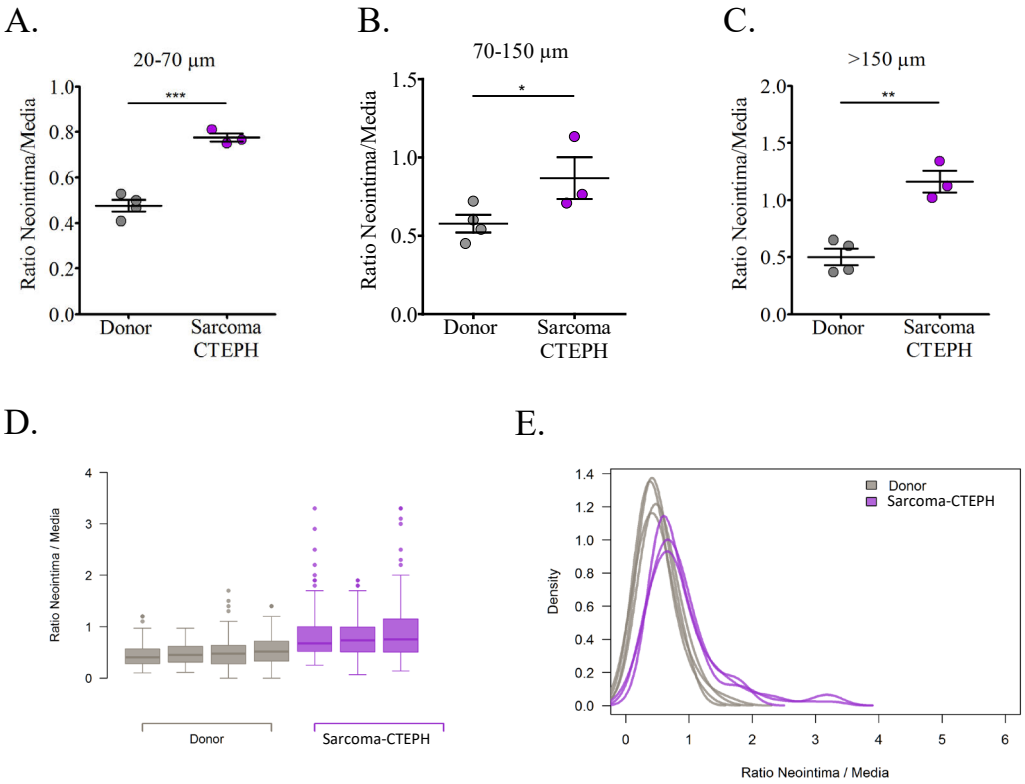

Figure 35: Computational assessment of the ratio neointima/media of pulmonary vessels from donor and sarcoma-CTEPH patients. Ratio neointima/media in A. Group 1: d = 20-70 µm; B. Group 2: d = 70-150 µm; C. Group 3: d > 150 µm; D: Boxplot of individual patients displaying the distribution of the ratio neointima/media; E. Distribution of the individual densities of the ratio neointima/media for each individual donor or patients sample. Data is represented as mean±SEM; (n(donors)=4), n(sarcoma)=3(*p<0.05, **p<0.01, ***p<0.001).

4.5.1.3. Collagen distribution in sarcoma-CTEPH patients in comparison to donors

Both staining methods, Sirius red and Trichrome, revealed increased collagen deposition in sarcoma CTEPH patients (Figure 36A). The quantification of the total collagen area confirmed the significant increase in sarcoma CTEPH (313.64%) in comparison to the respective donors (T(5) = 2.802, p < .05) (Figure 36B).

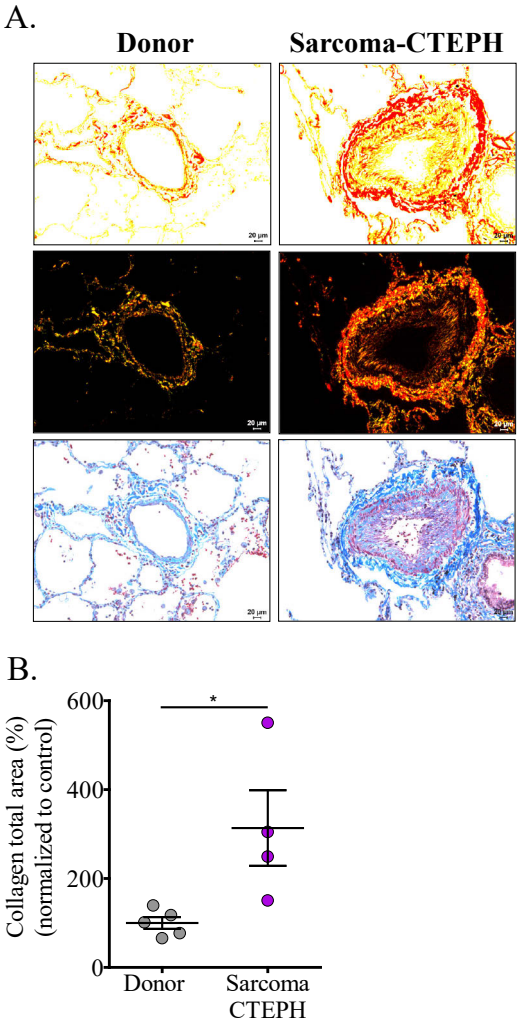

Figure 36: Visualization and quantification of total collagen area in human donor and Sarcoma CTEPH. A. Representative microphotographs of vessels with extensive collagen deposition characteristic for severe vascular remodelling; B. Measurement of the total collagen area in the respective samples. Scale bar 20 µm. Data is represented as mean±SEM; n(donor)=5; n(sarcoma)=4 (*p<0.05, **p<0.01, ***p<0.001).

4.6. Chapter VI: Histopathological and molecular characterization of CTEPH patients undergoing pulmonary endarterectomy (PEA)

Patients undergoing PEA are at most patients with fibrotic vessel obstuctions at central (proximal) level, including the segmental and subsegmental level (distal to the thromboemboli). Experienced centres, depending on the diagnostic tests, are further able to evaluate the types of lesion at the distal level and characterize them as patent (stenotic or non-completely occluded) and completely occluded.

4.6.1. Structural and cellular evaluation of PEA biorepository form CTEPH with ongoing course of the disease

Histopathological changes were comprehensively studied in samples from PEA, being distinguished as central (proximal) fibrous tissue and distal patent (spenotic, non-completely occluded) and completely occluded fibrous tissue and compared to the respective controls (Figure 37). In these samples, we phenotyped the vascular changes in terms of vascularization and collagen content, followed by microarray–based approach of genome wide expression profiling.

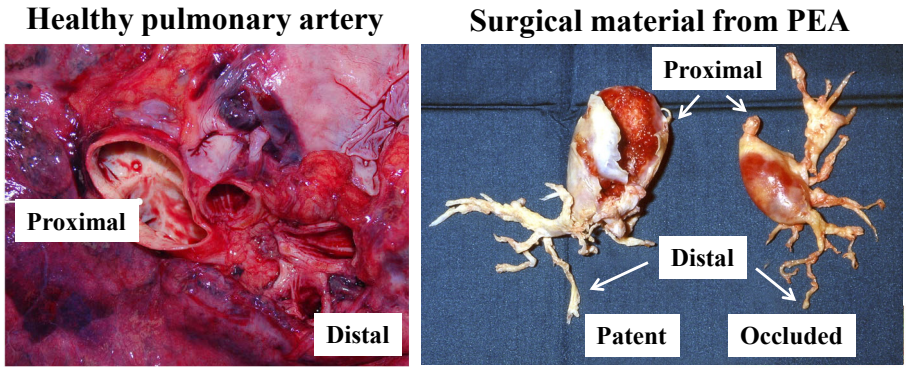

Figure 37: Representative images of healthy pulmonary artery and surgical material from PEA. Healthy main pulmonary artery and arteries at subsegmental/distal level (left) and biorepository from PEA marked with proximal material as well as distal patent and distal completely occluded tissue (right).

4.6.2. Recanalization in proximal and distal PEA biorepository

In CTEPH, the major vessel obstruction is a result of fibrotic organization of the thrombus, which in some cases affects the distal arteries in similar extent. Thus, in order to get an overview of the tissue phenotype, paraffin embedded PEA tissue from proximal as well distal patent and completely occluded was evaluated.

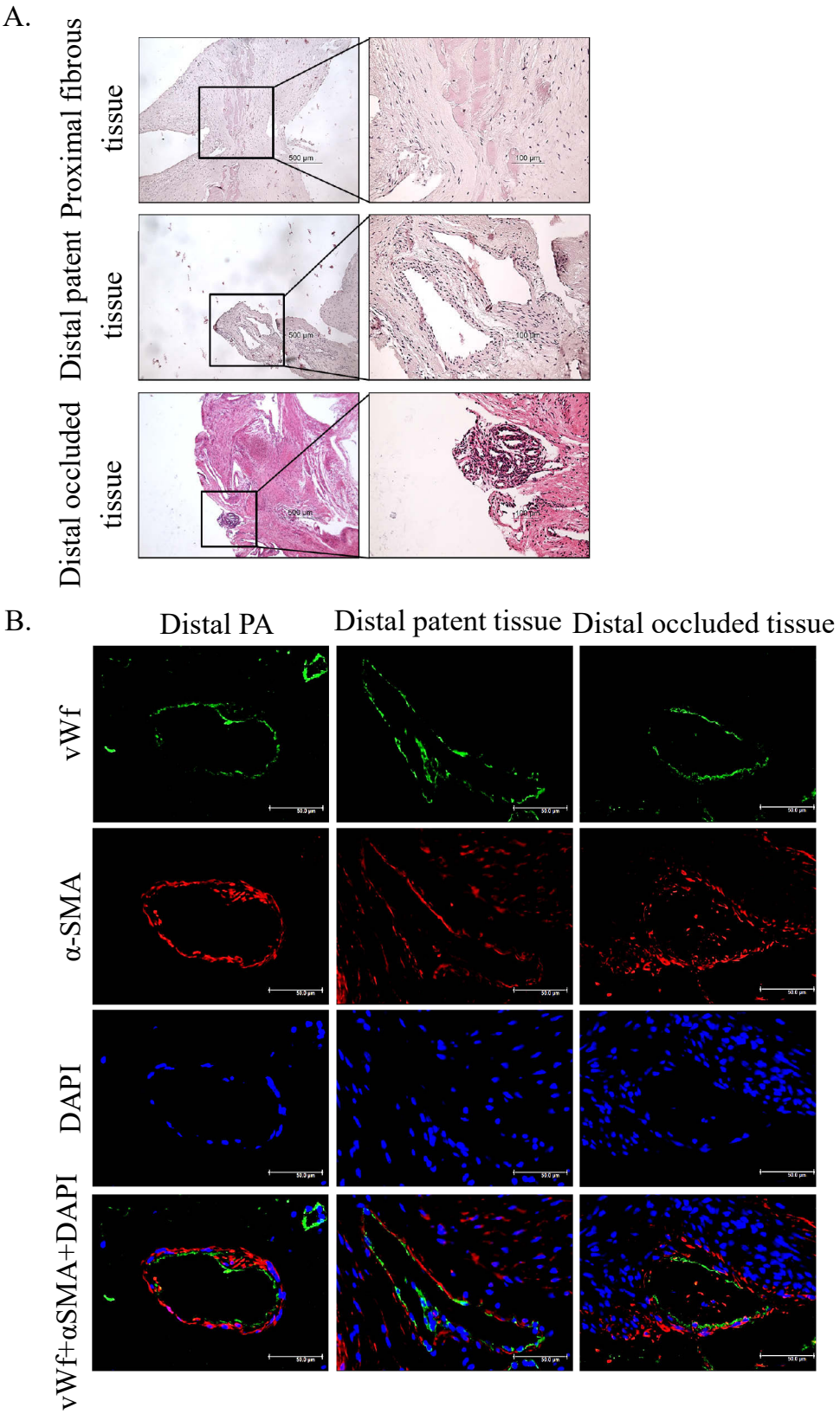

Figure 38: Proximal and distal PEA biorepository with recanalized regions. A. H&E staining of proximal and distal fibrous tissue. B. Evident recanalization was assessed by vWf (green), α-SMA (red), DAPI (blue) in distal patent and occluded tissue in comparison to distal pulmonary artery (PA). Scale bar 50µm (n=3).

The proximal endarterectomised tissue mainly resembled fibrinous structures with poor cellular composition. Vessel-like structures were observed in both distal patent and distal completely occluded tissue stained by H&E, may be due to extensive recanalization in the distal PEA tissue (Figure 38A). The recanalized regions were next confirmed to be von Willebrand factor (vWf) and α-smooth muscle actin (α-SMA) positive staining (Figure 38B).

4.6.3. Deposition of soluble and insoluble collagen in proximal and distal PEA biorepository

In order to characterize and compare the deposited collagen in the proximal and the distal (patent and occluded) fibrous tissue, a histological and biochemical evaluation was conducted employing Trichrome staining and Sircol assay (Figure 39).

As observed from Figure 39A the proximal fibrous tissue, exhibits extensive collagen deposition (in blue) and some fresh thrombi (in red), as well as poor cellular composition in comparison to the respective control. The distal patent and completely occluded fibrous tissue are as well collagen enriched, and to a certain extent with higher cellular composition of spindled shape cells, randomly distributed or in a network forming recanalized, vessel-like structures (Figure 39B).

When assessing the soluble collagen, from central and both distal (peripheral), patent or completely occluded tissue, in contrast to their respective controls, the results show a significant difference between the groups $F(4, 34) = 2.989$, $p < .05$). The post-hoc tests showed that the central fibrous tissue exhibits significantly lower amount of soluble collagen in comparison to the control proximal pulmonary artery (Dunnett, $p < .05$), while distal pulmonary artery is not different to distal patent (Dunnett, ns) and distal occluded (Dunnett, ns) as well as distal patent is not different to distal occluded (Dunnett, ns) (Figure 39C).

The insoluble collagen measurements showed a significant difference between the groups $F(4, 32) = 4.893$, $p < .01$). Although, the post-hoc tests revealed that the amount of insoluble collagen in the central fibrous tissue is not significantly different to the collagen in the proximal pulmonary artery (Tukey, ns), the insoluble collagen in the distal occluded tissue is significantly higher than in the distal pulmonary artery (Tukey, $p < .05$), while not different to distal patent tissue (Tukey, ns). Distal patent and distal completely occluded tissues were not different to each other (Tukey, ns) (Figure 39D).

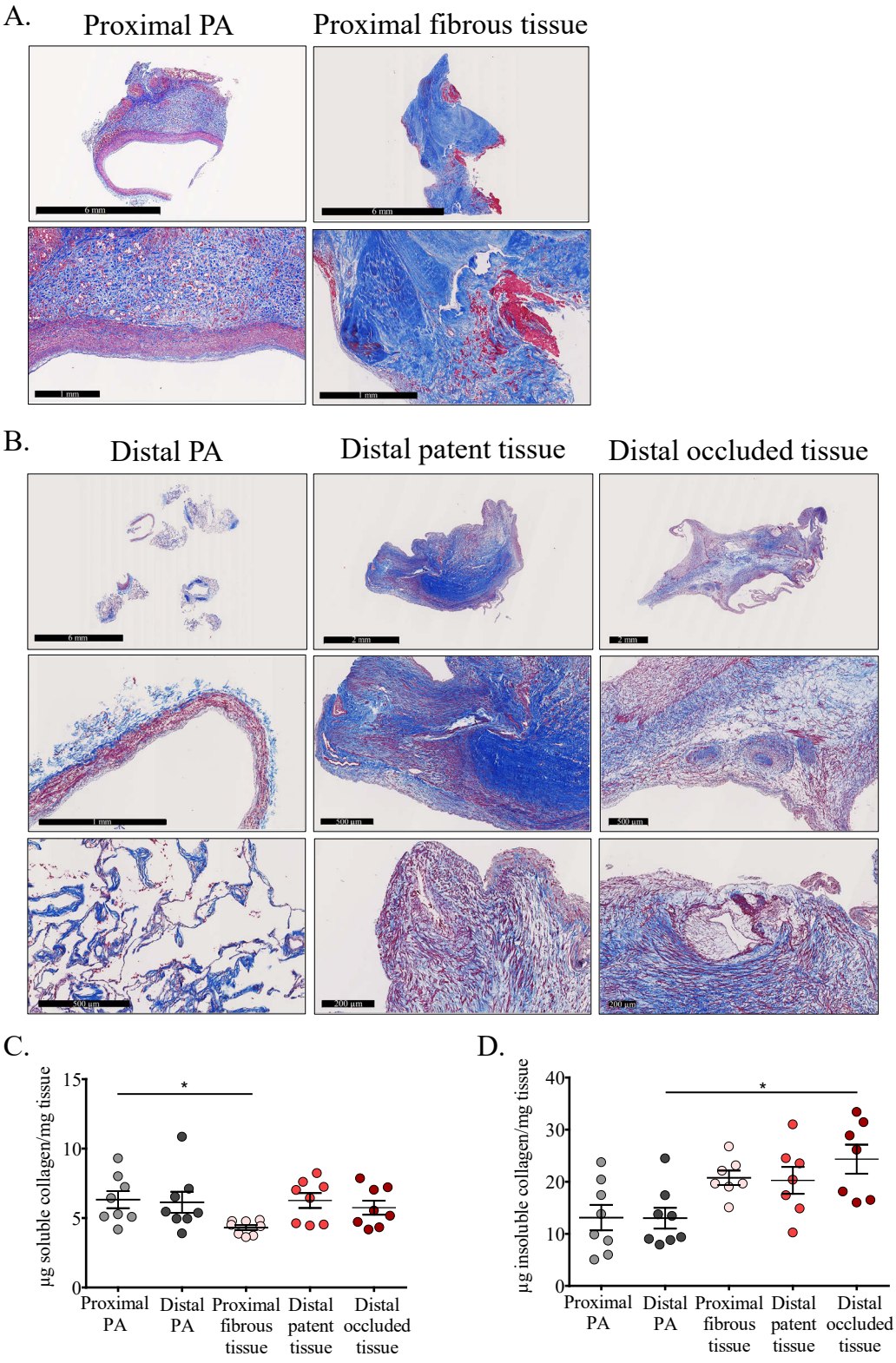

Figure 39: Characterization of the deposited collagen in PEA biorepository. A. Trichrome staining of proximal heathy pulmonary artery and proximal fibrous PEA tissue; B. Trichrome staining of distal heathy pulmonary artery and distal patent and fibrous PEA tissue; C. Quantification of the soluble collagen in PEA extracted tissue and respective controls; D. Quantification of the insoluble collagen in PEA tissue and respective controls; n=8. Data are represented as mean±SEM (*p<0.05, **p<0.01, ***p<0.001).

4.6.4. Genome wide expression profiling of proximal and distal PEA material

To investigate and compare the site-specific differential gene expression of proximal and distal stenotic and distal completely occluded biorepository, we performed microarray–based approach of genome wide expression profiling from these samples and their corresponding controls, including the pre-thrombus affected (PEA) pulmonary artery.

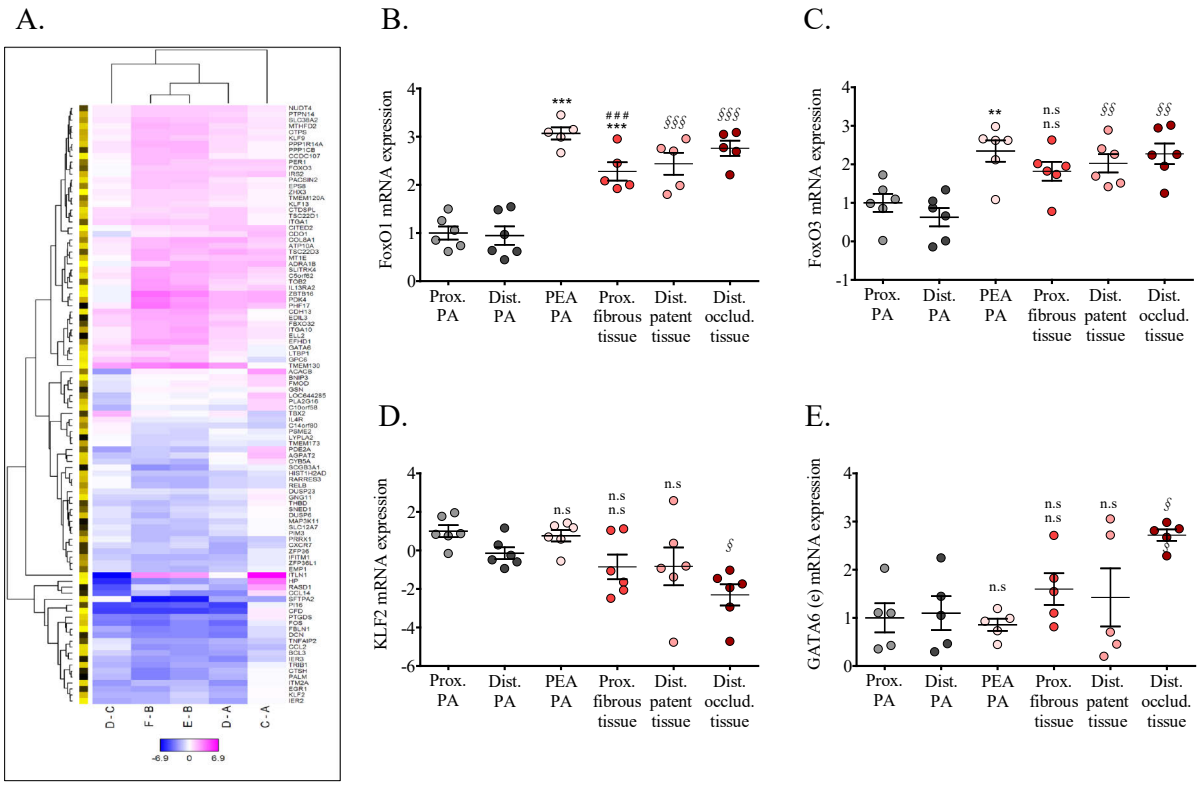

A. Proximal pulmonary artery; B. Distal pulmonary artery; C. PEA pulmonary artery;
B. D. Proximal fibrous tissue; E. Distal patent tissue; F. Distal occluded tissue

Figure 40: Gene regulation patterns of central, patent and completely occluded PEA repository in comparison to their respective contols. A. Heatmap of the top 100 differentially regulated genes selected by F value. Blue indicates relatively low expression, while red relatively high expression; mRNA expression of: B. FoxO1; C. FoxO3; D. KLF2; E. GATA6; n=6; Data are represented as mean±SEM (*p<0.05, **p<0.01, ***p<0.001 versus proximal PA; §p<0.05, §§p<0.01, §§§p<0.001 versus distal PA; $^{\#}$p<0.05, $^{\#\#}$p<0.01, $^{\#\#\#}$p<0.001 versus PEA PA).

As demonstrated in the heatmap, in both proximal and distal PEA material, similar as well as differential regulation of subset of genes was observed, when compared to the corresponding controls (Figure 40A). Importantly, microarray analysis suggests deregulation of several important transcription factor networks in the distal PEA tissue, including FoxO1 and 3, KLF2 and GATA6. Further on, we confirmed the results from the screening by real-time PCR.

As noticed from Figure 40B, for the FoxO1 gene expression, there was a significant difference between the groups $F(5, 26) = 27.633$, $p < .001$). FoxO1 was significantly upregulated in the

proximal fibrous tissue in comparison to the proximal (control) pulmonary artery (Tukey, $p < .001$). Furthermore, the PEA pulmonary artery was exhibiting extensive upregulation of FoxO1 in comparison to the control pulmonary artery (Tukey, $p < .001$). With regard to the distal compartment, FoxO1 expression in the distal patent tissue was significantly upregulated in contrast to the control distal pulmonary artery (Tukey, $p < .001$) as well as in the distal completely occluded tissue (Tukey, $p < .001$). FoxO1 expression in the distal patent and distal completely occluded were not significantly different to PEA pulmonary artery (Tukey, ns).

Next, we evaluated the FoxO3 mRNA expression levels in both proximal and distal PEA in contrast to their corresponding controls. The results showed a significant difference between the groups $F(5, 30) = 8.006$, $p < .001$). The expression of FoxO3 in the control pulmonary artery was not significantly different to proximal fibrous tissue (Tukey, ns), while it was significantly different to PEA pulmonary artery (Tukey, $p < .01$). The FoxO3 expression in the proximal fibrous tissue was not significantly changed to PEA pulmonary artery (Tukey, ns). FoxO3 levels were significantly upregulated in distal patent (Tukey, $p < .01$) as well as to distal completely occluded (Tukey, $p < .01$) tissue, in comparison to the corresponding control (Figure 40C).

When KLF2 was evaluated in terms of mRNA expression in both proximal and distal fibrous tissue, the results revealed a significant difference between the groups $F(5, 30) = 4.545$, $p < .01$). The KLF2 expression in the proximal fibrous tissue was not significantly regulated in comparison to the control pulmonary artery (Dunnett, ns) and PEA pulmonary artery to the proximal fibrous tissue (Dunnett, ns). The mRNA expression of distal patent tissue was not significantly different to the respective control (Dunnett, ns), but KLF2 was significantly upregulated in the distal occluded tissue (Dunnett, $p < .05$) (Figure 40D).

On the other hand, the mRNA expression profiling of embryonic GATA6 revealed a significant difference between the groups $F(5, 24) = 3.861$, $p < .05$). The GATA6 mRNA expression of the proximal fibrous tissue was not significantly changed in contrast to the control pulmonary artery (Tukey, ns) as well as to PEA pulmonary artery (Tukey, ns). Within the distal part, we haven`t observed significant changes in distal patent (Tukey, n.s.), but a significant upregulation of GATA6 in the distal occluded tissue (Tukey, $p < .05$) in contrast to the respective controls (Figure 40E).

4.7. Chapter VI: Chitinase-3-like-1 (CHI3L1), expression and their functional effects on vascular cells

4.7.1. Screening of CHI3L1 expression in donor, CTEPH and IPAH patients and their basal expression in human vascular and tumour lung cells

As an initial step, in order to confirm the results of the microarray screening and to better understand the regulation of CHI3L1 in the pathobiology of CTEPH, the expression pattern was evaluated in frozen lung sections subjected to laser capture microdissection (LCM) of pulmonary vessels, followed by RNA isolation and qPCR (Figure 41A). The results of the comparison of CHI3L1 revealed a significant difference between the groups $F(2, 15) = 4.539$, $p < .05$). The post-hoc tests showed that CTEPH LCM samples are presenting a significant upregulation of CHI3L1 expression ($\Delta Ct=3.05$; Tukey-HSD, $p < .05$), in comparison to the respective donors; while the IPAH samples were not significantly different to the donors ($\Delta Ct=1.22$; Tukey-HSD, ns), nor in comparison to CTEPH (Tukey-HSD, ns).

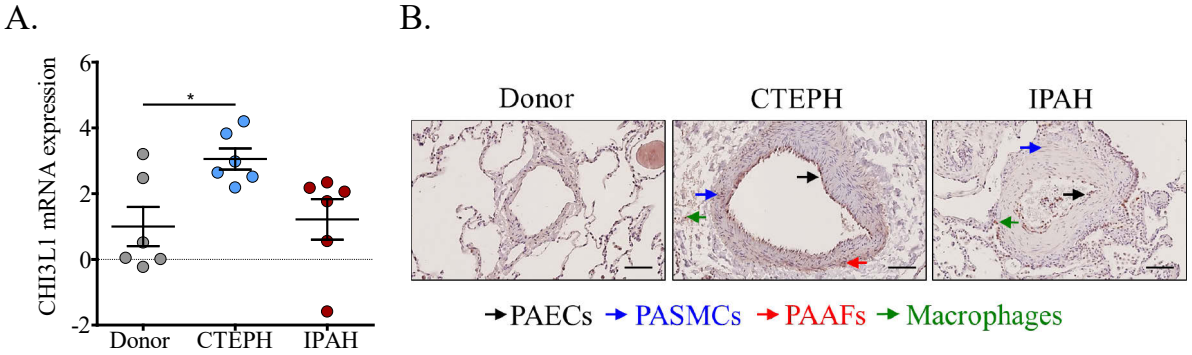

Figure 41: CHI3L1 expression in pulmonary vessels of donors, CTEPH and IPAH patients. A. mRNA expression analysis of CHI3L1 by qPCR. B. Representative immunohisto-microphotographs of human lung sections stained with CHI3L1 (dark brown). Scale bar: 20µm. Data is expressed as ΔCt, normalized to the donors and represented as mean±SEM (n=6; *p<0.05, **p<0.01, ***p<0.001).

The immunohistological staining showed a predominant localization of CHI3L1 in PAECs, PASMCs, macrophages and partly in the adventitia (PAAFs) of CTEPH pulmonary vessels as comapred to donors (Figure 41B). Expression of CHI3L1 was noticable in some IPAH patients as well.

Furthermore, when evaluating the basal mRNA expression, lung pericytes showed the highest abundance of CHI3L1, followed by PASMCs and PAAFs. The pulmonary microvascular ECs (hPMECs) presented the lowest mRNA levels of CHI3L1 among the tested cell types (Figure 42A). In contrast to the mRNA expression, CHI3L1 protein levels are highest in A549 tumour

cells, while PASMCs and PAAFs are presenting the lowest level of CHI3L1 protein expression (Figure 42B and 42C).

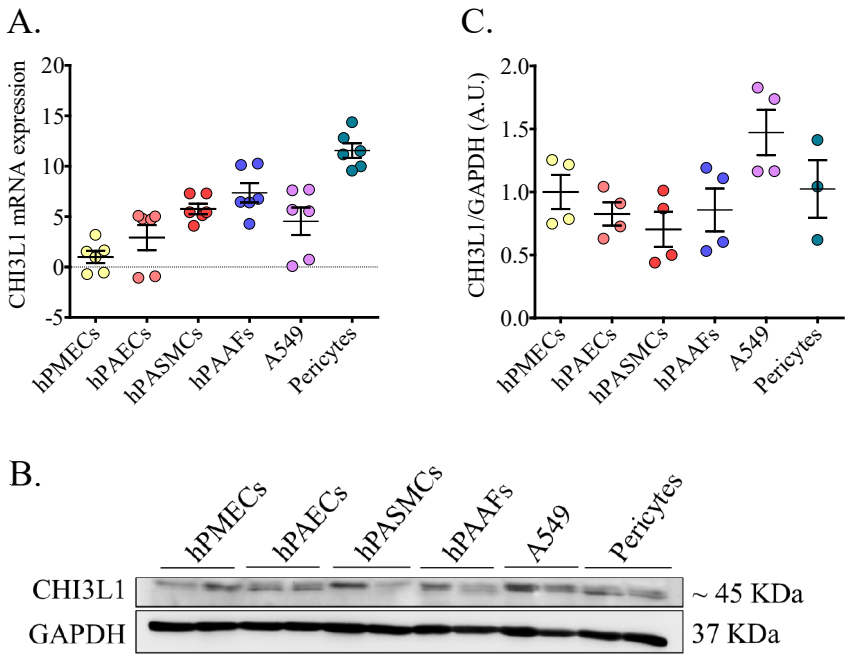

Figure 42: Evaluation of CHI3L1 basal mRNA and protein expression in human vascular and tumour lung cells. A. mRNA expression levels of CHI3L1 in human PMECs, PAECs, PASMCs, PAAFs, A549 and lung pericytes (n=3$_{\text{biological replicate}}$; n=2$_{\text{experimental replicate}}$); B. Representative Western blot image of protein levels of CHI3L1 in the listed cell types; C. Densitometry of protein levels of CHI3L1 (n=4, lung pericytes n=3). GAPDH was used as a loading control. Data is expressed as ΔCt (mRNA) or A.U. (proteins) and normalized to the expression of hPMECs.

4.7.2. CHI3L1 expression in human naïve (M0) and polarized-activated (M1 and M2) macrophages

To demonstrate whether the resting or activated macrophages will convey differential CHI3L1 mRNA and protein expression, their generation and polarization was conducted from peripheral blood mononuclear cells employing the protocols established in the lab of Dr. Rajkumar Savai. In order to compare the CHI3L1 levels in M0, M1 and M2 macrophages, an ANOVA is conducted. The results indicated a significant difference ($F(2, 18) = 4.629$, $p < .05$) and showed that M2 (anti-inflammatory) macrophages exhibited significantly lower CHI3L1 mRNA expression with ΔCt=-0.15 compared to M0 (Tukey-HSD, $p < .05$), while M1 (pro-inflammatory) macrophages were not presenting significant difference in CHI3L1 expression in contrast to the M0 macrophages (0.69; Tukey-HSD, ns). M1 and M2 macrophages were not significantly different from each other (Tukey-HSD, ns) in terms of CHI3L1 mRNA expression (Figure 43A).

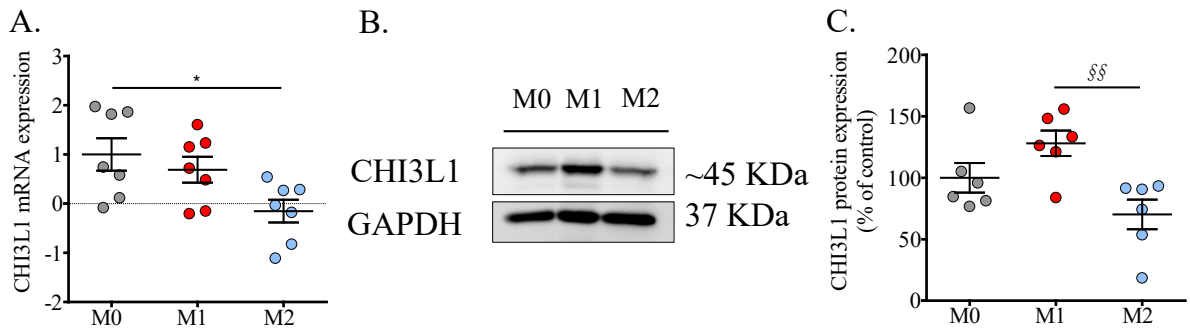

Figure 43: Evaluation of CHI3L1 basal mRNA and protein expression in human naïve (M0) and polarized (M1, M2) macrophages. A. mRNA expression levels of CHI3L1 in human macrophages normalized to M0 (n=7); B. Representative Western blot image of protein levels of CHI3L1 in the respective groups; C. Densitometry of protein levels of CHI3L1 (n=6). GAPDH was used as a loading control. mRNA data is expressed as ΔCt, protein level data are expressed as percentage of control (M0). Data are represented as mean±SEM (*p<0.05, **p<0.01, ***p<0.001; ; §p<0.05, §§p<0.01, §§§p<0.001 versus M1).

The results of the comparison of CHI3L1 protein levels in M0, M1 and M2 macrophages, indicate a significant difference ($F(2, 15) = 6.297$, $p < .05$). The post-hoc tests showed that M2 macrophages were having a significantly lower protein level with 70.21% compared to M1 (128.06%; Tukey-HSD, $p < .01$), but not to M0 (Tukey-HSD, ns). Also CHI3L1 expression in M1 and M0 macrophages did not significantly differ (Tukey-HSD, ns) (Figure 43B and 43C).

4.7.3. Effect of different PH-associated growth factors in the expression of CHI3L1 in lung vascular cells

To determine the effect of various growth factors (GFs) on CHI3L1 expression, we stimulated hPMECs, hPASMCs and hPAAFs with PH associated GFs that were found to be deregulated from the microarray screening.

4.7.3.1. Effect of different growth factors on the expression of CHI3L1 in human pulmonary microvascular endothelial cells (hPMECs)

hPMECs were stimulated with different GFs and cytokines such as VEGFA, IL6, IL8, IL13, IL18, CCL2, PDGF-BB, TGF-β and TNF-α. The results of the mRNA expression profiling showed a significant difference between the groups $F(9, 74) = 15.049$, $p < .001$). IL6 was significantly upregulating the CHI3L1 expression (Dunnett, $p < .01$), as well as the TNF-α (Dunnett, $p < .001$). The mRNA expression to VEGF, IL8, IL13, IL18, CCL2, PDGF-BB and TGF-β were not significantly different, despite the tendency to increase the CHI3L1 mRNA levels (Figure 44A).

The results of comparing protein levels of CHI3L1 where hPMECs were stimulated with different GFs showed no significant difference between the groups F(9, 20) = 0.470, ns) (Figure 44B and 44C.

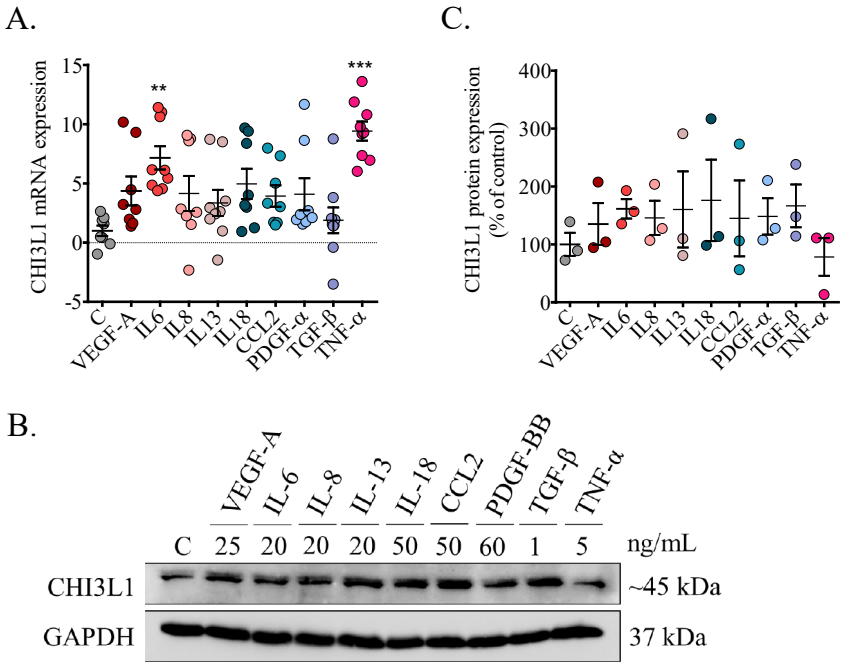

Figure 44: Growth factors effect on the CHI3L1 expression in human pulmonary microvascular endothelial cells. A. mRNA expression levels of CHI3L1 in human hPMECs normalized to controls ($n=3_{biological\ replicates}$; $n=3_{experimental\ replicates}$); B. Representative Western blot image of protein levels of CHI3L1 in the respective groups with the given concentrations of each GF; C. Densitometry of protein levels of CHI3L1 (n=3). GAPDH was used as a loading control. mRNA data is expressed as ΔCt, protein level data are expressed as percentage of control. Data are represented as mean±SEM (*p<0.05, **p<0.01, ***p<0.001).

4.7.3.2. Effect of different growth factors on the expression CHI3L1 in human pulmonary artery smooth muscle cells (hPASMCs)

hPASMCs were stimulated with different growth factors IL6, IL8, IL13, IL18, CCL2, PDGF-BB, TGF-β and TNF-α with the indicated concentrations as in Figure 45B. The results are compared using an ANOVA test and show a significant difference between the groups F(8, 66) = 28.701, p < .001). Stimulation of hPASMCs with IL13 caused significant downregulation of CHI3L1 at mRNA level (Dunnett, p < .01). Similarly, PDGF-BB decreased the CHI3L1 expression (Dunnett, p < .001), while TNF-α significantly upregulated the CHI3L1 (Dunnett, p < .001). The differences to IL6, IL8, IL18, CCL2 and TGF showed no significance (Figure 46A).

The results of comparing protein levels of CHI3L1, when hPMECs were stimulated with different GFs showed no significant difference between the groups F(8, 18) = 0.683, ns) (Figure 45B and 45C).

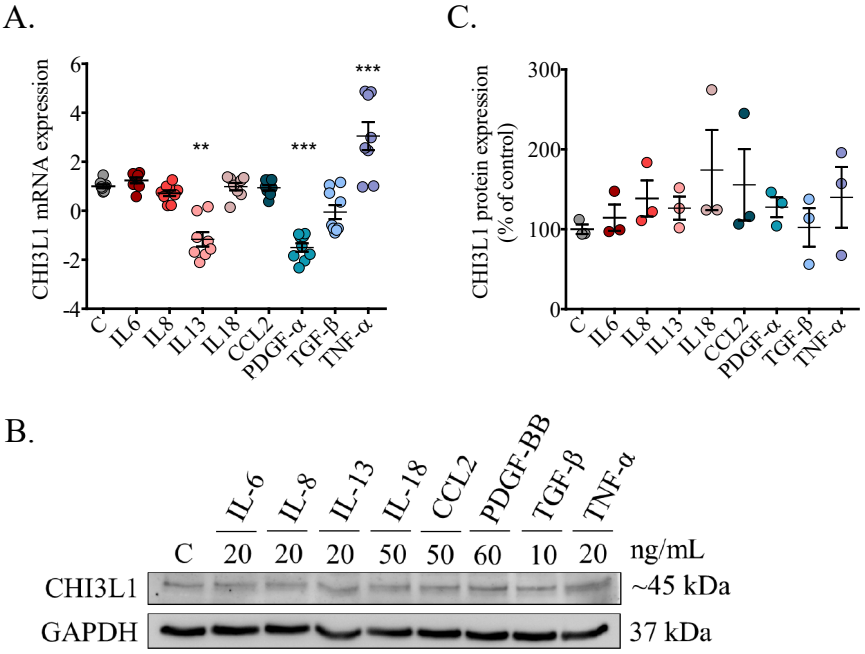

Figure 45: Growth factors effect on the CHI3L1 expression in human pulmonary artery smooth muscle cells. A. mRNA expression levels of CHI3L1 in human PASMCs normalized to controls ($n=3_{biological\ replicates}$; $n=3_{experimental\ replicates}$); B. Representative Western blot image of protein levels of CHI3L1 in the respective groups with the given concentrations of each GF; C. Densitometry of protein levels of CHI3L1 (n=3). GAPDH was used as a loading control. mRNA data is expressed as ΔCt, protein level data are expressed as percentage of control. Data are represented as mean±SEM (*p<0.05, **p<0.01, ***p<0.001).

4.7.3.3. Effect of different growth factors on the expression CHI3L1 in human pulmonary artery adventitial fibroblasts (hPAAFs)

hPAAFs were stimulated with different growth factors IL6, IL8, IL13, IL18, CCL2, PDGF-BB, TGF-β and TNF-α with the indicated concentrations Figure 46B. The results presented a significant difference between the groups F(8, 64) = 6.141, p < .001). TNF-α was significantly downregulating the CHI3L1 mRNA expression (Dunnett, p < .01). The stimulations with IL6, IL8, IL13, IL18, CCL2, PDGF and TGF did not significantly different results in comparison to controls, although IL6 tended to upregulate, while IL13 to downregulate CHI3L1 (Figure 46A).

No significant changes were observed at CHI3L1 protein level when hPAAFs were stimulated with different GFs F(8, 18) = 0.683, ns) (Figure 46B and 46C).

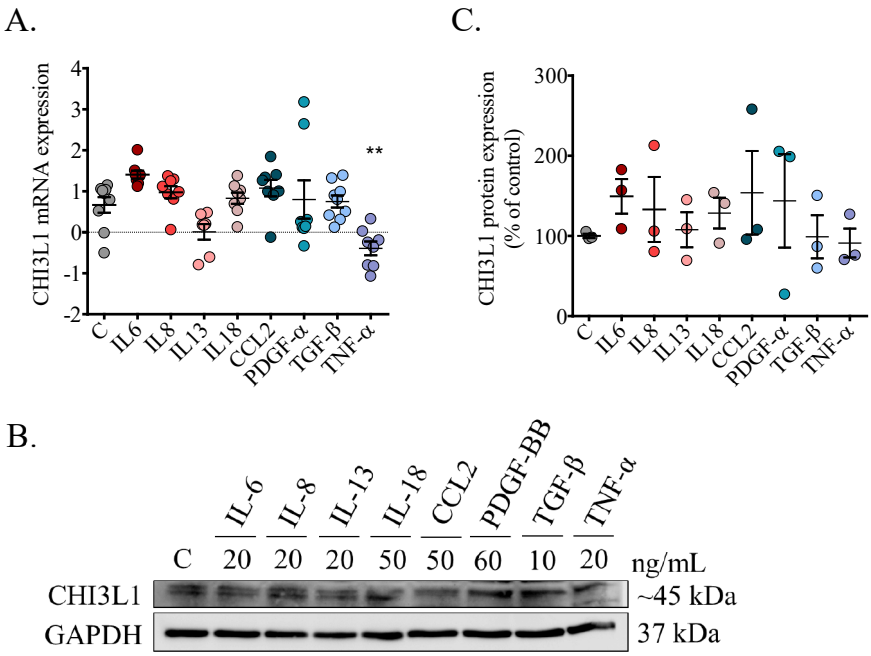

Figure 46: Growth factors effect on the CHI3L1 expression in human pulmonary artery adventitial fibroblasts. A. mRNA expression levels of CHI3L1 in human PAAFs normalized to controls ($n=3_{\text{biological replicates}}$; $n=3_{\text{experimental replicates}}$); B. Representative Western blot image of protein levels of CHI3L1 in the respective groups with the given concentrations of each GF; C. Densitometry of protein levels of CHI3L1 (n=3). GAPDH was used as a loading control. mRNA data is expressed as ΔCt, protein level data are expressed as percentage of control. Data are represented as mean±SEM (*p<0.05, **p<0.01, ***p<0.001).

4.7.4. Effect of recombinant CHI3L1 on the proliferation and apoptosis of vascular cells

As the expression of CHI3L1 was increased in pulmonary vasculature of CTEPH, we aimed to examine their functional role in modulation of cell proliferation, and apoptosis. Serum starved vascular cells (hPMECs, hPASMCs and hPAAFs) were stimulated with different concentrations of recombinant CHI3L1 for 24 hr, to identify the influence of CHI3L1 on proliferation (BrDU incorporation assay), and apoptosis (Cell death detection kit).

When hPMECs were stimulated with recombinant CHI3L1 in different concentration range (50-600 ng/mL) data revealed a strong increase in BrdU incorporation in +FCS controls in contrast to –FCS ($T(26.976) = -3.213$, $p < .01$). However, recombinant CHI3L1 in concentration of 50 ng/mL and 100 ng/mL increased the proliferation of hPMECs for approximately around 29%, although the difference was not significant according to the post-hoc tests (Figure 47A). Similarly, apoptosis assay showed a significant difference between

+FCS and –FCS (T(38) = 6.058, p < .001). The further comparison of +FCS with the other groups shows no significant difference between the groups F(5, 113) = 1.031, ns) (Figure 47B).

Furthermore, hPASMCs were stimulated with CHI3L1 in a similar manner as previously described. The results show a significant difference between +FCS and –FCS (T(40) = -2.446, p < .05) and a significant difference between the groups F(5, 103) = 3.778, p < .01). CHI3L1 with a concentration of 200 ng/mL significantly increased the proliferation of hPASMCs (151.33%; Tukey, p < .05) in comparison to +FCS control, while concentration of 100 ng/mL and 400 ng/mL increased the proliferation, even if the effect was not significant (Figure 47C).

CHI3L1 did not directly affect the apoptosis of hPASMCs. The results show a significant difference between +FCS and –FCS (T(22.069) = 6.271, p < .001). The further comparison of +FCS control with the stimulated groups shows no significant difference between the groups F(5, 113) = 1.031, ns)(Figure 47D).

Similarly, in hPAAFs the stimulation with CHI3L1 with different concentration had no significant influence on proliferation (F(5, 112) = 2.074, ns) (Figure 47E). Interestingly, CHI3L1 reduced the apoptosis of hPAAFs were stimulated with 200 ng/mL (to 82.89%; Dunnett, p < .05), 400 ng/mL (to 75.47%; Dunnett, p < .01) and 600 ng/mL (to 69.83%; Dunnett, p < .001), but not to 50 ng/mL and 100 ng/mL (Figure 47F).

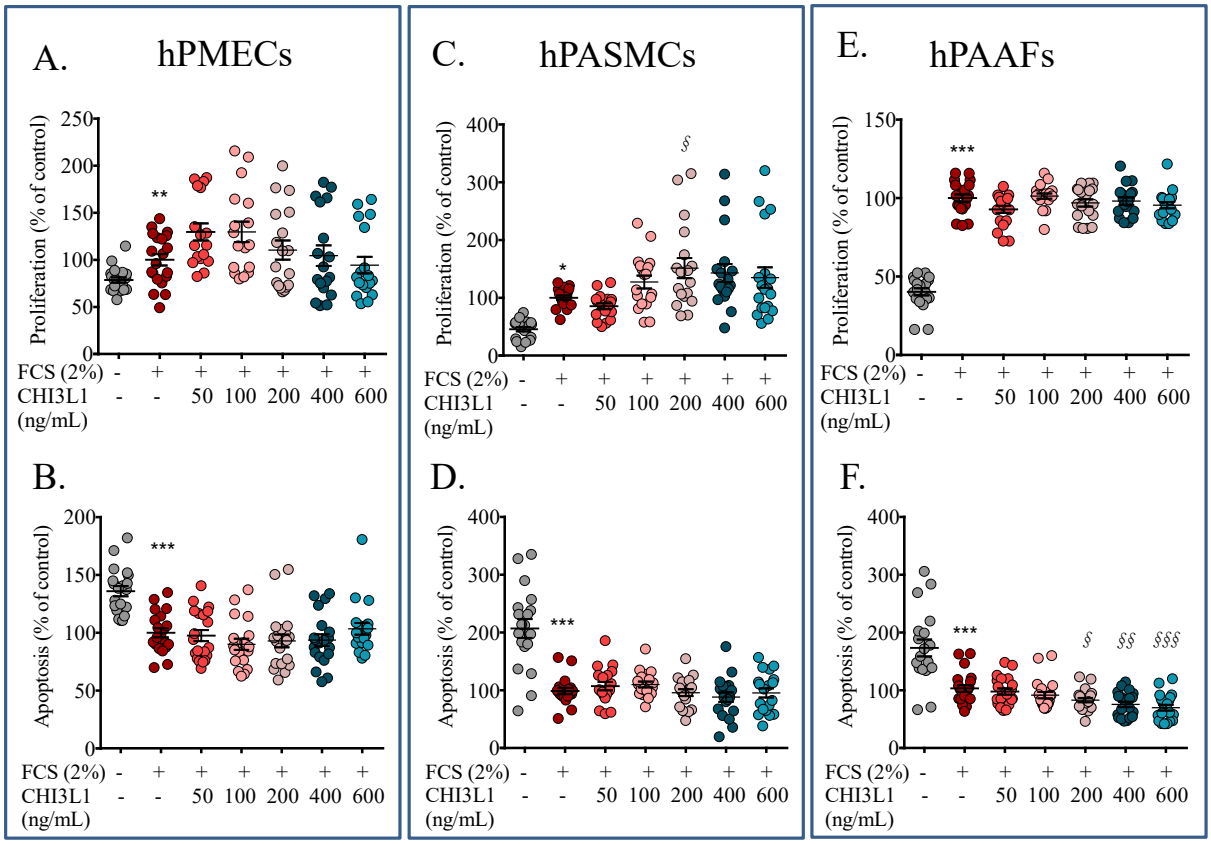

Figure 47: CHI3L1 effect on proliferation and apoptosis of vascular cells. Effects were tested with concentration of 50, 100, 200, 400, 600 ng/mL for all cell types employing BrdU incorporation assay for proliferation and ELISA based cell death detection kit for apoptosis; A. CHI3L1 proliferation effect on hPMECs; B. CHI3L1 apoptosis effect on hPMECs; C. CHI3L1 proliferation effect on hPASMCs; D. CHI3L1 apoptosis effect on hPASMCs; E. CHI3L1 proliferation effect on hPAAFs; F. CHI3L1 apoptosis effect on hPAAFs. Data ($n=3_{\text{biological replicates}}$; $n=6_{\text{technical replicates}}$) are expressed as percentage of control and represented as mean±SEM (*p<0.05, **p<0.01, ***p<0.001).

4.7.5. Effect of recombinant CHI3L1 on migration of vascular cells

To identify whether, CHI3L1 has a functional influence on motility, transwell migration assays have been employed for studying the motility of hPASMCs and hPAAFs. This method measures the capacity of cell motility toward a chemo-attractant gradient.

hPASMCs were stimulated with recombinant CHI3L1 at concentration of 200 ng/mL and 400 ng/mL. The results revealed a significant difference between the groups $F(3, 29) = 33.440$, $p < .001$). CHI3L1 increased the cell migration in both conditions, 200ng/mL (Tukey, $p < .05$) as well as to 400 ng/mL (Tukey, $p < .01$), while the serum stimulated and serum deprived controls were also statistically different to each other (Tukey, $p < .001$) (Figure 48A and 48B).

Additionally, the effect of CHI3L1 potentially induced migration was tested on hPAAFs. The results show a significant difference between the groups $F(3, 28) = 15.464$, $p < .001$). Similarly, CHI3L1 increased the cell migration when different concentration was applied. The post-hoc showed a statistically significant increase migration to 200ng/mL (Tukey, $p < .05$) as well as

to 400 ng/mL (Tukey, $p < .05$). Serum stimulated and serum deprived controls were also statistically different to each other (Tukey, $p < .05$) (Figure 48C and 48D).

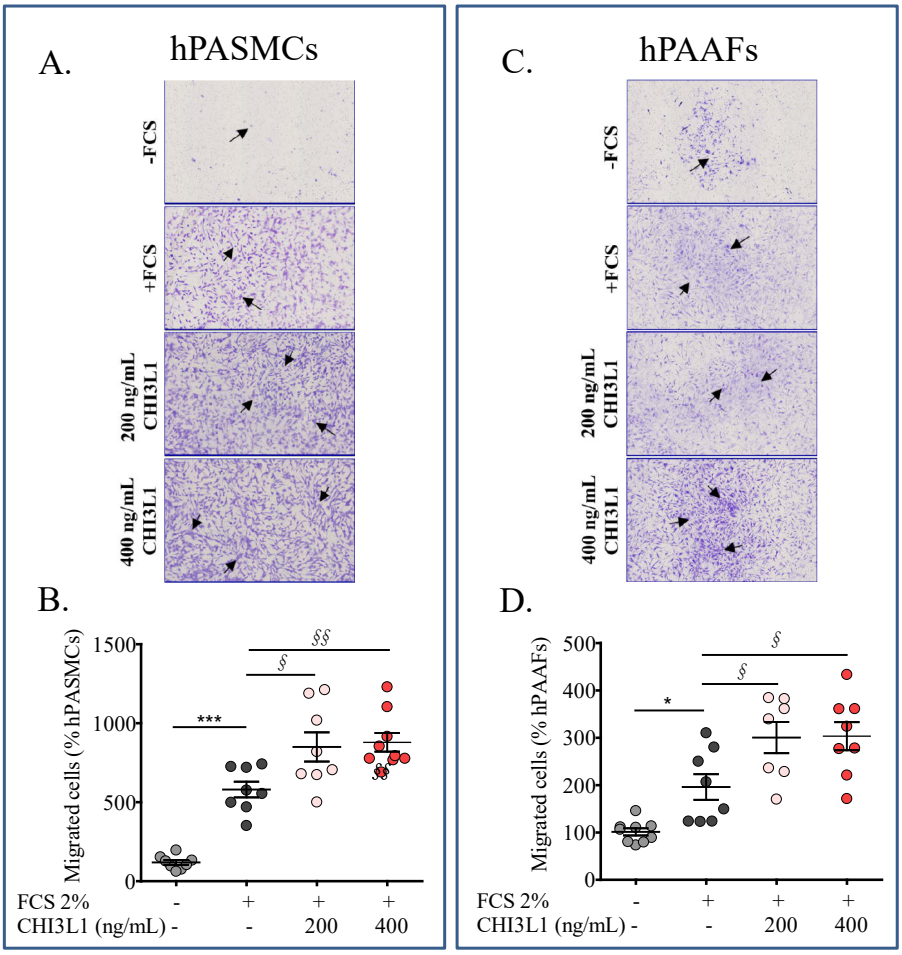

Figure 48: Effect of CHI3L1 on migration of hPASMCS and hPAAFs. Effects were tested with concentration of 200 and 400 ng/mL using Boyden chamber assay; A. Representative microphotographs of transwell membrane of CHI3L1induced hPASMCS migration; B. Quantification of the migrated hPASMCs; C. Representative microphotographs of transwell membrane of CHI3L1 induced hPAAFs migration; D. Quantification of the migrated hPAAFs; Data ($n=3_{\text{biological replicates}}$; $n=3_{\text{technical replicates}}$) are expressed as percentage of control and represented as mean±SEM (*p<0.05, **p<0.01, ***p<0.001).

4.7.6. Effect of CHI3L1 on contractility of hPASMCs

In order to evaluate the role of CHI3L1 in modulation of cell contractility, *in vitro* studies were carried on hPASMCs using rat tail collagen type 1 solution. Within the stimulated condition CHI3L1 was tested in serum deprived medium. We noted that the comparison of -FCS and GM (growth media) showed a significant difference ($T(6) = 7.707$, $p < .001$). Comparing –FCS with the other groups as well revealed a significant results ($F(3,12) = 13.38$, $p < .01$). The post-hoc tests confirms that, when hPASMCs are treated with 100 ng/mL CHI3L1, the gel size decreases, which suggest increased contractility up to 71.12% (Dunnett, $p < .001$). Similarly, as the concentration of CHI3L1 increased at 200 ng/mL and 400 ng/mL, we observed

comparable pattern of decreased gel size up to 72.30% (Dunnett, $p < .01$) and 76.93% (Dunnett, $p < .01$) respectively, in comparison to serum deprived control (Figure 49A and 49B).

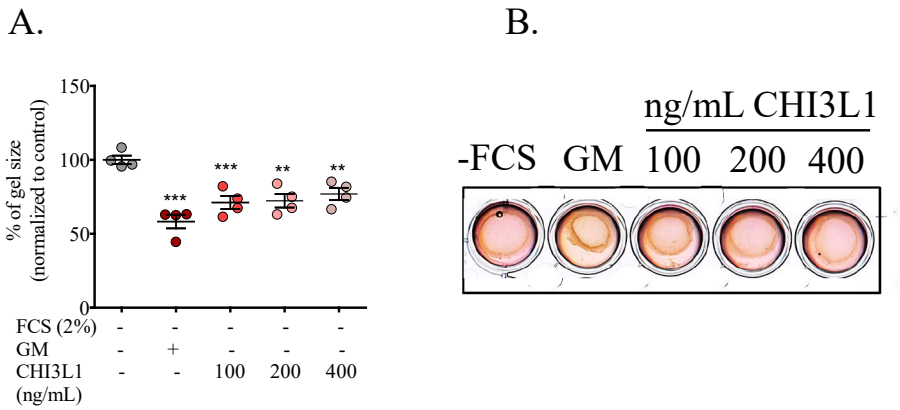

Figure 49: CHI3L1 induced contractility of hPASMCs. Effects were tested using concentration of CHI3L1 at 100, 200 and 400 ng/mL in serum deprived medium; A. Quantification of the contracted gels for different conditions; B. Representative image of the contracted gels under different conditions. Data ($n=4_{\text{biological replicates}}$) are expressed as percentage of control and represented as mean±SEM (*p<0.05, **p<0.01, ***p<0.001).

4.7.7. Effect of CHI3L1 on VEGF signalling pathway in hPMECs

To test whether CHI3L1 acting on hPMECs has a causative role in triggering the VEGF signalling pathway, we stimulated donor hPMECs with recombinant CHI3L1 with different concentrations.

Treatment with CHI3L1 resulted in significant difference between the groups in vascular endothelial growth factor receptor 2 (VEGFR2) using a one-sided ANOVA test $F(5, 18) = 2.723$, $p < .05$). Concentrations of 200 ng/mL (Tukey-HSD, $p < .05$) and 600 ng/mL (Tukey-HSD, $p < .05$) significantly increased the VEGFR2 expression at protein level, while cells stimulated with 50 ng/mL, 100 ng/mL and 400 ng/mL presented increased, but not significant tendency of VEGFR2 induction (Tukey-HSD, ns) (Figure 50A and 50B).

Stimulation of hPMECs with CHI3L1 did not affect the proteins levels of vascular endothelial growth factor receptor 1 (VEGFR1), as no significant difference between the groups $F(5, 18) = 0.856$, ns) was noted (Figure 50A and 50C).

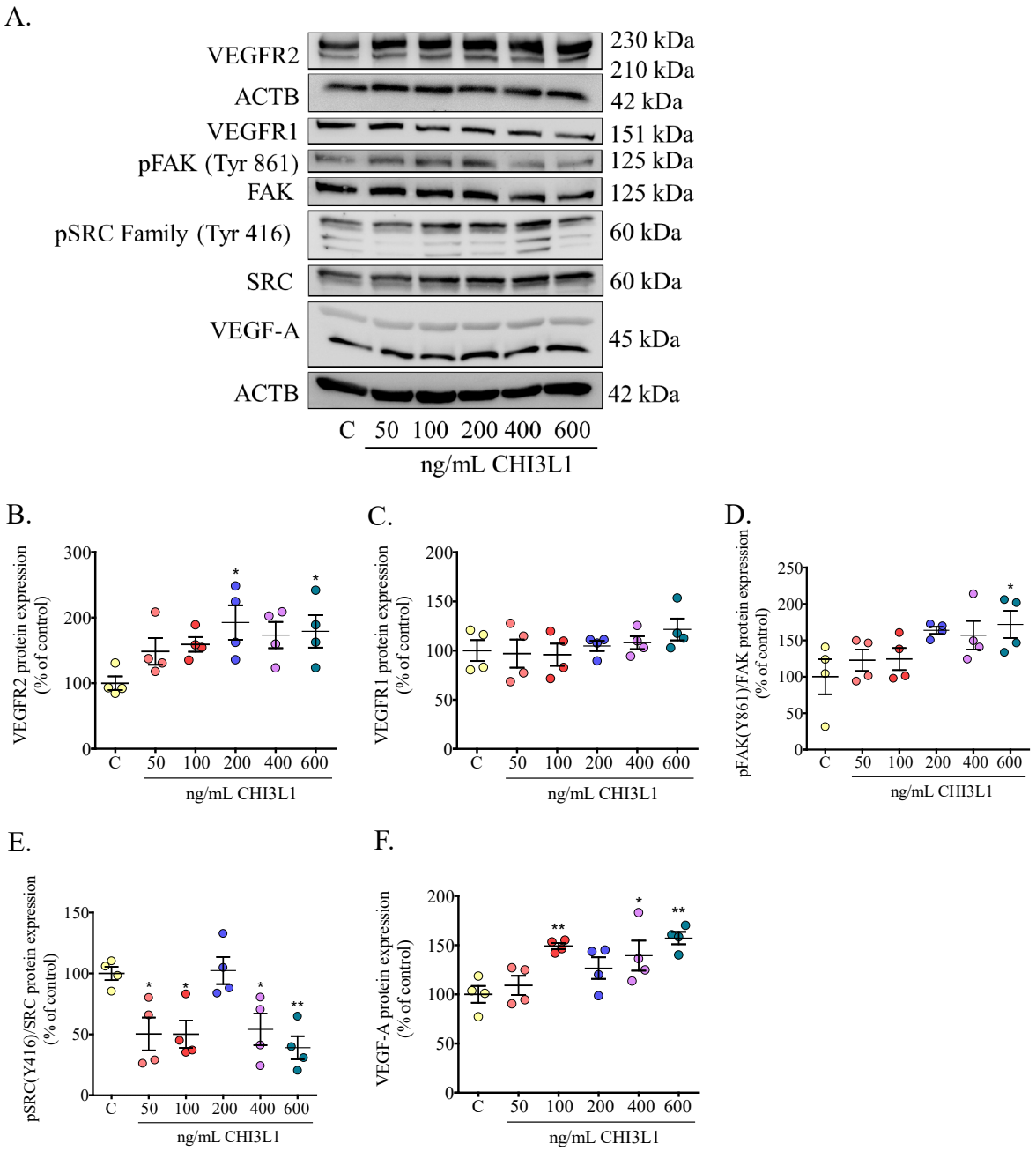

Figure 50: Effect of CHI3L1 on VEGF signalling pathway. A. Representative Western blot images of protein levels of selected VEGF signalling molecules (VEGFR2, VEGFR1, pFAK (Tyr861) in comparison to FAK, pSRC family (Tyr416) in comparison to SRC, and VEGFA protein expression) stimulated with 2-fold increasing concentration of CHI3L1. Densitometry of protein levels in response to CHI3L1 stimulation of: B. VEGFR2; C. VEGFR1; D. FAK (Y861) and FAK; E. SRC (Y416) and SRC; F. VEGF-A; B-actin (ACTB) was used as a loading control; (n=4). Protein levels data are expressed as percentage of control. Data are represented as mean±SEM (*p<0.05, **p<0.01, ***p<0.001).

Furthermore, we noted significant difference between the groups, with regard to the phosphorylation of the focal adhesion kinase (FAK) ($F(5, 18) = 2.701$, $p < .05$). CHI3L1 in concentration of 600 ng/mL significantly increased the phosphorylation of FAK at Tyr861

(Y861) (Tukey-HSD, $p < .05$) while the rest stimulations showed inclination, although not significantly different (Tukey-HSD, ns) (Figure 50A and 50D).

The results regarding phosphorylation of proto-oncogene tyrosine family protein kinases SRC (SRC) at Tyr416 (Y416) are suggesting significant difference between the groups $F(5, 18) = 6.420$, $p < .001$). The post-hoc tests show that 50 ng/mL (Tukey-HSD, $p < .05$), 100 ng/mL (Tukey-HSD, $p < .05$), 400 ng/mL (Tukey-HSD, $p < .05$) and 600 ng/mL (Tukey-HSD, $p < .01$) are significantly different to the control, while 200 ng/mL is not significantly different (Tukey-HSD, ns) (Figure 50A and 50E).

Vascular endothelial growth factor A (VEGFA) was significantly induced as well as a result of the CHI3L1 stimulation $F(5, 18) = 5.343$, $p < .01$). When cells were stimulated with different concentrations of recombinant CHI3L1 we observed significant increase of VEGFA protein levels at 100 ng/mL (Tukey-HSD, $p < .01$), 400 ng/mL (Tukey-HSD, $p < .05$) and 600 ng/mL (Tukey-HSD, $p < .01$), while 50 ng/mL and 200 ng/mL of CHI3L1 were not significantly different to the respective control (Tukey-HSD, ns) (Figure 50A and 50F).

4.7.8. *Ex-vivo* assessment of the vessel number in end-stage CTEPH

As end stage-CTEPH lung tissues suggested to have an increased angiogenic potential from the microarray data as well as from our microscopic observation, we evaluated the total (micro)vessel density as a number of von Willebrand factor (vWf), CD31- and CD34- positive vessels in the tissue section divided by the total area. When CTEPH were compared to donor samples, we observed a significant increase in the number of the vWF positive vessels ($T(4) = -7.646$, $p < .01$) (Figure 51A and 51B). Further on, the CD31 staining and vessel number quantification confirmed increased number of vessels in the CTEPH lung samples in comparison to the controls ($T(4.258) = -4.611$, $p < .01$) (Figure 51A and 51C). Similarly, the CD34+ vessel evaluation confirmed the result of increased vessel count in diseased conditions ($T(5.038) = -3.278$, $p < .05$) (Figure 51A and 51D).

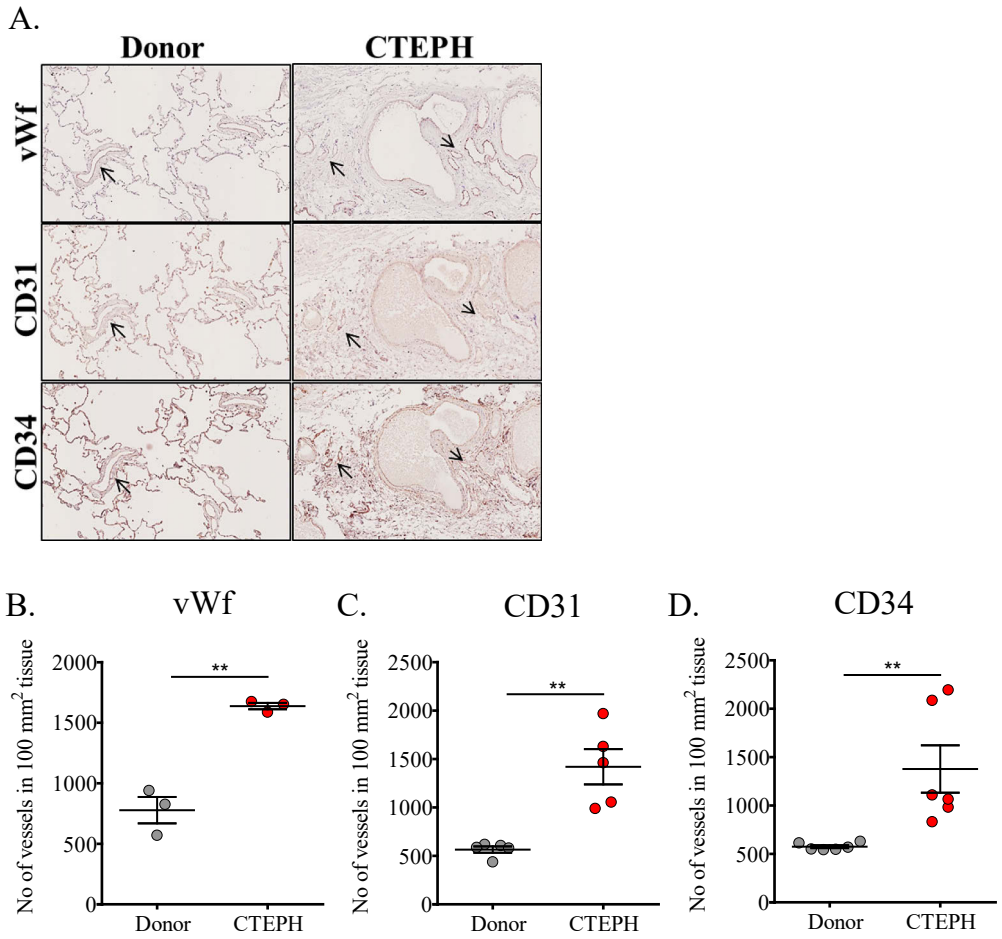

Figure 51: Total vessel density in explanted end-stage CTEPH in comparison to donors. A. Representative microphotographs of vessels within control and CTEPH lung samples stained with different markers for endothelial cells as vWf, CD31 and CD34; Field magnification 5x; Quantification of the number of the vessels visualized and identified by: B. vWf staining (n=3); C. CD31 staining (n=5); D. CD34 staining (n=6) ; Data are normalized to 100mm^2 tissue surface and represented as mean±SEM (*p<0.05, **p<0.01, ***p<0.001).

4.7.9. *Ex-vivo* effect of CHI3L1 on human precision cut lung sections in terms of vascular remodelling

Further, in order to evaluate the *ex-vivo* effect of CHI3L1 on vascular remodelling and downstream signaling pathways, the precision cut lung sections were used. Human living precision cut (300 µM thick) lung sections were kept at 37°C and 5% CO_2 in a humidified chamber for 10 days, being fully replenished after the fourth day of stimulation. CHI3L1 was diluted to final concentration in 1%FCS containing medium (Figure 52A).

To access the vascular remodelling, measurements of MWT and neointima were taken. The results regarding MWT were compared using a one-sided ANOVA test and show a significant difference between the groups $F(5, 17) = 5.812$, $p < .01$). Interestingly, CHI3L1 stimulation affected significantly the MWT in all the given concentrations: 200 ng/mL (Tukey-HSD, p <

.05), 400ng/mL (Tukey-HSD, p < .05), 800ng/mL (Tukey-HSD, p < .05) and 1200 ng/mL (Tukey-HSD, p < .01). The post-hoc tests showed that the 1% FCS is significantly different to 20% FCS (Tukey-HSD, p < .001) (Figure 52B and 52C). The results regarding the neointima/media ratio revealed no significant difference between the groups F(5, 17) = 0.717, ns) (Figure 52B and 52D).

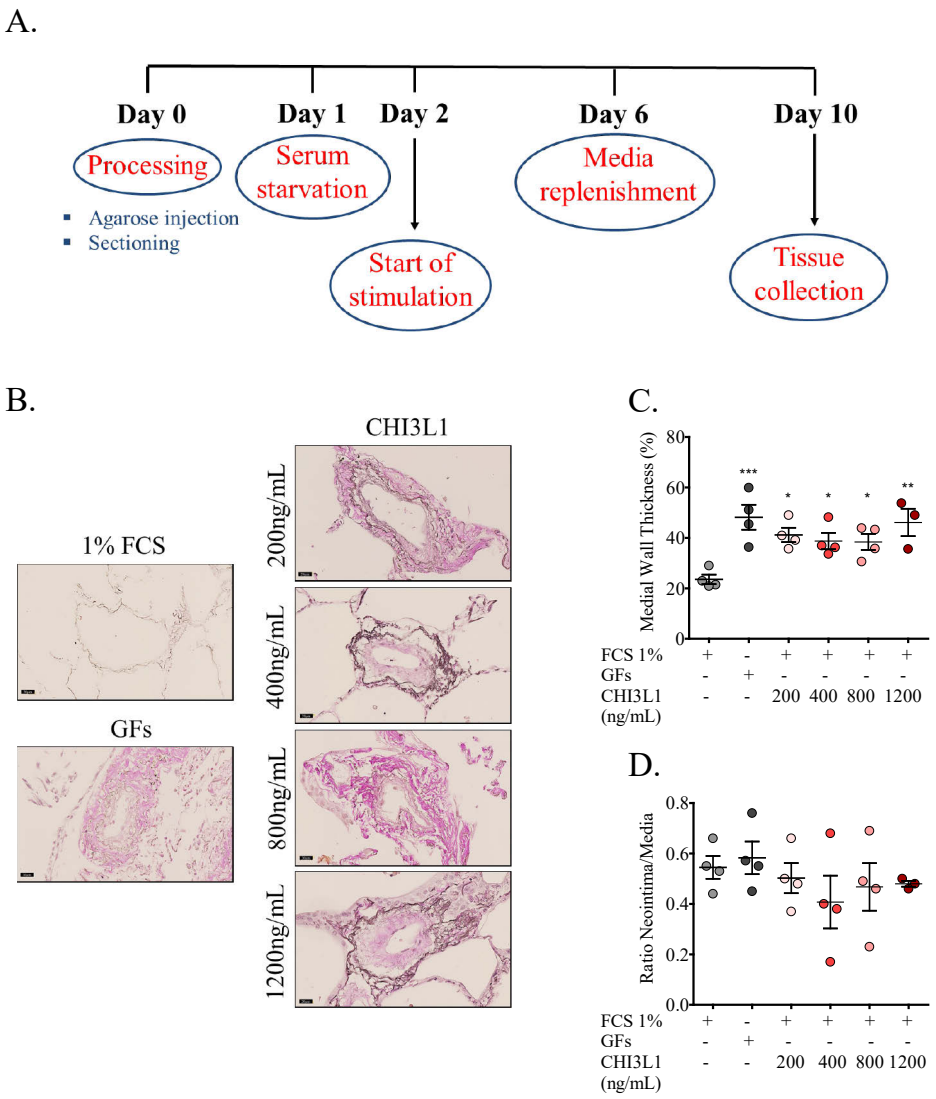

Figure 52: CHI3L1 ex-vivo induced vascular remodelling. Effects of recombinant CHI3L1 were tested at concentration of 200, 400, 800 and 1200 ng/mL. A. Schematic representation of the experimental plan; B. Representative microphotographs of vessels stained with Elastica Van Gieson from PCLS; B. Quantification of the medial wall thickness (MWT) in PCLS vessels shown as a percentage; C. Ratio neointima/media assessment of CHI3L1 stimulated PCLS. n=4 ≠ c(1200ng/mL)=3. Data is represented as mean±SEM (n=12; *p<0.05, **p<0.01, ***p<0.001)

mRNA from three biological PCLS replicates (controls and concentrations of CHI3L1 of 800 ng/mL and 1200 ng/mL) was isolated, pooled and subjected to microarray screening, in order to evaluate whether CHI3L1 has an differential effect on some genes and associated signalling pathways. As shown in Figure 53A, there was a transcriptional difference between 800 ng/mL

and 1200 ng/mL stimulated PCLS (red dots-top 20 significantly regulated genes) as well as compared to controls. The ten most significantly up- and down- regulated genes in both stimulated conditions are listed in Appendix (A-6 and A-7). KEGG pathway analysis revealed enrichment of several signalling pathways, in both experimental setups (800 ng/mL and 1200 ng/mL of CHI3L1 stimulation), where increased number of differentially regulated genes was found to be associated metabolic pathways, ubiquitin mediated proteolysis, followed by cellular senescence, endocytosis, etc. (Figure 53B). Surprisingly, the most prominently different pathway, with the condition of 1200 ng/mL stimulation according to where the most of the regulated genes fall in, is systemic lupus erythematosus (Figure 53C).

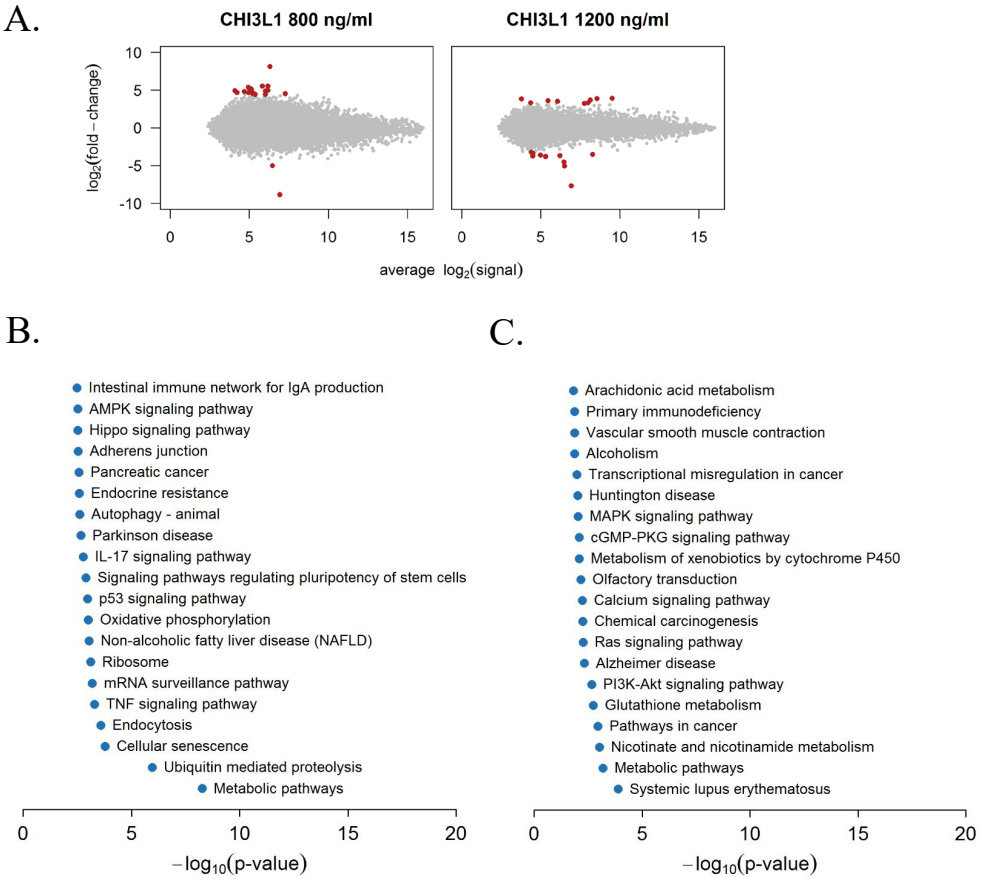

Figure 53: Gene regulation patterns of CHI3L1 stimulated PCLS and in silico KEGG pathway analysis. A. MDPlots to visualise the transcriptional difference between two different CHI3L1 concentrations used for PCLS stimulation, based on $\log_2$ (fold change) of p values plotted against the average $\log_2$ of the expression. KEGG signalling pathways affected by: B. 800 ng/mL CHI3L1 as $-\log_{10}$ p-value; C. 1200 ng/mL of CHI3L1 presented as $-\log_{10}$ p-value.

4.8. Chapter VII: ENPP2-LPA axis expression and their biological effects on vascular cells

4.8.1. Ectonucleotide Pyrophosphatase/Phosphodiesterase 2 (ENPP2) expression in donors, CTEPH and IPAH patients and their basal expression in human vascular and tumour lung cells

Similarly, as in the case of CHI3L1, in order to substantiate the results of the microarray screening and to better understand the regulation of ENPP2 in the pathophisiology of CTEPH, the expression pattern was evaluated in frozen lung sections subjected to laser capture microdissection (LCM) of pulmonary vessels, followed by RNA isolation and qPCR.

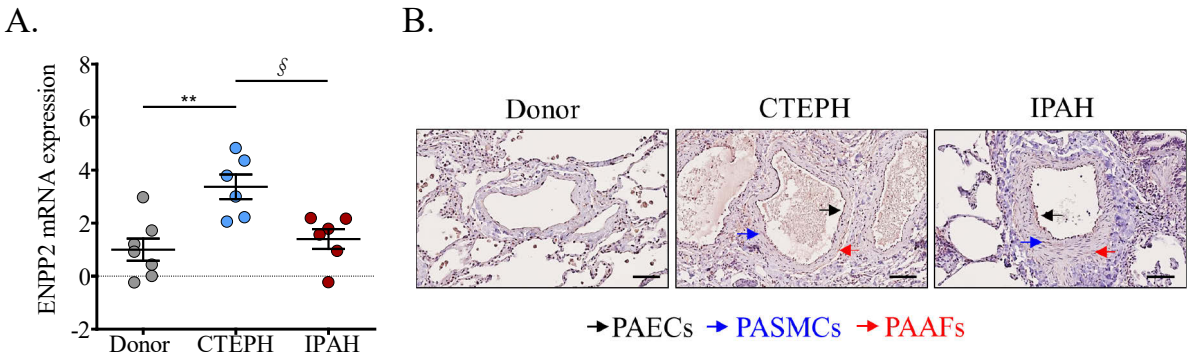

Figure 54: ENPP2 expression in pulmonary vessels of donors, CTEPH and IPAH patients. A. mRNA expression analysis of ENPP2 evaluated by qPCR. B. Representative immunohisto-microphotographs of human lung sections stained with ENPP2 (dark brown). Scale bar: 20µm. Data is expressed as ΔCt, normalized to the donors and represented as mean±SEM (n(donor)=7; n(CTEPH/IPAH)=6; *p<0.05, **p<0.01, ***p<0.001; ; §p<0.05, §§p<0.01, §§§p<0.001 versus CTEPH).

CTEPH LCM samples presented a significant upregulation of ENPP2 expression (ΔCt=3.37; Tukey-HSD, $p < .01$), in comparison to the respective donors; while the IPAH samples were not significantly different to the donors (ΔCt=1.40; Tukey-HSD, ns) in their ENPP2 expression. CTEPH and IPAH LCM samples differentiate in their ENPP2 expression (Tukey-HSD, $p < .05$) (Figure 54A). The immunohistological staining showed a predominant localization of ENPP2 in PAECs in patients with CTEPH, as well as expression in the PASMCs, and partially in the adventitia of pulmonary vessels (Figure 54B). Expression of ENPP2 was noticable in some IPAH patients as well.

Next, when evaluating the basal mRNA expression, lung pericytes along with hPASMCs showed the highest abundance of ENPP2, followed by hPAAFs (Figure 56A). In contrast to the mRNA expression, ENPP2 protein levels were not changed when compared to the hPMECs, or even less expressed as it is the case with hPAECs, hPASMCs and hPAAFs (Figure 55B and 55C).

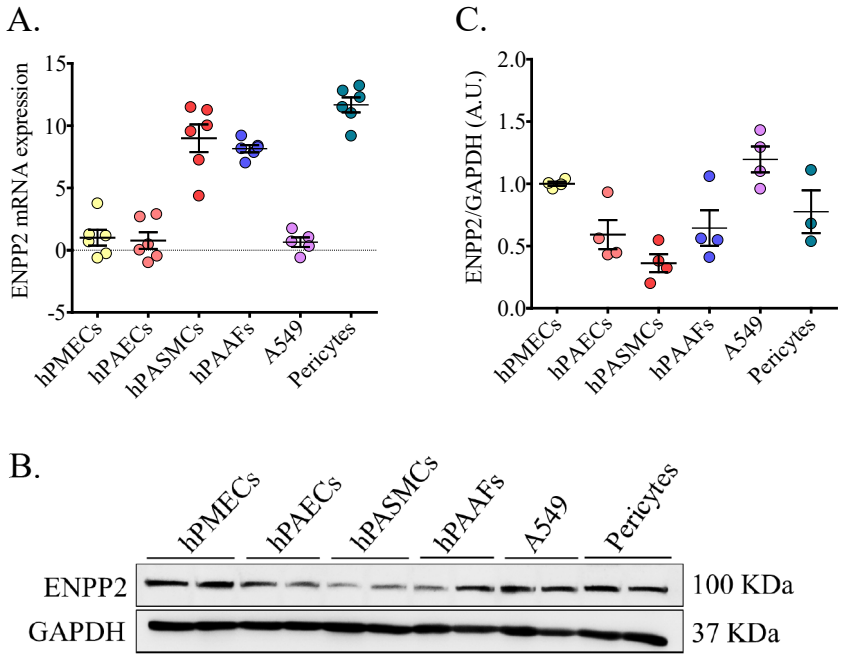

Figure 55: Evaluation of ENPP2 basal mRNA and protein expression in human vascular and tumour lung cells. A. mRNA expression levels of ENPP2 in human PMECs, PAECs, PASMCs, PAAFs, A549 and lung pericytes (n=3$_{\text{biological replicate}}$; n=2$_{\text{experimental replicate}}$); B. Representative Western blot image of protein levels of ENPP2 in the listed cell types; C. Densitometry of protein levels of ENPP2 (n=4, lung pericytes n=3). GAPDH was used as a loading control. Data is expressed as ΔCt (mRNA) or A.U. (proteins) and normalized to the expression of hPMECs.

4.8.2. ENPP2 expression in human naïve (M0) and polarized (M1,M2) macrophages

To demonstrate whether the resting or activated (pro- and anti- inflammatory) macrophages will convey differential ENPP2 expression, mRNA and protein levels were evaluated.

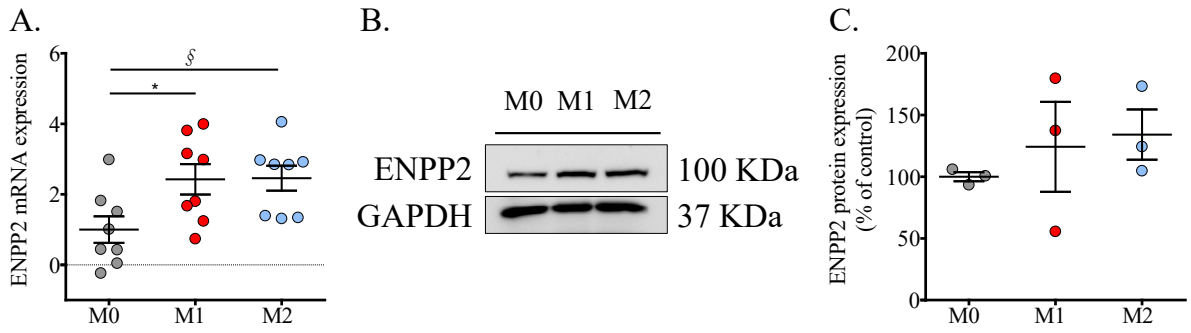

Figure 56: Evaluation of ENPP2 basal mRNA and protein expression in human naïve (M0) and polarized (M1, M2) macrophages. A. mRNA expression levels of ENPP2 in human macrophages normalized to M0 (n=8); B. Representative Western blot image of protein levels of ENPP2 in the listed groups; C. Densitometry of protein levels of ENPP2 (n=3). GAPDH was used as a loading control. mRNA data is expressed as ΔCt, protein level data are expressed as percentage of control (M0). Data are represented as mean±SEM (*p<0.05, **p<0.01, ***p<0.001; §p<0.05, §§p<0.01, §§§p<0.001 M2 versus M0).

The results of the comparison of the mRNA level between M0 (resting macrophages) and M1 (pro-inflammatory) and M2 (anti- inflammatory) indicated a significant difference ($F(2, 21) = 4.590$, $p < .05$). The post-hoc tests showed that both M2 (2.46; Tukey-HSD, $p < .05$) and M1 (2.43; Tukey-HSD, $p < .05$) are exhibiting significantly upregulated ENPP2 mRNA levels compared to M0, while the ENPP2 expression between M1 and M2 macrophages did not differ (Tukey-HSD, ns) (Figure 56A). When comparing the protein expression of ENPP2, the results indicate no significant difference within the resting and activated macrophages ($F(2, 6) = 0.527$, ns) (Figure 56B and 56C).

4.8.3. Effect of different PH-associated growth factors in the expression of CHI3L1 in lung vascular cells

To evaluate whether different GFs can act upstream to ENPP2 expression, we stimulated hPMECs, hPASMCs and hPAAFs with PH associated GFs that were found to be deregulated from the microarray screening.

4.8.3.1. Effect of different growth factors on the expression of ENPP2 in human pulmonary microvascular endothelial cells (hPMECs)

hPMECs, were stimulated with different growth factors VEGFA, IL6, IL8, IL13, IL18, CCL2, PDGF-BB, TGF-β and TNF-α at the indicated concentrations as in Figure 57B. The results showed a significant difference between the groups $F(9, 74) = 4.814$, $p < .001$). IL13 was significantly inducing the ENPP2 mRNA expression (Tukey, $p < .01$), while TNF-α showed tendency of induction. The rest of the GFs showed no significant difference in induction or decrease of the ENPP2 (Figure 57A). However, ENPP2 protein levels were not significantly regulated by any of the GF stimulations in hPMECs ($F(9, 20) = 0.473$, ns) (Figure 57B and 57C).

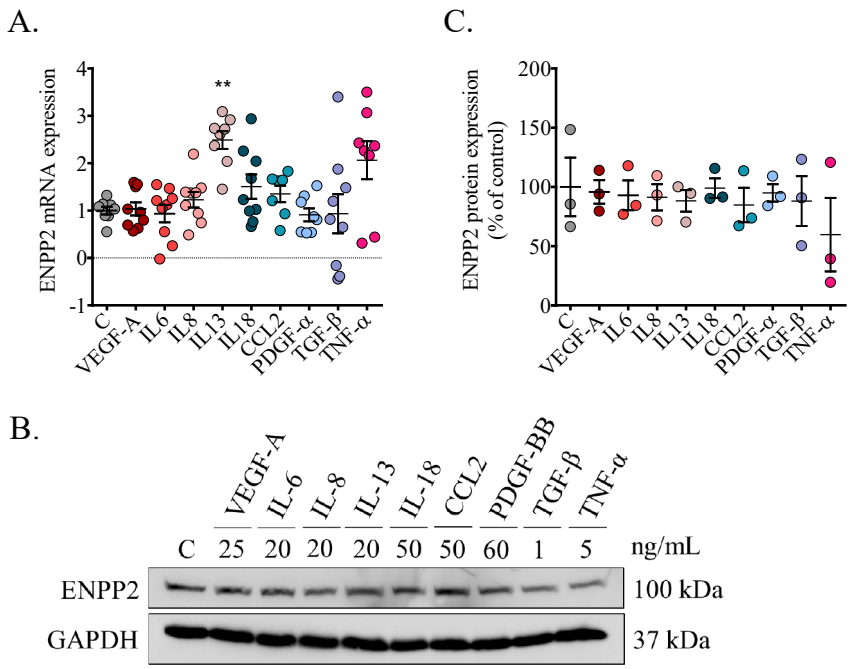

Figure 57: Growth factors effect on the ENPP2 expression in human pulmonary microvascular endothelial cells. A. mRNA expression levels of ENPP2 in human hPMECs normalized to controls ($n=3_{\text{biological replicates}}$; $n=3_{\text{experimental replicates}}$); B. Representative Western blot image of protein levels of ENPP2 in the respective groups with the given concentrations of each GF; C. Densitometry of protein levels of ENPP2 (n=3). GAPDH was used as a loading control. mRNA data is expressed as ΔCt, protein level data are expressed as percentage of control. Data are represented as mean±SEM (*p<0.05, **p<0.01, ***p<0.001).

4.8.3.2. Effect of different growth factors on the expression ENPP2 in human pulmonary artery smooth muscle cells (hPASMCs)

Similar to hPMECs, in hPASMCs, IL13 caused significant downregulation of ENPP2 mRNA expression (Dunnett, $p < .01$) along with TGF-β (Dunnett, $p < .05$) and TNF-α (Dunnett, $p < .001$). IL6, IL8, IL18 and CCL2 did not significantly influenced the ENPP2 expression (Figure 58A). However, similar to hPMECs, ENPP2 protein levels were not significantly regulated by any of the GF stimulations in hPASMCs ($F(8, 18) = 0.727$, ns) (Figure 58B and 58C).

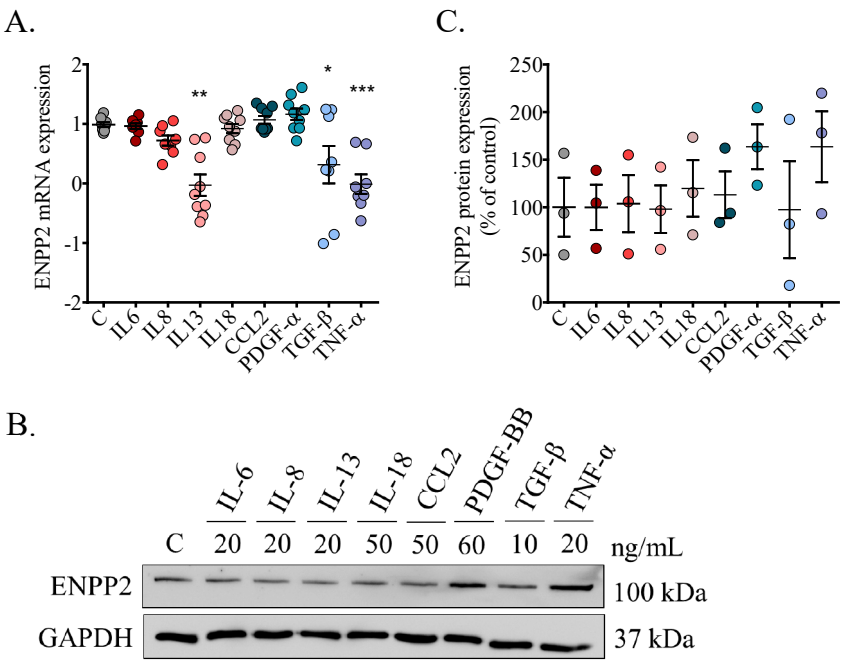

Figure 58: Growth factors effect on the ENPP2 expression in human pulmonary artery smooth muscle cells. A. mRNA expression levels of ENPP2 in human PASMCs normalized to controls ($n=3_{\text{biological replicates}}$; $n=3_{\text{experimental replicates}}$); B. Representative Western blot image of protein levels of ENPP2 in the respective groups with the given concentrations of each GF; C. Densitometry of protein levels of ENPP2 (n=3). GAPDH was used as a loading control. mRNA data is expressed as ΔCt, protein level data are expressed as percentage of control. Data are represented as mean±SEM (*p<0.05, **p<0.01, ***p<0.001).

4.8.3.3. Effect of different growth factors on the expression of ENPP2 in human pulmonary artery adventitial fibroblasts

In hPAAFs stimulated with different GFs, a significant difference between the groups was observed ($F(8, 69) = 29.484$, $p < .001$) (Figure 59A). IL6 (Dunnett, $p < .05$) and PDGF-BB (Dunnett, $p < .01$) were significantly inducing the ENPP2 mRNA levels, while TGF-β (Dunnett, $p < .001$) and TNF-α (Dunnett, $p < .001$) significantly reducing the mRNA levels. The changes to IL8, IL13 and IL18 and CCL2 were not significantly different (Figure 59A).

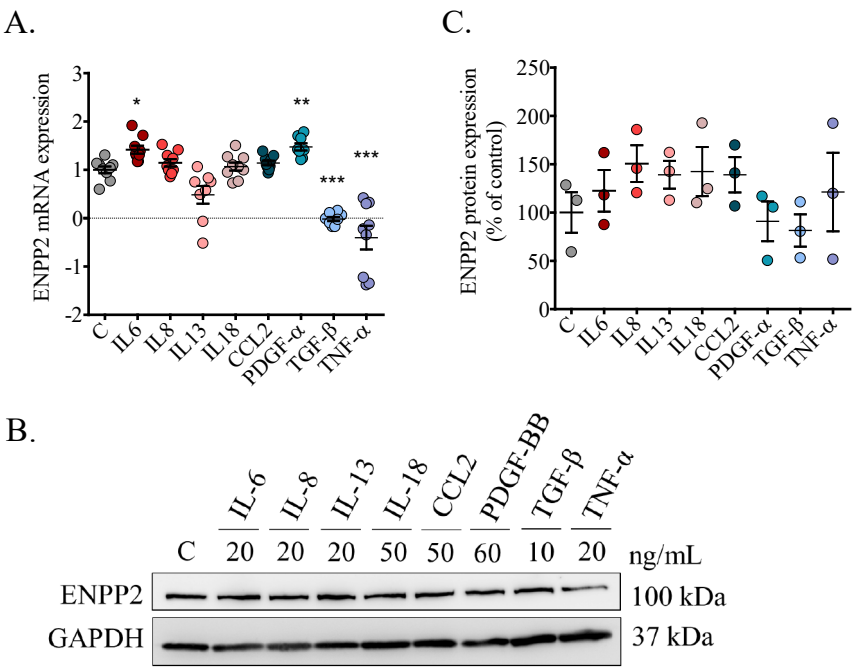

Figure 59: Growth factors effect on the ENPP2 expression in human pulmonary artery adventitial fibroblasts. A. mRNA expression levels of ENPP2 in human PAAFs normalized to controls ($n=3_{\text{biological replicates}}$; $n=3_{\text{experimental replicates}}$); B. Representative Western blot image of protein levels of ENPP2 in the respective groups with the given concentrations of each GF; C. Densitometry of protein levels of ENPP2 (n=3). GAPDH was used as a loading control. mRNA data is expressed as ΔCt, protein level data are expressed as percentage of control. Data are represented as mean±SEM (*p<0.05, **p<0.01, ***p<0.001).

No significant changes were observed at a ENPP2 protein level when hPAAFs were stimulated with different GFs (F(8, 18) = 0.727, ns) (Figure 59B and 59C).

4.8.4. Pharmacological effect of LPA on the proliferation and apoptosis of vascular cells

ENPP2 plays a role in hydrolysing the lysophoshpolipids, to produce lysophosphatidic acid (LPA), involved in wide variety of cellular processes. As the expression of ENPP2 was increased in LCM dissected CTEPH vessels, we examined their functional role in modulation of cell proliferation or apoptosis. Serum starved pulmonary vasular cells (hPMECs, hPASMCs and hPAAFs) were stimulated with LPA for 24 h at different concentrations to identify whether LPA exerts effects on proliferationa or apoptosis in a concentration dependent manner.

hPMECs were stimulated with LPA in different concentration range (1-80 ng/mL) in presence of 0.2% bovine serum albumin (BSA). Data revealed a strong increase in BrdU incorporation in +BSA controls in contrast to –FCS ($T(33) = -3.043$, $p < .01$) as well as no difference between +FCS and +BSA ($T(33) = 0.835$, ns). However, the further comparison of +BSA control with the stimulated LPA groups was significant $F(5, 96) = 3.945$, $p < .01$). LPA in concentration of

1 µM induced the hPMECs proliferation for approximately 22%, 5 µM for 27%, 10 µM for 32% and 40 µM for approximately 29%, although the post-hoc tests show no statistically significant differences in comparison to BSA (Figure 60A).

With regard to apoptosis, LPA showed an influence at a high concentration. The results showed a significant difference between -FCS and +BSA ($T(24.988) = 4.936$, $p < .001$), as well as no difference between +FCS and +BSA ($T(29.944) = 0.203$, ns) in terms of decrease in apoptosis. The further comparison of +BSA with the stimulated groups was significant $F(5, 111) = 31.130$, $p < .001$). The results suggested that a concentration of LPA at 80 µM (182.59%; Tukey, $p < .001$) significantly increased the apoptosis in hPMECs (Figure 60B).

Next, hPASMCs were stimulated with LPA in a similar manner as previously described. The results show a significant difference between ($T(24.241) = -9.923$, $p < .05$), as well as no difference between +FCS and +BSA ($T(35) = 0.479$, ns). The further comparison of +BSA with the stimulated groups is significant $F(5, 115) = 2.475$, $p < .05$). LPA in concentration of 1-40 µM showed a tendency to increase proliferation, although the post-hoc tests show no statistical significant differences in comparison to BSA (Figure 60C).

LPA did not directly affect the apoptosis of hPASMCs. The results show a significant difference ($T(15.140) = 9.143$, $p < .001$) as well as a difference between +FCS and +BSA ($T(19.199) = 4.007$, $p < .01$). The further comparison of +BSA with the other groups is significant $F(5, 102) = 3.809$, $p < .01$). The results suggested that a concentration of LPA at 40 µM (145.80; Tukey, $p < .05$), significantly increased the apoptosis in hPASMCs (Figure 60D).

Finally, potential proliferation effects of LPA were evaluated on hPAAFs, after the serum starvation of 24 hr, prior to their 24 hr stimulation. The +BSA control was significantly different to -FCS ($T(32) = -13.145$, $p < .001$) as well as no difference was noted between +FCS and +BSA ($T(32) = -1.277$, ns). The stimulation with LPA in different concentration showed mild increase of the proliferation of approximately 6-15%, which however was not significant in comparison to the control BSA ($F(5, 87) = 0.974$, ns) (Figure 60E).

The LPA induced apoptosis of hPAAFs was as well evaluated and the results showed a significant difference between -FCS and +BSA ($T(15.140) = 9.143$, $p < .001$) as well as no difference between +FCS and +BSA ($T(38) = 1.378$, ns). The further comparison of +BSA with the other groups is significant $F(5, 106) = 7.673$, $p < .001$). The stimulation with LPA in different concentration revealed significant increase of apoptosis in 10 µM stimulated cells

(187.72%; Tukey, p < .001), in 40 µM (179.97%; Tukey, p < .01) and 80 µM (162.86%; Tukey, p < .01), in comparison to the respective control (Figure 60F).

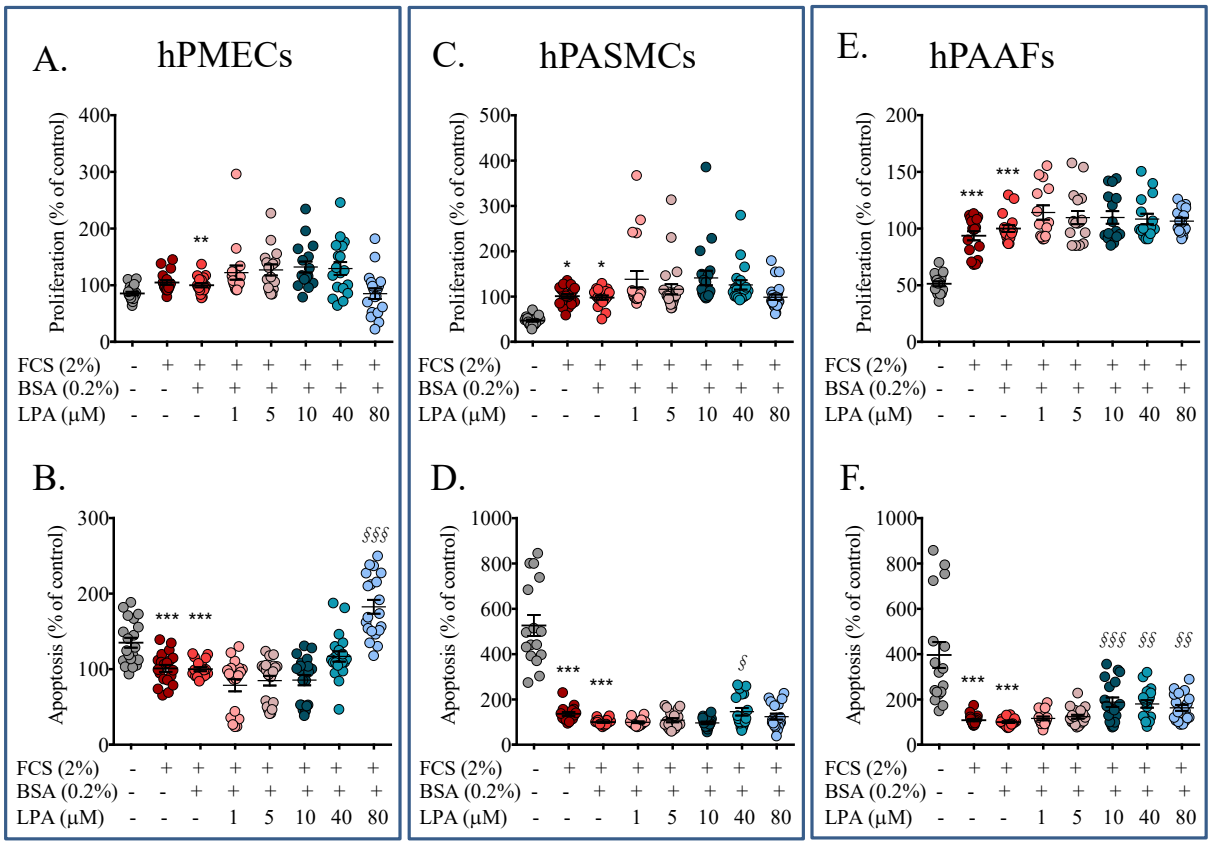

Figure 60: LPA effect on proliferation and apoptosis of vascular cells. Effects were tested with concentration of 1, 5, 10, 40 and 80 µM for all cell types employing BrdU incorporation assay for proliferation and ELISA based cell death detection kit for apoptosis; A. LPA proliferation effect on hPMECs; B. LPA apoptosis effect on hPMECs; C. LPA proliferation effect on hPASMCs; D. LPA apoptosis effect on hPASMCs; E. LPA proliferation effect on hPAAFs; F. LPA apoptosis effect on hPAAFs. Data ($n=3_{biological\ replicates}$; $n=6_{technical\ replicates}$) are expressed as percentage of control and represented as mean±SEM (*p<0.05, **p<0.01, ***p<0.001).

4.8.5. Effect of LPA on migration of hPASMCs and hPAAFs

To determine whether, LPA has a functional influence on motility and in a concentration dependency, transwell migration assays have been carried out for studying the migration of hPASMCs and hPAAFs.

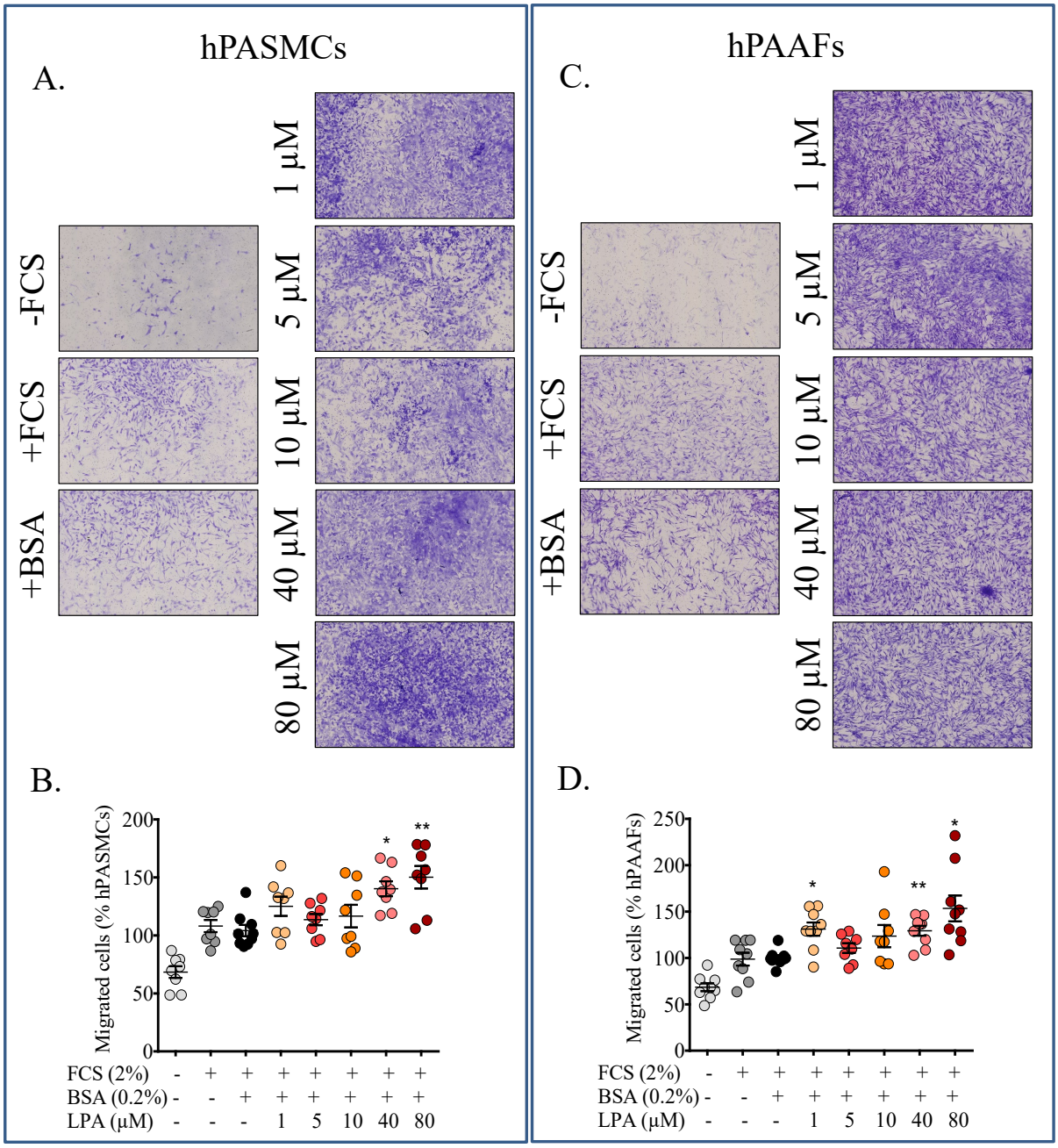

Figure 61: Effect of LPA on migration of hPASMCS and hPAAFs. Prior experiments, cells were serum starved for 24 h, then stimulated with different concentration of LPA using Boyden chamber assay; A. Representative microphotographs of transwell membrane of LPA induced hPASMCS migration; B. Quantification of the migrated hPASMCs; C. Representative microphotographs of transwell membrane of LPA induced hPAAFs migration; D. Quantification of the migrated hPAAFs; Data ($n=3_{\text{biological replicates}}$; $n=3_{\text{technical replicates}}$) are expressed as percentage of control and represented as mean±SEM (*p<0.05, **p<0.01, ***p<0.001).

hPASMCs were stimulated with LPA at concentration of 1, 5, 10, 40 and 80µM. The results showed a significant difference between -FCS and +BSA ($T(15) = -5.095$, $p < .001$), as negative and positive control, respectively, as well as no difference between +FCS and +BSA ($T(15) = 0.555$, ns) in terms of increased migration. The further comparison of +BSA with the stimulated groups was significant $F(5, 43) = 5.408$, $p < .01$). LPA significantly increased the cell migration

at 40 µM (140.28%; Tukey-HSD, $p < .05$) and 80 µM (150.17%; Tukey-HSD, $p < .01$) (Figure 61A and 61B).

In addition, the results regarding migration LPA hPAAFs showed a significant difference between -FCS and +BSA ($T(16) = -6.191$, $p < .001$) as control groups, as well as no difference between +FCS and +BSA ($T(16) = -0.180$, ns) in terms of increase of migration. Similarly, LPA increased the cell migration when different concentration was applied $F(5, 43) = 5.408$, $p < .01$). The results were suggesting that LPA significantly increased the hPAAFs migration at concentration of 1 µM (131.08%; Dunnett, $p < .05$), 40 µM (129.26%; Dunnett, $p < .01$) and 80 µM (153.37%; Dunnett, $p < .05$) (Figure 61C and 61D).

4.8.6. *Ex-vivo* effect of LPA on human precision cut lung slides (PCLS)

Further, in order to evaluate the *ex-vivo* effect of LPA and LPA inhibitor (PF8380) on vascular remodelling and downstream signaling pathways, the precision cut lung sections were treated with LPA +/- PF 8380 as described in Figure 62A.

LPA significantly increased the vascular remodelling in stimulated PCLS. The results are compared using a one-sided ANOVA test and showed a significant difference between the groups $F(4, 15) = 8.772$, $p < .01$). The GFs stimulated samples, served as a positive control and showed significant increase in comparison to 1% FCS treated group (Tukey-HSD, $p < .01$). Stimulation of the PCLS with LPA revealed increased MWT at different concentrations, 5µM LPA (Tukey-HSD, $p < .01$), 10µM LPA (Tukey-HSD, $p < .05$) and 50µM LPA (Tukey-HSD, $p < .05$) (Figure 62B and 62C). The results regarding the ratio show no significant difference between the groups $F(4, 15) = 0.495$, ns) (Figure 62B and 62D).

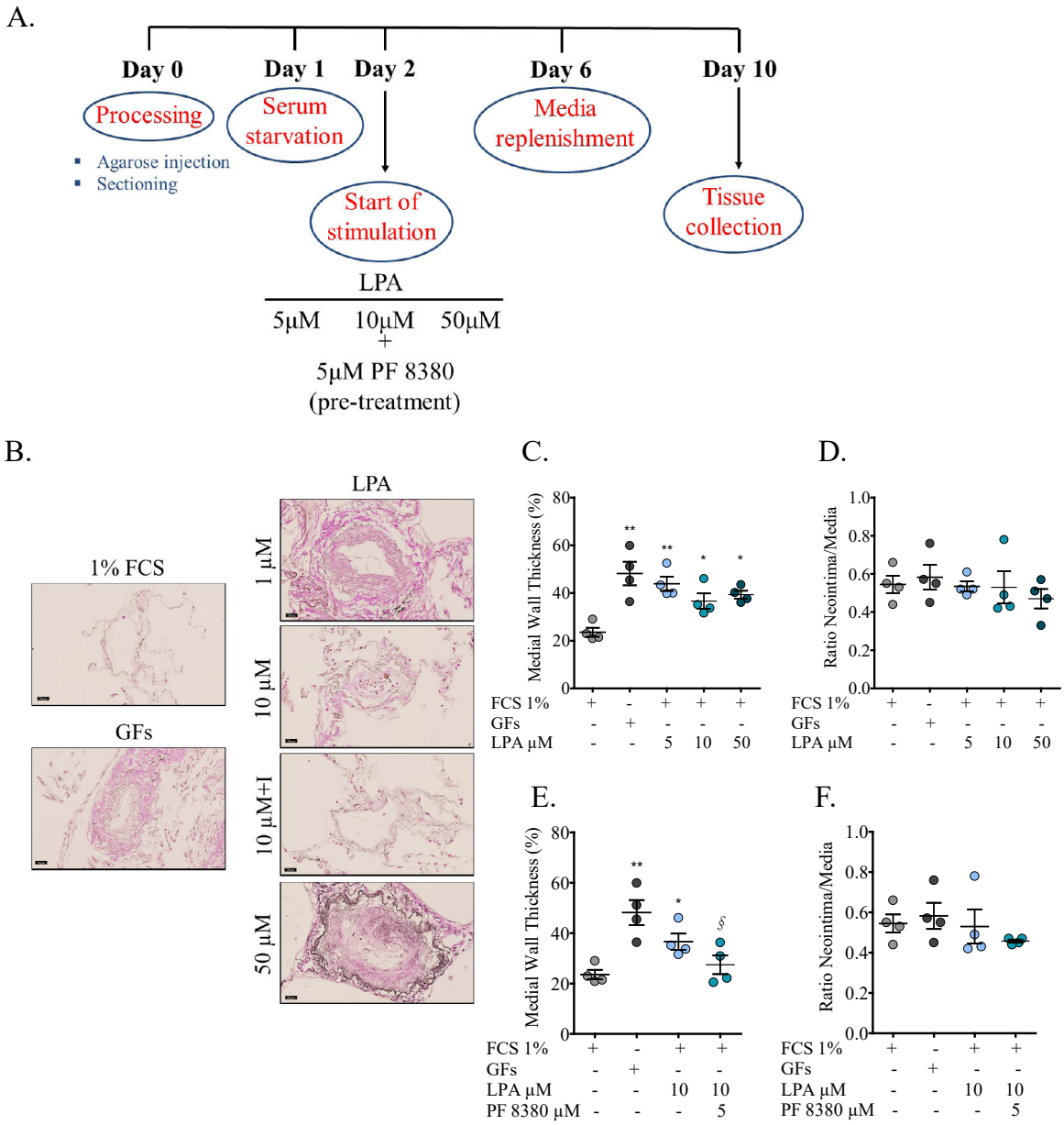

Figure 62: LPA *ex-vivo* induced vascular remodelling and effect of LPA specific inhibition. PCLS were treated with LPA (5, 10 and 50 µM); PF 8380 was used at PCLS stimulated with 10µM A. Schematic representation of the experimental plan and duration of the experiment; B. Representative microphotographs of vessels stained with Elastica Van Gieson from stimulated PCLS; B. Quantification of the medial wall thickness (MWT) in PCLS vessels shown as a percentage; C. Ratio neointima/media assessment of LPA stimulated PCLS. n=4. Data is represented as mean±SEM (n=12; *p<0.05, **p<0.01, ***p<0.001; ; §p<0.05, §§p<0.01, §§§p<0.001 versus GFs).

The inhibitor studies are compared using a one-sided ANOVA test and showed a significant difference between the groups $F(3, 12) = 9.204$, $p < .01$). As previously mentioned, the MWT of GFs stimulated samples, served as a positive control and showed significant increase in comparison to 1% FCS treated group (Tukey-HSD, $p < .01$). LPA at concentration of 10µM, leads to significant vascular remodelling (Tukey-HSD, $p < .05$). The PF 8380 has a potential

to diminish (decrease) this effect, however insignificantly (Tukey-HSD, ns). 20% FCS is significantly different from 10µM+PF8380 (Tukey-HSD, $p < .05$) (Figure 62E). The results regarding the neointima/media ratio showed no significant difference between the groups $F(3, 12) = 0.818$, ns) (Figure 62F).

4.8.7. The effect of ENPP2 reduction in mouse thrombosis model

To test whether ENPP2 has a causative role in the thrombus formation or resolution, a mouse model of inferior vena cava (IVC) ligation induced thrombosis was employed, on *Enpp2*$^{+/+}$ wild type (WT) and *Enpp2*$^{+/-}$ heterozygous (HZ) ENPP2 mice. Ultrasound measurements were taken on day 3, 7 and 14 post-ligation, while thrombus, organ harvest and blood cell counts were performed on day 7 and day 14 post-ligation (Figure 63).

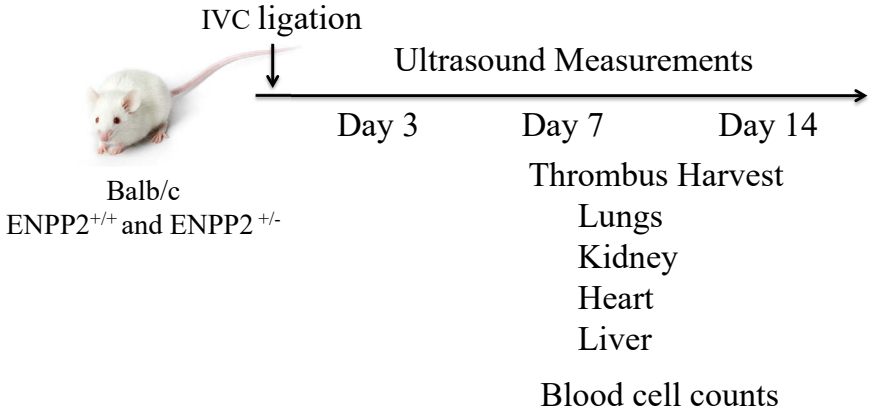

Figure 63: Schematic representation of the experimental plan of CTEPH thrombosis model. Ligation of IVC was performed on WT and HZ mice. Experiment was performed with three different time points, day 3, 7 and 14, thrombus measurements were taken at day 7 and 14, along with organ harvest and blood cell count.

Thrombus area, thrombus length and thrombus volume were evaluated within 3 different time points. The comparison of *Enpp2*$^{+/+}$ and *Enpp2*$^{+/-}$ regarding thrombus area over the three measurement points revealed that *Enpp2*$^{+/-}$ has significantly higher area in comparison to *Enpp2*$^{+/+}$ at Day 14 ($F(1, 6) = 3.869$, $p < .05$) (Figure 64A).

Thrombus length over the three measurement points significantly dropped $F(1, 6) = 7.758$, $p < .05$), while *Enpp2*$^{+/+}$ and *Enpp2*$^{+/-}$ mice didn`t present significant difference in the length in any of the time points ($F(1, 6) = 0.654$, ns) (Figure 64B).

Similarly, the thrombus volume also significantly decreased $F(1, 6) = 23.336$, $p < .01$) with HZ and WT being significantly quadratic (not linear) different from each other over time ($F(1, 6) = 7.743$, $p < .05$) (Figure 64C).

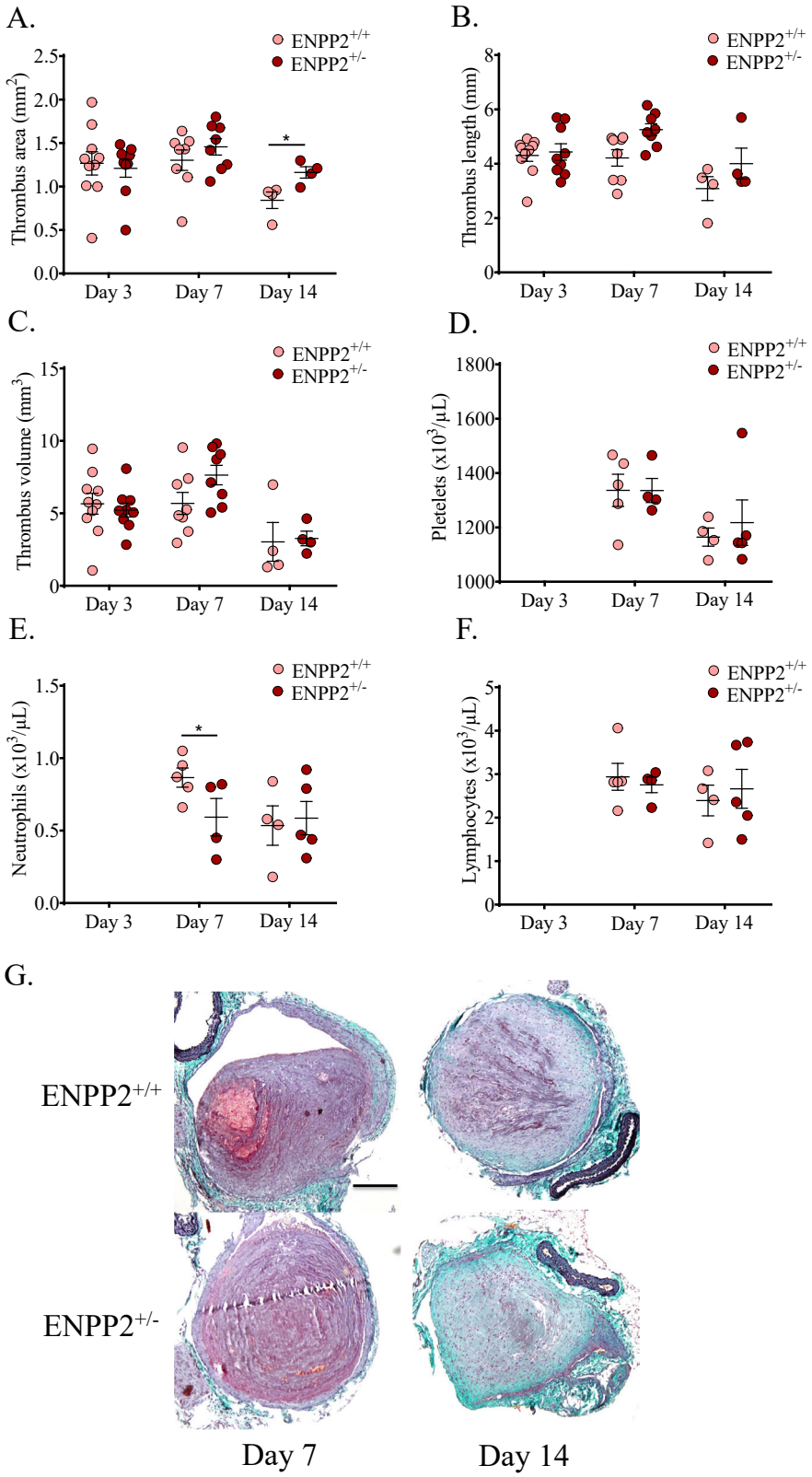

Figure 64: The effect of *Enpp2* partial deficiency in thrombosis model of CTEPH. Measurements were asses at three time points for both WT (*Enpp2*$^{+/+}$) and HZ (*Enpp2*$^{+/-}$) mice. Blood cells analysis was performed at day 7 and 14. Evaluation of the: A. Thrombus area; B. Length; C. Volume; D. Platelets; E. Neutrophils; F. Lymphocytes. Data is represented as mean±SEM (*p<0.05, **p<0.01, ***p<0.001).

In terms of platelets number, comparing the *Enpp2*$^{+/+}$ and *Enpp2*$^{+/-}$ there was no significant difference within all three time points (T(7) = -0.578, ns) (Figure 64D), while the neutrophils number was significantly altered at day 7 in the *Enpp2*$^{+/-}$ (T(7) = 2.009, $p < .05$) (Figure 64E). No significant change was noticed in the number of lymphocytes within all three time points (T(7) = -0.453, ns) (Figure 64F) .

5. Discussion

The pathophysiological and molecular mechanisms underlying chronic vascular scaring and/or distal vessel remodelling in CTEPH, are poorly comprehended. CTEPH as a rear, complex and multifactorial disease is generated by wide scope of clinical factors and alterations leading to PH and RV dysfunction (I. M. Lang et al., 2016; J. Pepke-Zaba, 2010); (Matthews & Hemnes, 2016). Importantly, this study delineates the histopathological and molecular similarities and differences between end-stage CTEPH and the well-studied form of PAH, IPAH. In addition, it identifies the resemblance in terms of both structural and molecular changes between patients with proximal (major) vessel CTEPH obliterations and distal vessel arteriopathy. Importantly, it also describes that the vascular remodelling intensity in recurrent CTEPH is independent of the site of obstruction. Next, it gives an overview of the distal vascular remodelling of patients who developed CTEPH due to sarcoma and further underwent for PEA surgery. Furthermore, by employing unbiased genome-wide expression profiling based approach, we identified the disease-specific genes and signalling pathways in end-stage CTEPH and functionally identified the key role of 2 differentially regulated genes CHI3L1 and ENPP2 in the initiation and/or maintenance of the vascular remodelling, both *in vitro* and *ex vivo*. Finally, we utilized the PEA repository to morphologically and molecularly characterize the ongoing CTEPH in terms of proximal and distal (patent or completely occluded) vascular remodelling. Taken together, this study conveys new insights in the histopathological and molecular features of CTEPH.

5.1. CTEPH exhibits distal histopathological resemblance to IPAH

The vascular lesions elucidating PH encompass eccentric intima thickening and fibrotic, plexiform, concentric, and dilation/angiomatoid formations, medial smooth muscle cell hypertrophy and increased adventitial thickness due to collagen deposition (Rubin M. Tuder 2007). In CTEPH, the histopathological features of microvascular (small vessel) disease present similarities to those seen in IPAH and Eisenmenger`s syndrome (Moser 1993, Azarian 1997, Yi et al 2000).

In our initial work, we characterized and compared the vascular remodelling in CTEPH with IPAH, in terms of assessing the medial hypertrophy and muscularization, intimal thickening and collagen deposition. Severe vascular wall thickening was observed in both CTEPH and IPAH, distinguished by Weigert–van Gieson staining in all types of vessels, d=20-70 µm, 70-150 µm and >150 µm (media and the newly formed intima, in comparison to the tiny vessel wall of the donors (Figure 7).

The morphometric analysis confirmed the presence of medial hypertrophy in CTEPH, in all different vessel diameters, in similar extent as in IPAH, and twice higher in comparison to the donor controls (Figure 8A-8C). Medial hypertrophy (represented as medial wall thickness - MWT) as a typical pathological feature of PH affects muscularized arteries (ranging between 70 and 500 μm in diameter), and precapillary vessels (below 70 μm in diameter) (Rubin M. Tuder 2007). Similarly to our findings, Moser and Bloor (Moser, Bloor, 1993) conducted morphometry on 234 vessels (25 to 100 μm in diameter) from the patients with CTEPH and discovered that the mean muscle mass of the muscular arteries and arterioles in the autopsy group was 41% greater than the value for the control group. Furthermore, a piglet animal model closely resembling CTEPH features, performed by ligation of the left pulmonary artery, followed by weekly transcatheter embolization of the right lower-lobe arteries (Mercier, 2013) confirmed our findings. Animals of the CTEPH group showed severe hypertrophy in obstructed and unobstructed territories, compared to the sham group. The distribution of the MWT values for each individual patient of CTEPH was similar to IPAH, in contrast to the donor samples. The MWT of IPAH samples were more homogenously distributed, in comparison to CTEPH, where some patients displayed higher variability to the rest of the corresponding samples (Figure 8D). The distribution of the individual densities of the MWT, revealed fairly Gaussian curve resemblance for both CTEPH and IPAH samples, presenting that some samples have bimodal distribution of the MWT values (8E). These findings suggest that, despite the unbiased selection of the explanted CTEPH tissues, the vessels didn`t show heterogeneous profile. On contrary, the distribution of the medial hypertrophy was independent of the fact whether vessels belong to the fully obstructed areas or those in high-share stress (or hyper-perfused), which is supported by the animal model of Mercier et al (Mercier, 2013). Furthermore, it has been reported that the narrowing of resistance vessels is heterogeneous. In PAH, approximately around 30% of the vessels were affected, while 70% of vessels had diameters not different from vessels of control subjects (Nina Rol at al 2017).

Notably, along with the media remodelling, increased intimal thickening was noticed in all different sized vessels in CTEPH and similarly in IPAH (Figure 9A-9C). Intimal lesions are accounted for decreasing the vessel lumen in a greatest extent, being characterized as intima thickening, and fibrotic, plexiform, concentric, and dilation/angiomatoid lesions (Rubin M. Tuder 2007). Eccentric intimal fibrosis and concentric laminar intimal fibroelastosis in patients with CTEPH has been reported by Moser and Bloor (Moser, Bloor, 1993) for around 67% and 80% among the 15 cases, respectively. Along with our findings, significant intimal thickening

of larger arteries (d=401-600 μm), as well as in the smaller arteries has been reported in CTEPH, although in contrast to PPH they were significantly smaller (Yi et al, 2000). The analysis of the distribution of the values for each individual patient of CTEPH and IPAH patients presented homogeneous distribution of the values for the ratio, in contrast to the donor samples (Figure 9D) as well as the individual densities confirming the Gaussian distribution suggesting that, vessels in CTEPH and IPAH patients are similarly affected by the neointima remodelling (Figure 9E).

Extensive muscularization of the pulmonary arteries is one of the well-known feature of PH, mainly affecting distal pulmonary arteries (d=70-500 μm), and precapillary vessels (d < 70 μm). Our results suggested that the small vessels with d = 20-70 μm are highly muscularized in diseased conditions, in both CTEPH and IPAH in a similar way, following a transition from decreased percentage of non-muscularized to increased percentage of fully muscularized vessels in CTEPH and similarly in IPAH (Figure 10A and 10C). Dorfmüller et al., have shown that in the previously mentioned CTEPH experimental model, animals presented severe remodelling of septal veins within the left lung and, to a lower extent, within the right lower lobe. Arterioles or venules (d = 50 μm) showed an increased muscularization in CTEPH left lungs and CTEPH right lower lobes, while they were attenuated in CTEPH right upper lobes and sham animals (Dorfmüller et al 2014). The results from the immunolocalization staining of α-SMA and vWf confirmed the increased immunoreactivity to cytoplasmic α-SMA in the medial layer, suggesting that vascular remodelling is present and prominent in both CTEPH and IPAH, in a similar extent, with vWf positive layer marking the lumen (Figure 10B).

An increased vascular tone is as well represented by adventitial thickening, caused by collagen deposition. Hereby, we confirmed that CTEPH is characterized by significantly increased level of total collagen area in comparison to donors. Interestingly, the CTEPH exhibited more prominent collagen deposition even in comparison to IPAH (Figure 11). The limitation of this method or the microscopic principle is that it can`t differentiate between vascular and systemic collagen, therefore the evaluation was performed on a complete tissue, as a total collagen measurement. The external diameter of pulmonary arteries is normally represented by adventitia for approximately 15% of the size of the vessel, while in IPAH arteries, the adventitial thickness increases up to 28% of artery diameter, predominantly due to collagen deposition (Chazova et al, 1995).

Taken together, all the structural changes in both forms of PH, IPAH and CTEPH, may be driven by a switch from “quiescent” towards “pro-proliferative”, “pro-migratory”, “apoptosis-

resistant" and "pro-inflammatory" vascular cells, leading to increased PVR and ultimately to RV failure (Gamen et al, 2016). To our knowledge, this is the first study comparing head-to-head the vascular remodelling in CTEPH and IPAH.

5.2. CTEPH manifests significantly divergent global transcriptional regulatory landscape in comparison to IPAH

Next, we hypothesized that the analysis of the global transcriptional regulatory landscape and networks in CTEPH will provide us the common or unique genes or mechanisms driving small vessel arteriopathy in CTEPH as compared to IPAH. For this purpose, we microdissected pulmonary vessels from donors and CTEPH and IPAH patients and performed genome-wide expression profiling using microarrays (Figure 12A and 12B). The transcriptomic analysis revealed a significant portion of genes which were similarly regulated in both CTEPH and IPAH (Figure 12C). Several of them are already known to be altered in IPAH, such as NFATC2, BMPR2, VEGFA, PDGFRA etc (Figure 12D). In PAH, activation of NFAT (nuclear factor of activated T cells), a Ca^{2+}/calcineurin-sensitive transcription factor, leads to decresed Kv current and Kv1.5 expression and increased [Ca2+]i, [K+]i, mitochondrial potential ($\Delta\Psi m$), and bcl-2 levels. These findings converge an apoptosis-resistant and pro-proliferative phenotype of PASMCs (Bonnet, 2007). BMPR2 is another gene which was downregulated in both IPAH and CTEPH. BMPR2 is a transmembrane serine/threonine kinase receptor as a part of TGF-β superfamily. It is involved in several signalling pathways that regulate cellular differentiation, proliferation and apoptosis via BMPs (Upton et all, 2013). Either loss of function or reduction in BMPR2 expression may be sufficient to develop PAH (Upton et all, 2013) which is in line with our findings, having the BMPR2 downregulated in the laser dissected vessels. The *in-vivo* experimental model of Cre-dependent BMPR-II ablation in the endothelium (Hong et al. 2008) or targeted overexpression of a dominant negative BMPR-II in smooth muscle cells (West et al.2005) causes spontaneous PAH in mice. VEGFA regulated by HIF1 has been implicated in the pathogenesis of PH. El Kasmi et al. have shown that conditioned medium (CM) from bovine fibroblasts from chronically hypoxic hypertensive calves (PH-Fibs) also induced transcription of Vegfa in naïve mouse, rat, and bovine macrophages. Human PH-Fib CM also induced VEGFA mRNA in naive human monocytes (Karim C. El Kasmi, 2014). Furthermore, altered PDGF signalling was shown to play an important role in the progression of PH. A study has shown that using a potent PDGF receptor antagonist STI571 (imatinib) reversed advanced PH in two different animal models (Ralph Theo Schermuly, 2005).

According to the microarray analysis, among the differentially identified genes with LogFC > 1, only a fraction of 17.65% were commonly regulated between CTEPH *vs.* donor and IPAH *vs.* donor. With respect to CTEPH, the total number of regulated genes were 1339, among them 618 genes were upregulated, while 721 downregulated in comparison to the donor controls (Figure 13A-13C). A study has reported gene expression profiles of ECs isolated from patients with CTEPH and normal tissue, where they found 1614 genes significantly regulated. Among these, 880 genes were upregulated in the CTEPH samples and 734 were downregulated (Song Gu, 2013). The most significantly regulated genes in this study were Prostaglandin-Endoperoxide Synthase 2 (PTGS2), T-Box 15 (TBX15), Flavin Containing Dimethylaniline Monoxygenase 3 (FMO3), Leucine Rich Repeat Containing 32 (LRRC32), UBA Like Domain Containing 2 (FAM100B). In our experimental setup, PTGS2 was significantly upregulated as well, while TBX15 was mildly upregulated, FMO3 was not regulated, while LRRC32 was downregulated, the results to FAM100B were not applicable. Chordin Like 1 (CHRDL1), FRAS1 Related Extracellular Matrix 1 (FREM1), Basonuclin 2 (BNC2), Acyl-CoA Dehydrogenase Long Chain (ACADL), Unc-13 Homolog C (UNC13C) were shown to be downregulated in the same study, while in our data CHRDL1 was the only gene to be downregulated, while the rest were not regulated or slightly upregulated. On one hand, these differences in the gene expression profiles suggest that using more complex system, such as microdissected vasculature, can enrich the gene expression analysis in contrast to purely isolated ECs. On the other hand, our experimental setup employs end-stage lung tissues, while ECs in the study listed above were isolated from PEA material, meaning, an on-going disease.

Among the gene selection of LogFC > 1, one of the commonly regulated genes in both, CTEPH *vs.* donor and IPAH *vs.* donor was NFATC2. As presented in the Volcano plots (Figure 13D) and in Table 19, CHI3L1 came as a gene which is upregulated in CTEPH, while down regulated in IPAH. Several other genes were regulated in opposite direction in CTEPH and IPAH, both in contrast to the donor. Chitinase-3-like-1 (CHI3L1) also known as YKL-40 (cartilage-glycoprotein 39) is a 40-kDa secreted heparin-, chitin- and collagen-binding lectin (Fusetti, Pijning, Kalk, Bos, & Dijkstra, 2003). CHI3L1 is secreted by broad spectrum of cells, such as neutrophils, macrophages, synovial cells, fibroblasts, connective tissue cells, ECs, SMCs, epithelial cells and tumour cells (Di Rosa, Malaguarnera, De Gregorio, Drago, & Malaguarnera, 2013). The physiological and biological functions of CHI3L1 are not delineated in detail (Kawada, Hachiya, Arihiro, & Muizoguchi, 2007). It is suggested that it affects the proliferation and differentiation of connective tissue cells (De Ceuninck et al., 2001; Recklies,

White, & Ling, 2002), inflammation and matrix remodelling (Di Rosa et al., 2013), activation of vascular endothelial cells (Malinda, Ponce, Kleinmann, Shackelton, & Millis, 1999) and angiogenesis (Francescone et al., 2011). Studies are showing that CHI3L1 expression is enhanced in patients with different lung diseases, such as idiopathic pulmonary fibrosis (IPF) for example the plasma levels of CHI3L1 in IPF patients correlate with the disease progression (Zhou et al., 2014). Increased CHI3L1 is associated with asthma and chronic obstructive pulmonary disease, suggesting its potential as a biomarker of underlying chronic inflammatory disease processes (Chupp et al., 2007; James et al., 2016).

Furthermore, one of the selected genes, ENPP2, showed a significant upregulation in CTEPH, while no change was detected in IPAH (Figure 13D). The physiological function of ENPP2 is to produce LPA, a lipid mediator (Kondo et al., 2014), involved in wide variety of processes such as cell migration, neurogenesis, angiogenesis, smooth-muscle contractions, platelet aggregation, and wound healing (Moolenaar et al., 2004). LPA may as well modulate endothelial cell function and endothelial permeability (Ishii et al., 2004; Moolenaar et al., 2004; Sarker et al., 2010). It has been postulated that LPA promotes fibroblast and monocyte differentiation into myofibroblast and fibrocyte, respectively (Shao et al., 2008; Tang et al., 2014).

Several similarly and differentially regulated signalling pathways were enriched in both CTEPH and IPAH. Interestingly, the most prominently regulated pathways in CTEPH and in contrast to IPAH were alcoholism, systemic lupus erythematosus and viral carcinogenesis (Figure 14A and 14B). The KEGG pathways analysis is based on the number of regulated genes falling into a particular set, and in this case most of them related to alcoholism, came to be significantly regulated in CTEPH. In contrast, the previously published data obtained from microarray of endothelial cells isolated from 5 CTEPH patients (Song Gu, 2013), suggested that cytokine-cytokine receptor interaction, Leishmaniasis, cell adhesion molecules (CAMs), Chagas disease and T cell receptor signalling pathway were among the most significantly upregulated pathways. The same study revealed that Focal adhesion, Neuroactive ligand-receptor interaction, Arrhythmogenic RV cardiomyopathy (ARVC), Calcium signalling pathway and Wnt signalling pathway were pathways associated with significantly downregulated genes.

With regard to the IPAH, signalling pathways related to lysosome and oxidative were among the most significantly regulated pathways (Figure 14A and 14B). As observed from Figure 15C, the majority of the genes determined by LogFC >1 fall into metabolic pathways were

upregulated in IPAH (Figure 14D). In IPAH, most of the genes supporting the lysosomal processes are upregulated, along with all upregulated genes in oxidative phosphorylation Figure (Figure 14D). Regulation of genes involved in metabolic pathways seems to be a common feature of CTEPH and IPAH. However, in contrast to IPAH, most of the differentially regulated metabolic genes in CTEPH were downregulated (14E).

To our knowledge, this is a first study to comprehensively evaluate the pathophysiological and molecular aspects of end-stage CTEPH and compare it with the well-studied form of PH, IPAH. Further studies are needed to understand how PH initiating factors, such as high share stress, hypoxia and/or inflammatory molecules trigger the underlying pathological phenotype and particular molecular mechanisms.

5.3. Central CTEPH manifest similar histopathological changes as peripheral CTEPH

As the initial screening of CTEPH explanted lung samples confirmed a nearly similar distribution of the vascular remodelling, despite the expected heterogeneity, we aimed to more specifically characterize the vascular lesions underlying patients with central (proximal, operable) and peripheral (distal, non-operable) course of CTEPH. Notably, we identified severe vascular wall thickening in both central and peripheral CTEPH in all different vessel sizes (Figure 15).

The morphometric analysis confirmed the presence of medial hypertrophy in both central (proximal) and peripheral (distal) CTEPH, with a similar tendency in all vessel sizes (Figure 16A-16C). Surprisingly, the central and the peripheral CTEPH showed similar levels of vascular remodelling and vasculopathy, despite the conflicting arguments in the scientific society. In these terms, we sought that the proximal occlusion in CTEPH will affect the distal vasculature in a similar manner, likewise the distal, non-surgically assessable obliterations both leading to microvascular disease. Apart of the present occlusions, many other factors can affect the occurrence of inflicted microvasculature, such as chronic hypoxia, high share-stress, circulating factors, endothelial dysfunction etc. Our findings are similar to those of Moser and Bloor (Moser, Bloor, 1993) reported before, whereas the morphometric analysis of vessels with d = 25-100 μm revealed increased vessel wall for the CTEPH samples in contrast to the control group. Aligned with that, the piglet CTEPH animal supported our findings to present severe hypertrophy in obstructed and unobstructed territories, compared to the sham group. (Mercier, 2013). The distribution of the MWT values in central or peripheral CTEPH was similar, despite the heterogeneity of the MWT values in central CTEPH (Figure 16D). The individual densities

of the MWT, showed Gaussian distribution for peripheral CTEPH and partially bimodal distribution for central CTEPH (16E). These findings suggest that, despite the proximity of the disease to the obstruction site or presence of distal disease, the vascular remodelling intensity showed similar tendency.

Next, we assessed the neointima/media ratio in central and peripheral CTEPH and compared to the respective donors. As expected along with the media remodelling, increased intimal thickening was noticed in all different sized vessels in central and peripheral CTEPH (Figure 17A-17C). As described before, Yi et al. were in charge of the discovery that a significant intimal thickening of larger arteries (d=401-600 μm), as well as smaller arteries prevailed in patients with CTEPH (Yi et al, 2000). Surprisingly, a significant difference between the central and peripheral CTEPH in terms of neointima deposition was observed. This can be explained by the fact that the peripheral lesions in CTEPH patients are inaccessible for PEA and remain unaffected. The distribution of the neointima/media ratio values for each individual patient of central and peripheral CTEPH, revealed indistinguishable and homogeneous distribution in comparison to the donors (Figure 17D). The distribution of the individual densities of the ratio resembled Gaussian distribution, suggesting that the neointima deposition is affected similarly, independently of the site of the disease (Figure 17E).

Adventitial thickening, caused by collagen deposition was one of the features of both central and peripheral CTEPH. As presented in Figure 18A and 18B, increased collagen total area was prominently noticed in central CTEPH, in contrast to the peripheral CTEPH. The organized thrombi in central CTEPH predisposes for fibrous plaques with angiogenesis and athero-sclerotic plaques (Arbustini et al., 2002). The intimal layer mainly displayed collagen and elastic fibres deposition and presence of α-SMA positive cells (A. L. Firth, Yao, et al., 2010; Owens et al., 2004), which may explain enhanced collagen deposition in the central CTEPH.

5.4. Genome wide expression profiling of central CTEPH manifests similar and unique global transcriptional regulatory landscape compared to peripheral CTEPH

Based on the histological findings, we postulated that the analysis of the global transcriptional regulatory landscape and networks will provide us knowledge on molecular mechanisms driving small vessel arteriopathy in central and peripheral CTEPH. To address, we microdissected pulmonary vessels from donors and central and peripheral CTEPH and performed genome-wide expression profiling using microarrays (Figure 19A). The mdplots showed that peripheral CTEPH encounters higher enrichment of regulated genes, while the

comparison between peripheral and central revealed diminished gene enrichment (Figure 19B). Interestingly, as presented by the heatmap displaying hierarchical clustering of the top 50 (selected by F-value) (Figure 19C), we encountered quite similar gene expression profiles for central and peripheral CTEPH. The result might exemplify the outcome that molecular mechanisms in both central and peripheral CTEPH might not be as different as expected. To that extent, among the all protein-coding genes with LogFC > 1 differential expression, only 43.02% of the genes were commonly regulated in central CTEPH in comparison to peripheral CTEPH (Figure 20A). Among the gene selection of LogFC > 1, the genes of previous interest, CHI3L1 and ENPP2 came to be among the significantly and commonly regulated genes in a similar direction in both, central and peripheral CTEPH (Figure 20D). In comparison to the previously reported study (Song Gu, 2013), in our experimental setup PTGS2 and TBX15 were highly upregulated in both, whereas FMO3 was upregulated only in peripheral CTEPH. However, the downregulated genes identified in the study by Song et al. such as CHRDL1, FREM, BNC2 ACADL were upregulated in our study, while UNC13C was slightly downregulated suggesting differences between two studies which could be explained by the nature of peripheral CTEPH samples.

Interestingly, four genes were regulated in opposite direction in central and peripheral CTEPH. MCEMP1, CKS1B, PRPF6 and HOXC6 were upregulated in central CTEPH, while downregulated in peripheral CTEPH. Similarly, the genes of interest CHI3L1 and ENPP2 were among the commonly regulated genes between central and peripheral CTEPH. On the other hand, MCEMP1, CKS1B, PRPF6, HOXC6 were downregulated in peripheral CTEPH compared to central CTEPH (Figure 21A and 21B). MCEMP1 has been identified as a novel transmembrane protein of human lung mast cells (Kang Li, 2005). It is speculated to be involved in regulating mast cell differentiation or immune responses. Increased expression of CKS1B is known to be associated with lymph node metastasis and poor prognosis in nasopharyngeal carcinoma (Lina Xu, 2017). Single nucleotide polymorphisms (SNPs) are the most common genetic variants in the human genome and have been shown to be associated with risk of human diseases, including cancers. The six novel SNPs in PRPF6 are associated with PRPF6 mRNA expression in lymphoblastoid cells (Yongchu Pan, 2016 or 17). HOXC6 has been implicated in gastric and colorectal cancer (Meiling Ji, 2016, Q. ZHANG, 2013). Within the central CTEPH or the proximal occlusion, the gene expression profiles of the organized white human PEA thrombi, manifest decreased expression of several vascular specific genes such as KDR, vascular endothelial cadherin (VE-catherin) and podoplanin

(PDPN), as well as angiopoetin 2 (ANGPT2), platelet endothelial cell adhesion molecule (PECAM 1), VEGFA etc. (Alias et al., 2014). Inflammatory markers, such as C-reactive protein (CRP) (R. Quarck et al., 2009), tumour necrosis factor alpha (TNF-α) (Langer et al., 2004) and monocyte chemoattractant protein-1 (MCP-1) (Kimura et al., 2001) are elevated in plasma and proximal thrombi of CTEPH patients, in correlation with the patient hemodynamic parameters. A study has reported that CRP induced NF-κB activation may be involved in the pathogenesis of CTEPH (Wynants et al., 2013).

Various comparable and distinct signalling pathways were enriched in both central and peripheral CTEPH. Interestingly, the most prominently regulated pathways in both central and peripheral CTEPH were metabolic pathways, pathways in cancer and PI3K-Akt signalling pathway, defined by number of differentially regulated genes in a specific pathway (Figure 22A and 22B). PI3K pathway for example, is one of the pathways activated in response to hypoxia, thus contributing to development of PAH (Xiao-Dong Xia, 2016). When potent inhibitors of PI3K/Akt, wortmannin and β-aminopropionitrile (β-APN), are used in rat model of hypoxia-induced PAH, the cross-linking of collagen (one of the PAH features) was significantly reversed. Few interesting pathways that predominantly take place in the peripheral part were systemic lupus erythematosus, alcoholism and vascular smooth muscle contraction. Regarding alcoholism, the KEGG pathway database (https://www.genome.jp/kegg-bin/show_pathway?hsadd05034) suggest that one of the primary mediators are dopaminergic ventral tegmental area (VTA) projections to the nucleus accumbens (NAc) have been identified. Depending on whether the exposure to alcohol is acute or chronic, different signalling pathways are further activated. Acute exposure affects dopamine release into the NAc, which activates D1 receptors, stimulating PKA signalling and subsequent CREB-mediated gene expression, while chronic alcohol exposure leads to an adaptive downregulation of this pathway, in particular of CREB function. Whether some of the medication that CTEPH patients take in the time-course of the disease before transplantation affects the dopamine release and consequently affecting the above listed signalling pathways, is not really known.

To our knowledge this is the first study differentiating between central and peripheral CTEPH in terms of histopathological characterization and molecular profiling. Further research is needed to delineate the reasoning behind the prevalence of one or the other condition.

5.5. Distal vessel remodelling in CTEPH is evenly distributed and independent on the disease site

In order to systematically assess the vascular changes of the macro- and micro- vasculature, an ex-vivo ink-injection was performed by cannulating the central pulmonary arteries and injecting the ink into the periphery of a case study patients with central and recurrent CTEPH (Figure 23). The areas of interest were those proximal to, thromboembolism and distal to thromboembolism. The pre-thrombus area (proximal to thromboembolism) was affected by extensive remodelling presented by concentric intimal lesions and medial hypertrophy (Figure 24C and 24F). The area of the central thromboembolism was fairly overwhelmed by intimal fibrosis and recanalization (Figure 24G-24I). Similarly, the distal to thromboembolism regions revealed existence of concentric, highly remodelled vascular lesions, characterized by intimal and medial thickening and extensive matrix deposition (Figure 24J-24O, 25). In corroboration of these findings, the study of Dorfmüller et al (Dorfmüller, 2014), with blue (bronchial systemic vessels) and green (pulmonary vessels) ink-injected patient from ineffective PEA, revealed an eccentric muscular fibrosis in the peripheral pulmonary arteries and recanalization, whereas both inks we mixed. These results suggested the direct connection between the bronchial and pulmonary veins within the lobar septa. Interestingly, the same study examined eight CTEPH (ineffective PEA and inaccessible by PEA) patients and reported organized thrombotic lesions, known as colander-like lesions, intimal fibrosis of small pre-septal venules, as well as interstitial remodelling. These characteristic features were observed as well in the Giessen and Paris cohort, so as in the case study.

Importantly, pre-, thrombus, and post-thrombus areas presented with severe vascular remodelling in terms of increased medial wall thickness in comparison to the baseline (26A). Next, the distribution of the MWT values for each individual site was similar for all the vessels, independently of the area they were taken from (Figure 26B). Interestingly, the distribution of the individual densities of the MWT, showed bimodal Gaussian curve for the pre-, post- and the thrombus part itself (Figure 26C) suggesting that in this particular patient some of the vessels were extremely remodelled, while some were having normal values of MWT, although the mean of the twice higher than the baseline. In accordance with our results, it has been reported that the narrowing of resistance vessels is heterogeneous. In PAH, approximately around 30% of the vessels were affected, while 70% of vessels had diameters not different from vessels of control subjects (Nina Rol at al 2017).

The neointima formation was again confirmed by the neointima/media ratio for the pre-, thrombus and the post-thrombus for all sizes of the vessels. In the pre-thrombus part, 20-70 μm vessels were by value close to baseline, while the 70-150 μm and > 150 μm vessels, the ratio was twice to three times increased, respectively (Figure 27A). Similarly, the pre-, thrombus- and the post-thrombus presented homogeneous distribution of the values of the neointima/media ratio (Figure 27B) and the distribution of the individual densities of the ratio resembled Gaussian curve for all CTEPH sites (27C). These results suggest that the neointima is uniformly formed independently on the disease site. As expected, the total collagen area (%) was increased in the pre-, thrombus and post-thrombus is a similar manner, suggesting a random distribution of the collagen, independently of the area affected by the disease (Figure 28).

5.6. Different lung lobes from patients with CTEPH dispense a uniform distribution of distal vessel remodelling

As presented in Figure 29 and 30A-30C, severe medial hypertrophy was observed in both central and peripheral lobes of central CTEPH patients and it was characteristic for all sizes of the vessels. The distribution of the MWT values within the central or the peripheral CTEPH lobes was similar, and different from the donor (Figure 30D). The individual densities of the MWT, showed Gaussian distribution for both central and peripheral CTEPH lobes (Figure 30E). The neointima/media ratio positively correlated with the growth of MWT. All sizes of the vessels 20-70 μm, 70-150 μm and >150 μm displayed increased ratio in both central and peripheral lobes (Figure 31A-31C). Neointima/media ratios were evenly distributed within the central or the peripheral CTEPH lobes, and different from the donor (Figure 31D). The individual densities of the ratio, showed Gaussian distribution for both central and peripheral CTEPH lobes (Figure 31E). Collagen deposition was evaluated as before, and the outcome was similar. Central CTEPH lobes were exhibiting significantly higher values of total collagen area, along with the peripheral lobes (Figure 32).

These findings suggest that, despite the proximity of the disease to the obstruction site or presence of distal disease as a secondary outcome, the vascular remodelling intensity showed similar tendency.

5.7. Sarcoma-CTEPH patients present comprehensive vascular remodelling, similar to end-stage CTEPH patients

Pulmonary sarcoma is an extremely rare neoplasm affecting the pulmonary arteries, characterized by tumour cells that undergo endothelial, fibroblastic, or myofibroblastic differentiation (Daniel T. Matthews, Anna R. Hemnes 2016). A study has reported only 2 cases of pulmonary artery sarcoma in a series of 200 consecutive PEAs highlighting that sarcoma can actually mimic CTEPH (Bernard 2006). In corroboration, evaluation of the MWT revealed extensive vascular remodelling in sarcoma-CTEPH patients, in a similar extent as all CTEPH patients listed above (Figure 33 and 34A-34C). In contrast to the donors, the distribution of the MWT values within the sarcoma patients was higher (Figure 34D), while individual densities of the MWT, showed a significant shift in the distribution of the values, according to the Gaussian curve and in comparison, to the donors (Figure 34E). Likewise, the neointina/media ratio presented significant increase in sarcoma-CTEPH for all vessel sizes (Figure 35A-35C). The neointima/media values in the sarcoma patients were higher than the donors (Figure 35D) and the individual densities of the MWT, showed a Gaussian distribution in comparison to the donors (Figure 35E). The evaluation the collagen deposition confirmed the significant increase in total collagen area in sarcoma CTEPH (Figure 36A and 36B).

These results are suggesting that indeed, patients with sarcoma exhibit PH histopathological phenotype, more specifically close to those purely diagnosed with CTEPH.

5.8. PEA biorepository presents with tissue repair phenotype

In operable CTEPH, the organized thrombi affecting the proximal and segmental to subsegmental arteries, known as neointima is tightly adhered to the medial layer of the pulmonary arteries, which may completely obstruct the lumen of the artery (I. Lang, 2015). As a consequence, the intimal surface roughens and in order to restore the blood circulation and potentially decrease the PVR, recanalization (bands and webs) takes place (P. F. Fedullo et al., 2001). The lesions of CTEPH patients were described as: neointima, thrombotic, atherosclerotic and recanalized lesions. Regarding the composition of infiltrated cells in the organized thrombi, several studies confirmed presence and similar distribution of macrophages, T- and B- lymphocytes and neutrophils (Arbustini et al., 2002; Bernard & Yi, 2007; Rozenn Quarck et al., 2015). We have found that, the recanalization quite often takes place in the distal (or segmental to subsegmental) vascular tissue (Figure 38A and 38B), most likely due to hypoxia or high-share stress or circulating progenitor cells (Firth, A. L., 2010).

The recanalization is regulated by both pro- and anti- angiogenic factors (Ribatti, 2009). However, a mixed findings were reported in the literature. Zabini et al. (2012) reported that several angiostatic factors, such as collagen type I, PF4 and IP-10 are present in PEA material (Zabini et al., 2012). On the other hand, Naito et al. (2018) have been able to demonstrate that ECs isolated from PEA express not only high proliferative potential, but they have extensive angiogenic capacity, confirmed by greater degree of tube formation of these cells (Naito et al. 2018).

As the extracted neointima layer contains collagen and elastic fibres, as well as presence of α-SMA positive cells, (Owens, Kumar, & Wamhoff, 2004), we characterized the collagen deposition, according to the solubility in acid and pepsin. As appreciated from Figure 39C, the levels of soluble collagen are decreased in proximal fibrous tissue in comparison to the respective control, whereas levels of insoluble collagen are increased in distal completely occluded tissue (Figure 39D). The increased levels of insoluble collagen in distal occluded tissues suggest a newly formed collagen fibres which is observed during periods of rapid growth, development, tissue repair, remodelling and wound healing (Christine Theoret, 2016).

5.8.1. Several transcription factors are regulated in proximal and distal PEA

The global transcriptome of both proximal and distal PEA material brought insights into several deregulated and important TFs, including FoxO1 and 3, KLF2 and GATA6. Further on, we confirmed the results from the screening by real-time PCR. Growing evidence indicates that TFs have been implicated in the pathogenesis of PH and RV dysfunction (Pullamsetti et al., 2017).

In our study, FOXO1 was upregulated in both proximal and distal fibrous tissue, while FOXO3 only from distal perspective (Figure 40A-40C), emphasizing their involvement in the hyperproliferative and apoptosis-resistant phenotype of PASMCs, one of the hallmark of PAH (Savai et al. 2014). FOXOs control various cellular responses (Eijkelenboom & Burgering, 2013) and have been implicated in vascular structural maintenance (Mahajan et al., 2012; Oellerich & Potente, 2012). In general, FoxO1 and FoxO3 play a role in angiogenesis as well as in vascular remodelling (Potente et al., 2005). In addition, we identified significant downregulation of KLF2 in distal completely occluded tissue (Figure 40D), suggesting the influence of shear stress on KLF2 expression. Previous studies have reported that KLF2 is exclusively expressed in ECs and upregulated upon exposure to sustained shear stress (Dekker

et al., 2002). Further, shear stress induced KLF2 is shown to directly affect the eNOS levels, as an essential regulator of vascular reactivity and tone (Huang et al., 1995).

GATA-6 is a transcription factor which is highly expressed in quiescent vasculature, particularly in vascular SMCs, maintaining their contractile phenotype and lost upon vascular injury (Mano et al., 2015; Nishida et al., 2002). In our experimental setup, we observed significant increase of GATA6 in the distal completely occluded tissue (Figure 40E), suggesting that it may play a role in the pathogenesis of PH by regulating ET-1, plasminogen activator inhibitor-1 (PAI-1), matrix metallopeptidase 1 (MMP1), matrix metallopeptidase 10 (MMP10) etc (Ghatnekar et al., 2013).

To date, this is the first study that evaluated the transcriptional profile (coding and non-coding RNAs) of central and distal (segmental and subsegmental) vascular fibrous tissue from PEA. Previously, a study has shown differential expression of 185 lncRNAs in CTEPH proximal tissues compared with healthy control tissues and 464 regulated enhancer-like lncRNAs and overlapping, antisense or nearby mRNA pairs (Gu, 2014).

5.9. CHI3L1 is expressed in end-stage CTEPH and regulates vast varieties of cellular processes

CHI3L1 is enzymatically inactive molecule, secreted by endothelial cells, vascular smooth muscle cells macrophages, neutrophils, synovial cells, fibroblasts, connective tissue cells, epithelial cells and tumour cells (Di Rosa et al., 2013). CHI3L1 plays a protective role by enhancing inflammation and cell death, while in repair it plays a pro-fibrotic role by contributing to fibroblast proliferation and matrix deposition (Zhou et al., 2014). Increased CHI3L1 is associated with asthma and chronic obstructive pulmonary disease, suggesting its role in chronic inflammatory disease processes (Chupp et al., 2007; James et al., 2016).

As our results present, CHI3L1 has been upregulated in laser microdissected vessels from CTEPH (Figure 13D and 41A), and predominantly localized within PAECs and macrophages in patients with CTEPH, as well as in the media (PASMCs), and partially in the adventitia (PAAFs) of pulmonary vessels (Figure 41B). In addition, at basal level, among all the screened cell types, lung pericytes presented with highest expression of CHI3L1 at mRNA level, followed by PASMCs and PAAFs (Figure 42A), while CHI3L1 protein levels are highest in A549 tumour cells (Figure 42B and 42C). Indeed, increased levels of CHI3L1 was reported in lung cancer cells, in the lung tumour tissue and blood of patients with lung cancer (Bing Ma, 2015 or 2016).

Macrophages play a role in initiation, regulation and resolution of innate immune responses (Di Rosa 2012). On one hand, macrophages can be classically activated (M1), in the presence of interferon (IFN)-γ and lipopolysaccharide (LPS). On the other hand, when stimulated with IL-4 and IL-13, macrophages can undergo alternative activation towards an M2 phenotype (M2) (Di Rosa 2012). Since macrophages were shown increased immunoreactivity of CHI3L1 in CTEPH lungs, we examined the mRNA and protein levels of naïve and M1 and M2 macrophages. Similar to the published literature (Di Rosa, 2012), we found that M2 macrophages showed decreased CHI3L1 mRNA and protein expression in comparison to M1 macrophages (Figure 43A-43C).

5.9.1. Pro-PH factors drive a deregulation of CHI3L1 expression in vascular cells

Different pro-PH growth factors such as VEGFA, IL6, IL8, IL13, IL18, CCL2, PDGF-BB, TGF-β and TNF-α were shown to affect the vascular cellular proliferation, differentiation and migration (Schermuly, 2005; M Kathryn Steiner, 2009, Sung-Hyun Park 2014, Brian B. Graham, 2013). Our results suggested that among these, IL6 and TNF-α can induce the mRNA expression of CHI3L1 in PMECs, while IL13 and PDGF-BB downregulated CHI3L1 in hPASMCs. Similarly, TNF-α increased the CHI3lL1 mRNA levels in hPASMCs, yet in PAAFs it caused mRNA downregulation. Protein levels of CHI3L1 were not affected in all the cells types, implying that the 24 h time point was inefficient for protein synthesis and secretion (Figure 44-46).

5.9.2. CHI3L1 exhibits pro-proliferative, anti-apoptotic, pro-migratory and pro-contractile effects on vascular cells

The biological function of CHI3L1 is not completely delineated, although is speculated that it affects the proliferation and differentiation of connective tissue cells (De Ceuninck et al., 2001; Recklies et al., 2002), inflammation and matrix remodelling (Di Rosa et al., 2013), activation of vascular endothelial cells (Malinda et al., 1999) and angiogenesis (Francescone et al., 2011). In response to injury, CHI3L1 can be secreted from the differentiated macrophages and activated endothelial cells, further inducing proliferation and migration of SMCs (Nakashima, Raines, Plump, Breslow, & Ross, 1998).

Significant proliferation was noticed when hPASMCs were stimulated with 200 ng/mL recombinant CHI3L1 (Figure 47C), while hPMECs showed tendency to increased proliferation in response to CHI3L1 stimulation (Figure 47A). hPAAFs have shown no response to proliferation (Figure 47E). Likewise, a study implied a modest effect on proliferation of

PMECs (~25% increase in cell proliferation) and that proliferation was not significantly altered by the introduction of YKL-40 (CHI3L1) in colon cancer cells (Rong Shao, 2009). On contrary, proliferation of CHI3L1 overexpression hepatocellular carcinoma cell line was significantly increase than in control cells at 96 hours after seeding (Qing-Chong Qiu, 2018).

Significant decrease in apoptosis or more specifically inhibition of apoptosis was demonstrated in the case of hPAAFs, when different concentrations of recombinant CHI3L1 were used (200-600 ng/mL) (Figure 47B, 47D, 47F). In line with our findings, Sohn et al. have demonstrated that in an animal model on hyperoxia-induced acute lung injury, CHI3L1 protects against hyperoxia-induced oxidant injury, DNA injury and cell death (Sohn et al, 2010).

One of the suggested biological functions of CHI3L1 is inducing migration of different vascular and tumour cells (Nakashima et al., 1998). We also found that hPASMCs and hPAAFs (Figure 48), stimulated with recombinant CHI3L1 in two different concentrations can persuade migration of the listed cells. Interestingly, this effect wasn`t obtained by concentration dependency, rather the uptake of the cells was saturated after using already higher concentration of CHI3L1. Effect of migration on hPMECs was tested as well, although unsuccessfully, probably due to the cell morphology and sensitivity (data not shown).

CHI3L1 is overexpressed in human glioblastoma samples compared to normal issue. It has been proven that CHI3L1 affects glioma cell invasion through regulation of MMP-2 expression, adhesion to ECM, cytoskeleton rearrangement and contractility (Qu et al 2011). These findings set us a basis to explore the contractility potential of hPASMCs in stimulation of different doses of CHI3L1. Interestingly, the effect was not concentration dependent, most likely due to decreased sensitivity of the cells to higher concentration of CHI3L1 (Figure 49).

5.9.3. CHI3L1 induces VEGFA expression and activates VEGF signalling via FAK

A significant amount of angiogenic factors are secreted in a tumour microenvironment, further activating vascular endothelial cells towards angiogenic responses (Douglas Hanahan and Robert A. Weinber, 2011). However, it´s not clear whether VEGF and CHI3L1 act dependently or independently in terms of increased angiogenesis. A study has reported that, U87 brain tumour cells express high levels of CHI3L1 and VEGF (Francescone et al., 2011). When YKL-40 expression was inhibited, a reduction of VEGF was observed, suggesting the regulatory role of CHI3L1 in the VEGF production. Similarly, in order to delineate the role of VEGF in CHI3L1 expression, a neutralizing anti-VEGF antibody was used for 24 h, showing no effect on CHI3L1 production. Surprisingly, inhibition of VEGF for 1 week induced expression of

CHI3L1 (Saidi et al., 2008). VEGFA binds to and activates VEGFR-1 and VEGFR-2. VEGFR-1 has a high affinity for VEGFA, which is one order higher than that of VEGFR-2, whereas its tyrosine kinase activity is approximately 10-fold weaker than that of VEGFR-2, therefore their signalling cascade is not fully understood (Masabumi Shibuya, 2011). The signalling activation encounters FAK to transmit the downstream effectors (Hood JD et al 2003).

In this study, we observed VEGFR2 mediated activation of VEGF signalling in response to CHI3L1 stimulation, supported by phosphorylation of FAK Y^{861} which has been shown to moderate angiogenic responses (R Shao, 2009). We tested the affect in "chronic conditions" of 24 h stimulation, on contrary to the already published literature, however, the effect was similar (Figure 51). VEGFR1 after binding to VEGF, activates autophosphorylation of specific tyrosine residues, followed by binding and activation of Src family (Francescone et al., 2011). We didn`t observe any changes in the VEGFR1 expression, which probably affected the activation of the SRC family. However, we have shown that the CHI3L1-VEGFA-VEGFR2 can cause angiogenesis via activation of pFAK Y^{861} in chronic exposure conditions (Figure 50).

5.9.4. Vessel number is increased in end-stage CTEPH in contrast to donors

Increased antigenic potential, has been evaluated by our microarray data and our microscopic observation of CTEPH lungs samples. Although there has been controversy on the topic, the common knowledge is that in PAH, inward remodelling, loss of precapillary vessels (pruning) and impaired vascular regeneration contribute to the severe reduction of pulmonary vascular bed (Seeger, Pullamsetti, 2013). However, significant evidence is suggesting that angiogenesis *per se* takes place in CTEPH, affecting the vasa vasorum and causing broncho-pulmonary shunt (Dorfmuller 2014). A patient with Behçet disease, diagnosed with acute massive PE, after 16 months, presented chronic PE with hypertrophy of right bronchial artery, which connects with vasa vasora to supply distal pulmonary arteries (Hsin-Yu Tsai, 2011).

Here, we evaluated the total (micro) vessel density as a number of Von Willebrand factor (vWf), CD31- and CD34- positive vessels in the tissue section divided by the total area and as anticipated we observed increase number within all markers used to evaluate positive staining (Figure 51).

5.9.5. CHI3L1 drives vascular remodelling in living human precision cut lung sections

Lack of proper animal model of CTEPH and an increasing trend of using an organ culture to functionally evaluate the *ex-vivo* effects, encouraged us to test whether the pure, recombinant CHI3L1 will affect directly the remodelling of the pulmonary vessel in a living human

precision cut lung sections (Figure 52). Surprisingly, different concentrations of CHI3L1 induced similar effect of increased MWT, suggesting that in *ex-vivo* chronic conditions, CHI3L1 on its own can cause mild proliferation, extensive migration and contraction of vascular cells, contributing to vascular remodelling.

The microarray analysis revealed a transcriptional difference between the two simulated conditions of 800 ng/mL and 1200 ng/mL (Figure 53). The most up- or down- regulated genes belonged to the metabolic pathways, as KEGG pathway analysis indeed revealed an enrichment of these pathways in both of the stimulated conditions. In accordance, the binding of carbohydrates by CHI3L1 provide a link to glycomics (Coffman, 2008). Thus, further work is needed to delineate the role of CHI3L1 in the pathogenesis of CTEPH.

5.10. ENPP2 is expressed in end-stage CTEPH and regulates some cellular processes

ENPP2 or ATX is a secreted lysophospholipase D, a member of the nucleotide pyrophosphatase (NPP) family of ectoenzymes and exoenzymes (van Meeteren et al., 2006).

ENPP2 is stored in the α-granules of resting human platelets and released upon platelet aggregation, leading to the production of LPA (Leblanc et al., 2014). LPA is also known to promote human platelet activation by inducing platelet shape change and calcium mobilization, thereby potentially playing a role in thrombosis and thrombus formation (Teo et al., 2009).

As shown previously in our work, ENPP2 has been upregulated in laser microdissected vessels from CTEPH (Figure 13D and 54A), and predominantly localized within hPAECs in patients with CTEPH. Some positive staining was noticed in hPASMCs, as well in hPAAFs of pulmonary vessels (54B). In addition, at basal level, among all the screened cell types, lung pericytes, hPASMCs and hPAAFs presented with highest expression of ENPP2 at mRNA level (Figure 55A), whereas protein levels are highest in A549 tumour cells and hPMECs (Figure 55B and 55C). The higher protein levels of ENPP2 in hPMECs can be explained by the fact that ENPP2 maintains the expression of receptors required for VEGF and lysophospholipids to accelerate angiogenesis, which can also be amplified in cancer related angiogenesis and cancer progression. (Malgorzata M. Ptaszynska, 2010).

Since, ENPP2 and its product LPA, are involved in wide variety of processes such as cell migration, neurogenesis, angiogenesis, smooth-muscle contractions, platelet aggregation, and wound healing (Moolenaar et al., 2004), we aimed to check whether they play a role in initiation, regulation and resolution of innate immune responses (Di Rosa 2012). The mRNA levels of ENPP2 in M1 and M2 macrophages in comparison to naïve macrophages were

increased, suggesting that ENPP2 is upregulated in both pro- and anti-inflammatory macrophages (Uzma Saqib, 2018). The protein levels of ENPP2 in M1 or M2 macrophages were insignificantly changed; due to the lower sample number, we are unable to withdraw any conclusions (Figure 57).

5.10.1. Pro-PH factors guide a deregulation of ENPP2 expression in vascular cells

Our results suggested that pro-PH factor like IL13 induce the mRNA expression in hPMECs, while in hPASMC, along with TGF-β and TNF-α it downregulated ENPP2 expression. Interestingly, in hPAAFs, IL6 and PDGF-BB increased the mRNA levels, while TGF-β and TNF-α decreased them. Protein levels of ENPP2 were not affected in all the cells types, implying that the 24 h time point was inefficient for protein synthesis and secretion (Figure 57-59).

5.10.2. ENPP2-LPA axis converges several cellular effects

LPA is known to promote fibroblast and monocyte differentiation into myofibroblast and fibrocyte, respectively (Shao et al., 2008; Tang et al., 2014) and dedifferentiation, proliferation and migration of cultured vascular smooth muscle cells (Boguslawski et al., 2002; Gennero et al., 1999).

Although significant proliferation wasn`t evaluated when vascular cells were stimulated with LPA, nonetheless, we observed a proliferative tendency from approximately 5-30% in all the vascular cells tested. A study reported more significant outcome, where LPA induced a 3.9±0.6-fold increase in proliferation in vascular smooth muscle cells (Kim, 2006).

Significant increase in apoptosis demonstrated with higher concentrations of LPA was used in stimulation of the vascular cells, starting from 10 µM for hPAAFs up to 80 µM, while hPMECs were more resistance and showed increased apoptosis levels at 80 µM LPA. hPASMCs were affected towards higher apoptosis in 40 and 80 µM (Figure 60). On contrary to our findings, LPA has been found to protect intestinal epithelial cells from apoptosis by inhibiting the mitochondrial pathway at concentration of 10 µM (Wenlin Deng, 2002).

As one of the suggested biological functions of LPA is inducing migration of different vascular and tumour cells (Wenlin Deng, 2002, Boguslawski et al., 2002, Martina Stähle, 2003). We also found that stimulated hPASMCs and hPAAFs, can persuade migration in different concentrations of LPA, with an accent on higher doses, to a certain instance at a concentration dependent manner (Figure 61). Effect of migration on hPMECs was tested as well, although

unsuccessfully, due to technical difficulties or the cell morphology and sensitivity (data not shown).

5.10.3. LPA drives vascular remodelling in living human precision cut lung sections

As described above, lack of proper animal model of CTEPH and an increasing trend of using an organ culture to functionally evaluate the *ex-vivo* effects, encouraged us to test whether LPA will directly affect the remodelling of the pulmonary vessel in a living human precision cut lung sections (Figure 62). Surprisingly, different concentrations of LPA induced similar effect of increased medial wall thickness, suggesting that in *ex-vivo* chronic conditions, LPA on its own can cause mild proliferation and extensive migration, contributing to vascular remodelling. Interestingly, when we used potent and direct ENPP2 inhibitor, which modulates the LPA levels in vivo and in vitro, we observed decrease in the medial wall thickness in comparison to the stimulated control (Gierse 2010).

5.10.4. Loss of ENPP2 didn`t influence thrombus formation or resolution in a mouse thrombosis model of CTEPH

LPA signalling protects mouse pulmonary vasculature from hypoxia induced remodelling, whereas LPA deficiency affects the endothelin signalling, indulging endothelin-A receptor, in contrast to endothelin-B signalling (Cheng et al., 2012). Hence, LPA can undoubtedly influence the function of both, endothelial and smooth muscle cells, creating a pulmonary hypertensive sequelae. However, in contrast to vascular remodelling effects induced by ENPP2, ENPP2 exerted mild or no effects on thrombus formation or resolution in a mouse model of inferior vena cava (IVC) ligation induced thrombosis. Except of increased thrombus area at day 14 in the *Enpp2*$^{+/-}$ mice, we didn`t observe any other significant changes (Figure 64). The first cell type to invade the thrombus is neutrophils, as they are essential for early thrombus resolution (Sharma 2018). In a rat model of stasis DVT, neutropenia was found to be associated with larger thrombi on day 7 and increased thrombus fibrosis (Manu Varma, 2004). However, we observed slight changes in neutrophil count at day 7 in *Enpp2*$^{+/-}$ in contrast to *Enpp2*$^{+/+}$ (Figure 64E).

To our knowledge, this is the first study implying that ENPP2-LPA axis plays a role in the pathogenesis of PH, and specifically CTEPH and further work is needed to substantiate the molecular mechanisms contributing to disease development.

6. Future outlook

The data presented in this study comprehensively evaluate the pathophysiological and molecular aspects of end-stage CTEPH and compare it with the well-studied form of PH, IPAH. Moreover, this is the first study differentiating between central and peripheral CTEPH in terms of histopathological characterization and molecular profiling. However, further studies are needed to understand how PH initiating factors, such as high share stress, hypoxia and/or inflammatory molecules trigger the underlying pathological phenotype and particular molecular mechanisms in CTEPH, as well as the prevalence of one or the other condition, in terms of proximity of the disease.

In our initial studies, we were able to demonstrate that CHI3L1 and ENPP2, differently regulated genes between CTEPH and IPAH, and similarly regulated in proximal and distal CTEPH, are involved in pulmonary vascular remodelling *in vitro* and *ex vivo* via regulation of pro-proliferative, pro-migratory and pro-contractile mechanisms, suggesting a potential contribution to the pathogenesis of CTEPH. It will be interesting to examine if other PH factors, such as share stress or hypoxia will be able to induce similar changes of CHI3L1 or ENPP2 levels in vascular cells. For that purpose, donor hPMECs will be exposed to different levels of share stress and along with hPASMCs and hPAAFs to hypoxia, whereas expression and localization of CHI3L1 and ENPP2 will be evaluated.
Furthermore, studies to identify the exact molecular mechanisms downstream of CHI3L1 and ENPP2 shall be undertaken, by performing knockdowns of these genes in vascular cells and revealing how exactly they contribute to the pro-migratory and pro-angiogenic phenotype.

As mentioned before, ENPP2 is stored in the α-granules of resting human platelets and released upon platelet aggregation, leading to the production of LPA (Leblanc et al., 2014). LPA signalling on the other hand protects mouse pulmonary vasculature from hypoxia induced remodelling (Cheng et al., 2012). Therefore it would be interesting to know whether the combined thrombosis animal model of IVF ligation and hypoxia will create pulmonary hypertensive sequelae (Figure 65).

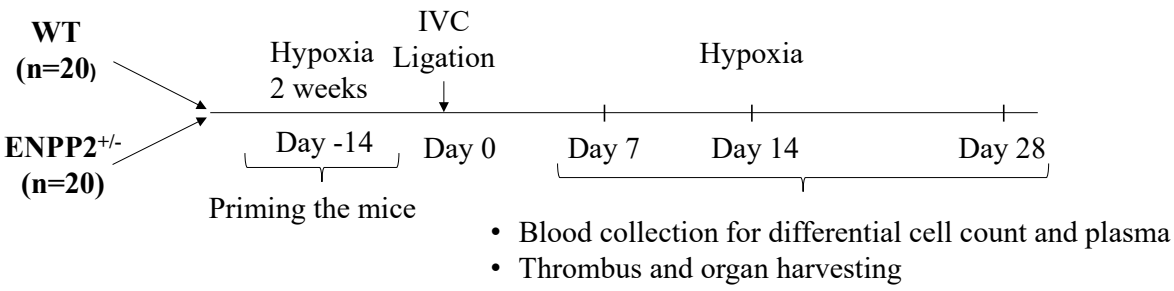

Figure 65: Schematic representation of the experimental plan of hypoxia-CTEPH thrombosis model. Ligation of IVC will be performed on WT and HZ mice. Experiment will be conducted with three different time points, day 7, 14 and 28. And ligation will follow after 2 weeks of hypoxia exposure

As the transcriptional profile of central and distal (segmental and subsegmental) vascular fibrous tissue from PEA was evaluated and several transcription factors came to be regulated in both, patent and completely occluded tissue, it will be of a great value to understand and estimate their functional role in the pathogenesis of the ongoing CTEPH. This work will be carried out, by overexpression or knockdown of the evaluated TFs in ECs and hPASMCs isolated from PEA. Finally, the relevance of these transcription gactors in the attenuation of CTEPH phenotype *in vivo* will be strengthened by completing the ongoing animal experiments with hemodynamic parameters and histological evaluations.

Summary

Chronic thromboembolic pulmonary hypertension (CTEPH) is considered to be a rare disease, with an epidemiology likely to be similar to that of pulmonary arterial hypertension (PAH). CTEPH is a subgroup of pulmonary hypertension (PH) with a cumulative incidence between 0.1 and 9.1% in patients with reported pulmonary embolism (I. M. Lang & Madani, 2014). Clinical evidence from registries demonstrates that CTEPH occurs at a prevalence of 17-20 per million in the general population (I. M. Lang et al., 2016). The state-of-the-art therapeutic strategy is pulmonary endarterectomy (PEA). Yet, a well-known fact in the field is that, approximately only 60% of the patients are eligible for surgery and even more, significant number of patients develop persistent/recurrent PH after PEA. This consecutive outcome is most likely a consequence of the production and release of mediators from endothelial cells or platelets, or both stimulated by pulmonary hypertensive state (Galiè & Kim, 2006; Remková et al., 2015). Furthermore, around 25% of patients with subsegmental obstruction are candidates for balloon angioplasty (BPA), and/or medical therapy, developed and used in the past few years. Ultimately and very rarely, however if all the therapeutic strategies fail, patients will undergo for lung transplantation. Searching for better alternative treatments is however limited as the pathophysiological and molecular mechanisms generating central (proximal) disease and/or distal (peripheral) vessel arteriopathy in CTEPH and the mechanistic differences/similarities with other groups of PH are sparsely understood.

Hence, better understanding of the pathophysiology and molecular mechanisms driving and orchestrating the development of CTEPH is mandatory in order to identify effective alternative treatments especially for patients with absence of proximal obliteration. The existence of microvascular disease in CTEPH was at first acknowledged by Moser and Bloor in a lung tissues obtained from biopsy or at autopsy of CTEPH patients (Moser & Bloor, 1993). Along with other authors, they highlighted the observation that vascular pulmonary hypertensive lesions in CTEPH are indistinguishable from the one underlying idiopathic PAH. On one hand, the vascular lesions exhibited intimal thickening, eccentric intimal fibrosis, intimal fibromuscular proliferation, medial hypertrophy and presence of plexiform lesions (Moser & Bloor, 1993; G. G. Pietra et al., 2004). On the other hand, it was postulated that the vascular remodelling distal to the organized thromboembolic obstruction may be similarly distributed in the lung areas of complete and non-complete occlusion CTEPH (G. Simonneau et al., 2017).

Based on prior research, the following research questions are of interest to better understand the CTEPH: (1) Are the molecular and histological imprints of CTEPH comparable or distinct

to the extensively studied PAH? (2) Are there significant differences from histological or molecular aspect between the vascular lesions in proximal (central) and distal (peripheral) CTEPH? More precisely, whether the lung areas distal to the organized thromboembolic obstruction being completely and non-completely obstructed (hypo- and hyper-perfused areas) convey a distinct phenotype and genotype. (3) Is the small vessel arteriopathy homogeneously distributed in different lobes, irrespective of the site of the disease? (4) Are the lung biopsies from patients who develop PH due to sarcoma resembling the "classical" histopathological changes observed in CTEPH? (5) Are the completely occluded biorepositories from PEA, in terms of histological and gene regulatory networks similar or distinct to the non-completely occluded areas complying with high-share stress? (6) What is the functional role of the unbiasedly selected targets in terms of development or maintenance of CTEPH?

In order to answer these research questions, this thesis aim to histologically and molecularly characterize the end-stage CTEPH enfolding several facets and further, the ongoing CTEPH in terms of central and occluded (completely and non-completely) vascular lesions.

First, in a carefully selected, multi-centre biorepositories, human samples have been collected and investigated to identify whether vascular remodelling in the end-stage CTEPH is as similar as in the other groups of PH, esp. in the well-studied idiopathic PAH (IPAH) group. Different morphometric approaches, such as medial wall thickness, neointima/media ratio and collagen deposition has been measured to assess the vascular remodelling. Next, the analysis of global transcriptional regulatory landscape in CTEPH and IPAH was performed from laser capture microdissected vessels, followed by microarrays and subsequent bioinformatic analysis to identify the common or the unique mechanisms driving small vessel arteriopathy in CTEPH as compared to IPAH. These findings suggest that the distal vascular remodelling in CTEPH, represented by intima thickening, medial hypertrophy and muscularization and adventitial thickening, resemble vascular remodelling in IPAH. Furthermore, we identified that CTEPH manifests significantly divergent global transcriptional regulatory landscape in comparison to IPAH.

Second, we evaluated whether the distal histological and molecular changes between central (proximal) and peripheral (distal) CTEPH are similar or distinct, in a comparable work frame to the previous experimental setup. We noted that central CTEPH manifest similar histological changes as peripheral CTEPH, while the global transcriptional regulatory landscape of central CTEPH manifests similar as well as unique signaling pathways regulation in contrast to the peripheral CTEPH.

Third, applying similar approach, we discovered that small vessel arteriopathy is homogeneously distributed in different lobes, irrespective of the site of the disease. Interestingly, the pre-affected as well as the post-affected areas showed similar distribution of the vascular remodelling intensity, confirming that the site affected by hypo-perfusion resembles the site with hyper-perfused flow in terms of vascular remodelling.

Forth, similarly patients who develop PH due to sarcoma and underwent PEA present comprehensive vascular remodelling, similar to end-stage CTEPH patients.

Fifth, based on histological and molecular analysis suggest that PEA biorepository presents with tissue repair phenotype, and especially in those areas distal to the central occlusion which are defined as non-completely and completely occluded regions.

Sixth, we reveal that CHI3L1 and ENPP2, differently regulated genes between CTEPH and IPAH, and similarly regulated in proximal and distal CTEPH, are involved in pulmonary vascular remodelling *in vitro* and *ex vivo* via regulation of pro-proliferative, pro-migratory and pro-contractile mechanisms, suggesting a potential contribution to the pathogenesis of CTEPH.

Taken together, further studies are needed to understand how exact factors, such as high share stress, hypoxia or inflammatory molecules trigger the interlaying pathological and molecular mechanisms in CTEPH.

Zusammenfassung

Chronische thromboembolische pulmonale Hypertonie (CTEPH) ist eine seltene Krankheit mit einer Epidemiologie, der der pulmonalen arteriellen Hypertonie (PAH) ähnelt. CTEPH ist eine Untergruppe der pulmonalen Hypertonie (PH), die zwischen 0,1% und 9,1% bei Patienten mit einer gemeldeter Lungenembolie auftritt (I. M. Lang & Madani, 2014). Klinische Daten belegen, dass CTEPH in der Allgemeinbevölkerung mit einer Prävalenz von 17 bis 20 pro eine Million Individuen auftritt (I. M. Lang, Dorfmüller & Vonk Noordegraaf, 2016). Die beste bekannte Therapiestrategie ist die pulmonale Endarteriektomie (PEA). Allerdings kommen nur etwa 60% der Patienten für eine Operation in Frage und eine signifikant höhere Anzahl von Patienten entwickelt eine persistierende/rezidivierende PH nach der PEA. Diese PH ist sehr wahrscheinlich eine Folge der Produktion und Freisetzung von Mediatoren aus Endothelzellen oder Blutplättchen oder beiden, die durch den pulmonalen hypertensitiven Zustand stimuliert werden (Galiè & Kim, 2006; Remková, Šimková & Valkovičová, 2015). Darüber hinaus sind rund 25% der Patienten mit subsegmentaler Obstruktion Kandidaten für eine Ballonangioplastie (BPA) und/oder eine medizinische Therapie, die in den letzten Jahren entwickelt und angewendet wurde. Schließlich und sehr selten, wenn alle therapeutischen Strategien versagen, erhalten Patienten eine Lungentransplantation. Die Suche nach besseren alternativen Therapien ist jedoch begrenzt, da die pathophysiologischen und molekularen Mechanismen, die eine zentrale (proximale) Erkrankung und/oder eine distale (periphere) Gefäßarteriopathie bei CTEPH hervorrufen und die mechanistischen Unterschiede/Ähnlichkeiten mit anderen Arten der PH bisher nur wenig verstanden sind.

Daher ist ein besseres Verständnis der Pathophysiologie und der molekularen Mechanismen, die die Entwicklung von CTEPH treiben und beeinflussen, unabdingbar, um wirksame alternative Therapien zu identifizieren. Dies gilt insbesondere für Patienten ohne proximale Obliteration. Das Vorliegen einer Kleingefäßerkrankung bei CTEPH wurde als erstes von Moser und Bloor in einem durch Biopsie oder Autopsie von CTEPH-Patienten gewonnenem Lungengewebe nachgewiesen (Moser & Bloor, 1993). Zusammen mit anderen Autoren hoben sie hervor, dass vaskuläre pulmonale hypertensive Läsionen bei CTEPH nicht von denen der idiopathischen PAH zu unterscheiden sind. Einerseits zeigten die Gefäßläsionen eine Intimaverdickung, exzentrische Intimalfibrosen, intimale fibromuskuläre Proliferationen, mediale Hypertrophie sowie das Vorhandensein plexiformer Läsionen (Moser & Bloor, 1993; G. G. Pietra et al., 2004). Andererseits wurde postuliert, dass die vaskuläre Remodellierung distal zu der organisierten thromboembolischen Obstruktion eine ähnliche Verteilung in den

Lungenbereichen der vollständigen und nicht vollständigen CTEPH-Okklusion aufweist (Simonneau et al., 2017).

Ausgehend von früheren Forschungsarbeiten sind die folgenden Forschungsfragen für ein besseres Verständnis von CTEPH von Interesse: (1) Sind die molekularen und histologischen Abdrücke von CTEPH mit denen der intensiv untersuchten PAH vergleichbar oder verschieden? (2) Gibt es signifikante Unterschiede aus histologischer oder molekularer Perspektive zwischen den Gefäßläsionen bei proximaler (zentraler) und distaler (peripherer) CTEPH? Genauer gesagt, weisen die zur organisierten thromboembolischen Obstruktion distalen Lungenbereiche, die vollständig oder nicht vollständig blockiert sind (hypo- und hyperperfundierte Bereiche), einen unterschiedlichen Phänotyp und Genotyp auf. (3) Ist die kleine Gefäßarteriopathie unabhängig vom Ort der Erkrankung homogen in verschiedenen Lappen verteilt? (4) Sind die Lungenbiopsien von Patienten, die aufgrund eines Sarkoms eine PH entwickeln, den bei CTEPH beobachteten „klassischen“ histopathologischen Veränderungen ähnlich? (5) Sind die vollständig verschlossenen Biorepositorien von PEA in Bezug auf histologische und genregulatorische Netzwerke ähnlich oder verschieden von den nicht vollständig verschlossenen Bereichen, die einen hohen Stressanteil aufweisen? (6) Welche funktionale Rolle spielen die zufällig ausgewählten Ziele bei der Entwicklung oder dem Bestehen von CTEPH?

Um diese Forschungsfragen zu beantworten, hat die vorliegende Arbeit das Ziel CTPEH im Endstadium histologisch und molekular aus verschiedenen Sichtweisen zu charakterisieren. Darüber hinaus soll eine bestehende CTEPH in Bezug auf zentrale und verschlossene (vollständig und nicht vollständig) Gefäßläsionen untersucht werden.

Erstens wurden in sorgfältig ausgewählten multizentrischen Biorepositorien humane Proben gesammelt und untersucht. Damit sollte festgestellt werden, ob die vaskuläre Remodellierung im CTEPH-Endstadium ähnlich zu anderen Gruppen von PH ist, insbesondere in der extensiv untersuchten Gruppe der idiopathischen PAH (IPAH). Dazu wurden verschiedene morphometrische Ansätze wie die mediale Wandstärke, das Neointima / Media-Verhältnis und die Kollagenablagerung genutzt, um die Remodellierung der Gefäße zu messen und zu bewerten. Weiterhin wurden die globalen regulatorischen Transkriptionslandschaften in CTEPH und IPAH an mikrodissezierten Gefäßen mit Lasereinfang analysiert. Anschließend wurden Microarrays und eine bioinformatische Analyse durchgeführt, um die gemeinsamen oder einzigartigen Mechanismen zu identifizieren, die die Arteriopathie kleiner Gefäße in CTEPH im Vergleich zu IPAH treiben. Diese Ergebnisse legen nahe, dass die distale

Gefäßumbildung bei CTEPH, charakterisiert durch Intimaverdickung, mediale Hypertrophie und Muskularisation sowie adventitiale Verdickung, der Gefäßumbildung bei IPAH ähnelt. Darüber hinaus stellten wir fest, dass CTEPH im Vergleich zu IPAH eine signifikant abweichende globale regulatorische Transkriptionslandschaft aufweist.

Zweitens haben wir untersucht, ob die distalen histologischen und molekularen Veränderungen zwischen zentralem (proximalem) und peripherem (distalem) CTEPH ähnlich oder unterschiedlich sind. Dies erfolgte in einem vergleichbaren Design wie im vorherigen Versuchsaufbau. Die Ergebnisse zeigen, dass die zentrale CTEPH ähnliche histologische Veränderungen aufweist wie die periphere CTEPH. Allerdings zeigt die globale Transkriptionsregulationslandschaft der zentralen CTEPH im Gegensatz zur peripheren CTEPH zwar ähnliche aber auch einzigartige Regulation der Signalwege.

Drittens stellten wir mit einem ähnlichen Untersuchungsdesign fest, dass die Arteriopathie der kleinen Gefäße unabhängig vom Ort der Erkrankung homogen in verschiedenen Lappen verteilt ist. Interessanterweise zeigten sowohl die vorher als auch hinterher betroffene Stelle eine ähnliche Verteilung der Intensität der Gefäßumbildung. Dies bestätigt, dass der von der Hypoperfusion betroffene Bereich hinsichtlich der Gefäßumbildung dem Bereich mit hyperperfusiertem Fluss ähnelt.

Viertens, weisen Patienten, die aufgrund eines Sarkoms eine PH entwickeln sowie eine PEA durchlaufen haben, eine umfassende Gefäßumbildung ähnlich wie CTEPH-Patienten im Endstadium auf.

Fünftens, deuten die Ergebnisse der histologischen und molekularen Analysen darauf hin, dass das PEA-Biorepository einen Gewebereparaturphänotyp aufweist. Dies zeigt sich insbesondere in den Bereichen, die distal zur zentralen Okklusion liegen (nicht vollständige und vollständige verschlossene Bereiche).

Sechstens zeigen wir, dass CHI3L1 und ENPP2, unterschiedlich regulierte Gene zwischen CTEPH und IPAH und ähnlich reguliert in proximaler und distaler CTEPH, in vitro und ex vivo an der Remodellierung der Lungengefäße beteiligt sind. Dies erfolgt durch positive Wachstums-, Migrations- und Kontraktile-Mechanismen, die auf einen möglichen Beitrag zur Pathogenese von CTEPH hindeuten.

References

Ackermann, M., Gaumann, A., Mentzer, S. J., Hinrichs, J. B., Warnecke, G., Hoeper, M. M., . . . Jonigk, D. (2017). Plexiform vasculopathy in chronic thromboembolic pulmonary hypertension. *American Journal of Respiratory and Critical Care Medicine, 196*(8), e48-e51.

Aldred, M. A., Comhair, S. A., Varella-Garcia, M., Asosingh, K., Xu, W., Noon, G. P., . . . Coldren, C. D. (2010). Somatic chromosome abnormalities in the lungs of patients with pulmonary arterial hypertension. *Am J Respir Crit Care Med, 182*(9), 1153-1160. doi: 10.1164/rccm.201003-0491OC.

Alias, S., Redwan, B., Panzenboeck, A., Winter, M. P., Schubert, U., Voswinckel, R., . . . Lang, I. M. (2014). Defective angiogenesis delays thrombus resolution: a potential pathogenetic mechanism underlying chronic thromboembolic pulmonary hypertension. *Arterioscler Thromb Vasc Biol, 34*(4), 810-819. doi: 10.1161/ATVBAHA.113.302991.

Arbustini, E., Morbini, P., D'Armini, A., Repetto, A., Minzioni, G., Piovella, F., . . . Tavazzi, L. (2002). Plaque composition in plexogenic and thromboembolic pulmonary hypertension: the critical role of thrombotic material in pultaceous core formation. *Heart, 88*(1), 177-182.

Archer, S. L., Gomberg-Maitland, M., Maitland, M. L., Rich, S., Garcia, J. G., & Weir, E. K. (2008). Mitochondrial metabolism, redox signaling, and fusion: a mitochondria-ROS-HIF-1alpha-Kv1.5 O2-sensing pathway at the intersection of pulmonary hypertension and cancer. *Am J Physiol Heart Circ Physiol, 294*(2), H570-578. doi: 10.1152/ajpheart.01324.2007.

Baile, E. M. (1996). The Anatomy and Physiology of the Bronchial Circulation. *Journal of Aerosol Medicine, 9*(1), 1-6.

Balabanian, K., Foussat, A., Dorfmüller, P., Durand-Gasselin, I., Capel, F., Bouchet-Delbos, L., . . . Humbert, M. (2002). CX3C Chemokine Fractalkine in Pulmonary Arterial Hypertension. *American Journal of Respiratory and Critical Care Medicine, 165*(10), 1419-1425. doi: 10.1164/rccm.2106007.

Bernard, J., & Yi, E. S. (2007). Pulmonary thromboendarterectomy: a clinicopathologic study of 200 consecutive pulmonary thromboendarterectomy cases in one institution. *Hum Pathol, 38*(6), 871-877. doi: 10.1016/j.humpath.2006.11.017.

Bieker, J. J. (2001). Kruppel-like factors: three fingers in many pies. *J Biol Chem, 276*(37), 34355-34358. doi: 10.1074/jbc.R100043200.

Blauwet, L. A., Edwards, W. D., Tazelaar, H. D., & McGregor, C. G. (2003). Surgical Pathology of Pulmonary Thromboendarterectomy. A Study of 54 Cases From 1990 to 2001. *Human Pathology, 34*(12), 1290-1298. doi: 10.1016/S0046-8177(03)00469-6.

Bogatcheva, N. V., Garcia, J. G., & Verin, A. D. (2002). Molecular mechanisms of thrombin-induced endothelial cell permeability. *Biochemistry (Mosc), 67*(1), 75-84.

Boguslawski, G., Grogg, J. R., Welch, Z., Ciechanowicz, S., Sliva, D., Kovala, A. T., . . . English, D. (2002). Migration of vascular smooth muscle cells induced by sphingosine 1-phosphate and related lipids: potential role in the angiogenic response. *Exp Cell Res, 274*(2), 264-274. doi: 10.1006/excr.2002.5472.

Bonderman, D., Jakowitsch, J., Adlbrecht, C., Schemper, M., Kyrle, P., Schönauer, V., . . . Lang, I. (2005). Medical conditions increasing the risk of chronic thromboembolic pulmonary hypertension. *Thromb Haemost, 93*(3), 512-516.

Bonderman, D., Jakowitsch, J., Redwan, B., Bergmeister, H., Renner, M.-K., Panzenböck, H., . . . Lang, I. M. (2008). Role for Staphylococci in Misguided Thrombus Resolution of Chronic Thromboembolic Pulmonary Hypertension. *Arteriosclerosis, Thrombosis, and Vascular Biology, 28*(4), 678-684. doi: doi:10.1161/ATVBAHA.107.156000.

Bonderman, D., Turecek, P. L., Jakowitsch, J., Weltermann, A., Adlbrecht, C., Schneider, B., . . . Lang, I. M. (2003). High prevalence of elevated clotting factor VIII in chronic thromboembolic pulmonary hypertension. *Thromb Haemost, 90*(3), 372-376. doi: 10.1160/TH03-02-0067.

Bonderman, D., Wilkens, H., Wakounig, S., Schäfers, H.-J., Jansa, P., Lindner, J., . . . Lang, I. M. (2009). Risk factors for chronic thromboembolic pulmonary hypertension. *European Respiratory Journal, 33*(2), 325-331. doi: 10.1183/09031936.00087608.

Bonderman, D., Wilkens, H., Wakounig, S., Schafers, H. J., Jansa, P., Lindner, J., . . . Lang, I. M. (2009). Risk factors for chronic thromboembolic pulmonary hypertension. *Eur Respir J, 33*(2), 325-331. doi: 10.1183/09031936.00087608.

Brinkmann, V. (2007). Sphingosine 1-phosphate receptors in health and disease: mechanistic insights from gene deletion studies and reverse pharmacology. *Pharmacol Ther, 115*(1), 84-105. doi: 10.1016/j.pharmthera.2007.04.006.

Bussink, A. P., Speijer, D., Aerts, J. M., & Boot, R. G. (2007). Evolution of mammalian chitinase(-like) members of family 18 glycosyl hydrolases. *Genetics, 177*(2), 959-970. doi: 10.1534/genetics.107.075846.

Cannon, J. E., Su, L., Kiely, D. G., Page, K., Toshner, M., Swietlik, E., . . . Pepke-Zaba, J. (2016). Dynamic Risk Stratification of Patient Long-Term Outcome After Pulmonary Endarterectomy: Results From the United Kingdom National Cohort. *Circulation, 133*(18), 1761-1771. doi: 10.1161/CIRCULATIONAHA.115.019470.

Chatelain, R. E., & Dardik, B. N. (1988). Increased DNA replication in the arterial adventitia after aortic ligation. *Hypertension, 11*(2 Pt 2), I130-134. doi: 10.1161/01.hyp.11.2_pt_2.i130.

Chavin, S. I., & Weidner, S. M. (1984). Blood Clotting Factor IX. Loss of activity after cleavage of sialic acid residues. *The Journal of Biological Chemistry, 259*(6), 3387-3390.

Chelladurai, P., Seeger, W., & Pullamsetti, S. S. (2012). Matrix metalloproteinases and their inhibitors in pulmonary hypertension. *Eur Respir J, 40*(3), 766-782. doi: 10.1183/09031936.00209911.

Cheng, H. Y., Dong, A., Panchatcharam, M., Mueller, P., Yang, F., Li, Z., . . . Smyth, S. S. (2012). Lysophosphatidic acid signaling protects pulmonary vasculature from hypoxia-induced remodeling. *Arterioscler Thromb Vasc Biol, 32*(1), 24-32. doi: 10.1161/ATVBAHA.111.234708.

Christman, B. W., McPherson, C. D., Newman, J. H., King, G. A., Bernard, G. R., M., G. B., & Loyd, J. E. (1992). An imbalance between the excretion of thromboxane and prostacyclin metabolites in pulmonary hypertension. *The New England Journal of Medicine, 327*(2), 70-75.

Chupp, G. L., Lee, C. G., Jarjour, N., Shim, Y. M., Holm, C. T., He, S., . . . Elias, J. A. (2007). A Chitinase-like Protein in the Lung and Circulation of Patients with Severe Asthma. *The New England Journal of Medicine, 357*(1), 2016-2027.

Cohn, D. M., Roshani, S., & Middeldorp, S. (2007). Thrombophilia and venous thromboembolism: implications for testing. *Semin Thromb Hemost, 33*(6), 573-581. doi: 10.1055/s-2007-985753.

Cool, C. D., Stewart, J. S., Werahera, P., Miller, G. J., Williams, R. L., Voelkel, N. F., & Tuder, R. M. (1999). Three-Dimensional Reconstruction of Pulmonary Arteries in Plexiform Pulmonary Hypertension Using Cell-Specific Markers. Evidence for a Dynamic and Heterogeneous Process of Pulmonary Endothelial Cell Growth. *American Journal of Pathology, 155*(2).

D'Alonzo, G. E., Barst, R. J., Ayres, S. M., Bergofsky, E. H., Brundage, B. H., Detre, K. M., . . . Wu, M. (1991). Survival in Patients with Primary Pulmonary Hypertension: Results

from a National Prospective Registry. *Annals of Internal Medicine, 115*(5), 343-349. doi: 10.7326/0003-4819-115-5-343.

Dartevelle, P., Fadel, E., Mussot, S., Chapelier, A., Herve, P., de Perrot, M., . . . Simonneau, G. (2004). Chronic thromboembolic pulmonary hypertension. *European Respiratory Journal, 23*(4), 637-648. doi: 10.1183/09031936.04.00079704.

Davie, N. J., Gerasimovskaya, E. V., Hofmeister, S. E., Richman, A. P., Jones, P. L., Reeves, J. T., & Stenmark, K. R. (2006). Pulmonary artery adventitial fibroblasts cooperate with vasa vasorum endothelial cells to regulate vasa vasorum neovascularization: a process mediated by hypoxia and endothelin-1. *The American journal of pathology, 168*(6), 1793-1807. doi: 10.2353/ajpath.2006.050754.

De Ceuninck, F., Gaufillier, S., Bonnaud, A., Sabatini, M., Lesur, C., & Pastoureau, P. (2001). YKL-40 (cartilage gp-39) induces proliferative events in cultured chondrocytes and synoviocytes and increases glycosaminoglycan synthesis in chondrocytes. *Biochem Biophys Res Commun, 285*(4), 926-931. doi: 10.1006/bbrc.2001.5253.

Dekker, R. J., van Soest, S., Fontijn, R. D., Salamanca, S., de Groot, P. G., VanBavel, E., . . . Horrevoets, A. J. (2002). Prolonged fluid shear stress induces a distinct set of endothelial cell genes, most specifically lung Kruppel-like factor (KLF2). *Blood, 100*(5), 1689-1698. doi: 10.1182/blood-2002-01-0046.

Di Rosa, M., Malaguarnera, G., De Gregorio, C., Drago, F., & Malaguarnera, L. (2013). Evaluation of CHI3L-1 and CHIT-1 expression in differentiated and polarized macrophages. *Inflammation, 36*(2), 482-492. doi: 10.1007/s10753-012-9569-8.

Diller, G.-P., Eijl, S. v., Okonko, D. O., Howard, L. S., Ali, O., Thum, T., . . . Wharton, J. (2008). Circulating Endothelial Progenitor Cells in Patients With Eisenmenger Syndrome and Idiopathic Pulmonary Arterial Hypertension. *Circulation, 117*(23), 3020-3030. doi: doi:10.1161/CIRCULATIONAHA.108.769646.

Distler, J. H. W., Hirth, A., Kurowska-Stolaroska, M., Gay, R. E., & Distler, O. (2003). Angiogenic and angiostatic factors in the molecular control of angiogenesis. *The Quarterly Journal of Nuclear Medicine, 47*(3), 149-161.

Dorfmüller, P., Gunther, S., Ghigna, M. R., Thomas de Montpreville, V., Boulate, D., Paul, J. F., . . . Mercier, O. (2014). Microvascular disease in chronic thromboembolic pulmonary hypertension: a role for pulmonary veins and systemic vasculature. *Eur Respir J, 44*(5), 1275-1288. doi: 10.1183/09031936.00169113.

Dorfmüller, P., ZARKA, V., DURAND-GASSELIN, I., MONTI, G., BALABANIAN, K., GARCIA, G., . . . HUMBERT, M. (2002). Chemokine RANTES in Severe Pulmonary Arterial Hypertension. *American Journal of Respiratory and Critical Care Medicine, 165*(4), 534-539. doi: 10.1164/ajrccm.165.4.2012112.

Du, L., Sullivan, C. C., Chu, D., Cho, A. J., Kido, M., Wolf, P. L., . . . Thistlethwaite, P. A. (2003). <nejmoa021650.pdf>. *The New England Journal of Medicine, 384*(6), 500-509.

Eijkelenboom, A., & Burgering, B. M. (2013). FOXOs: signalling integrators for homeostasis maintenance. *Nat Rev Mol Cell Biol, 14*(2), 83-97. doi: 10.1038/nrm3507.

Evans, C. E., Humphries, J., Waltham, M., Saha, P., Mattock, K., Patel, A., . . . Smith, A. (2011). Upregulation of hypoxia-inducible factor 1 alpha in local vein wall is associated with enhanced venous thrombus resolution. *Thromb Res, 128*(4), 346-351. doi: 10.1016/j.thromres.2011.05.006.

Farber, H. W., & Loscalzo, J. (2004). Pulmonary arterial hypertension. *The New England Journal of Medicine, 351*(16), 1655-1665.

Fedullo, P., Kerr, K. M., Kim, N. H., & Auger, W. R. (2011). Chronic thromboembolic pulmonary hypertension. *Am J Respir Crit Care Med, 183*(12), 1605-1613. doi: 10.1164/rccm.201011-1854CI.

Fedullo, P. F., Augur, W. R., Kerr, K. M., & Rubin, L. J. (2001). Current Concepts. Chronic Thrombembolic Pulmonary Hypertension. *N Engl J Med, 345*(20), 1465-1472.

Firth, A. L., Mandel, J., & Yuan, J. X. (2010). Idiopathic pulmonary arterial hypertension. *Dis Model Mech, 3*(5-6), 268-273. doi: 10.1242/dmm.003616.

Firth, A. L., Remillard, C. V., & Yuan, J. X. (2007). TRP channels in hypertension. *Biochim Biophys Acta, 1772*(8), 895-906. doi: 10.1016/j.bbadis.2007.02.009.

Firth, A. L., Yao, W., Ogawa, A., Madani, M. M., Lin, G. Y., & Yuan, J. X. (2010). Multipotent mesenchymal progenitor cells are present in endarterectomized tissues from patients with chronic thromboembolic pulmonary hypertension. *Am J Physiol Cell Physiol, 298*(5), C1217-1225. doi: 10.1152/ajpcell.00416.2009.

Firth, A. L., Yuill, K. H., & Smirnov, S. V. (2008). Mitochondria-dependent regulation of Kv currents in rat pulmonary artery smooth muscle cells. *American Journal of Physiology-Lung Cellular and Molecular Physiology, 295*(1), L61-L70. doi: 10.1152/ajplung.90243.2008.

Francescone, R. A., Scully, S., Faibish, M., Taylor, S. L., Oh, D., Moral, L., . . . Shao, R. (2011). Role of YKL-40 in the angiogenesis, radioresistance, and progression of glioblastoma. *J Biol Chem, 286*(17), 15332-15343. doi: 10.1074/jbc.M110.212514.

Frey, M. K., Alias, S., Winter, M. P., Redwan, B., Stubiger, G., Panzenboeck, A., . . . Lang, I. M. (2014). Splenectomy is modifying the vascular remodeling of thrombosis. *J Am Heart Assoc, 3*(1), e000772. doi: 10.1161/JAHA.113.000772.

Funkhouser, J. D., & Aronson, N. N., Jr. (2007). Chitinase family GH18: evolutionary insights from the genomic history of a diverse protein family. *BMC Evol Biol, 7*, 96. doi: 10.1186/1471-2148-7-96.

Fusetti, F., Pijning, T., Kalk, K. H., Bos, E., & Dijkstra, B. W. (2003). Crystal structure and carbohydrate-binding properties of the human cartilage glycoprotein-39. *J Biol Chem, 278*(39), 37753-37760. doi: 10.1074/jbc.M303137200.

Galiè, N., Hoeper, M. M., Humbert, M., Torbicki, A., Vachiery, J. L., Barbera, J. A., . . . Simonneau, G. (2009). Guidelines for the diagnosis and treatment of pulmonary hypertension. *Eur Respir J, 34*(6), 1219-1263. doi: 10.1183/09031936.00139009.

Galiè, N., Humbert, M., Vachiery, J. L., Gibbs, S., Lang, I., Torbicki, A., . . . Group, E. S. C. S. D. (2016). 2015 ESC/ERS Guidelines for the diagnosis and treatment of pulmonary hypertension: The Joint Task Force for the Diagnosis and Treatment of Pulmonary Hypertension of the European Society of Cardiology (ESC) and the European Respiratory Society (ERS): Endorsed by: Association for European Paediatric and Congenital Cardiology (AEPC), International Society for Heart and Lung Transplantation (ISHLT). *Eur Heart J, 37*(1), 67-119. doi: 10.1093/eurheartj/ehv317.

Galiè, N., & Kim, N. H. (2006). Pulmonary microvascular disease in chronic thromboembolic pulmonary hypertension. *Proc Am Thorac Soc, 3*(7), 571-576. doi: 10.1513/pats.200605-113LR.

Gallinaro, L., Cattini, M. G., Sztukowska, M., Padrini, R., Sartorello, F., Pontara, E., . . . Casonato, A. (2008). A shorter von Willebrand factor survival in O blood group subjects explains how ABO determinants influence plasma von Willebrand factor. *Blood, 111*(7), 3540-3545. doi: 10.1182/blood-2007-11-122945.

Gándara, E. E., Kovacs, M. J., Kahn, S. R., Wells, P. S., Anderson, D. A., Chagnon, I., . . . Rodger, M. A. (2013). Non-OO blood type influences the risk of recurrent venous thromboembolism: a cohort study. *Thromb Haemost, 110*(6), 1172-1179.

Gao, N., Flynn, D. C., Zhang, Z., Zhong, X.-S., Walker, V., Liu, K. J., . . . Jiang, B.-H. (2004). G1 cell cycle progression and the expression of G1 cyclins are regulated by PI3K/AKT/mTOR/p70S6K1 signaling in human ovarian cancer cells. *Am J Physiol Cell Physiol, 287*(1), C281-C291.

Garcia, J., & Schaphorst, K. (1995). Regulation of endothelial cell gap formation and paracellular permeability. *J Investig Med, 43*(1), 117-126.

Garcia, J. G., Siflinger-Birnboim, A., Bizios, R., Del Vecchio, P. J., Fenton, J. W., 2nd, & Malik, A. B. (1986). Thrombin-induced increase in albumin permeability across the endothelium. *J Cell Physiol, 128*(1), 96-104. doi: 10.1002/jcp.1041280115.

Gavilanes-Oleas, F. A., Alves-Jr, J. L., Fernandes, C. J. C., Prada, L. F. L., Salibe-Filho, W., Terra-Filho, M., . . . Souza, R. (2018). Use of direct oral anticoagulants for chronic thromboembolic pulmonary hypertension. *Clinics, 73*(216), 1-2.

Gennero, I., Xuereb, J.-M., Simon, M.-F., Girolami, J.-P., Bascands, J.-L., Chap, H., . . . Sié, P. (1999). Effects of Lysophosphatidic Acid on Proliferation and Cytosolic Ca11 of Human Adult Vascular Smooth Muscle Cells in Culture. *Thrombosis Research, 94*(1), 317-326.

Ghatnekar, A., Chrobak, I., Reese, C., Stawski, L., Seta, F., Wirrig, E., . . . Trojanowska, M. (2013). Endothelial GATA-6 deficiency promotes pulmonary arterial hypertension. *Am J Pathol, 182*(6), 2391-2406. doi: 10.1016/j.ajpath.2013.02.039.

Ghofrani, H.-A., Simonneau, G., D'Armini, A. M., Fedullo, P., Howard, L. S., Jaïs, X., . . . Kim, N. H. (2017). Macitentan for the treatment of inoperable chronic thromboembolic pulmonary hypertension (MERIT-1): results from the multicentre, phase 2, randomised, double-blind, placebo-controlled study. *The Lancet Respiratory Medicine, 5*(10), 785-794. doi: 10.1016/s2213-2600(17)30305-3.

Ghofrani, H. A., D'Armini, A. M., Grimminger, F., Hoeper, M. M., Jansa, P., Kim, N. H., . . . Group, C.-S. (2013). Riociguat for the treatment of chronic thromboembolic pulmonary hypertension. *N Engl J Med, 369*(4), 319-329. doi: 10.1056/NEJMoa1209657.

Giaid, A., Yanagisawa, M., Langleben, D., Michel, R. P., Levy, R., Shennib, H., . . . Stewart, D. J. (1993). Expression of Endothelin-1 in the lungs of patients with pulmonary hypertension. *The New England Journal of Medicine, 328*(24), 1732-1739.

Gill, J. C., Endres-Brooks, J., Bauer, P. J., Marks, W. J., Jr., & Montgomery, R. R. (1987). The effect of ABO blood group on the diagnosis of von Willebrand disease. *Blood, 69*(6), 1691-1695.

Golembeski, S. M., West, J., Tada, Y., & Fagan, K. A. (2005). Interleukin-6 Causes Mild Pulmonary Hypertension and Augments Hypoxia-Induced Pulmonary Hypertension in Mice. *Chest, 128*(1), 572S-573S.

Gong, Z., Xing, S., Zheng, F., & Xing, Q. (2014). Increased expression of chitinase 3-like 1 in aorta of patients with atherosclerosis and suppression of atherosclerosis in apolipoprotein E-knockout mice by chitinase 3-like 1 gene silencing. *Mediators Inflamm, 2014*, 905463. doi: 10.1155/2014/905463.

Goodrich, J. A., & Tjian, R. (2010). Unexpected roles for core promoter recognition factors in cell-type-specific transcription and gene regulation. *Nat Rev Genet, 11*(8), 549-558. doi: 10.1038/nrg2847.

Hamsten, A., Wiman, B., de Faire, U., & Blombäck, M. (1985). Increased Plasma Levels of a Rapid Inhibitor of Tissue Plasminogen Activator in Young Survivors of Myocardial Infarction. *New England Journal of Medicine, 313*(25), 1557-1563. doi: 10.1056/nejm198512193132501.

Hoeper, M. M., Bogaard, H. J., Condliffe, R., Frantz, R., Khanna, D., Kurzyna, M., . . . Badesch, D. B. (2013). Definitions and diagnosis of pulmonary hypertension. *J Am Coll Cardiol, 62*(25 Suppl), D42-50. doi: 10.1016/j.jacc.2013.10.032.

Hoeper, M. M., Madani, M. M., Nakanishi, N., Meyer, B., Cebotari, S., & Rubin, L. J. (2014). Chronic thromboembolic pulmonary hypertension. *The Lancet Respiratory Medicine, 2*(7), 573-582. doi: 10.1016/s2213-2600(14)70089-x.

Hoeper, M. M., Mayer, E., Simonneau, G., & Rubin, L. J. (2006). Chronic thromboembolic pulmonary hypertension. *Circulation, 113*(16), 2011-2020. doi: 10.1161/CIRCULATIONAHA.105.602565.

Hojoong Kim, G. L. Y. J. (2009). Pulmonary Vascular Remodeling Distal to Pulmonary Artery Ligation Is Accompanied by Upregulation of Endothelin Receptors and Nitric Oxide Synthase. *Experimental Lung Research, 26*(4), 287-301. doi: 10.1080/019021400404555.

Huang, P. L., Huang, Z., Mashimo, H., Bloch, K. D., Moskowitz, M. A., Bevan, J. A., & Fishman, M. C. (1995). Hypertension in mice lacking the gene for endothelial nitric oxide synthase. *Letters to Nature, 377*(1), 239-242.

Humbert, M., Gianpaola, M., Brenot, F., Sitbon, O., Portier, A., Grangeot-Keros, L., . . . Emilie, D. (1995). Increased Interleukin-1 and Interleukin-6 Serum concentrations in severe primary pulmonary hypertension. *Am J Respir Crit Care Med, 151*(1), 1628-1631.

Inami, T., Kataoka, M., Shimura, N., Ishiguro, H., Yanagisawa, R., Kawakami, T., . . . Satoh, T. (2015). Incidence, avoidance, and management of pulmonary artery injuries in percutaneous transluminal pulmonary angioplasty. *Int J Cardiol, 201*, 35-37. doi: 10.1016/j.ijcard.2015.08.052.

Ishii, I., Fukushima, N., Ye, X., & Chun, J. (2004). Lysophospholipid receptors: signaling and biology. *Annu Rev Biochem, 73*, 321-354. doi: 10.1146/annurev.biochem.73.011303.073731.

Jais, X., Ioos, V., Jardim, C., Sitbon, O., Parent, F., Hamid, A., . . . Humbert, M. (2005). Splenectomy and chronic thromboembolic pulmonary hypertension. *Thorax, 60*(12), 1031-1034. doi: 10.1136/thx.2004.038083.

James, A. J., Reinius, L. E., Verhoek, M., Gomes, A., Kupczyk, M., Hammar, U., . . . Dahlén, S.-E. (2016). Increased YKL-40 and Chitotriosidase in Asthma and Chronic Obstructive Pulmonary Disease. *American Journal of Respiratory and Critical Care Medicine, 193*(2), 131-142. doi: 10.1164/rccm.201504-0760OC.

Jeffery, T. K., & Morrell, N. W. (2002). Molecular and cellular basis of pulmonary vascular remodeling in pulmonary hypertension. *Prog Cardiovasc Dis, 45*(3), 173-202. doi: 10.1053/pcad.2002.130041.

Jenkins, D. (2015). Pulmonary endarterectomy: the potentially curative treatment for patients with chronic thromboembolic pulmonary hypertension. *Eur Respir Rev, 24*(136), 263-271. doi: 10.1183/16000617.00000815.

Jenkins, D., Madani, M., Fadel, E., D'Armini, A. M., & Mayer, E. (2017). Pulmonary endarterectomy in the management of chronic thromboembolic pulmonary hypertension. *Eur Respir Rev, 26*(143). doi: 10.1183/16000617.0111-2016.

Jonigk, D., Golpon, H., Bockmeyer, C. L., Maegel, L., Hoeper, M. M., Gottlieb, J., . . . Laenger, F. (2011). Plexiform lesions in pulmonary arterial hypertension composition, architecture, and microenvironment. *Am J Pathol, 179*(1), 167-179. doi: 10.1016/j.ajpath.2011.03.040.

Jurk, K., & Kehrel, B. E. (2005). Platelets: Physiology and Biochemistry. *Seminars in Thrombosis and Hemostasis, 31*(4), 381-392.

Karimi, M., & Cohan, N. (2010). Cancer-associated thrombosis. *Open Cardiovasc Med J, 4*(1), 78-82.

Kawada, M., Hachiya, Y., Arihiro, A., & Muizoguchi, E. (2007). Role of mammalian chitinases in inflammatory conditions. *Keio J Med, 56*(1), 21-27.

Kim, J., Keys, J. R., & Eckhart, A. D. (2006). Vascular smooth muscle migration and proliferation in response to lysophosphatidic acid (LPA) is mediated by LPA receptors coupling to Gq. *Cell Signal, 18*(10), 1695-1701. doi: 10.1016/j.cellsig.2006.01.009.

Kim, N. H., Delcroix, M., Jenkins, D. P., Channick, R., Dartevelle, P., Jansa, P., . . . Mayer, E. (2013). Chronic thromboembolic pulmonary hypertension. *J Am Coll Cardiol, 62*(25 Suppl), D92-99. doi: 10.1016/j.jacc.2013.10.024.

Kim, N. H., & Lang, I. M. (2012). Risk factors for chronic thromboembolic pulmonary hypertension. *European Respiratory Review, 21*(123), 27-31. doi: 10.1183/09059180.00009111.

Kimura, H., Okada, O., Tanabe, N., Tanaka, Y., Terai, M., Takiguchi, Y., . . . Kuriyama, T. (2001). Plasma Monocyte Chemoattractant Protein-1 and Pulmonary Vascular Resistance in Chronic Thromboembolic Pulmonary Hypertension. *Am J Respir Crit Care Med, 164*(1), 319-324.

Klinger, J. R., Abman, S. H., & Gladwin, M. T. (2013). Nitric oxide deficiency and endothelial dysfunction in pulmonary arterial hypertension. *Am J Respir Crit Care Med, 188*(6), 639-646. doi: 10.1164/rccm.201304-0686PP.

Kondo, M., Ishizawa, T., Enooku, K., Tokuhara, Y., Ohkawa, R., Uranbileg, B., . . . Ikeda, H. (2014). Increased serum autotaxin levels in hepatocellular carcinoma patients were caused by background liver fibrosis but not by carcinoma. *Clin Chim Acta, 433*, 128-134. doi: 10.1016/j.cca.2014.03.006.

Kuypers, F. A. (1998). Phodpholipid asymmetry in health and disease. *Current Opinion in Hematology, 5*(1), 122-131.

Kyrgios, I., Galli-Tsinopoulou, A., Stylianou, C., Papakonstantinou, E., Arvanitidou, M., & Haidich, A. B. (2012). Elevated circulating levels of the serum acute-phase protein YKL-40 (chitinase 3-like protein 1) are a marker of obesity and insulin resistance in prepubertal children. *Metabolism, 61*(4), 562-568. doi: 10.1016/j.metabol.2011.09.004.

Kyrle, P. A., Minar, E., Hirschl, M., Bialonczyk, C., Stain, M., Schneider, B., . . . Eichinger, S. (2000). High Plasma Levels of Factor VIII and the Risk of Recurrent Venous Thromboembolism. *The New England Journal of Medicine, 343*(7), 457-462.

Lammers, S., Scott, D., Hunter, K., Tan, W., Shandas, R., & Stenmark, K. R. (2012). Mechanics and Function of the Pulmonary Vasculature: Implications for Pulmonary Vascular Disease and Right Ventricular Function *Comprehensive Physiology*.

Lang, I. (2010). Advances in understanding the pathogenesis of chronic thromboembolic pulmonary hypertension. *Br J Haematol, 149*(4), 478-483. doi: 10.1111/j.1365-2141.2010.08142.x.

Lang, I. (2015). Chronic thromboembolic pulmonary hypertension: a distinct disease entity. *Eur Respir Rev, 24*(136), 246-252. doi: 10.1183/16000617.00001115.

Lang, I., Meyer, B. C., Ogo, T., Matsubara, H., Kurzyna, M., Ghofrani, H. A., . . . Brenot, P. (2017). Balloon pulmonary angioplasty in chronic thromboembolic pulmonary hypertension. *Eur Respir Rev, 26*(143). doi: 10.1183/16000617.0119-2016.

Lang, I. M., Dorfmuller, P., & Vonk Noordegraaf, A. (2016). The Pathobiology of Chronic Thromboembolic Pulmonary Hypertension. *Ann Am Thorac Soc, 13 Suppl 3*, S215-221. doi: 10.1513/AnnalsATS.201509-620AS.

Lang, I. M., & Gaine, S. P. (2015). Recent advances in targeting the prostacyclin pathway in pulmonary arterial hypertension. *European Respiratory Review, 24*(138), 630-641. doi: 10.1183/16000617.0067-2015.

Lang, I. M., & Madani, M. (2014). Update on chronic thromboembolic pulmonary hypertension. *Circulation, 130*(6), 508-518. doi: 10.1161/CIRCULATIONAHA.114.009309.

Lang, I. M., Marsh, J. J., Olman, M. A., Moser, K. M., & Schleef, R. R. (1994). Parallel analysis of tissue-type plasminogen activator and type 1 plasminogen activator inhibitor in plasma and endothelial cells derived from patients with chronic pulmonary thromboemboli. *Circulation, 90*(2), 706-712. doi: doi:10.1161/01.CIR.90.2.706.

Lang, I. M., Pesavento, R., Bonderman, D., & Yuan, J. X. (2013). Risk factors and basic mechanisms of chronic thromboembolic pulmonary hypertension: a current understanding. *Eur Respir J, 41*(2), 462-468. doi: 10.1183/09031936.00049312.

Langer, F., Schramm, R., Bauer, M., Tscholl, D., Kunihara, T., & Schafers, H. J. (2004). Cytokine response to pulmonary thromboendarterectomy. *Chest, 126*(1), 135-141. doi: 10.1378/chest.126.1.135.

Lankeit, M., Friesen, D., Schäfer, K., Hasenfuß, G., Konstantinides, S., & Dellas, C. (2013). A simple score for rapid risk assessment of non-high-risk pulmonary embolism. *Clinical Research in Cardiology, 102*(1), 73-80. doi: 10.1007/s00392-012-0498-1.

Le Gal, G., Delahousse, B., Lacut, K., Malaviolle, V., Regina, S., Blouch, M.-T., . . . Gruel, Y. (2007). Fibrinogen Aα-Thr312Ala and factor XIII-A Val34Leu polymorphisms in idiopathic venous thromboembolism. *Thrombosis Research, 121*(3), 333-338. doi: https://doi.org/10.1016/j.thromres.2007.05.003.

Leblanc, R., Lee, S. C., David, M., Bordet, J. C., Norman, D. D., Patil, R., . . . Peyruchaud, O. (2014). Interaction of platelet-derived autotaxin with tumor integrin alphaVbeta3 controls metastasis of breast cancer cells to bone. *Blood, 124*(20), 3141-3150. doi: 10.1182/blood-2014-04-568683.

Lee, H., Goetzl, E. J., & An, S. (2000). Lysophosphatidic acid and sphingosine 1-phosphate stimulate endothelial cell wound healing. *Am J Physiol Cell Physiol, 278*(1), C612-C618.

Lee, S. D., Shroyer, K. R., Markham, N. E., Cool, C. D., Voelkel, N. F., & Tuder, R. M. (1998). Monoclonal endothelial cell proliferation is present in primary but not secondary pulmonary hypertension. *The Journal of clinical investigation, 101*(5), 927-934. doi: 10.1172/JCI1910.

Lelli, K. M., Slattery, M., & Mann, R. S. (2012). Disentangling the many layers of eukaryotic transcriptional regulation. *Annu Rev Genet, 46*, 43-68. doi: 10.1146/annurev-genet-110711-155437.

Li, J.-F., Lin, Y., Yang, Y.-H., Gan, H.-L., Liang, Y., Liu, J., . . . Wang, C. (2013). Fibrinogen Aα Thr312Ala Polymorphism Specifically Contributes to Chronic Thromboembolic Pulmonary Hypertension by Increasing Fibrin Resistance. *PLoS One, 8*(7), e69635. doi: 10.1371/journal.pone.0069635.

Libreros, S., Garcia-Areas, R., & Iragavarapu-Charyulu, V. (2013). CHI3L1 plays a role in cancer through enhanced production of pro-inflammatory/pro-tumorigenic and angiogenic factors. *Immunol Res, 57*(1-3), 99-105. doi: 10.1007/s12026-013-8459-y.

Lin, M.-J., Leung, G. P. H., Zhang, W.-M., Yang, X.-R., Yip, K.-P., Tse, C.-M., & Sham, J. S. K. (2004). Chronic Hypoxia–Induced Upregulation of Store-Operated and Receptor-Operated Ca²⁺ Channels in Pulmonary Arterial Smooth Muscle Cells. *Circulation Research, 95*(5), 496-505. doi: doi:10.1161/01.RES.0000138952.16382.ad.

Luscher, T. F., & Barton, M. (2000). Endothelins and endothelin receptor antagonists: therapeutic considerations for a novel class of cardiovascular drugs. *Circulation, 102*(19), 2434-2440. doi: 10.1161/01.cir.102.19.2434.

Ma, W.-h., Wang, X.-l., Du, Y.-m., Wang, Y.-b., Zhang, Y., Wei, D.-e., . . . Bu, B.-l. (2012). Association between human cartilage glycoprotein 39 (YKL-40) and arterial stiffness in essential hypertension. *BMC Cardiovascular Disorders, 12*(35), 1-7.

Madani, M., Ogo, T., & Simonneau, G. (2017). The changing landscape of chronic thromboembolic pulmonary hypertension management. *Eur Respir Rev, 26*(146). doi: 10.1183/16000617.0105-2017.

Madani, M. M., & Jamieson, S. W. (2006). Technical advances of pulmonary endarterectomy for chronic thromboembolic pulmonary hypertension. *Semin Thorac Cardiovasc Surg, 18*(3), 243-249. doi: 10.1053/j.semtcvs.2006.09.003.

Mahajan, S. G., Fender, A. C., Meyer-Kirchrath, J., Kurt, M., Barth, M., Sagban, T. A., . . . Rauch, B. H. (2012). A novel function of FoxO transcription factors in thrombin-stimulated vascular smooth muscle cell proliferation. *Thromb Haemost, 108*(1), 148-158. doi: 10.1160/TH11-11-0756.

Majesky, M. W., Dong, X. R., Hoglund, V., Mahoney, W. M., Jr., & Daum, G. (2011). The adventitia: a dynamic interface containing resident progenitor cells. *Arterioscler Thromb Vasc Biol, 31*(7), 1530-1539. doi: 10.1161/ATVBAHA.110.221549.

Malinda, K. M., Ponce, L., Kleinmann, H. K., Shackelton, L. M., & Millis, S. J. T. (1999). Gp38k, a Protein Synthesized by Vascular Smooth Muscle Cells, Stimulates Directional Migration of Human Umbilical Vein Endothelial Cells. *Experimental Cell Research, 250*(1), 168-173.

Mano, T., Luo, Z., Malendowicz, S. L., Evans, T., & Walsh, K. (2015). Reversal of GATA-6 Downregulation Promotes Smooth Muscle Differentiation and Inhibits Intimal Hyperplasia in Balloon-Injured Rat Carotid Artery. *Circ Res, 84*(1), 647-654.

Marsh, J. J., Chiles, P. G., Liang, N.-C., & Morris, T. A. (2013). Chronic thromboembolic pulmonary hypertension-associated dysfibrinogenemias exhibit disorganized fibrin structure. *Thrombosis Research, 132*(6), 729-734. doi: https://doi.org/10.1016/j.thromres.2013.09.024.

Matthews, D. T., & Hemnes, A. R. (2016). Current concepts in the pathogenesis of chronic thromboembolic pulmonary hypertension. *Pulm Circ, 6*(2), 145-154. doi: 10.1086/686011.

Mayer, E., Jenkins, D., Lindner, J., D'Armini, A., Kloek, J., Meyns, B., . . . Dartevelle, P. (2011). Surgical management and outcome of patients with chronic thromboembolic pulmonary hypertension: results from an international prospective registry. *J Thorac Cardiovasc Surg, 141*(3), 702-710. doi: 10.1016/j.jtcvs.2010.11.024.

McCallum, C. J., Peake, I. R., Newcombe, R. G., & Bloom, A. L. (1983). Factor VIII levels and blood group antigens. *Thromb Haemost, 50*(3), 757.

McNeil, K., & Dunning, J. (2007). Chronic thromboembolic pulmonary hypertension (CTEPH). *Heart, 93*(9), 1152-1158. doi: 10.1136/hrt.2004.053603.

Mercier, O., & Fadel, E. (2013). Chronic thromboembolic pulmonary hypertension: animal models. *European Respiratory Journal, 41*(5), 1200-1206. doi: 10.1183/09031936.00101612.

Mercier, O., Tivane, A., Dorfmuller, P., de Perrot, M., Raoux, F., Decante, B., . . . Fadel, E. (2013). Piglet model of chronic pulmonary hypertension. *Pulm Circ, 3*(4), 908-915. doi: 10.1086/674757.

Meyrick, B., Clarke, S. W., Symons, C., Woodgate, D. J., & Reid, L. (1974). Primary pulmonary hypertension. A case report including electronmicroscopic study. *Brit J Dis Chest, 68*(1), 11-20.

Michelakis, E. D., McMurtry, M. S., Wu, X.-C., Dyck, J. R. B., Moudgil, R., Hopkins, T. A., . . . Archer, S. L. (2002). Dichloroacetate, a Metabolic Modulator, Prevents and Reverses Chronic Hypoxic Pulmonary Hypertension in Rats. Role of Increased Expression and Activity of Voltage-Gated Potassium Channels. *Circulation, 105*(2), 244-250.

Michelsen, A. E., Rathcke, C. N., Skjelland, M., Holm, S., Ranheim, T., Krohg-Sorensen, K., . . . Halvorsen, B. (2010). Increased YKL-40 expression in patients with carotid atherosclerosis. *Atherosclerosis, 211*(2), 589-595. doi: 10.1016/j.atherosclerosis.2010.02.035.

Mohanty, D., Ghosh, K., Marwaha, N., Kaur, S., Chauhan, A. P., & Das, K. C. (1984). Major blood group antigens--a determinant of factor VIII levels in blood? *Thromb Haemost, 51*(3), 414.

Moolenaar, W. H., van Meeteren, L. A., & Giepmans, B. N. (2004). The ins and outs of lysophosphatidic acid signaling. *Bioessays, 26*(8), 870-881. doi: 10.1002/bies.20081.

Morrell, N. W., Adnot, S., Archer, S. L., Dupuis, J., Jones, P. L., MacLean, M. R., . . . Weir, E. K. (2009). Cellular and molecular basis of pulmonary arterial hypertension. *J Am Coll Cardiol, 54*(1 Suppl), S20-31. doi: 10.1016/j.jacc.2009.04.018.

Morris, T. A., Marsh, J. J., Chiles, P. G., Magaña, M. M., Liang, N.-C., Soler, X., . . . Woods, V. L., Jr. (2009). High prevalence of dysfibrinogenemia among patients with chronic thromboembolic pulmonary hypertension. *Blood, 114*(9), 1929-1936. doi: 10.1182/blood-2009-03-208264.

Moser, K. M., & Bioor, C. M. (1993). Pulmonary Vascular Lesions Occurring in Patients With Chronic Major Vessel Thromboembolic Pulmonary Hypertension. *Chest, 103*(3), 685-692. doi: 10.1378/chest.103.3.685.

Moser, K. M., Cantor, J. P., Olman, M., Villespin, I., Graif, J. L., Konopka, R., . . . Petersen, C. (1991). Chronic Pulmonary Thromboembolism in Dogs Treated With Tranexamic Acid. *Circulation, 83*(4), 1371-1379.

Moshtaghi-Kashanian, G. R., Gholamhoseinian, A., Hoseinimoghadam, A., & Rajabalian, S. (2006). Splenectomy changes the pattern of cytokine production in beta-thalassemic patients. *Cytokine, 35*(5-6), 253-257. doi: 10.1016/j.cyto.2006.09.003.

Moudgil, R., Michelakis, E. D., & Archer, S. L. (2006). The role of k+ channels in determining pulmonary vascular tone, oxygen sensing, cell proliferation, and apoptosis: implications in hypoxic pulmonary vasoconstriction and pulmonary arterial hypertension. *Microcirculation, 13*(8), 615-632. doi: 10.1080/10739680600930222.

Naeije, R., & Eddahibi, S. (2004). Serotonin in Pulmonary Arterial Hypertension. *Am J Respir Crit Care Med, 170*(1), 209-210.

Naito, A., Sakao, S., Lang, I. M., Voelkel, N. F., Jujo, T., Ishida, K., . . . Tatsumi, K. (2018). Endothelial cells from pulmonary endarterectomy specimens possess a high angiogenic potential and express high levels of hepatocyte growth factor. *BMC Pulm Med, 18*(1), 197. doi: 10.1186/s12890-018-0769-3.

Nakashima, Y., Raines, E. W., Plump, A. S., Breslow, J. L., & Ross, R. (1998). Upregulation of VCAM-1 and ICAM-1 at Atherosclerosis-Prone Sites on the Endothelium in the ApoE-Deficient Mouse. *Arteriosclerosis, Thrombosis, and Vascular Biology, 18*(5), 842-851. doi: 10.1161/01.Atv.18.5.842.

Nijkeuter, M., Hovens, M. M. C., Davidson, B. L., & Huismann, M. V. (2006). Resolution of Thromboemboli in Patients With Acute Pulmonary Embolism. A Systematic Review. *Chest, 129*(1), 192-197.

Nillson, I. M., Ljungnér, H., & Tengborn, L. (1985). Two different mechanisms in patients with venous thrombosis and defective fibrinolysis: low concentration of plasminogen activator or increased concentration of plasminogen activator inhibitor. *British Medical Journal, 290*(1), 1453-1456.

Nishida, W., Nakamura, M., Mori, S., Takahashi, M., Ohkawa, Y., Tadokoro, S., . . . Sobue, K. (2002). A triad of serum response factor and the GATA and NK families governs the transcription of smooth and cardiac muscle genes. *J Biol Chem, 277*(9), 7308-7317. doi: 10.1074/jbc.M111824200.

Oellerich, M. F., & Potente, M. (2012). FOXOs and sirtuins in vascular growth, maintenance, and aging. *Circ Res, 110*(9), 1238-1251. doi: 10.1161/CIRCRESAHA.111.246488.

Ogawa, A., Firth, A. L., Yao, W., Madani, M. M., Kerr, K. M., Auger, W. R., . . . Yuan, J. X. (2009). Inhibition of mTOR attenuates store-operated Ca2+ entry in cells from endarterectomized tissues of patients with chronic thromboembolic pulmonary hypertension. *Am J Physiol Lung Cell Mol Physiol, 297*(4), L666-676. doi: 10.1152/ajplung.90548.2008.

Ogawa, A., & Matsubara, H. (2015). Balloon Pulmonary Angioplasty: A Treatment Option for Inoperable Patients with Chronic Thromboembolic Pulmonary Hypertension. *Front Cardiovasc Med, 2*, 4. doi: 10.3389/fcvm.2015.00004.

Ogo, T., Fukuda, T., Tsuji, A., Fukui, S., Ueda, J., Sanda, Y., . . . Yasuda, S. (2017). Efficacy and safety of balloon pulmonary angioplasty for chronic thromboembolic pulmonary hypertension guided by cone-beam computed tomography and electrocardiogram-gated area detector computed tomography. *Eur J Radiol, 89*, 270-276. doi: 10.1016/j.ejrad.2016.12.013.

Olman, M., Marsh, J. J., Lang, I. M., Moser, K. M., Binder, B. R., & Schleef, R. R. (1992). Endogenous Fibrinolytic System in Chronic Large-Vessel Thromboembolic Pulmonary Hypertension. *Circulation, 86*(4), 1241-1248.

Olschewski, H., Rose, F., Schermuly, R., Ghofrani, H. A., Enke, B., Olschewski, A., & Seeger, W. (2004). Prostacyclin and its analogues in the treatment of pulmonary hypertension. *Pharmacol Ther, 102*(2), 139-153. doi: 10.1016/j.pharmthera.2004.01.003.

Olschweski, H., Simmoneau, G., Galie, N., Higenbottam, T., Naeije, R., Rubin, L., . . . Seeger, W. (2002). Inhaled Iloprost for Severe Pulmonary Hypertension. *The New England Journal of Medicine, 347*(5), 322-329.

Orstavik, K. H., Magnus, P., Reisner, H., Berg, K., Graham, J. B., & Nance, W. (1985). Factor VIII and factor IX in a twin population. Evidence for a major effect of ABO locus on factor VIII level. *American journal of human genetics, 37*(1), 89-101.

Owens, G. K., Kumar, M. S., & Wamhoff, B. R. (2004). Molecular Regulation of Vascular Smooth Muscle Cell Differentiation in Development and Disease. *Physiol Rev, 84*(1), 767-801.

Paramo, J. A., Colucci, M., & Collen, D. (1985). Plasminogen activator inhibitor in the blood of patients with coronary artery disease. *British Medical Journal, 291*(1), 573-574.

Park, G. Y., Lee, Y. G., Berdyshev, E., Nyenhuis, S., Du, J., Fu, P., . . . Christman, J. W. (2013). Autotaxin production of lysophosphatidic acid mediates allergic asthmatic inflammation. *Am J Respir Crit Care Med, 188*(8), 928-940. doi: 10.1164/rccm.201306-1014OC.

Parthvi, R., Sikachi, R. R., Agrawal, A., Adial, A., Vulisha, A., Khanijo, S., & Talwar, A. (2017). Pulmonary hypertension associated with antiphospholipid antibody: Call for a screening tool? *Intractable Rare Dis Res, 6*(3), 163-171. doi: 10.5582/irdr.2017.01044.

Peacock, A., Simonneau, G., & Rubin, L. (2006). Controversies, uncertainties and future research on the treatment of chronic thromboembolic pulmonary hypertension. *Proc Am Thorac Soc, 3*(7), 608-614. doi: 10.1513/pats.200605-114LR.

Pepke-Zaba, J. (2010). Diagnostic testing to guide the management of chronic thromboembolic pulmonary hypertension: state of the art. *Eur Respir Rev, 19*(115), 55-58. doi: 10.1183/09059180.00007209.

Pepke-Zaba, J., Delcroix, M., Lang, I., Mayer, E., Jansa, P., Ambroz, D., . . . Simonneau, G. (2011). Chronic thromboembolic pulmonary hypertension (CTEPH): results from an international prospective registry. *Circulation, 124*(18), 1973-1981. doi: 10.1161/CIRCULATIONAHA.110.015008.

Pepke-Zaba, J., Ghofrani, H. A., & Hoeper, M. M. (2017). Medical management of chronic thromboembolic pulmonary hypertension. *Eur Respir Rev, 26*(143). doi: 10.1183/16000617.0107-2016.

Pepke-Zaba, J., Jansa, P., Kim, N. H., Naeije, R., & Simonneau, G. (2013). Chronic thromboembolic pulmonary hypertension: role of medical therapy. *European Respiratory Journal, 41*(4), 985-990. doi: 10.1183/09031936.00201612.

Perros, F., Montani, D., Dorfmuller, P., Durand-Gasselin, I., Tcherakian, C., Le Pavec, J., . . . Humbert, M. (2008). Platelet-derived growth factor expression and function in idiopathic pulmonary arterial hypertension. *Am J Respir Crit Care Med, 178*(1), 81-88. doi: 10.1164/rccm.200707-1037OC.

Piazza, G., & Goldhaber, S. Z. (2011). Current concepts: Chronic Thromboembolic Pulmonary Hypertension. *The New England Journal of Medicine, 364*(4), 351-360.

Pietra, G. G., Capron, F., Stewart, S., Leone, O., Humbert, M., Robbins, I. M., . . . Tuder, R. M. (2004). Pathologic assessment of vasculopathies in pulmonary hypertension. *J Am Coll Cardiol, 43*(12 Suppl S), 25S-32S. doi: 10.1016/j.jacc.2004.02.033.

Pietra, G. G., Edwards, W. D., Kay, J. M., Rich, S., Kernis, J., Schloo, B., . . . Williams, G. W. (1994). Histopathology of Primary Pulmonary Hypertension. A Qualitative and Quantitative Study of Pulmonary Blood Vessels From 58 Patients in the National Heart, Lung, and Blood Institute, Primary Pulmonary Hypertension Registry. *Circulation, 80*(5), 1198-1206.

Pollock, D. M., Keith, T. L., & Highsmith, R. F. (1995). Endothelin receptors and calcium signaling. *The FASEB Journal, 9*(12), 1196-1204.

Potente, M., Urbich, C., Sasaki, K., Hofmann, W. K., Heeschen, C., Aicher, A., . . . Dimmeler, S. (2005). Involvement of Foxo transcription factors in angiogenesis and postnatal neovascularization. *J Clin Invest, 115*(9), 2382-2392. doi: 10.1172/JCI23126.

Pullamsetti, S., Kiss, L., Ghofrani, H. A., Voswinckel, R., Haredza, P., Klepetko, W., . . . Schermuly, R. T. (2005). Increased levels and reduced catabolism of asymmetric and symmetric dimethylarginines in pulmonary hypertension. *The FASEB Journal, 19*(9), 1175-1177. doi: 10.1096/fj.04-3223fje.

Pullamsetti, S. S., Kojonazarov, B., Storn, S., Gall, H., Salazar, Y., Wolf, N., . . . Savai, R. (2017). Lung cancer–associated pulmonary hypertension: Role of microenvironmental inflammation based on tumor cell–immune cell cross-talk. *Sci Transl Med, 9*(1), 1-16.

Pullamsetti, S. S., Schermuly, R., Ghofrani, A., Weissmann, N., Grimminger, F., & Seeger, W. (2014). Novel and emerging therapies for pulmonary hypertension. *Am J Respir Crit Care Med, 189*(4), 394-400. doi: 10.1164/rccm.201308-1543PP.

Quarck, R., Nawrot, T., Meyns, B., & Delcroix, M. (2009). C-reactive protein: a new predictor of adverse outcome in pulmonary arterial hypertension. *J Am Coll Cardiol, 53*(14), 1211-1218. doi: 10.1016/j.jacc.2008.12.038.

Quarck, R., Wxnants, M., Verbeken, E., Meyns, B., & Delcroix, M. (2015). Contribution of inflammation and impaired angiogenesis to the pathobiology of chronic thromboembolic pulmonary hypertension. *Eur Respir J, 46*(2), 431-443. doi: 10.1183/13993003.00962-2015.

Rabinovitch, M. (2012). Molecular pathogenesis of pulmonary arterial hypertension. *J Clin Invest, 122*(12), 4306-4313. doi: 10.1172/JCI60658.

Rai, P. R., Cool, C. D., King, J. A., Stevens, T., Burns, N., Winn, R. A., . . . Voelkel, N. F. (2008). The cancer paradigm of severe pulmonary arterial hypertension. *Am J Respir Crit Care Med, 178*(6), 558-564. doi: 10.1164/rccm.200709-1369PP.

Ranchoux, B., Harvey, L. D., Ayon, R. J., Babicheva, A., Bonnet, S., Chan, S. Y., . . . Perez, V. J. (2018). Endothelial dysfunction in pulmonary arterial hypertension: an evolving landscape (2017 Grover Conference Series). *Pulm Circ, 8*(1), 2045893217752912. doi: 10.1177/2045893217752912.

Rathcke, C. N., & Vestergaard, H. (2009). YKL-40 - an emerging biomarker in cardiovascular disease and diabetes. *Cardiovascular Diabetology, 8*(1), 61. doi: 10.1186/1475-2840-8-61.

Recklies, A. D., White, C., & Ling, H. (2002). The chitinase 3-like protein human cartilage glycoprotein 39 (HC-gp39) stimulates proliferation of human connective-tissue cells

and activates both extracellular signal-regulated kinase- and protein kinase B-mediated signalling pathways. *Biochemical Journal, 365*(1), 119-126.

Reesink, H. J., Meijer, R. C., Lutter, R., Boomsma, F., Jansen, H. M., Kloek, J. J., & Bresser, P. (2006). Hemodynamic and Clinical Correlates of Endothelin-1 in Chronic Thromboembolic Pulmonary Hypertension. *Circulation Journal, 70*(1), 1058-1063.

Remková, A., Šimková, I., & Valkovičová, T. (2015). Platelet abnormalities in chronic thromboembolic pulmonary hypertension. *Int J Clin Exp Med, 8*(6), 9700-9707.

Renkema, G. H., Boot, R. G., Au, F. L., Donker-Koopman, W. E., Strijland, A., Muijsers, A. O., . . . Aerts, J. M. F. G. (1998). Chitotriosidase, a chitinase, and the 39-kDa human cartilage glycoprotein, a chitin-binding lectin, are homologues of family 18 glycosyl hydrolases secreted by human macrophages. *Eur J Biochem, 251*(1), 504-509.

Ribatti, D. (2009). Endogenous inhibitors of angiogenesis: A historical review. *Leukemia Research, 33*(5), 638-644.

Roca, B., & Roca, M. (2015). The new oral anticoagulants: Reasonable alternatives to warfarin. *Cleve Clin J Med, 82*(12), 847-854. doi: 10.3949/ccjm.82a.14052.

Rondbjerg, A. K., Omerovic, E., & Vestergaard, H. (2011). YKL-40 levels are independently associated with albuminuria in type 2 diabetes. *Cardiovascular Diabetology, 10*(54), 1-6.

Sacks, R. S., Remillard, C. V., Agange, N., Auger, W. R., Thistlethwaite, P. A., & Yuan, J. X. J. (2006). Molecular Biology of Chronic Thromboembolic Pulmonary Hypertension. *Seminars in Thoracic and Cardiovascular Surgery, 18*(3), 265-276. doi: https://doi.org/10.1053/j.semtcvs.2006.09.004.

Sakao, S., Hao, H., Tanabe, N., Kasahara, Y., Kurosu, K., & Tatsumi, K. (2011). Endothelial-like cells in chronic thromboembolic pulmonary hypertension: crosstalk with myofibroblast-like cells. *Respir Res, 12*, 109. doi: 10.1186/1465-9921-12-109.

Sakao, S., Taraseviciene-Stewart, L., Lee, J. D., Wood, K., Cool, C. D., & Voelkel, N. F. (2005). Initial apoptosis is followed by increased proliferation of apoptosis-resistant endothelial cells. *The FASEB Journal, 19*(9), 1178-1180.

Sanchez, O., Marcos, E., Perros, F., Fadel, E., Tu, L., Humbert, M., . . . Eddahibi, S. (2007). Role of endothelium-derived CC chemokine ligand 2 in idiopathic pulmonary arterial hypertension. *Am J Respir Crit Care Med, 176*(10), 1041-1047. doi: 10.1164/rccm.200610-1559OC.

Sarker, M. H., Hu, D.-E., & Fraser, P. A. (2010). Regulation of Cerebromicrovascular Permeability by Lysophosphatidic Acid. *Microcirculation, 17*(1), 39-46.

Savai, R., Al-Tamari, H. M., Sedding, D., Kojonazarov, B., Muecke, C., Teske, R., . . . Pullamsetti, S. S. (2014). Pro-proliferative and inflammatory signaling converge on FoxO1 transcription factor in pulmonary hypertension. *Nat Med, 20*(11), 1289-1300. doi: 10.1038/nm.3695.

Schermuly, R. T., Dony, E., Ghofrani, H. A., Pullamsetti, S., Savai, R., Roth, M., . . . Grimminger, F. (2005). Reversal of experimental pulmonary hypertension by PDGF inhibition. *J Clin Invest, 115*(10), 2811-2821. doi: 10.1172/JCI24838.

Shao, D. D., Suresh, R., Vakil, V., Gomer, R. H., & Pilling, D. (2008). Pivotal Advance: Th-1 cytokines inhibit, and Th-2 cytokines promote fibrocyte differentiation. *J Leukoc Biol, 83*(6), 1323-1333. doi: 10.1189/jlb.1107782.

Sharma, S., & Lang, I. M. (2018). Current understanding of the pathophysiology of chronic thromboembolic pulmonary hypertension. *Thromb Res, 164*, 136-144. doi: 10.1016/j.thromres.2017.06.011.

Shlyonsky, V., Naeije, R., & Mies, F. (2014). Possible role of lysophosphatidic acid in rat model of hypoxic pulmonary vascular remodeling. *Pulm Circ, 4*(3), 471-481. doi: 10.1086/677362.

Simonneau, G., Montani, D., Celermajer, D. S., Denton, C. P., Gatzoulis, M. A., Krowka, M., . . . Souza, R. (2019). Haemodynamic definitions and updated clinical classification of pulmonary hypertension. *European Respiratory Journal, 53*(1), 1801913. doi: 10.1183/13993003.01913-2018.

Simonneau, G., Torbicki, A., Dorfmuller, P., & Kim, N. (2017). The pathophysiology of chronic thromboembolic pulmonary hypertension. *Eur Respir Rev, 26*(143). doi: 10.1183/16000617.0112-2016.

Skoro-Sajer, N., Mittermayer, F., Panzenboeck, A., Bonderman, D., Sadushi, R., Hitsch, R., . . . Lang, I. M. (2007). Asymmetric dimethylarginine is increased in chronic thromboembolic pulmonary hypertension. *Am J Respir Crit Care Med, 176*(11), 1154-1160. doi: 10.1164/rccm.200702-278OC.

Soon, E., Holmes, A. M., Treacy, C. M., Doughty, N. J., Southgate, L., Machado, R. D., . . . Morrell, N. W. (2010). Elevated levels of inflammatory cytokines predict survival in idiopathic and familial pulmonary arterial hypertension. *Circulation, 122*(9), 920-927. doi: 10.1161/CIRCULATIONAHA.109.933762.

Southwood, M., MacKenzie Ross, R. V., Kuc, R. E., Hagan, G., Sheares, K. K., Jenkins, D. P., . . . Pepke-Zaba, J. (2016). Endothelin ETA receptors predominate in chronic thromboembolic pulmonary hypertension. *Life Sci, 159*, 104-110. doi: 10.1016/j.lfs.2016.02.036.

Stenmark, K. R., Frid, M. G., Yeager, M., Li, M., Riddle, S., McKinsey, T., & El Kasmi, K. C. (2012). Targeting the adventitial microenvironment in pulmonary hypertension: A potential approach to therapy that considers epigenetic change. *Pulmonary Circulation, 2*(1), 3-14. doi: 10.4103/2045-8932.94817.

Stenmark, K. R., Meyrick, B., Galie, N., Mooi, W. J., & McMurtry, I. F. (2009). Animal models of pulmonary arterial hypertension: the hope for etiological discovery and pharmacological cure. *Am J Physiol Lung Cell Mol Physiol, 297*(6), L1013-1032. doi: 10.1152/ajplung.00217.2009.

Suntharalingam, J., Goldsmith, K., van Marion, V., Long, L., Treacy, C. M., Dudbridge, F., . . . Morrell, N. W. (2008). Fibrinogen Aα Thr312Ala polymorphism is associated with chronic thromboembolic pulmonary hypertension. *European Respiratory Journal, 31*(4), 736-741. doi: 10.1183/09031936.00055107.

Suresh, K., & Shimoda, L. A. (2016). Lung Circulation. *Compr Physiol, 6*(2), 897-943. doi: 10.1002/cphy.c140049.

Sutendra, G., Bonnet, S., Rochefort, G., Haromy, A., Folmes, K. D., Lopaschuk, G. D., . . . Michelakis, E. D. (2010). Fatty Acid Oxidation and Malonyl-CoA Decarboxylase in the Vascular Remodeling of Pulmonary Hypertension. *Science Translational Medicine, 2*(44), 44ra58-44ra58. doi: 10.1126/scitranslmed.3001327.

Suzuki, E., Evans, T., Lowry, J., Truong, L., Bell, D. W., Testa, J. R., & Walsh, K. (1996). The Human GATA-6 Gene: Structure, Chromosomal Location, and Regulation of Expression by Tissue-Specific and Mitogen-Responsive Signals. *Genomics, 38*(1), 283-290.

Tang, N., Zhao, Y., Feng, R., Liu, Y., Wang, S., Wei, W., . . . Li, L. (2014). Lysophosphatidic acid accelerates lung fibrosis by inducing differentiation of mesenchymal stem cells into myofibroblasts. *J Cell Mol Med, 18*(1), 156-169. doi: 10.1111/jcmm.12178.

Teo, S. T., Yung, Y. C., Herr, D. R., & Chun, J. (2009). Lysophosphatidic acid in vascular development and disease. *IUBMB Life, 61*(8), 791-799. doi: 10.1002/iub.220.

Thompson, K., & Rabinovitch, M. (1996). Exogenous Leukocyte and endogenous elastases can mediate mitogenic activity in pulmonary artery smooth muscle cells by release of extracellular matrix-bound basic fibroblast growth factor. *J Cell Physiol, 166*(1), 495-505.

Tonelli, A. R., Haserodt, S., Aytekin, M., & Dweik, R. A. (2013). Nitric oxide deficiency in pulmonary hypertension: Pathobiology and implications for therapy. *Pulm Circ, 3*(1), 20-30. doi: 10.4103/2045-8932.109911.

Toshner, M., & Pepke-Zaba, J. (2014). Chronic thromboembolic pulmonary hypertension: time for research in pathophysiology to catch up with developments in treatment. *F1000prime reports, 6*, 38-38. doi: 10.12703/P6-38.

Townsley, M. I. (2013). Structure and composition of pulmonary arteries, capillaries, and veins. *Compr Physiol, 2*(1), 675-709. doi: 10.1002/cphy.c100081.

Tu, L., De Man, F. S., Girerd, B., Huertas, A., Chaumais, M. C., Lecerf, F., . . . Guignabert, C. (2012). A critical role for p130Cas in the progression of pulmonary hypertension in humans and rodents. *Am J Respir Crit Care Med, 186*(7), 666-676. doi: 10.1164/rccm.201202-0309OC.

Tu, L., Dewachter, L., Gore, B., Fadel, E., Dartevelle, P., Simonneau, G., . . . Guignabert, C. (2011). Autocrine fibroblast growth factor-2 signaling contributes to altered endothelial phenotype in pulmonary hypertension. *Am J Respir Cell Mol Biol, 45*(2), 311-322. doi: 10.1165/rcmb.2010-0317OC.

Tuder, R. M., Abman, S. H., Braun, T., Capron, F., Stevens, T., Thistlethwaite, P. A., & Haworth, S. G. (2009). Development and pathology of pulmonary hypertension. *J Am Coll Cardiol, 54*(1 Suppl), S3-9. doi: 10.1016/j.jacc.2009.04.009.

Tuder, R. M., Davis, L. A., & Graham, B. B. (2012). Targeting energetic metabolism: a new frontier in the pathogenesis and treatment of pulmonary hypertension. *Am J Respir Crit Care Med, 185*(3), 260-266. doi: 10.1164/rccm.201108-1536PP.

Tuder, R. M., Groves, B., Badesch, D. B., & Voelkel, N. F. (1994). Exuberant endothelial cell growth and elements of inflammation are present in plexiform lesions of pulmonary hypertension. *The American journal of pathology, 144*(2), 275-285.

Tura-Ceide, O., Aventín, N., Piccari, L., Morén, C., Guitart-Mampel, M., Garrabou, G., . . . Barberà, J. A. (2016). Endothelial dysfunction in patients with chronic thromboembolic pulmonary hypertension (CTEPH). *European Respiratory Journal, 48*(suppl 60), PA3606. doi: 10.1183/13993003.congress-2016.PA3606.

van Meeteren, L. A., Ruurs, P., Stortelers, C., Bouwman, P., van Rooijen, M. A., Pradere, J. P., . . . Jonkers, J. (2006). Autotaxin, a secreted lysophospholipase D, is essential for blood vessel formation during development. *Mol Cell Biol, 26*(13), 5015-5022. doi: 10.1128/MCB.02419-05.

Varma, M. R., Moaveni, D. M., Dewyer, N. A., Varga, A. J., Deatrick, K. B., Kunkel, S. L., . . . Henke, P. K. (2004). Deep vein thrombosis resolution is not accelerated with increased neovascularization. *J Vasc Surg, 40*(3), 536-542. doi: 10.1016/j.jvs.2004.05.023.

Vlot, A. J., Koppelmann, S. J., Meijers, J. C. M., Damas, C., van den Berg, H. M., Bouma, B. N., . . . Willems, G. M. (1996). Kinetics of Factor VIII-von Willebrand Factor Association. *Blood, 87*(5), 1809-1816.

von Hundelshausen, P., & Weber, C. (2007). Platelets as immune cells: bridging inflammation and cardiovascular disease. *Circ Res, 100*(1), 27-40. doi: 10.1161/01.RES.0000252802.25497.b7.

Waltham, M., Burnand, K. G., Collins, M., McGuinness, C. L., Singh, I., & Smith, A. (2003). Vascular endothelial growth factor enhances venous thrombus recanalisation and organisation. *Thromb Haemost, 89*(1), 169-176.

Wilkens, H., Konstantinides, S., Lang, I. M., Bunck, A. C., Gerges, M., Gerhardt, F., . . . Mayer, E. (2018). Chronic thromboembolic pulmonary hypertension (CTEPH): Updated Recommendations from the Cologne Consensus Conference 2018. *Int J Cardiol, 272S*, 69-78. doi: 10.1016/j.ijcard.2018.08.079.

Wilkins, M. R., Wharton, J., Grimminger, F., & Ghofrani, H. A. (2008). Phosphodiesterase inhibitors for the treatment of pulmonary hypertension. *Eur Respir J, 32*(1), 198-209. doi: 10.1183/09031936.00124007.

Wolf, M., Boyer-Neumann, C., Parent, F., Eschwege, V., Jaillet, H., Meyer, D., & Simmoneau, G. (2000). Thrombotic risk factors in pulmonary hypertension. *European Respiratory Journal, 15*(1), 395-399.

Wong, C. L., Szydlo, R., Gibbs, S., & Laffan, M. (2010). Hereditary and acquired thrombotic risk factors for chronic thromboembolic pulmonary hypertension. *Blood Coagul Fibrinolysis, 21*(3), 201-206. doi: 10.1097/MBC.0b013e328331e664.

Wu, S., Haynes, J., Taylor, J. T., Obiako, B. O., Stubbs, J. R., Li, M., & Stevens, T. (2003). Ca_v3.1 (α_{1G}) T-Type Ca²⁺ Channels Mediate Vaso-Occlusion of Sickled Erythrocytes in Lung Microcirculation. *Circulation Research, 93*(4), 346-353. doi: doi:10.1161/01.RES.0000087148.75363.8F.

Wynants, M., Vengethasamy, L., Ronisz, A., Meyns, B., Delcroix, M., & Quarck, R. (2013). NF-kappaB pathway is involved in CRP-induced effects on pulmonary arterial endothelial cells in chronic thromboembolic pulmonary hypertension. *Am J Physiol Lung Cell Mol Physiol, 305*(12), L934-942. doi: 10.1152/ajplung.00034.2013.

Xu, W., Koeck, T., Lara, A. R., Neumann, D., DiFilippo, F. P., Koo, M., . . . Erzurum, S. C. (2007). Alterations of cellular bioenergetics in pulmonary artery endothelial cells. *Proceedings of the National Academy of Sciences of the United States of America, 104*(4), 1342-1347. doi: 10.1073/pnas.0605080104.

Yaoita, N., Shirakawa, R., Fukumoto, Y., Sugimura, K., Miyata, S., Miura, Y., . . . Horiuchi, H. (2014). Platelets Are Highly Activated in Patients of Chronic Thromboembolic Pulmonary Hypertension. *Arteriosclerosis, Thrombosis, and Vascular Biology, 34*(11), 2486-2494. doi: doi:10.1161/ATVBAHA.114.304404.

Yazici, B., & Yolacan, S. (2007). A comparison of various tests of normality. *Journal of Statistical Computation and Simulation, 77*(2), 175-183. doi: 10.1080/10629360600678310.

Yeager, M. E., Halley, G. R., Golpon, H. A., Voelkel, N. F., & Tuder, R. M. (2001). Microsatellite Instability of Endothelial Cell Growth and Apoptosis Genes Within Plexiform Lesions in Primary Pulmonary Hypertension. *Circulation Research, 88*(1), e2-e11. doi: doi:10.1161/01.RES.88.1.e2.

Yi, E. S., Kim, H., Ahn, H., Strother, J., Morris, T., Masliah, E., . . . Friedman, P. J. (2000). Distribution of Obstructive Intimal Lesions and Their Cellular Phenotypes in Chronic Pulmonary Hypertension. A Morphometric and Immunohistochemical Study. *Am J Respir Crit Care Med, 162*(1), 1577-1586.

Yuan, J. X., & Rubin, L. J. (2005). Pathogenesis of pulmonary arterial hypertension: the need for multiple hits. *Circulation, 111*(5), 534-538. doi: 10.1161/01.CIR.0000156326.48823.55.

Yuan, X.-J., Wang, J., Juhaszova, M., Gaine, S. P., & Rubin, L. J. (1998). Attenuated K+ channel gene transcription in primary pulmonary hypertension. *The Lancet, 351*(9104), 726-727. doi: 10.1016/s0140-6736(05)78495-6.

Zabini, D., Nagaraj, C., Stacher, E., Lang, I. M., Nierlich, P., Klepetko, W., . . . Olschewski, A. (2012). Angiostatic factors in the pulmonary endarterectomy material from chronic thromboembolic pulmonary hypertension patients cause endothelial dysfunction. *PLoS One, 7*(8), e43793. doi: 10.1371/journal.pone.0043793.

Zhao, Y., & Natarajan, V. (2013). Lysophosphatidic acid (LPA) and its receptors: role in airway inflammation and remodeling. *Biochim Biophys Acta, 1831*(1), 86-92. doi: 10.1016/j.bbalip.2012.06.014.

Zhou, Y., Peng, H., Sun, H., Peng, X., Tang, C., Gan, Y., . . . Herzog, E. L. (2014). Chitinase 3-like 1 suppresses injury and promotes fibroproliferative responses in Mammalian lung fibrosis. *Sci Transl Med, 6*(240), 240ra276. doi: 10.1126/scitranslmed.3007096.

Appendix

A-1: List of Top 25 upregulated genes in CTEPH *vs.* donor

Symbol	Entrez gene name	LogFC CTEPH-Donor
HBD	Hemoglobin delta	3.85
HBB	Hemoglobin beta	3.78
HBA2	Hemoglobin.alpha 2	3.70
HAS1	Hyaluronan synthase 1	2.90
CXCL8	Chemokine (C-X-C motif) ligand 8	2.64
FOSB	FBJ murine osteosarcoma viral oncogene homolog B	2.52
LMOD1	Leiomodin 1 (smooth muscle)	2.35
ACKR1	Atypical chemokine receptor 1 (Duffy blood group)	2.35
ENPP2	Ectonucleotide pyrophosphatase/phosphodiesterase 2	2.35
VSIG8	V-set and immunoglobulin domain containing 8	2.31
SSC5D	Scavenger receptor cysteine rich family. 5 domains	2.31
CHIT1	Chitinase 1 (chitotriosidase)	2.29
NR4A2	Nuclear receptor subfamily 4. group A. member 2	2.29
KIAA1683	Carboxypeptidase X (M14 family). member 2	2.25
CPXM2	Coiled-coil domain containing 3	2.25
CCDC3	Periostin osteoblast specific factor	2.23
POSTN	Fc fragment of IgG binding protein	2.19
FCGBP	Amyloid beta (A4) precursor protein-binding. family B. member 3	2.15
APBB3	MT-RNR2-like 9 (pseudogene)	2.14
MTRNR2L9	Actin. gamma 2 smooth muscle. enteric	2.13
ZDHHC11	Zinc finger DHHC-type containing 11	2.13
ITGAX	Integrin alpha X (complement component 3 receptor 4 subunit)	2.12
BCAM	Basal cell adhesion molecule (Lutheran blood group)	2.10
NFATC2	Nuclear factor of activated T-cells. cytoplasmic. calcineurin-dependent 2	2.07

A-2: List of Top 25 downregulated genes in CTEPH *vs.* donor

Symbol	Entrez gene name	LogFC CTEPH-Donor
APMAP	adipocyte plasma membrane associated protein	-1.99
ST8SIA6	ST8 alpha-N-acetyl-neuraminide alpha-2.8-sialyltransferase 6	-2.01
IGJ	immunoglobulin J polypeptide. linker protein for immunoglobulin alpha and mu polypeptides	-2.02
PCDH17	protocadherin 17	-2.03
PCDHB15	protocadherin beta 15	-2.03
AGTR2	angiotensin II receptor. type 2	-2.04
S100A12	S100 calcium binding protein A12	-2.04
SCN7A	sodium channel. voltage gated. type VII alpha subunit	-2.05
SPTLC2	serine palmitoyltransferase. long chain base subunit 2	-2.05
ABCC4	ATP-binding cassette. sub-family C (CFTR/MRP). member 4	-2.09
CYP1B1	cytochrome P450. family 1. subfamily B. polypeptide 1	-2.11
GANC	glucosidase. alpha; neutral C	-2.12
HS3ST3B1	heparan sulfate (glucosamine) 3-O-sulfotransferase 3B1	-2.17
CCDC85A	coiled-coil domain containing 85A	-2.19
CCL13	chemokine (C-C motif) ligand 13	-2.29
CPA3	carboxypeptidase A3 (mast cell)	-2.29
LIPG	lipase. endothelial	-2.35
SCGB3A2	secretoglobin. family 3A. member 2	-2.43
HEY1	hes-related family bHLH transcription factor with YRPW motif 1	-2.46
S100A8	S100 calcium binding protein A8	-2.59
PSAT1	phosphoserine aminotransferase 1	-2.72
SERPINA3	serpin peptidase inhibitor. clade A (alpha-1 antiproteinase. antitrypsin). member 3	-2.93
TMEM100	transmembrane protein 100	-2.94
FCN3	ficolin (collagen/fibrinogen domain containing) 3	-3.50
DKK2	dickkopf WNT signaling pathway inhibitor 2	-3.54

A-3: List of primers for qRT-PCR

Gene	Species	Sequences (5‘-3‘)	Annealing Temperature (◦C)
B2M	human	F: AGATGAGTATGCCTGCCGTG R: TCATCCAATCCAAATGCGGC	60
CHI3L1	human	F: ATGATGTGACGCTCTACGGC R: ACTCTGGGTGTTGGAGGCTA	60
ENPP2	human	F: GCCCTCCATTAATCATCTTC R: CAGTGGCCAAAGTGTATAAG	60
FOXO 1	human	F: CAATGGAACATCCCAAGAAG R: CAAGGAGAGGCCAACTGTAA	60
FOXO3	human	F: GCTGAAGGATCACTGAGGAA R: CAGTCTCTGCTGGGTTAGGA	60
KLF2	human	F: GGGGTGAGTTCCCCATTCTG R: CCAATGCACACAACAGGTGG	60
GATA6	human	F: TTTGCAACGTGCCTTGAAGT R: CTGTACACTCAGGGAGCCACA	60

A-4: List of primary antibodies

Antibody	Source	Dilution WB	Dilution IHC/ICC	Company
smooth muscle actin (Cy3-labeled)	rabbit		1:200	Sigma Aldrich
ACTB	mouse	1:4000		Sigma Aldrich
smooth muscle actin	mouse		1:700	Sigma Aldrich
vWf	mouse		1:300	Novus
vWf	rabbit		1:900	Agilent
CHI3L1	goat	1 µg/mL	10 µg/mL	R&D
ENPP2	mouse	1:100	1:1000	Abcam
pFAK	mouse		1:800	Santa Cruz
FAK	mouse		1:500	Santa Cruz
pSRC	rabbit		1:1000	Cell signaling
SRC	rabbit		1:1000	Cell signaling
VEGFR2	rabbit		1:1000	Cell signaling
VEGFR1	rabbit		1:1000	Cell signaling
VEGFA	rabbit		1:1000	Abcam
GAPDH	mouse		1:4000	Novus
CD31	mouse	Ready to use		Dako
CD34	mouse	1:50		Dako

A-5: Table list of secondary antibodies

Antibody	Dilution	Company
AlexaFluor488 anti-rabbit IgG	1:1000	Life Technologies
HRP conjugated anti-rabbit IgG	1:40000	Sigma Aldrich
HRP conjugated anti-mouse IgG	1:30000	Sigma Aldrich
HRP conjugated anti-goat IgG	1:1000	R&D

A-6: List of the top 10 up- and down- regulated genes in CHI3L1 (800 ng/mL)-stimulated PCLS

Symbol	Entrez gene name	LogFC CHI3L1 (800 ng/mL-control)
PDP2	pyruvate dehyrogenase phosphatase catalytic subunit 2	8.11
PRSS38	protease, serine, 38	5.55
CATIP	ciliogenesis associated TTC17 interacting protein	5.54
TNIP3	TNFAIP3 interacting protein 3	5.36
PPEF2	protein phosphatase, EF-hand calcium binding domain 2	5.14
PGLYRP2	peptidoglycan recognition protein 2	4.98
GAPDHS	glyceraldehyde-3-phosphate dehydrogenase, spermatogenic	4.94
ZNF232	zinc finger protein 232	4.88
KCNG4	potassium channel, voltage gated modifier subfamily G, member 4	4.81
KCNQ4	potassium channel, voltage gated KQT-like subfamily Q, member 4	4.80
TSTD1	thiosulfate sulfurtransferase (rhodanese)-like domain containing 1	-1.13
MSMB	microseminoprotein, beta-	-1.44
BPIFA1	BPI fold containing family A, member 1	-1.91
STAP1	signal transducing adaptor family member 1	-2.61
LOC100130539	uncharacterized LOC100130539	-2.81
GDF6	growth differentiation factor 6	-3.56
PDX1	pancreatic and duodenal homeobox 1	-3.58
PIGM	phosphatidylinositol glycan anchor biosynthesis, class M	-4.13
REV1	REV1, polymerase (DNA directed)	-4.99
FRAT1	frequently rearranged in advanced T-cell lymphomas 1	-8.83

A-7: List of the top 10 up- and down- regulated genes in CHI3L1 (1200 ng/mL)-stimulated PCLS

Symbol	Entrez gene name	LogFC CHI3L1 (1200 ng/mL-control)
BPIFA1	BPI fold containing family A, member 1	3.94
MSMB	microseminoprotein, beta-	3.87
RTL1	retrotransposon-like 1	3.85
GIMAP1	GTPase, IMAP family member 1	3.66
LILRA2	leukocyte immunoglobulin-like receptor, subfamily A (with TM domain), member 2	3.59
PCDH17	protocadherin 17	3.51
CPNE7	copine VII	3.33
RPE65	retinal pigment epithelium-specific protein 65kDa	3.31
FAM92B	family with sequence similarity 92, member B	3.29
MYCN	v-myc avian myelocytomatosis viral oncogene neuroblastoma derived homolog	3.22
GDF6	growth differentiation factor 6	-3.21
TSTD1	thiosulfate sulfurtransferase (rhodanese)-like domain containing 1	-3.36
ADAMTS13	ADAM metallopeptidase with thrombospondin type 1 motif, 13	-3.51
PDX1	pancreatic and duodenal homeobox 1	-3.60
PIGM	phosphatidylinositol glycan anchor biosynthesis, class M	-3.66
STAP1	signal transducing adaptor family member 1	-3.73
RNF186	ring finger protein 186	-3.78
REV1	REV1, polymerase (DNA directed)	-4.5
LOC100130539	uncharacterized LOC100130539	-5.04
FRAT1	frequently rearranged in advanced T-cell lymphomas 1	-7.68

Publication list

Publications

- Iloska et al**. Proximal vs. distal end-stage CTEPH: Insights from histopathological and molecular perspective.** *Manuscript in preparation.*
- Cheladurai, Iloska et al. **Sirt1 in pulmonary vascular remodelling and right ventricular hypertrophy**. *Manuscript in preparation.*
- Anabela Bensimon-Brito, Srinath Ramkumar, Giulia Boezio, Stefan Guenther, Carsten Kuenne, Héctor Sánchez-Iranzo, Dijana Iloska, Janett Piesker, Soni Pullamsetti, Nadia Mercader, Dimitris Beis, Didier Stainier. **Cardiac valve regeneration in adult zebrafish: importance of TGFß signaling in recellularization.** Submitted in *Dev Cell.*
- Li M, Riddle S, Zhang H, D'Alessandro A, Flockton A, Serkova NJ, Hansen KC, Moldvan R, McKeon BA, Frid M1, Kumar S, Li H, Liu H, Caánovas A, Medrano JF, Thomas MG, **Iloska D**, Plecitá-Hlavatá L, Ježek P, Pullamsetti S, Fini MA, El Kasmi KC, Zhang Q, Stenmark KR**. Metabolic Reprogramming Regulates the Proliferative and Inflammatory Phenotype of Adventitial Fibroblasts in Pulmonary Hypertension Through the Transcriptional Corepressor C-Terminal Binding Protein-1**. Circulation. 2016 Oct 11;134(15):1105-1121
- Josipovic I, Fork C, Preussner J, Prior KK, **Iloska D**, Vasconez AE, Labocha S, Angioni C, Thomas D, Ferreirós N, Looso M, Pullamsetti SS, Geisslinger G, Steinhilber D, Brandes RP, Leisegang MS. **PAFAH1B1 and the lncRNA NONHSAT073641 maintain an angiogenic phenotype in human endothelial cells**. Acta Physiol (Oxf). 2016 Sep;218(1):13-27.

Conference participation

- DZL 2019 Annual meeting, **Poster and short presentation** – *Proximal vs. distal end-stage CTEPH: Insights from histopathological and molecular perspective*, Mannheim, Germany, February 2019
- 13th PVRI Annual World Congress on Pulmonary Vascular Disease, **Presentation** – *Defective angiogenesis is a major contributor of CTEPH*, Barcelona, Spain, January 2019
- 13th PVRI Annual World Congress on Pulmonary Vascular Disease, **Poster presentation** – *Proximal vs. distal end-stage CTEPH: Insights from histopathological and molecular perspective*, Barcelona, Spain, January 2019
- German-French Lung Retreat, **Poster presentation** – *Unique molecular and histopathological imprint of end-stage CTEPH*, Paris, France, September 2018
- Cardiovascular Development and Regeneration Conference, Weinstein 2018, **Poster** – *Zebrafish heart valve regeneration: A model for valve recellularization*, Nara, Japan, May 2018
- 6th World Symposium on Pulmonary Hypertension, **Poster presentation** – *End-stage chronic thromboembolic pulmonary hypertension: Unique molecular and histopathological imprint*, Nice, France, February 2018

- DZL 2018 Annual meeting, **Poster presentation** – *End-stage chronic thromboembolic pulmonary hypertension: Unique molecular and histopathological imprint*, Bad Nauheim, Germany, February 2018
- ERS International congress 2017, **Poster presentation** – *Proangiogenic and wound healing molecular and histopathological fingerprint of chronic thromboembolic pulmonary hypertension*, Milan, Italy, September 2017
- International CTEPH conference, **Poster presentation** – *Proangiogenic and wound healing molecular and histological fingerprint of chronic thromboembolic pulmonary hypertension*, Leuven, Belgium, June 2017
- ECCPS symposium, **Poster and short presentation** – *Proangiogenic and wound healing molecular and histological fingerprint of chronic thromboembolic pulmonary hypertension*, Bad Nauheim, Germany, June 2017
- DZL 2017 Annual meeting, **Poster and short presentation** – *Proangiogenic and wound healing molecular and histological fingerprint of chronic thromboembolic pulmonary hypertension*, Munich, Germany, January 2017
- PH DACH Symposium, **Poster presentation** – Molecular and histological phenotyping of chronic thromboembolic pulmonary hypertension, Heidelberg, November 2016
- DZL 2016 Annual meeting, **Poster presentation** – *Characterization of distal vessel remodelling in CTEPH*, Hannover, Germany, January 2016
- American Thoracic Society, ATS 2015, **Presentation and poster presentation**– *Characterization of distal vessel remodelling in CTEPH*, Denver, Colorado, USA, May 2015
- DZL 2015 Annual meeting, **Poster presentation** – *Characterization of distal vessel remodelling in CTEPH*, Hannover, Germany, February, 2016
- **Symposium**, *Programming the Lung – Epigenetic control of lung biology through histone and chromatine modification*, Castle Weilburg, Germany, November 2012
- 22nd IUBMB- 37th FEBS Congress, **Poster** – *Global proteomic analysis of outer membrane vesicles derived from the probiotic Escherichia coli strain Nissle 1917*, Sevilla, Spain, 2012
- Vth Research day, Faculty of Pharmacy, University of Barcelona, Barcelona, Spain, April, 2012
- Seminar and experimental session, Use of fluorescence spectroscopy in the study of drugs, proteins and membranes, University of Applied Sciences Northwestern, Basel, Switzerland, December 2011
- 33rd Primatijada, **Presentation** - *Type of proteinuria described in comparing four methods for total protein determination in urine*, Zlatar, Serbia, May 2006
- 33rd Primatijada, **Presentation** - *Type of proteinuria described in comparing four methods for total protein determination in urine*, Zlatar, Serbia, May 2006
- Summer school, *Fine chemicals – evaluation of methods for their production*, Silesian University of Technology, Gliwice, Poland, July 2005

Erklärung zur Dissertation

„Hiermit erkläre ich, dass ich die vorliegende Arbeit selbständig und ohne unzulässige Hilfe oder Benutzung anderer als der angegebenen Hilfsmittel angefertigt habe. Alle Textstellen, die wörtlich oder sinngemäß aus veröffentlichten oder nichtveröffentlichten Schriften entnommen sind, und alle Angaben, die auf mündlichen Auskünften beruhen, sind als solche kenntlich gemacht. Bei den von mir durchgeführten und in der Dissertation erwähnten Untersuchungen habe ich die Grundsätze guter wissenschaftlicher Praxis, wie sie in der „Satzung der Justus-Liebig-Universität Gießen zur Sicherung guter wissenschaftlicher Praxis“ niedergelegt sind, eingehalten sowie ethische, datenschutzrechtliche und tierschutzrechtliche Grundsätze befolgt. Ich versichere, dass Dritte von mir weder unmittelbar noch mittelbar geldwerte Leistungen für Arbeiten erhalten haben, die im Zusammenhang mit dem Inhalt der vorgelegten Dissertation stehen, oder habe diese nachstehend spezifiziert. Die vorgelegte Arbeit wurde weder im Inland noch im Ausland in gleicher oder ähnlicher Form einer anderen Prüfungsbehörde zum Zweck einer Promotion oder eines anderen Prüfungsverfahrens vorgelegt. Alles aus anderen Quellen und von anderen Personen übernommene Material, das in der Arbeit verwendet wurde oder auf das direkt Bezug genommen wird, wurde als solches kenntlich gemacht. Insbesondere wurden alle Personen genannt, die direkt und indirekt an der Entstehung der vorliegenden Arbeit beteiligt waren. Mit der Überprüfung meiner Arbeit durch eine Plagiatserkennungssoftware bzw. ein internetbasiertes Softwareprogramm erkläre ich mich einverstanden.“

_____ _____

Ort, Datum Unterschrift

Acknowledgements

"I learned that courage was not the absence of fear, but the triumph over it. The brave man is not he who does not feel afraid, but he who conquers that fear."

Nelson Mendela

First of all, I would like to thank my supervisor **Dr. Soni Savai Pullamsetti** for her support, encouragement and help during my doctoral work. Sincere gratitude for the opportunity to start my research carrier at Max Planck Institute for Heart and Lung Research, Bad Nauheim as well as to enhance my knowledge within the lab or throughout international trainings as well as attending conferences.

I would like to thank **Prof. Dr. med. Werner Seeger** for the very productive discussions and scientific input, especially since CTEPH is still a challenging and yet unexplored field.

Special thanks to **Dr. Rory Morty** for providing me the indispensable experience and knowledge by joining the International PhD Programme, Molecular Biology and Medicine of Lung (MBML).

Thanks to **Dr. Rajkumar Savai** for his assistance and the provided protocols while realization of this thesis.

My sincere gratitude to **Prof. Dr. med. Eckhard Mayer and Dr. Stefan Gut,** with whom I spent most of the time during the first two years of my PhD, waiting for samples in the operation theatre at Kerckhoff-Klinik. Thank you for that and for all the support and scientific discussions, whenever a clarity and "surgical" mind precision was required.

I thank **Dr. Jochen Wilhelm** for performing genome-wide expression array analysis and distribution analysis of the morphometric data; as well as for generously sharing his knowledge and guidance to broaden the perspectives of this work.

Many thanks to **Prof. Dr. med. Ludger Fink** from the Institute of Pathology and Cytology, UEGP, Wetzlar, Germany for providing intact proximal and distal pulmonary arteries used as controls for the endarterectomised material as well as for the great ideas while developing this project.

I would like to thank **Dr. Maria Rosa Ghigna** from the Service Anatomie Pathologique, Hôpital Marie Lannelongue, Paris, France and **Peter Dorfmüller** from the Institute of Pathology, University Clinic Giessen and Marburg Peter, for providing precious samples from CTEPH patients of the Paris cohort.

As well, special thanks to **Prof. Susan S. Smyth,** MD, PhD from University of Kentucky, College of Medicine, Lexington KY, USA for providing a breeding pair of *Enpp2+/-* mice.

Many thanks to **Prof. Dr. Irene Lang** and **Smriti Sharma** from the Medical University of Vienna, Internal Medicine II, Austria for the helpful discussions and performing animal experiments of inferior vena cava ligation.

Thanks to **Dr. Lavinia Neubert** and **Borchert Paul** from Hannover Medical School for performing *ex-vivo* ink injection procedure of a CTEPH lung after transplantation as well as providing valuable human samples and enabling the "wrapping up" of this story.

Thanks to all the current and past members of **AG Morty** and **AG Savai**, for their assistance and help as well as for our "chatty" moments.

Thanks a bunch to my dear colleagues from **Ag Pullamsetti.** They weren`t just colleagues, rather more than good friends, having to share same or similar paths. **Dr. Swati Dabral**, thanks for the scientific input and help on this project and thesis revision, as well for all the unforgettable memories in the lab and during our trips. **Dr. Elisabetta Gamen**, thank you for our daily scientific debates on CTEPH or HDACs and mostly for keeping my back in good or bad times, memorable trips and the one to follow. **Dr. Hamza Al-tamari** thanks for all the advices and help as well as for the funny discussions we had. Thanks to **Dr. Prakash Chelladurai** for the scientific and life talks during this path and to **Dr. Christian Mücke** for the challenging conversations and experiences. Thanks to **Chanil Valasarajan** for his selfless aid on this project, especially in the last couple of months. Special thanks to **Natascha Wilker** for her technical assistance throughout the work and moreover thanks for your support and listening to my blabbing and complaints. Many thanks to the future doctors, **Ylia Salazar** and **Pouya Sarvari**, for being there, helping and encouraging all these years. As well, thanks to **Sreenath Nayakanti**, **Edibe Avci, Leili Jafari**, who would step-in, every time assistance was needed and **Golnaz Hesami** for the genotyping of the ENPP2 mice.

I would like to thank **Monika Haselbauer**, **Uta Eule**, the **IT department** and the **HR department** at MPI for their excellent cooperation.

Thanks to my dear friends from home, **Stefan, Ratka, Biljana, Jelena** and others. They were there for all the ups and downs on this path, celebrating every success as well as believing in me, supporting and caring.

My parents and my brother Stefco, I can`t thank them enough for their unconditional love, patience and support. These years of doubts and fears, peaks and valleys, wound`t have been bearable, if it wasn't for you. Thank you for making me the way I am today.

My husband, Prof. Dr. Michael Leyer, who came in my life at the last year of this path. Thank you for all the understanding, encouraging my motivation, "feeding" my endurance through the remaining bit and the "epic" discussions on statistics. I know what follows isn`t going to be easy, as I am sure that whatever comes, will be good, side by side with you.

Last, but not least, my genuine appreciation to all the **selfless donors, CTEPH patients**...You made this piece of work extraordinary... And I hope to have contributed a "tiny" bit to the global knowledge in order to set a background for making your path easier in the years that follow.